Nanoparticles functionalized with human antibodies for multimodal molecular imaging of atherosclerosis

Mélusine Larivière

université de BORDEAUX

THÈSE PRÉSENTÉE

POUR OBTENIR LE GRADE DE

DOCTEUR DE L'UNIVERSITÉ DE BORDEAUX

École doctorale : Sciences de la Vie et de la Santé

Spécialité : Bioimagerie

Par Mélusine LARIVIÈRE

Nanoparticles functionalized with human antibodies for multimodal molecular imaging of atherosclerosis

Sous la direction de : Gisèle CLOFENT-SANCHEZ, DR CNRS, Université de Bordeaux, Bordeaux, France

Co-directeur : Christoph Eugen HAGEMEYER, Group leader, ACBD, Monash University, Melbourne, Australia

Soutenue le 19 décembre 2016

Membres du jury :

Mme NAVARRO-TEULON Isabelle, CR à l'IRCM, Montpellier	Rapporteur
M. BOQUET Didier, DR au CEA, Saclay	Rapporteur
M. WATIER Hervé, PU-PH à l'Université François Rabelais, Tours	Examinateur
Mme CRAUSTE-MANCIET Sylvie, PU-PH à l'Université de Bordeaux	Examinateur
M. BESSEDE Alban, Président de la société ImmuSmol, Pessac	Examinateur
Mme CLOFENT-SANCHEZ Gisèle, DR au CNRS, Bordeaux	Examinateur
M. HAGEMEYER Christoph, Group Leader au ACBD, Melbourne	Examinateur

C'est en essayant continuellement que l'on finit par réussir. Donc plus ça rate, plus on a de chances que ça marche.

[Claude Piéplu, Devise Shadock]

It is by continuously trying that one eventually succeeds. Hence the more you mess up, the more it may finally work.

[Claude Piéplu, Shadock saying]

Acknowledgments

Merci à mes rapporteurs d'avoir accepté d'examiner ce travail de thèse, ainsi qu'aux membres du jury de leur intérêt pour ces travaux.

Plus que jamais dans ce marathon qu'est la fin de thèse, mes remerciements vont à Gisèle Clofent-Sanchez. Pour son immense soutien, sa foi en mes supposées capacités, et -je crois pouvoir le dire- son amitié. À toutes les bières partagées : celles pour célébrer une victoire, noyer une défaite, régler un conflit ou simplement discuter. À nos aventures passées, en Australie, en Thaïlande et ailleurs, et pour celles à venir. Pour les moments de loose (je pense en particulier à ce vol retour de Marseille où on a pris un tel orage sur la gueule qu'il a fallu attendre 2 heures qu'ils rouvrent la tour de contrôle pour qu'on puisse décoller !), les moments de gloire (hé, quand même, tu les as eus ces financements !) et tous les moments de doute qui ne t'ont jamais fait passer l'envie de rire. Merci. Beaucoup.

Merci infiniment à toute l'équipe de Bordeaux. Jeanny, sa disponibilité et son humour pince-sans-rire, Marie-Jo et son rire qui ramène le soleil en plein cœur de l'hiver, Stéphane pour ses conseils, Audrey toujours motivée et Florence toujours enthousiaste. À Ségolène, parce que tu feras toujours partie de l'équipe. Un merci tout particulier à Cyril qui m'a évité la pendaison en me sortant d'affaire lors de la mise en page de ce document, merci également pour ton patient enseignement pendant cette année de manips communes.

Merci à mes collègues du RMSB et de la PTIB, pour les bons conseils et les bons moments.

A massive thank you guys to all the Melbourne team. To my supervisor Christoph for his patience and trust. To all the team for being so friendly, helpful and patient. Cheers to you, the Tall timber brekkies and the TGIF labmeetings/beergardens! To Shweta for teaching me everything about sub-cloning and production, for the indian food and the kindness. Thank you Karen for the hospitality, the bike, the Sunday arvo coffees and strolls, and so much more. Thank you Hannah for being so ooowesome, for the puns I didn't get and the ones I did. For the food and laugh sessions we shared, and the kiwi toasts! Thanks Lok for the geekiness, the Lucky Coq and Exploding kittens. Thank you Mei for the interesting discussions, for being so nice and friendly. Thank you Austrian Thomas for the bike repair service, the Thursday steak nights and the nice promenades to the market or along the Yarra.

Thank you French Thomas, brother-in-lab, for the taste of France when I was feeling homesick. À la santé de Dikkenek, des Casseurs Flowteurs, des embuscades, des grands-packs-de-Carlton-comme-ça-il-en-restera, du switch magique et des black-listing xD Si c'est pas à Melbourne ce sera à Caen, à Bordeaux, peu importe tant qu'on y trouve à boire. Merci au reste de la french team pour avoir fait de cette année un très très grand cru qui restera dans les anals.

Merci encore et toujours à ma famille pour votre amour, votre soutien, vos zourseries et tout le reste. Bien sûr on ne choisit pas les trottoirs de Manille, de Paris ou d'Alger pour apprendre à marcher… Être née quelque part au milieu des champs de betteraves c'était peut-être un hasard, grandir si bien entourée c'est un sacré coup de bol.

Un vieux dicton dit qu'on n'a que ce qu'on mérite, alors, malgré tout le boulot qu'elle représente, cette thèse ne sera jamais un si grand accomplissement que votre amitié à tous, gens divers, étranges et merveilleux. Pour mes Pounaches, les Guindoules, La Bande de Potes™, la team Vovinam, les vieux amis perdus de vus et retrouvés, ceux qui sont loin des yeux, pas du cœur et tous les autres. MER.FUCKING.CI. Et à la vôtre !

Je voudrais continuer à ne *pas* féliciter les éternels insatisfaits qui sont allés voir de l'autre côté si l'herbe était plus verte. Franchement, on n'était pas bien là ? Maintenant y a des chaises vides, c'est pas feng-shui.

Pour finir, sans bande son ces 3 années n'auraient pas été les mêmes, celles d'avant non plus du reste. Merci, dans le désordre et de manière non exhaustive, à : Les Casseurs Flowteurs, Bruno Mars, Pink Floyd, Chill Bump, Mindless Self Indulgence, The Arctic Monkeys, Chinese Man, Boby Lapointe, Die Antwoord, Joan Jett, Maroon 5, Nine Inch Nails, Mozart…

Table of content

Abbreviation list

aa	amino-acid
Ab	antibody
AITP	autoimmune thrombocytopenic purpura
APC	antigen-presenting cell
ApoE mouse	ApoE KO or ApoE-/- mouse
BCA	bicinchoninic acid
BCR	B cell receptor
bp	base pairs
CDR	complementarity determining region
CT	computed tomography
CT	computed tomography
CVDs	cardiovascular diseases
Da	Dalton
DC	dendritic cells
EC	endothelial cells
Fc	cristalizable fragment
Fe	Iron
Gd	Gadolinium
GT	Glanzmann thrombasthenia
HDL	high-density lipoprotein
HTRF	homogeneous time resolved fluorescence
HuAb	human antibody
Ig	immunoglobulin
IHC	immuno histochemistry
kDa	kiloDalton
LDL	low-density lipoprotein
mAb	monoclonal antibody
MGE	multi-gradient echo
MM LDL	minimally-modified low-density lipoproteins

MR	magnetic resonance
NIRAF	near-infrared autofluorescence
NIRF	near-infrared fluorescence
NP	nanoparticle
PBS	phosphate buffer saline
PCR	polymerase chain reaction
PET	positron emission tomography
PFA	paraformaldehyde
PhAb	phage-antibody
ROS	reactive oxygen species
RT	room temperature
scFv	single chain variable fragment
SDS-PAGE	sodium dodecyl sulfate polyacrylamide gel electrophoresis
SMC	smooth muscle cells
SPECT	single photon emission computed tomography
SPIO	Superparamagnetic iron oxide
T	Tesla
TEM	transmission electron microscopy
VH	variable heavy (domain of Ig)
VL	variable light (domain of Ig)
VUSPIO	Versatile Ultrasmall superparamagnetic iron oxide
WHO	world health organization

Introduction

The research project presented in this thesis aims at tackling one of the most important health condition worldwide, called atherosclerosis, from which originate most acute cardio-vascular events. Atherosclerosis is a lifelong-developing condition, originating from multiple lifestyle, environmental and genetic factors, that can eventually lead to lethal events like myocardial infarction or stroke.

The team I joined for this work has an expertise in antibody selection by phage display technology, with applications in the field of cardiovascular pathologies, and particularly in atherosclerosis. Naturally, beyond the fundamental research interest, they have looked into potential applications: new biomarkers discovery, diagnosis and its therapeutic-coupled counterpart, theranostics.

With the aim to propose a non-invasive diagnosis method, a collaboration with chemists had been set up, which has led to the development of contrast agents for MRI imaging based on iron oxide nanoparticles. Those have been extensively studied in the ApoE-/- mouse, fed a high cholesterol diet, model of the pathology, and proof-of-concepts had been obtained.

In this context, I was enrolled with the aim to try and improve the diagnosis possibilities by the introduction of multimodal imaging. Fluorescent imagers, including a tomograph, had been acquired by the Bordeaux University and were emerging as a valuable tool for small animal imaging. At the same time, a long-lasting collaboration with the team of Dr Hagemeyer, in Melbourne, was offering the double opportunity of taking in a new site-specific conjugation method, and of undertaking yet another imaging technology: positron emission tomography.

It so happened that during the past three years, I have learnt and put to use several conjugation methods, immunoglobulin biology and production techniques, various image construction technologies and the way to interpret them. You are now reading the modest, yet as faithful as achievable, report of these three years of research.

In a first part, I will present the atherosclerotic disease, its importance and pathophysiology, and the variety of actors involved in its development and evolution, which can serve as so many targets for molecular diagnosis.

I will then introduce the imaging technologies available for the diagnosis of atherosclerosis and examples of contributions to the field.

The third part will address the monoclonal antibodies history, and summarize the methods available for their obtainment and production.

In a fourth part I will detail the project design, material and methods, and results, with regards to antibodies generation and conjugation. Finally, achievements in targeted imaging will be highlighted.

To conclude with, I will discuss the accomplishments and contingencies of this project, the lessons learned and future perspectives.

Section 1

Context of the project

1 Relevance of the topic: importance of cardio-vascular diseases

According to the World Health Organization (WHO) "*Cardiovascular diseases (CVDs) are a group of disorders of the heart and blood vessels and include coronary heart disease (heart attacks), cerebrovascular disease (stroke), raised blood pressure (hypertension), peripheral artery disease, rheumatic heart disease, congenital heart disease and heart failure.*" Figure 1 presents the cardiovascular death rate, per country, over a year (data 2012).

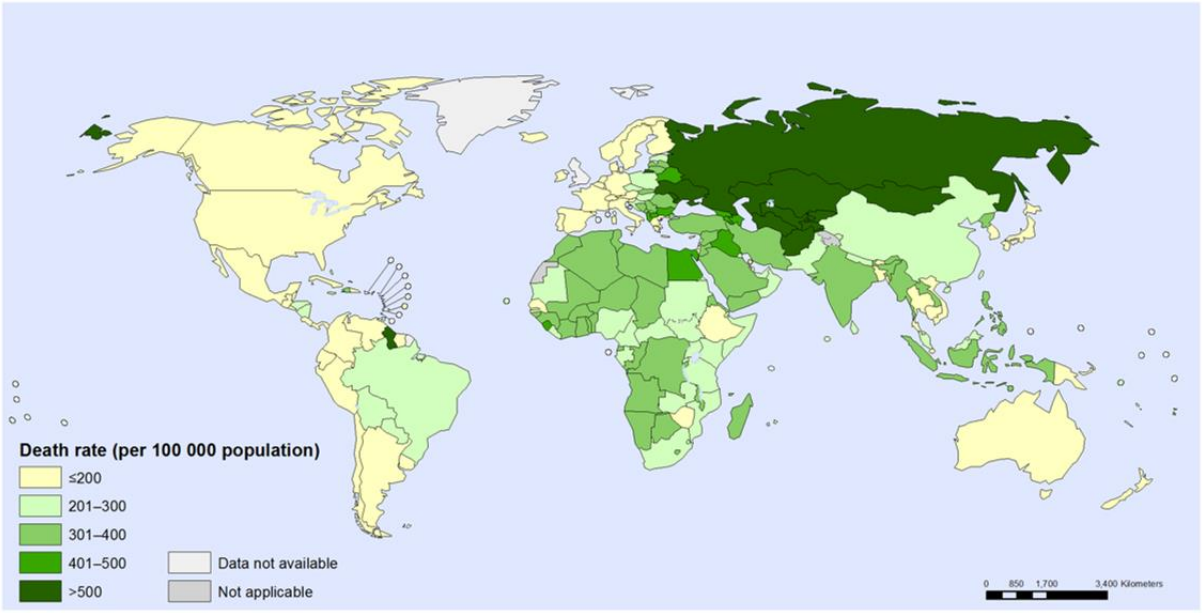

Figure 1: Map of the cardiovascular diseases mortality. Age-standardized death rate per 100,000 population, both sexes, in 2012, per country. From Global Health Observatory Map Gallery, http://gamapserver.who.int/mapLibrary.

Official statistics state that 17.5 million people die each year from CVDs, which is around 31% of all deaths worldwide. Furthermore, 80% of all CVD deaths are likely due to heart attacks and strokes, "[which cause] *are usually the presence of a combination of risk factors, such as tobacco use, unhealthy diet and obesity, physical inactivity and harmful use of alcohol, hypertension, diabetes and hyperlipidaemia.*" [1] (http://www.who.int/cardiovascular_diseases/en/, consulted 08/2016)

They are usually acute events caused by a blockage, preventing blood circulation to the heart or brain. The most common reasons for this are a pathological thickening of the aortic walls (stenotic atheroma plaque) or thrombi (ruptured atheroma plaque). These atheroma plaques slowly develop over the lifetime of an individual, leading to a chronic condition called atherosclerosis, which can go unnoticed for years.

The chance for a given individual to suffer from cardio-vascular diseases can be evaluated based on risk factors, which are gathered for interpretation through a score. There are two of them:

1/ The Framingham score is the most used worldwide, it evaluates the 10-years risk of cardiovascular events (even non-lethal) and includes sex, age, total blood cholesterol, HDL cholesterol level, smoking habit, presence or absence of diabetes and hypertension. Each of these gives a rating, if the global score exceeds 20% an individual is considered at risk. 2/ The SCORE (Systemic COronary Risk Estimation) score is only used in Europe and renders certain geographic epidemiological discrepancies. It evaluates the 10-years risk of dying from a cardiovascular event and takes into account roughly the same indicators as its counterpart.

An initial assessment and risk stratification for susceptible patients are based on these scores. The first level of intervention is lifestyle and dietary measures, then lipid-lowering drugs and ultimately in the acute phases surgery to remove the blockade and revascularize the ischemic organ.

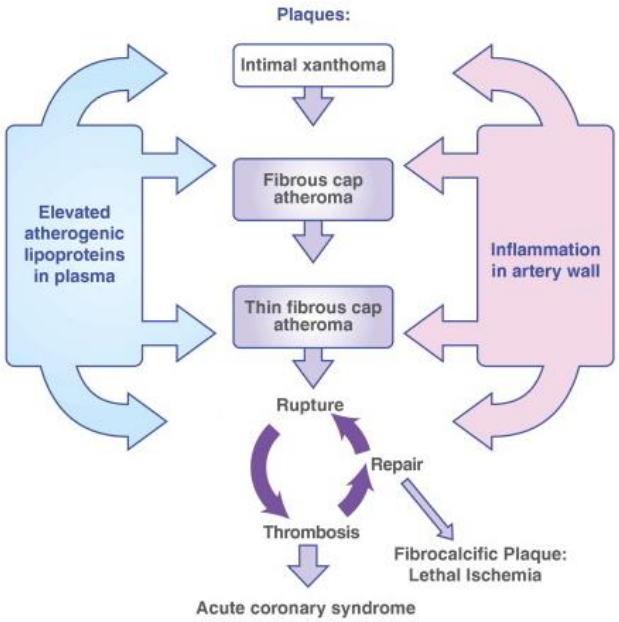

Figure 2: Influence of lipidemia and inflammation on the pathogenesis of atherosclerosis. Modified from Insull et al., 2009.

2 Pathogenesis and pathophysiology of atherosclerosis

Atherosclerosis gradually develops for fifty or more years throughout the life of an individual before leading to chronic ischemic complications or acute events. Two main factors influence this pathogenesis: 1/ an increased level of circulating atherogenic lipoproteins and 2/ local immuno-inflammatory factors, as shown in Figure 2.

"*Atherosclerosis is a multifocal, smoldering, immunoinflammatory disease of medium-sized and large arteries fuelled by lipids*." [2] Its slow, quiet progression generally remains unnoticed, explaining how over 50% of people dying from a sudden cardiovascular event were otherwise symptom-free[3].

2.1 Natural history of the pathology

Table 1: Classification and description of atherosclerosis stages. SMCs: smooth muscle cells ; TCFA: thin cap fibro-atheroma.

Evolution of the lesion[4]	AHA classification[5]	Histopathology
Clinically silent lesions		
1. Intimal thickening		Normal accumulation of SMCs in the intima; absence of lipid or macrophage foam cells
2. Intimal xanthoma or fatty streaks	I. isolated macrophage foam cells	Subendothelial accumulation of foam cells in intima without necrotic core or fibrous cap
Progressive lesions, inconsistently symptomatic		
1a. Pathologic intimal thickening	II. multiple foam cell layers formed III. isolated extracellular lipid pool	SMCs in a proteoglycan-rich matrix with areas of extracellular lipid accumulation without necrosis
1b. With erosion		Same as above, with luminal thrombosis
2a. Fibrous cap atheroma	IV. confluent extracellular lipid core formed V. fibromuscular tissue layers produced	Well-formed necrotic core with overlying fibrous cap
2b. With erosion		Same as above, with luminal thrombosis; no communication of thrombus with necrotic core
Usually symptomatic		
3. TCFA		Thin fibrous cap, infiltrated with macrophages and lymphocytes, rare SMCs, and an underlying necrotic core
a. With rupture	VI. surface defect, hematoma, thrombosis	Fibroatheroma with cap disruption; luminal thrombus communicates with underlying necrotic core
4. Calcified nodule	VII. calcification predominates	Eruptive nodular calcification with underlying fibrocalcific plaque
5. Fibrocalcific plaque	VIII. fibrous tissue changes predominates	Collagen-rich plaque usually with significant stenosis; contains large areas of calcification with few inflammatory cells; necrotic core may be present

Table 1 presents the lifelong evolution of the lesions. Early in life, from childhood or adolescence, non-pathologic intimal lesions develop under the influence of local hemodynamic stress. It usually takes place at the branching points of major arteries, and consists in smooth muscle cells (SMC) accumulation which thickens the vascular wall (*intimal thickening*)[6].

Secondarily, low-density lipoproteins (LDL) accumulate on the endothelial surface, forming structures called fatty streaks, which in turn trigger the recruitment, activation, and differentiation of monocytes into macrophages. LDLs are oxidized following a two-steps process, yielding first minimally-modified LDL (MM LDL), then oxidized LDL (oxLDL) in which ApoB is oxidized as well, leading to its recognition by the scavenger receptor of macrophages and thus the formation of foam cells[4]. Activated endothelial cells (EC) express P-selectin. This surface receptor binds monocytes and provokes the subendothelial accumulation of LDL-laden macrophages foam cells. In this environment, platelets also display more inflammation-associated adhesion receptors like P-selectin, intracellular adhesion molecule 1 (ICAM1), or glycoproteins Ibα and αIIbβ3 (GPIbα, GPαIIbβ3); they participate in the binding of oxLDL and leukocytes [6,7], and the development of the plaque (intimal *xanthoma or fatty streaks*).

Progressive atherosclerotic lesions (Figure 3) occur as the result of (i) a serum surcharge of low-density lipoproteins (LDL); (ii) a sustained activation of the inflammatory system within the vascular wall.

LDL accumulate into the cytoplasm of endothelial cells and smooth muscle cells, and in the extracellular matrix, where they undergo oxidization by reactive oxygen species (ROS) resulting from the inflammatory environment. The secretion of chemokines by SMCs and macrophages in turn draws more monocytes, T-and B-lymphocytes, neutrophils, granulocytes and dendritic cells (DCs) to the arterial wall. The recruitment and activation of leukocytes has been shown to be a platelet-mediated phenomenon[8,9]. SMCs proliferate in a proteoglycan-rich matrix, leading to a *pathologic intimal thickening.*

Extracellular proteoglycans secreted by smooth muscle cells bind lipids, and contribute to their extracellular accumulation. They eventually coalesce into lipid pools that cause cell necrosis. Necrotic tissue and oxidized lipids accumulate, forming lipid-rich necrotic cores in the intima, which architecture is progressively disrupted. *Fibrous cap atheroma* results from the extensive remodeling and fibrous tissue build-up over the necrotic cores, at the blood interface, by the SMCs[6].

Thin-cap fibro-atheroma is the typical rupture-prone lesion, usually in persons aged over 55. The fibrous cap is locally weakened by proteolytic enzyme activity, and scattered calcifications appear. The increasingly large necrotic core becomes hypoxic, triggering local neovascularization. Fragile and leaky newly-formed vessels facilitate further invasion of immune cells and release of soluble factors into their surroundings. Furthermore, intraplaque hemorrhage may occur from these imperfect vessels, causing an accumulation of erythrocyte-derived phospholipids, free cholesterol, hemoglobin and iron. These mechanisms ultimately result in plaque destabilization[10,11].

When the thrombogenic lipid core is exposed to the lumen, platelets as well as the coagulation cascade become activated, producing a massive thrombus that can extend into the arterial lumen, and result in a potentially life-threatening event such as acute coronary syndromes and stroke.

Alternatively, the ruptured cap can remain asymptomatic and heal, by reforming its fibrous tissue. When this rupture-healing sequence occurs repeatedly, multiple layers of scar tissue thicken the vascular wall, with a risk of stenosis. A significant stenosis restricts the blood flow and may cause ischemia. When it occurs inside the coronary arteries the symptoms are a chronic condition called angor, which must be monitored and may necessitate reperfusion surgery[6,12].

The calcification process occurs throughout all these steps, initially as small aggregates and later as large nodules, which are additional sites for thrombosis if exposed to the blood flow.

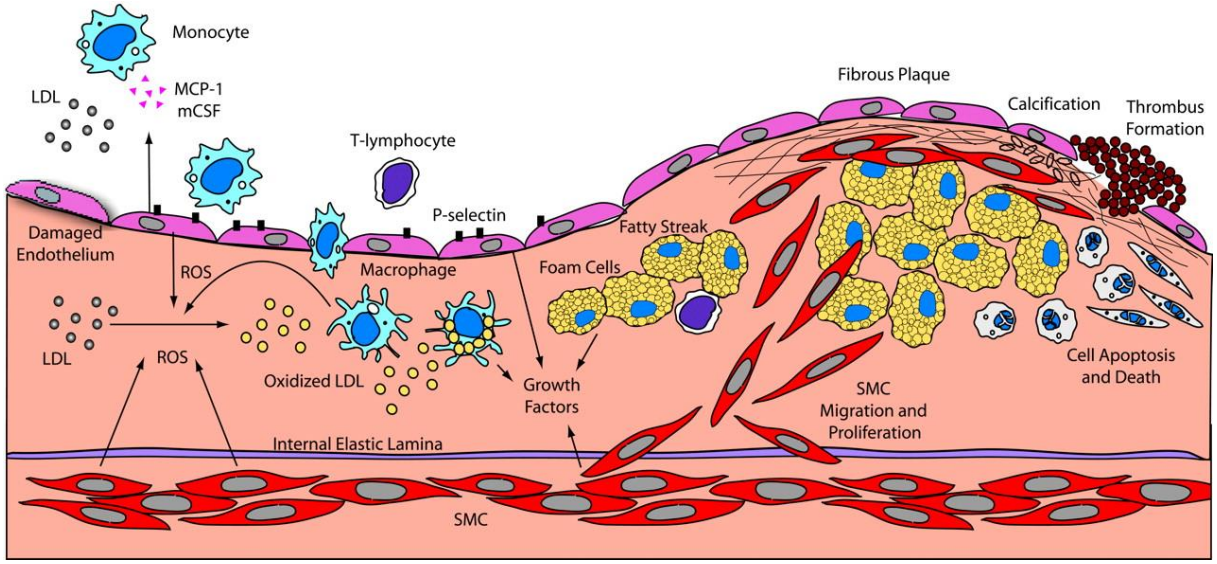

Figure 3: Key players in atheroma initiation and evolution. From Madamanchi et al., Arterioscler Thromb Vasc Biol, 2005.

2.2 Soluble factors

As described previously, atherogenesis results from the interaction of blood factors, either exogenous or secreted locally by the cells of the vessel wall, and inflammation-drawn immune cells. This chapter will precise the known role of some of these soluble factors and cellular actors and their complex interactions as summarized on Figure 3.

2.2.1 Low-density lipoprotein

Low-density lipoproteins (LDL) are protein-lipid complexes, synthetized by the liver from cholesterol, apolipoproteins (Apo), phospholipids, triglycerides and liposoluble vitamins. They are the bloodstream cholesterol-carrier, allowing its distribution throughout the organism to be

integrated into the cell membranes or to serve as a precursor for biomolecules synthesis. Although cholesterol is mandatory for the organism to function, too much cholesterol has been proven to be harmful: its role in atherosclerosis is paramount and undisputed, and its serum levels reduction is the first line of therapeutic intervention for the prevention of cardio-vascular events.

Indeed, the initiating event of atherosclerosis seems to be the transport of LDL across the endothelium into the artery wall (Figure 4, 1). This is a concentration-dependent process that does not require receptor-mediated endocytosis. Within the extracellular matrix they are retained by association with proteoglycans and collagen fibers[12,13].

Early atherosclerotic lesions, called fatty streaks, develop as a result of lipids exposure to the oxidative environment of the artery wall (Figure 4, 2). ECs and SMCs have been shown to be responsible for the primary oxidation of LDLs[14,15], leading to their internalization by monocytes, via several mechanisms (detailed in 2.3.1). Minimally modified LDL (MM-LDL) seem to trigger early recruitment of monocytes into the subendothelial space and further lead their conversion into macrophages(Figure 4, 3)[16,17]. This in turn enriches the microenvironment in reactive

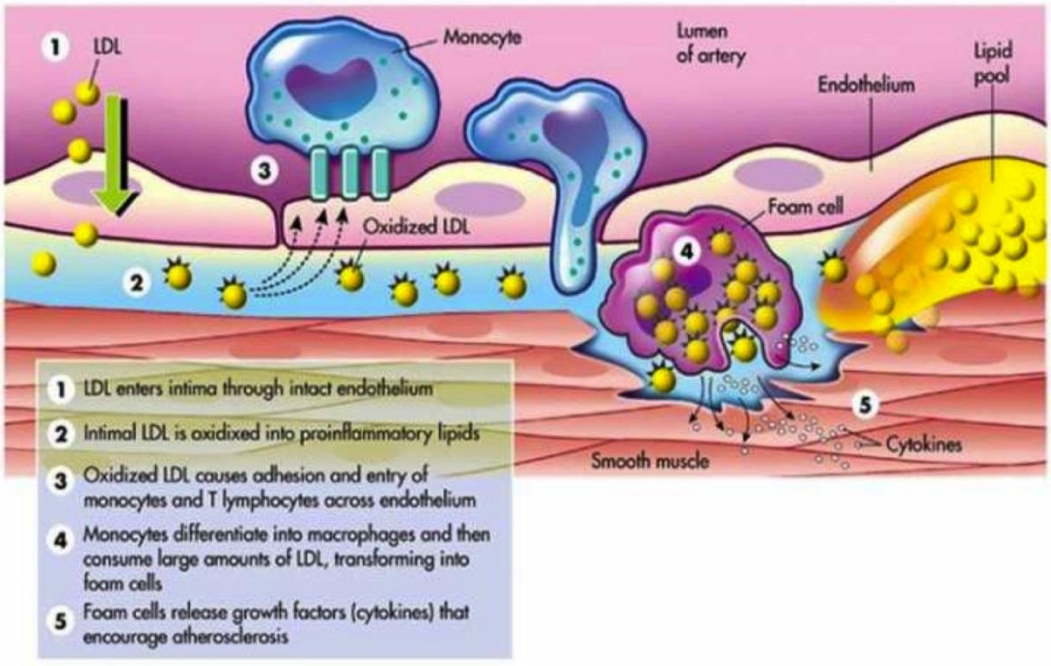

Figure 4: LDL participation in atherogenesis. Modified from Crawford et al., 2001, Cardiology.

oxygen species that turns MM-LDL, recognized by the LDL receptor (LDL-R) into highly oxidized LDL (oxLDL). OxLDL bind scavenger receptors (SRs) on the macrophages surface, triggering phagocytosis. When the macrophage elimination capacity is overwhelmed, cholesterol starts to accumulate as cholesteryl ester droplets in their cytosol, leading to the characteristic foam cell aspect (Figure 4, 4)[12]. Eventually the surcharge causes many of these cells to die, contributing to

the necrotic core of the plaque[13]. Interestingly, cholesterol-lowering therapies have proven efficient in reducing the occurrence of acute events in patients at risk[18,19], which accounts for the role of atherogenic lipoproteins in the end-stages of the pathology.

2.2.2 Reactive oxygen species

Reactive oxygen species (ROS) are oxygen-containing chemical compounds. Most abundant ROS are free oxygen radicals, oxygen ions and peroxides. They are usually formed as byproducts of the normal metabolism by mitochondrial electron transport chain and bear important roles in cell signaling and homeostasis.

In the vessel walls, additional enzymatic systems are involved, namely xanthine oxidase, a dysfunctional or uncoupled endothelial nitric oxide synthase (eNOS) and NADPH oxidase, which produces peroxydases and is able to activate the other two[20]. Under physiological conditions, ROS are involved in different signaling pathways and regulate an ensemble of functions such as vasodilatation/constriction, cell growth and proliferation, apoptosis, and inflammatory responses[21]. Furthermore, the presence of antioxidant enzymes such as superoxide dismutase, catalase, glutathione peroxidase, and paraoxonase, is meant to control the ROS production and prevent any harmful effect.

In the case of atherogenesis, vascular wall cells (EC, SMC) and infiltrating cells (monocytes, macrophages, lymphocytes, platelets), under the combined influence of hypercholesterolemia and inflammation, contribute to ROS production, overwhelming the ROS-detoxifying mechanisms, ultimately causing oxidative stress and leading to the oxidative modification of lipoproteins and phospholipids[20,22].

Global oxidative stress impairs the endoplasmic reticulum (ER) function, leading to improperly modified proteins that are thought to participate in the unfolded protein response (UPR) pathway. The UPR, through its role in inflammation and EC dysfunction, has been shown to contribute to all phases of atherosclerotic development[23,24].

2.2.3 Cytokines

The important number of cells involved in atherogenesis release as many cytokines with various effects, -non-exhaustively- summarized in Table 2. We will detail the role of some of them.

Table 2: Cytokines classification according to their role in atherogenesis. From Tousoulis et al., European Heart Journal, 2016. IL: interleukin, TNF: tumor necrosis factor, IFN: interferon, GM-CSF: granulocyte monocyte colony stimulating factor, MCP: monocyte chemoattractant protein, TGF: transforming growth factor.

Pro-atherogenic cytokines	**Disputed role**	**Anti-atherogenic cytokines**
IL-1β, IL-4, IL-6, IL-8, IL-12, IL-15, IL-18, IL-20, IL-21, IL-23, IL-32 TNFα, IFNα, IFNβ, IFNγ, GM-CSF, cyclophilin A, oncostatin M MCP-1	IL-2, IL-17	IL-5, IL-10, IL-13, IL-19, IL-27, IL-33, IL-35, IL-37 TGFβ

In the early stages of atherogenesis, activated endothelial cells express the monocyte-activating proteins MCP- 1 (CCL2), which interact with CCR2 receptors, leading to the recruitment of monocytes, and GM-CSF, triggering their proliferation and retention[12]. Monocytes recruitment and their differentiation into macrophages is a paramount process in atherogenesis.

TNFα and IL-1 signaling affects almost all cells involved in atherogenesis by promoting the expression of cytokines, adhesion molecules, and the migration and mitogenesis of vascular smooth muscle and endothelial cells. B lymphocytes bear a controversial role: early studies on LDLR-/- mice showed that depletion in all B cell subtypes increased atherosclerotic lesions; however, recent work by Kyaw et al.[25] and Ait-Oufella et al.[26] observed that B cell depletion by anti-CD20 monoclonal antibody reduced the atherosclerotic lesions. In a new study published this year, Tay et al. clarified the dispute by pointed out a proatherogenic role of the B2 lymphocytes subtype, which produces TNFα, a key cytokine in atherosclerosis development, particularly in unstable atherosclerotic lesions. B2 cells promoted atherosclerosis by augmenting TNFα production in lesion macrophages, increasing apoptosis and lesion inflammation, a phenomenon that also involved IL-1β and MCP-1 expression [27].

On the other hand, the immunomodulatory activity of regulatory T cells (see 2.3.1) is partly mediated by the secretion of anti-inflammatory and atheroprotective cytokines including TGF-β, IL-10 and IL-35. IL-10 alone appears to possess multiple anti-atherogenic properties, among which down-regulation of TNFα production [28].

2.2.4 MMPs

Matrix metalloproteinases are a family of enzymes involved in the remodeling of the extracellular matrix, secreted by SMCs, ECs, and macrophages. They can schematically be either atheroprotective, stabilizing the plaque by promoting smooth muscle cell migration and proliferation; or on the contrary, induce matrix destruction, angiogenesis, leucocyte infiltration, and apoptosis, favoring plaque rupture. Notably, an increased expression of MMP-1, -2, -3, -7, -8, -9, -12 and -13 in macrophages lining the lipid core, or in SMCs of the shoulder regions of plaques, have been linked to an augmented risk of rupture. For example, MMP9 produced by macrophages are overexpressed in vulnerable areas of plaques. A study enhancing this enzyme's expression was conducted in ApoE-/- mice, showing an increased plaque rupture[29]. Another class of proteinases, called cathepsins, have also been linked to atheroma destabilization. A mouse model deficient for this enzyme showed its role in the early leukocytes infiltration, degradation of the elastic lamina, endothelium invasion, neovascularization, and fibrous cap rupture[30].

2.3 Cellular actors

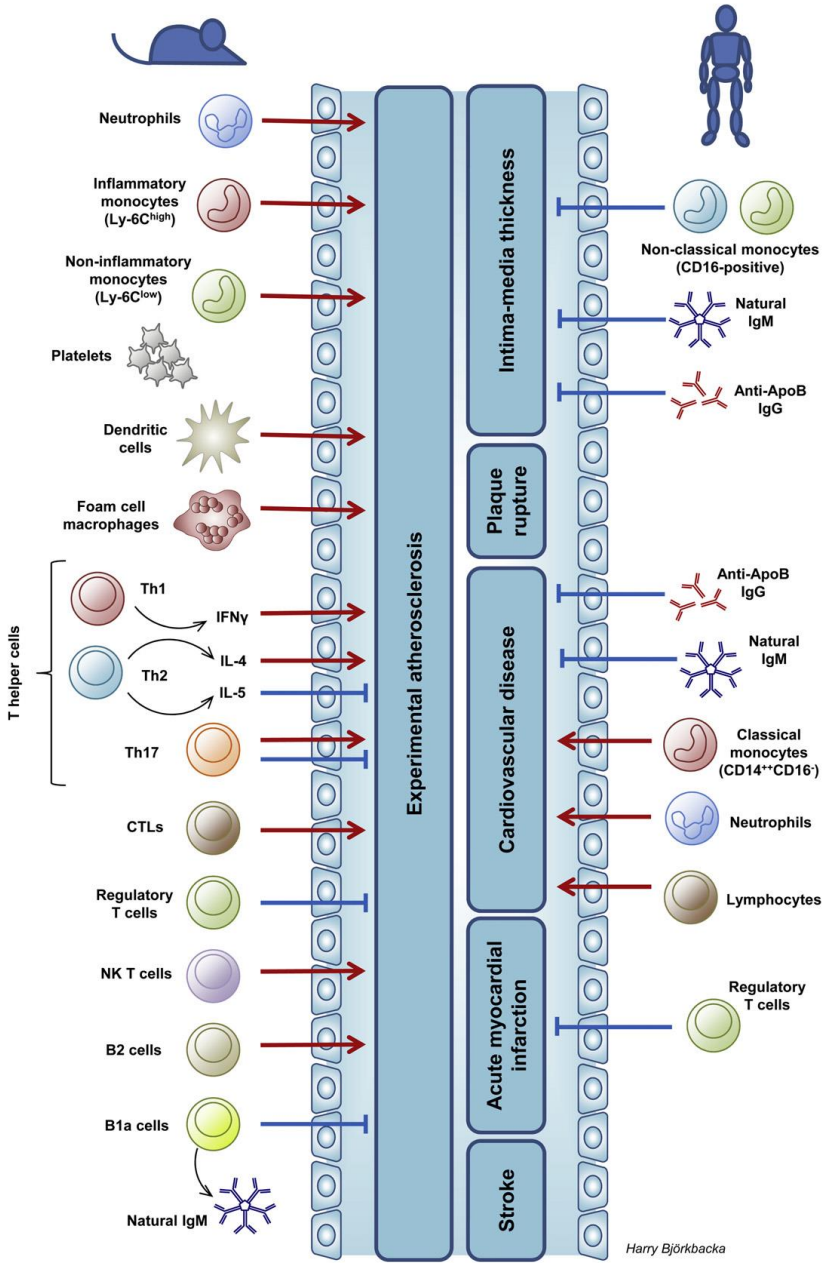

Figure 5: The role of different immune cell populations in experimental atherosclerosis in mice and in prediction of cardiovascular disease risk in humans. Red arrows indicate a role in facilitating atherosclerosis development in mice or positive association in humans. Blue arrows indicate an inhibition of atherosclerosis development in mice or negative association in humans. From Björkbacka et al., Atherosclerosis, 2013.

2.3.1 Immune cells

Inflammation is a recognized feature of atherogenesis involving both innate and adaptive immune cells[31], as shown by Figure 5. Recruitment of monocytes in the vascular wall, macrophage differentiation and proliferation represent a hallmark in the pathology of atherosclerotic lesions. They contribute to the processes that underlie atherogenesis such as

lipid accumulation, secretion of pro-inflammatory cytokines, and extracellular matrix remodeling.

The heterogeneity and complexity of the macrophage population have been recently pointed out, reflecting the diversity and complexity of the lesions microenvironment, the most extensively studied being M1 and M2 macrophages[32]. Lymphocytes Th1 and Th2 are also important contributors to the pathology and they interplay with the corresponding subsets of macrophages. M1 macrophages induced by LPS and IFNγ stimulation reflect the Th1 response of T cells, they express the pro-inflammatory cytokines IL-1β, IL-6, IL-8, IL-12, and TNFα; hence they are usually considered as pro-atherogenic. By contrast, M2 macrophages induced by IL-4 (M2a), immune complexes (M2b), or IL-13/IL-10 (M2c), largely reflect the Th2 response of T cells. They are considered anti-inflammatory and express IL-10, CD36, scavenger receptor-A and mannose receptor[33].

B lymphocytes also play a role depending on their different subtypes, and in atherosclerosis they accumulate both in the atherosclerotic intima and associated adventitia. Depletion of innate-like B cells (B1a cells) secreting natural antibodies was associated with an increase in arterial lesion area[34] whereas CD20-targeted B cells, and more recently anti-BAFF receptor depletion markedly reduced the progression of atherosclerosis in ApoE-/- and LDLR-/- mice, thus identifying conventional B2 cells as pro-atherogenic[35,36]. Moreover, the observation of activation and oligoclonal expansion of T cells has suggested the presence of inciting antigens that sustain T cell recruitment within coronary lesions[37]. Processes of B cell hypersomatic mutation, isotype switch, and affinity maturation have been described in tertiary lymphoid organs (TLO) in the coronary plaques investigated[37,38]. Thus, macrophages, T cells, and B cells appear as important contributors to the pathophysiology of atherosclerosis, being involved both in inflammatory and immune responses.

2.3.2 Non immune cells

Endothelial cells (EC) are a kind of epithelial cells that line the totality of the blood and lymphatic circulatory system. Beyond their role as an interface between blood (or lymph) and tissues, they bear multiple biological roles such as molecules filtration, hemostasis, leukocytes recruitment, hormonal signaling, and blood vessels tone (vasoconstriction/dilatation) in collaboration with vascular smooth muscle cells (SMC).

EC are in direct contact to blood-flow and able to sense variations in hemodynamic forces, to which they respond by modulating the liberation of vasoactive substances or on the long-term by regulating transcription pathways that adapt their phenotype[39]. It has been observed that early atherosclerotic lesions follow a nonrandom distribution pattern, leading to the hypothesis that they were linked to local variations in shear stress via biomechanically-activated transcription factors[40]. In a study by Parmar et al., the transcription factor Kruppel-like factor 2

(KLF2) was shown to be upregulated in areas with low hemodynamic stress and considered atheroprotected. On the contrary, decreasing its expression triggers a parallel decrease in eNOS expression levels, but induces a proinflammatory phenotype via IL-1β–dependent VCAM-1 and E-selectin expression, as well as a TNFα–dependent induction of tissue factor (TF) [41]; all features traditionally associated with atherogenesis.

Additionally, upon injury or inflammation, EC downregulate prostaglandins that prevent platelet activation and express molecules such as fibronectin, ICAM-1, P-selectin, E-selectin, integrin αIIbβ3 and vWF which promote platelet adhesion[42], leading to thrombosis.

EC also share a role with smooth muscle cells in LDL modifications through mechanisms involving generation of free radicals[14], transition metals[43], and the action of phospholipases[15].

Finally, vascular SMC, in addition to their role in intimal thickening (see 2.1), secrete proteoglycans, collagen and elastic fibers of the extracellular matrix, which participate in LDL retention as well as remodeling of the vascular wall[12].

2.3.3 Platelets

Platelets are small non-cellular elements of the blood, derived from the cytoplasmic fragmentation of megakaryocytes in the bone marrow. Although non-traditionally regarded as immune cells, platelets role is not limited to thrombus formation. Indeed, they were shown to bear pathogen recognition properties, to cross-talk and recruit leukocytes to infection sites, and to modulate inflammation[7].

In atherosclerosis their localization, as observed by Van Lammeren and colleagues, was mainly associated to intraplaque hemorrhages, leaky microvessels and mural thrombi. More surprisingly, platelets were also observed outside microvessels, mainly in the shoulder regions of the plaque, suggesting that extravasation of platelets can occur without erythrocytes leakage[44].

They are now recognized as key players in innate and adaptive immune responses[45,46]. They were notably shown to modulate the T-effector/T-reg balance via the CD40 ligand[47,48]. The CD40 ligand (CD40L) is a transmembrane molecule of crucial interest in cell signaling in innate and adaptive immunity. It is mainly expressed by activated T lymphocytes and platelets. Platelet-derived CD40L has also been reported to support B cell differentiation and immunoglobulin class switching in mice[49]. Additionally, several cytokines released by activated platelets have been demonstrated to modulate monocyte and macrophage function. Moreover platelet–leukocyte interactions largely contribute to oxLDL uptake and foam cell formation[50]. In a recent study, we underlined the presence of platelets not only in thrombi and intraplaque hemorrhage (IPH) but also in atheroma burden, around necrotic areas and neovessels, shedding light on the rationale for targeting platelets within atherosclerotic lesions[51].

2.4 Towards molecular markers

As a conclusion, atherosclerosis gradually develops and goes unnoticed for decades. All of the actors detailed above could serve as so many targets for specific, molecular imaging of the atheroma plaque and help improve the first diagnosis or secondary prevention. Given the right markers and assessment tools, many deaths could be avoided.

References

1. WHO | Cardiovascular diseases (CVDs). *WHO* Available at: http://www.who.int/entity/cardiovascular_diseases/en/index.html. (Accessed: 22nd August 2016)

2. Falk, E. Pathogenesis of Atherosclerosis. *J. Am. Coll. Cardiol.* **47,** C7–C12 (2006).

3. Go, A. S. *et al.* Heart Disease and Stroke Statistics—2014 Update. *Circulation* **129,** e28–e292 (2014).

4. Virmani, R., Kolodgie, F. D., Burke, A. P., Farb, A. & Schwartz, S. M. Lessons From Sudden Coronary Death A Comprehensive Morphological Classification Scheme for Atherosclerotic Lesions. *Arterioscler. Thromb. Vasc. Biol.* **20,** 1262–1275 (2000).

5. Stary, H. C. Natural History and Histological Classification of Atherosclerotic Lesions. *Arterioscler. Thromb. Vasc. Biol.* **20,** 1177–1178 (2000).

6. Insull Jr., W. The Pathology of Atherosclerosis: Plaque Development and Plaque Responses to Medical Treatment. *Am. J. Med.* **122,** S3–S14 (2009).

7. Nording, H. M., Seizer, P. & Langer, H. F. Platelets in Inflammation and Atherogenesis. *Front. Immunol.* **6,** (2015).

8. Kuijper, P. H. *et al.* Platelet-dependent primary hemostasis promotes selectin- and integrin-mediated neutrophil adhesion to damaged endothelium under flow conditions. *Blood* **87,** 3271–3281 (1996).

9. Page, C. & Pitchford, S. Neutrophil and platelet complexes and their relevance to neutrophil recruitment and activation. *Int. Immunopharmacol.* **17,** 1176–1184 (2013).

10. Kolodgie, F. D. *et al.* Intraplaque hemorrhage and progression of coronary atheroma. *N. Engl. J. Med.* **349,** 2316–2325 (2003).

11. Virmani, R. *et al.* Atherosclerotic plaque progression and vulnerability to rupture: angiogenesis as a source of intraplaque hemorrhage. *Arterioscler. Thromb. Vasc. Biol.* **25,** 2054–2061 (2005).

12. Navab, M. *et al.* The Yin and Yang of Oxidation in the Development of the Fatty Streak A Review Based on the 1994 George Lyman Duff Memorial Lecture. *Arterioscler. Thromb. Vasc. Biol.* **16,** 831–842 (1996).

13. Libby, P., Lichtman, A. H. & Hansson, G. K. Immune Effector Mechanisms Implicated in Atherosclerosis: From Mice to Humans. *Immunity* **38,** 1092–1104 (2013).

14. Morel, D. W., DiCorleto, P. E. & Chisolm, G. M. Endothelial and smooth muscle cells alter low density lipoprotein in vitro by free radical oxidation. *Arterioscler. Thromb. Vasc. Biol.* **4,** 357–364 (1984).

15. Steinbrecher, U. P., Parthasarathy, S., Leake, D. S., Witztum, J. L. & Steinberg, D. Modification of low density lipoprotein by endothelial cells involves lipid peroxidation and degradation of low density lipoprotein phospholipids. *Proc. Natl. Acad. Sci. U. S. A.* **81,** 3883–3887 (1984).

16. Cushing, S. D. *et al.* Minimally modified low density lipoprotein induces monocyte chemotactic protein 1 in human endothelial cells and smooth muscle cells. *Proc. Natl. Acad. Sci. U. S. A.* **87,** 5134–5138 (1990).

17. Vora, D. K. *et al.* Induction of P-Selectin by Oxidized Lipoproteins Separate Effects on Synthesis and Surface Expression. *Circ. Res.* **80,** 810–818 (1997).

18. Schwartz, G. G. Effects of Atorvastatin on Early Recurrent Ischemic Events in Acute Coronary Syndromes<SUBTITLE>The MIRACL Study: A Randomized Controlled Trial</SUBTITLE> *JAMA* **285,** 1711 (2001).

19. Group, H. P. S. C. MRC/BHF Heart Protection Study of cholesterol lowering with simvastatin in 20 536 high-risk individuals: a randomised placebocontrolled trial. *The Lancet* **360,** 7–22 (2002).

20. Li, H., Horke, S. & Förstermann, U. Vascular oxidative stress, nitric oxide and atherosclerosis. *Atherosclerosis* **237,** 208–219 (2014).

21. Zhang, D. X. & Gutterman, D. D. Mitochondrial reactive oxygen species-mediated signaling in endothelial cells. *Am. J. Physiol. - Heart Circ. Physiol.* **292,** H2023–H2031 (2007).

22. Madamanchi, N. R., Vendrov, A. & Runge, M. S. Oxidative Stress and Vascular Disease. *Arterioscler. Thromb. Vasc. Biol.* **25,** 29–38 (2005).

23. Zhou, J., Lhoták, Š., Hilditch, B. A. & Austin, R. C. Activation of the Unfolded Protein Response Occurs at All Stages of Atherosclerotic Lesion Development in Apolipoprotein E–Deficient Mice. *Circulation* **111,** 1814–1821 (2005).

24. Gargalovic, P. S. *et al.* The Unfolded Protein Response Is an Important Regulator of Inflammatory Genes in Endothelial Cells. *Arterioscler. Thromb. Vasc. Biol.* **26,** 2490–2496 (2006).

25. Kyaw, T. *et al.* Conventional B2 B cell depletion ameliorates whereas its adoptive transfer aggravates atherosclerosis. *J. Immunol. Baltim. Md 1950* **185,** 4410–4419 (2010).

26. Ait-Oufella, H. *et al.* B cell depletion reduces the development of atherosclerosis in mice. *J. Exp. Med.* **207,** 1579–1587 (2010).

27. Tay, C. *et al.* B cell-specific depletion of TNFα inhibits atherosclerosis development and plaque vulnerability to rupture by reducing cell death and inflammation. *Cardiovasc. Res.* cvw186 (2016). doi:10.1093/cvr/cvw186

28. Tousoulis, D., Oikonomou, E., Economou, E. K., Crea, F. & Kaski, J. C. Inflammatory cytokines in atherosclerosis: current therapeutic approaches. *Eur. Heart J.* ehv759 (2016). doi:10.1093/eurheartj/ehv759

29. Gough, P. J. Macrophage expression of active MMP-9 induces acute plaque disruption in apoE-deficient mice. *J. Clin. Invest.* **116,** 59–69 (2005).

30. Liu, J. *et al.* Lysosomal Cysteine Proteases in Atherosclerosis. *Arterioscler. Thromb. Vasc. Biol.* **24,** 1359–1366 (2004).

31. Weber, C., Zernecke, A. & Libby, P. The multifaceted contributions of leukocyte subsets to atherosclerosis: lessons from mouse models. *Nat. Rev. Immunol.* **8,** 802–815 (2008).

32. Fenyo, I. M. & Gafencu, A. V. The involvement of the monocytes/macrophages in chronic inflammation associated with atherosclerosis. *Immunobiology* **218,** 1376–1384 (2013).

33. Mantovani, A., Garlanda, C. & Locati, M. Macrophage diversity and polarization in atherosclerosis: a question of balance. *Arterioscler. Thromb. Vasc. Biol.* **29,** 1419–1423 (2009).

34. Kyaw, T. *et al.* B1a B lymphocytes are atheroprotective by secreting natural IgM that increases IgM deposits and reduces necrotic cores in atherosclerotic lesions. *Circ. Res.* **109,** 830–840 (2011).

35. Kyaw, T. *et al.* Depletion of B2 but Not B1a B Cells in BAFF Receptor-Deficient ApoE −/− Mice Attenuates Atherosclerosis by Potently Ameliorating Arterial Inflammation. *PLOS ONE* **7,** e29371 (2012).

36. Kyaw, T. *et al.* BAFF Receptor mAb Treatment Ameliorates Development and Progression of Atherosclerosis in Hyperlipidemic ApoE −/− Mice. *PLOS ONE* **8,** e60430 (2013).

37. Burioni, R. *et al.* Antigen-driven evolution of B lymphocytes in coronary atherosclerotic plaques. *J. Immunol. Baltim. Md 1950* **183,** 2537–2544 (2009).

38. Hamze, M. *et al.* Characterization of resident B cells of vascular walls in human atherosclerotic patients. *J. Immunol. Baltim. Md 1950* **191,** 3006–3016 (2013).

39. Davies, P. F. Flow-mediated endothelial mechanotransduction. *Physiol. Rev.* **75,** 519–560 (1995).

40. Gimbrone, M. A., Topper, J. N., Nagel, T., Anderson, K. R. & Garcia-Cardeña, G. Endothelial dysfunction, hemodynamic forces, and atherogenesis. *Ann. N. Y. Acad. Sci.* **902,** 230-239-240 (2000).

41. Parmar, K. M. *et al.* Integration of flow-dependent endothelial phenotypes by Kruppel-like factor 2. *J. Clin. Invest.* **116,** 49–58 (2006).

42. Linden, M. D. & Jackson, D. E. Platelets: Pleiotropic roles in atherogenesis and atherothrombosis. *Int. J. Biochem. Cell Biol.* **42,** 1762–1766 (2010).

43. Heinecke, J. W., Rosen, H. & Chait, A. Iron and copper promote modification of low density lipoprotein by human arterial smooth muscle cells in culture. *J. Clin. Invest.* **74,** 1890–1894 (1984).

44. van Lammeren, G. W. *et al.* Platelets enter atherosclerotic plaque via intraplaque microvascular leakage and intraplaque hemorrhage: A histopathological study in carotid plaques. *Atherosclerosis* **222,** 355–359 (2012).

45. Herter, J. M., Rossaint, J. & Zarbock, A. Platelets in inflammation and immunity. *J. Thromb. Haemost.* **12,** 1764–1775 (2014).

46. Morrell, C. N., Aggrey, A. A., Chapman, L. M. & Modjeski, K. L. Emerging roles for platelets as immune and inflammatory cells. *Blood* **123,** 2759–2767 (2014).

47. Lievens, D. *et al.* Platelet CD40L mediates thrombotic and inflammatory processes in atherosclerosis. *Blood* **116,** 4317–4327 (2010).

48. Ferdous, F. & Scott, T. A comparative examination of thrombocyte/platelet immunity. *Immunol. Lett.* **163,** 32–39 (2015).

49. Aloui, C. *et al.* The signaling role of CD40 ligand in platelet biology and in platelet component transfusion. *Int. J. Mol. Sci.* **15,** 22342–22364 (2014).

50. Badrnya, S. *et al.* Platelets mediate oxidized low-density lipoprotein-induced monocyte extravasation and foam cell formation. *Arterioscler. Thromb. Vasc. Biol.* **34,** 571–580 (2014).

51. Jacobin-Valat, M.-J. *et al.* Nanoparticles functionalised with an anti-platelet human antibody for in vivo detection of atherosclerotic plaque by magnetic resonance imaging. *Nanomedicine Nanotechnol. Biol. Med.* **11,** 927–937 (2015).

3 Atheroma imaging

3.1 Intravascular imaging

Intravascular imaging contributed to the understanding of atherosclerosis in humans and to the translation of novel therapies to the clinic [1]. These imaging modalities involve the introduction in the arteries of an intra-vascular catheter and are usually used to access: the plaque burden, the fibrous cap, the coronary remodeling and/or necrotic core rich plaques. These technics require that the patients be anticoagulated, typically with heparin, before inserting the guidewire into the coronary artery. Next to the risk linked with the surgery, only some parts of the vascular tree are accessible by these techniques and only patients at high risk, usually those with a first ischemic episode, are followed-up using this kind of imaging.

3.1.1 X-ray angiography

X-ray angiography consists in introducing a catheter via a peripheral artery to inject a radio-opaque contrast media, such as iodine-based contrast agent, under X-ray monitoring. This modality remains a reference to determine the severity of coronary luminal obstruction [2] and is particularly useful to monitor revascularization. Although this latter operation effectively relieves ischemia, it has proved disappointing in preventing myocardial infarction or prolonging life [3]. In addition, this imaging method only gives information about luminal stenosis, and two thirds of acute coronary events are a result of angiographically insignificant atherosclerotic lesions, mostly due to outward remodeling [4].

3.1.2 Intravascular ultrasound

Intravascular ultrasound (IVUS) was one of the first techniques used to assess the morphological features of plaque and, to a lesser extent, its composition [5]. IVUS is an echography method that uses differential sound waves reflection to display a live image. As an ultrasound pulse encounters a boundary between two tissues the beam will be partially reflected depending on the different mechanical properties of both media. The intensity of the backscatter signal is processed into gray scale with a spatial resolution of 100-200 µm, although by tuning transducer frequency, better resolutions of down to 40 µm have been achieved[6]. Its unmatched penetration depth (4–8 mm) compared to other intravascular methods makes it a good tool to determine artery wall morphology [7], plaque volume [8] and calcification [9]. In that sense, IVUS is superior to X-ray angiography in diagnosing dissections, determining the extent of arterial stenosis, and is commonly used during angioplasty to guide stent deployment. However, because of its limited spatial resolution, IVUS is insufficient to decipher fine plaque morphology, e.g. thin fibrous cap atheroma (TFCA). Furthermore, the IVUS gray scale signal does not allow for accurately discriminating the elements of plaque composition because their relationship with the original acoustic signal is distorted during the scan conversion process [10]. Nevertheless,

the analysis of the IVUS acoustic signal before demodulation and scan conversion, called IVUS-radiofrequency (RF) analysis, can overcome some of the limitations inherent to conventional gray-scale IVUS imaging [11]. Indeed, this data analysis method is supposedly more directly related to the interaction of ultrasound with the tissue. Another feature called elastography consists in measuring the local rate of plaque deformation in response to the pulsating force of blood pressure to assess vessel wall and plaque characteristics [12]. TFCA being stiffer than lipid-rich plaques, such ultrasound based technic holds considerable promise for the identification of vulnerable plaques.

3.1.3 Optical coherence tomography

The development of optical coherence tomography (OCT) technology was originally published by Fujimoto and his team at the MIT in 1991 [13]. Its underlying concept is close to this of ultrasonography, except that it uses light waves instead of sound. Because light propagates at high speed, the time-delay in tissue-reflected light is measured using low-coherence interferometry[14]. Near-infrared light reflects from the interfaces and backscattering sites of a sample, allowing the reconstruction, from multiple longitudinal scans at a series of lateral locations, a two-dimensional image of the surface hit by the beam [15]. OCT has a medium penetration depth of 2-3 mm and a resolution of 10 µm, provided a contrast flush of saline solution is used to clear the blood column and allow a transparent path for the light beam. Its usefulness for atheroma imaging was demonstrated *in vitro* in 1996 by the same team [16]. High resolution and high contrast between tissue constituents allowed for both the assessment of structural details and the ability to penetrate heavily calcified tissue, making OCT a promising tool for intravascular diagnostics [17,18] although its limited penetration provide less information on plaque volume. Additionally, absorption of light being strongly dependent on molecular composition, OCT imaging could collect spectroscopic properties of tissues and enhance the gathered data [16]. In clinic, this method is able to distinguish TFCA plaques [19], which is a paramount feature consistent with the risk of rupture [20].

Next to the discovery of new targets for molecular imaging of atherosclerosis [21], the utility of OCT should be further improved by combining enhanced light scattering OCT, contrast agents [22,23] and targeting particles. E.g. the first trails published by Jefferson et al.[24] who recently designed a molecular probe consisting of iron oxide particles functionalized with anti-human monoclonal antibodies against VCAM-1, and E-selectin. The probe was able to bind cultured EC under physiological flow conditions.

3.1.4 Hybrid intravascular imaging

Lately, hybrid intravascular imaging catheters have been developed that take advantage of the association of two imaging modalities to balance each other's drawbacks.

For example, a bimodal imaging catheter has been developed by the teams of Jaffer and Tearney, in Boston, that combines OCT and near-infrared fluorescence (NIRF) imaging. Its usefulness was demonstrated in vivo in a rabbit model of atherosclerosis and ex vivo on cadaveric human coronary artery[25].

Recently, it was used to analyze the distribution of plaque near-infrared autofluorescence (NIRAF) signal with respect to OCT-delineated plaque morphological features[26]. The study found that coronary arterial NIRAF intensity was elevated focally in plaques with a high-risk morphological phenotype. This new setting was able to distinguish fibroatheroma, plaque rupture, and fibroatheroma associated with in-stent restenosis. It also demonstrated the feasibility and safety of this approach for intra-coronary imaging in humans.

In further experiments, a NIRF marker specific for certain plaque features, i.e. inflammation, or MMP activity was injected and the signal combined with newly-developed high-resolution OCT anatomical information was collected, allowing for high resolution molecular imaging (communication, G.J. Tearney, 2016).

3.2 Non-invasive imaging

Because they are less risky than the above and don't require a hospitalization, non-invasive methods would allow for systematic risk assessment in larger groups of patients, based on their hazard ratio, to improve the prevention of acute cardio-vascular events and deaths. To match from the outside the level of information collected on the inside, sufficient resolution images are needed. Two main modalities have been able to –at least partially- fulfill these expectations. Magnetic resonance imaging (MRI) and nuclear imaging have lately been used to evaluate atherosclerosis *in vivo*. Main characteristics of the different technics are summarized in Table 3.

Table 3: Comparison of Imaging Modalities. Modified from: Krishnan, 2010, IEEE Transactions on Magnetics

	Radiation used	Spatial Resolution	Temporal Resolution	Sensitivity	Quantity of Contrast Agent used	Summary / Comments
Positron Emission Tomography	High-energy γ – rays	1-2 mm	10 s to min	10^{-11} – 10^{-12} M	Nanograms	Sensitive Quantitative Needs Cyclotron
Single Photon Emission Tomography	Low-energy γ - rays	1-2 mm	min	10^{-10} – 10^{-11} M	Nanograms	Many available probes
Computed Tomography	X-rays	50-200 µm	min	Not well characterized	Not applicable	Good for bone, tumors, not for soft tissue
Magnetic Resonance Imaging	Radio waves	25-100 µm	min to hours	10^{-3} – 10^{-5} M	Micrograms to Nanograms	Highest resolution Morphological and functional imaging Low sensitivity, slow
Ultrasound Imaging	Ultrasound	250-500 µm	real time	Not well characterized	Micrograms to Nanograms	Quantitative Good sensitivity, Fast good resolution No tissue contrast

3.2.1 Ultrasound imaging

3.2.1.1 Principle

Explained in 3.1.2.

3.2.1.2 Atherosclerosis imaging

In its non-invasive, non-targeted modality, ultrasound imaging (US) main utility in atherosclerosis is the measurement of carotid intima-media thickening (IMT), predictable for future risk of ischemic coronary events and stroke in patients from middle-age and older. Trans-esophageal application of ultrasounds at the thoracic aorta level is also widely accepted to detect local atherosclerotic plaque [27].

Molecular imaging is allowed is this setting by coupling antibodies that recognize various molecular structures to microbubbles. Although presenting with a relatively unfavorable contrast-to-noise ratio, thrombi imaging has been achieved with platelet integrin GPIIb/IIIa or fibrin–targeted antibodies [28]. *In vitro* studies of microbubbles functionalized with both a monoclonal antibody to VCAM-1, MVCAM.A(429) and a synthetic polymeric sLex (PAA-sLex) with affinity to P-selectin, , perfused through flow chambers at physiologically relevant shear stresses have shown promises for molecular imaging of atherosclerotic plaques [29].

3.2.2 Near infrared fluorescence imaging

Near infrared fluorescence characterizes emission wavelengths between 650 nm and 1,000 nm. These high wavelength, low energy radiations present the advantages of an increased penetration depth due to limited tissue-photon absorption compared to lower wavelengths, and a reduced detected endogenous fluorescence. Altogether, this offers an improved signal-to-noise ratio, or target-to-background ratio.

A number of imaging modalities take advantage of these properties, notably fluorescent molecular tomography (FMT). Potential applications to atheroma imaging were demonstrated using the protease-activatable NIRF imaging agent Prosense750 (VisEn Medical)[30]. Other NIRF imaging agents currently in development were shown useful for the visualization of atheroma inflammation, calcification, and angiogenesis [31].

However promising, available contrast agents remain limited to pre-clinical research and will require regulatory approval, in addition to necessary developments in the imaging technology for its to be used in the clinics[14].

3.2.3 Nuclear imaging

3.2.3.1 Principle

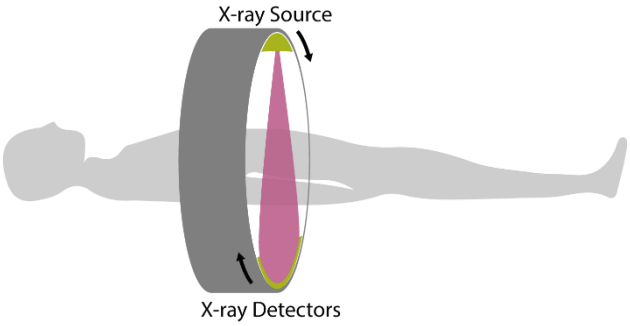

Schematic principle of CT scan

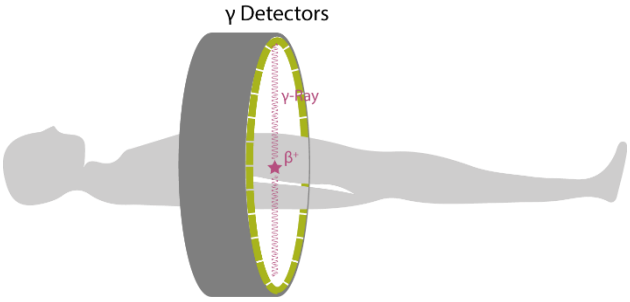

Schematic principle of PET scan

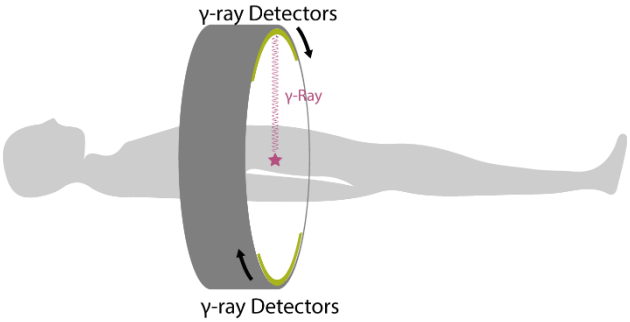

Schematic principle of SPECT scan

3.2.3.1.1 Computed tomography (CT)

CT is a radiographic method where a beam of X-rays is emitted by a source and collected by a detector placed at the opposite side of the X-rays source. The setting rotates around the area to be scanned, while the body moves through the machine to acquire data in all three directions. The attenuation of the X-ray beam as it moves through the tissues is a function of the atom density. Computed reconstruction of this 3D-collected data is used to produce tomographic images which are virtual "slices" rendering the attenuation properties of the scanned area. *In fine*, computed tomography is used to generate a 3D image from a large series of 2D

radiographic images taken around a single axis of rotation and showing a contrast based on tissue density differences.

3.2.3.1.2 Positron emission tomography

Positron emission tomography (PET) is based on the detection of two gamma radiations emitted in opposite directions following the annihilation of electrons from the imaged tissues with tracer-issued positrons. Its sensitivity and resolution are respectively in the picomolar and millimeter range.

3.2.3.1.3 Single photon emission computed tomography

In contrast with PET, tracers used in SPECT emit gamma radiations that are measured directly. Not unlike CT, a gamma camera acquires multiple 2D images from multiple angles and a computer is then used to yield a 3D data set through a tomographic reconstruction. This data set may be analyzed as thin slices along any chosen axis of the body. Although SPECT is 10 to 100 times less sensitive than PET due to lower photon statistic, it is quite useful owing to their lower cost than PET and the possibility of using multiple probes simultaneously. Photon "selection" by the collimator detector, if reducing the sensitivity, increases the spatial resolution to submillimeter range.

3.2.3.2 Application to atherosclerosis imaging

In cardio-vascular imaging, CT main application is in the assessment of coronary arteries plaque calcification, which predictive value is disputed [27]. A recent modality, contrast-enhanced multi-detector computed tomography (MDCT) may help characterize different components of atherosclerotic plaques (lipid-rich, fibrous and calcified plaques), although the overall lack of soft tissue contrast render localization tricky; in addition to the necessary radiation exposure, this make this modality unsuitable for non-symptomatic patients screening and follow-up [27]. It is however broadly used in combination with other methods such as PET or SPECT to associate the anatomic and metabolic information.

A passive targeting modality has used 18F-fluorodeoxyglucose (FDG) as a β^+-emitting analog of glucose for PET imaging. Upon internalization via glucose transporters, FDG undergoes phosphorylation by hexokinase to FDG-6-phosphate. However, differently from glucose-6-phosphate, FDG-6-phosphate does not undergo further metabolism and accumulates irreversibly in the cell in proportion to exogenous glucose utilization. This is of interest because vulnerable atherosclerotic plaques have been shown to accumulate more FDG than stable plaques by Rudd et al. in a clinic study [32]. They first showed that PET can be used to detect inflammatory atherosclerotic plaques, and subsequent studies confirmed the usefulness of FDG [33–35]. However, since FDG is accumulated by any metabolically active cell, concerns were raised

about its specificity. Additionally, coronary imaging with this agent is rendered tricky by the high glucose consumption, leading to FDG accumulation, in the myocardium[36].

Besides glucose uptake, numerous other metabolic and signaling pathways associated with plaque vulnerability have been targeted with nuclear imaging modalities. Some take advantage of the existence of natural ligands, relevant to a given feature of atherosclerosis to directly label them with radioelements and serve as a radiotracer. For example, monocyte recruitment is known as one of the early plaque development feature. As such, it was proposed to use ^{99m}Tc-labeled MCP-1 to monitor this process[37]. Radiotracer uptake correlated with a pathological macrophage infiltration within the plaque. In another study, ^{99m}Tc-labeled Annexin V was used to follow macrophage apoptosis[38], an important phenomenon in necrotic core build-up and rupture. Also prominent in fibrous cap erosion, matrix metalloproteinase (MMP) activity was studied by Fujimoto and colleagues [39] with a ^{99m}Tc-labeled MMP inhibitor. This broad MMP specific tracer allowed for the assessment of dietary modification and statin therapy efficiency on MMP activity.

The interest of macrophage targeting was also demonstrated by Hyafil et al.[40]. This team used the macrophage-specific iodine-based contrast agent N1177 (Nanoscan Imaging) in conjunction with the classical tracer ^{18}F-FDG. The intensity of enhancement detected in the aortic wall of atherosclerotic rabbits on CT scans strongly correlated with a high metabolic activity of ^{18}F-FDG PET, corresponding to an intense macrophage infiltration on immunohistological sections. Altogether, enhanced macrophage and metabolic activity are a good indicator of plaque risk of rupture.

Other studies used a radiolabeled RGD peptide to target the integrin αvβ3 expressed on platelets. ^{18}F-Galacto-RGD demonstrated specific uptake in atherosclerotic lesions of mouse aorta[41], and in stenotic lesions of patients scheduled for carotid endarterectomy[42]. Seo et al.[43] proposed a ^{64}Cu-labeled LyP-1 dendrimer able to detect activated macrophages-p32 protein and allowing to visualize atherosclerotic plaque in ApoE−/− mice with PET-CT. VCAM is another relevant target in the assessment of early atherosclerotic lesions: an ^{18}F-labeled peptide internalized by endothelial cells through VCAM-1–mediated binding permitted non-invasive PET-CT imaging of inflammatory atherosclerosis in ApoE-/- mice[44].

Finally, antibodies are targeting agents of choice and were proven useful for nuclear imaging of atherosclerosis. Torzewski and colleagues used oxidation-specific antibodies, labeled with ^{125}I, to assess oxidation and accumulation of LDL in lipid-rich atherosclerotic lesions, a known feature of plaque activity and unstability[45]. In another study, an antibody fragment targeting the ligand-induced binding sites (LIBS) of platelet glycoprotein IIb/IIIa was labeled with ^{18}F and used to detect carotid thrombi formation in ApoE-/- mice[46].

3.2.4 Magnetic resonance imaging

3.2.4.1 Principle

Magnetic resonance imaging (MRI) relies on the property of atoms nuclei, such as the single proton of the hydrogen atom, to behave like extremely small magnets (termed “spins”) that can, placed in a static magnetic field (B_0), absorb and reemit electromagnetic waves at a frequency proportional to B_0, called the Larmor frequency. MRI consists in mapping over space these nucleus resonances. Due to their natural abundance, hydrogen atoms from water and fatty molecules compose most of the signal contrast.

In more details, under the influence of a static B_0 (usually of 1.5T or 3T for clinical scanners), the spins are first excited thanks to radiofrequencies (electromagnetic waves) produced by an emission coil, and subsequently allowed to relax, thereby emitting radiofrequencies which are gathered by an emission coil, creating the MR signal (Figure 6).To construct an image the MR signal is encoded over space in phase and frequency thanks to magnetic gradients (30 to 45 mT/m) superimposed prior and during the RF reemission. In MRI, measured signal is determined by the pulse sequence applied in the NMR imaging procedure and, among other factors, depends on 1: the density of the nuclear spins associated with hydrogen atoms, so called proton density; 2: the spin-lattice relaxation time T_1 that reflects how fast the longitudinal magnetization returns to its equilibrium value; 3: the spin-spin relaxation time, also known as

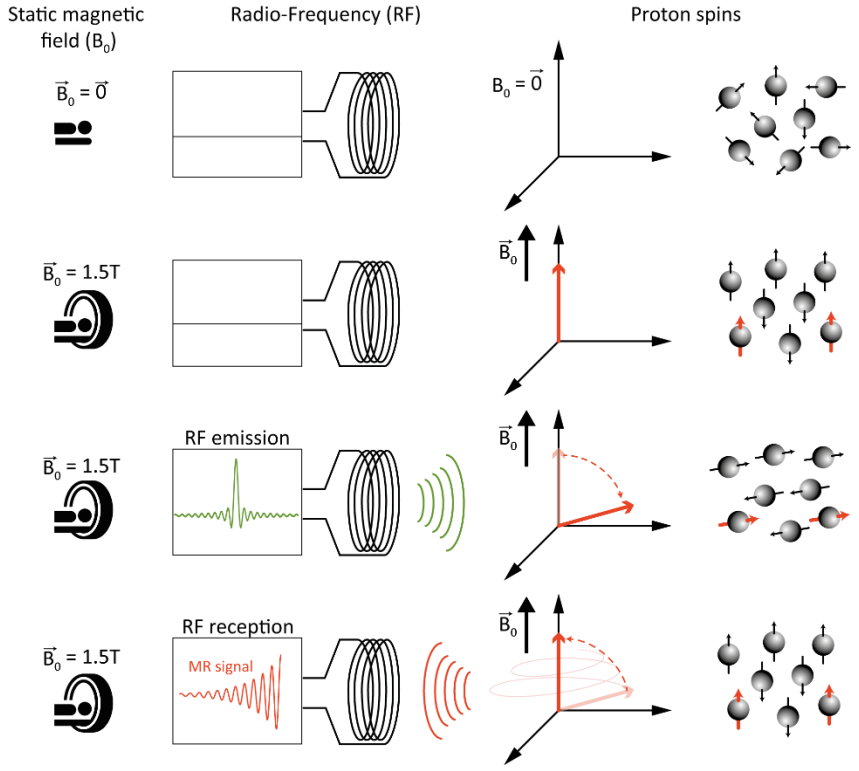

Figure 6: Principle of MR signal detection.

T_2, which represents the loss of coherence of the transverse magnetization. These properties are highly tissue-dependent, which allows by tuning the pulse sequence, for creating MR tissue contrasts, such as T_1- or T_2-weighted images.

3.2.4.2 Structural characterization of atherosclerotic plaque

MRI has demonstrated substantial potential in phenotyping vascular disease as it could be used to differentiate plaque components on the basis of biophysical and biochemical properties such as chemical composition, water content, physical state, molecular motion, or diffusion [47]. The greatest strength of MRI for characterizing atherosclerotic plaque is the availability of multi-contrast T_1-T_2 weighted protocols utilizing bright-blood, black-blood, and time-of-flight (TOF) techniques. While Bright blood sequences do not affect the blood signal, Black blood sequences rely on the elimination of the flowing blood signal and represent a general approach for characterizing the vessel wall. In an opposite manner, TOF sequences tend to minimize the signal of stationary tissues allowing for the visualization of the vascular lumen. As an example, Chu et al. [48] have developed a mapping method, called Morphology Enhanced Probability maPS (MEPPS), allowing for discriminating different plaque components thanks to the automatized combination of TOF images and black blood T_1/Contrast enhanced (CE) T_1/T_2 weighted images (Figure 7).

In clinical studies, the injection of gadolinium as a contrast agent have demonstrated differential

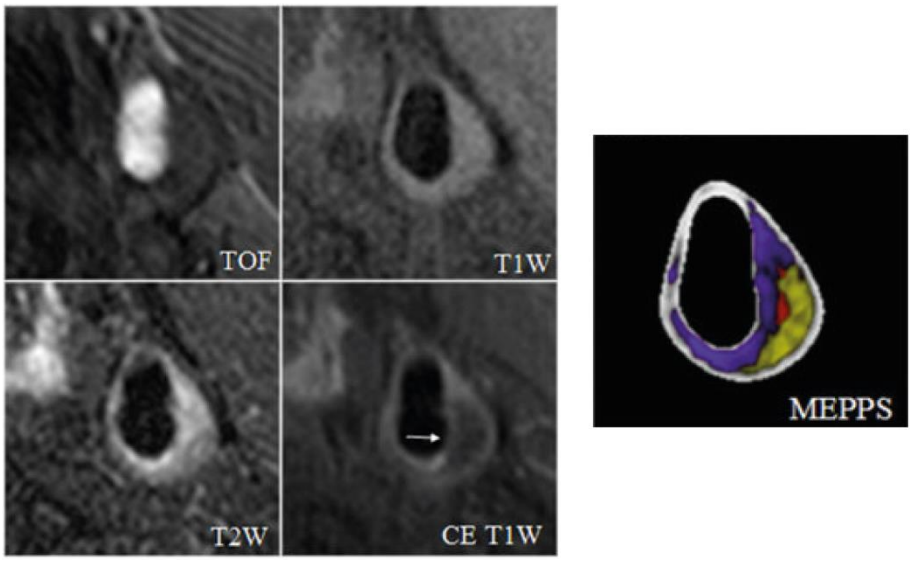

Figure 7: Structural characterization of atherosclerotic plaques by a combination of sequences. Time-of-flight (TOF), T1-weighted (T1W), T2-weighted (T2W), and contrast enhanced (by an injection of Gadolinium) T1-weighted (CE-T1W) MR images are combined to produce the automated Morphology Enhanced Probability maPS (MEPPS). Loose matrix is shown in purple, lipid-rich necrotic core in yellow, and intraplaque hemorrhage in red on the MEPPS image. From Chu et al., 2009, JACC. Cardiovascular imaging.

enhancement of carotid plaque tissues. Strong enhancement generally suggests an uptake within a highly permeable vascular structure and loose extracellular matrix. These features are usually markers of inflammation in the vascular wall[49]. The effects of a lipid-lowering therapy (atorvastatin) on plaque composition were assessed by MRI-based MEPPS method over a 3-years follow-up. Statistically significant plaque lipid depletion was observed in treated subjects compared to the placebo group, and plaque regression was observed in some cases[50].

Vascular MRI has high spatial, temporal, and soft-tissue contrast resolution. Particularly apt for investigating *in vivo* large vessels such as aorta, carotid and femoral arteries[51] yet cardiac and respiratory motion limit coronary imaging.

Here it should be pointed that, unlike CT examination, MRI provides imaging without ionizing radiation, rendering it suitable for repetitive/longitudinal clinical studies. In this context, Silvera et al. have demonstrated[52] the complementary value of MRI and PET for the evaluation of atherosclerotic plaque and a recent preclinical study showed the clear advantages of using

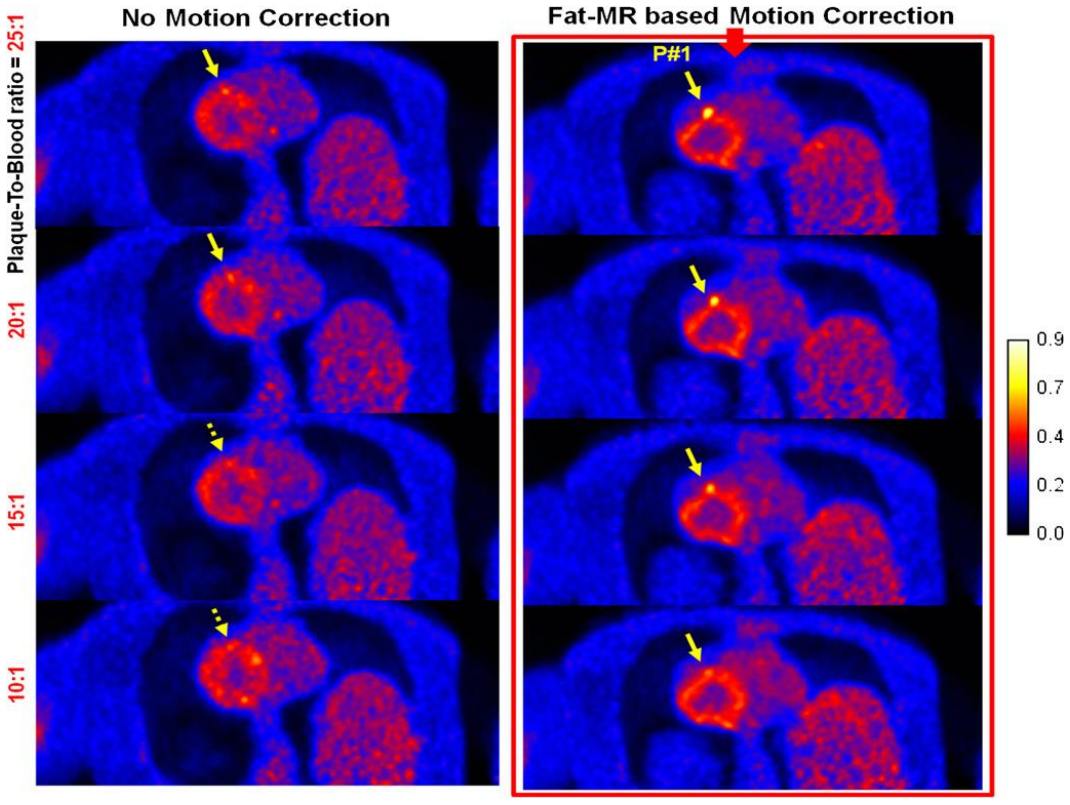

Figure 8: Contribution of PET/MRI to coronary atheroma imaging. PET slices reconstructed without (left), and with (right) fat-MR based motion correction. Each of the four frames corresponds to a different plaque radioactivity ratio (compared to blood activity level): 10, 15, 20 and 25, respectively, from the bottom to the top. The yellow arrows point to the plaque, in a coronary vessel (a heart ventricule is visible next to it in red). The fat-MR based motion correction significantly improves image reconstruction and plaque detection. From Petibon et al., 2014, Physics in Medicine and Biology.

simultaneous PET/MRI as compared to PET/CT or MRI alone[53]. In addition, dramatic improvement in terms of plaque detectability has been obtained using a motion correction technic allowed by PET and MRI simultaneous acquisitions[54] (Figure 8).

Beyond the mere structural characteristics of the atherosclerotic vessels, being able to image clinically relevant biological process of the pathology would allow deciphering between the plaque burden and its propensity to cause an acute cardio-vascular event.

3.2.4.3 Cellular and molecular atheroma targeting

As atherosclerosis is a complex pathological process, a wide variety of actors can be used to specifically image its underlying processes[21]. Some biological properties of the plaque components can be directly taken advantage of.

For example, considering the key role of intraplaque macrophages in atherosclerotic inflammation, numerous particles have been developed and tested in preclinical studies that take advantage of the phagocytic properties of these cells. Briley-Saebo et al.[55] have shown that dextran-based USPIOs (Feridex) with a diameter lower than 20 nm can be used to passively target intraplaque macrophages in atherosclerotic rabbits. They also corroborate the negative signal obtained using the T2w gradient echo acquisition with GRASP sequences able to generate positive signal enhancement (bright spot MR images) in areas containing USPIO (Figure 9).

A similar passive targeting was achieved in mice: cages of human ferritin protein, loaded with magnetite particles (diameter 6 nm)[56]; or FeCo/graphitic-carbon nanocrystals (diameter of 7nm) were used as negative contrast agents [57]. Although these studies were based on nanoparticles with a small hydrodynamic diameter, other teams have demonstrated that lipid-based

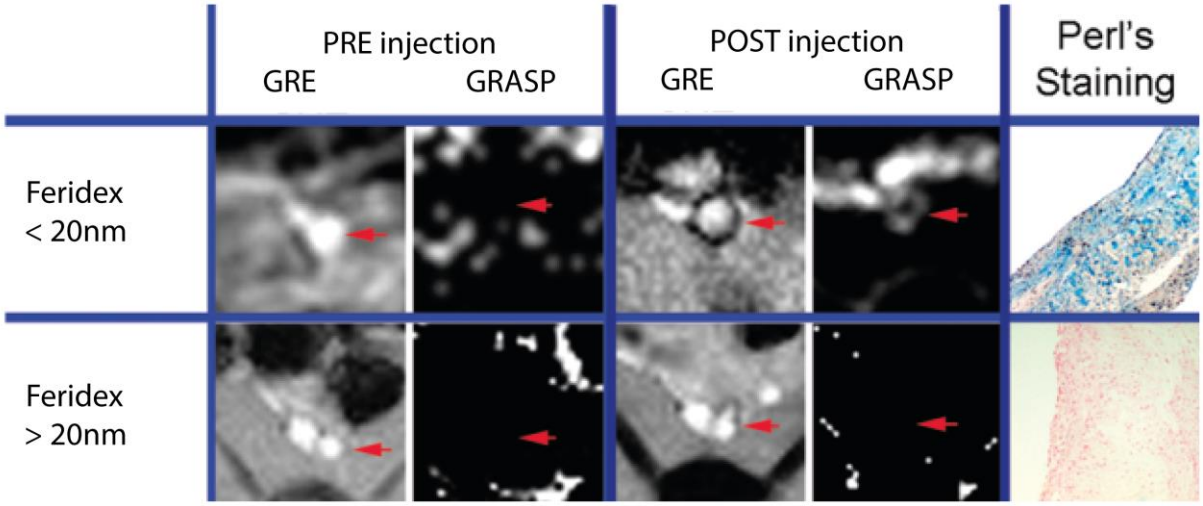

Figure 9: Passive macrophage targeting using Feridex nanoparticles. Representative T_2w gradient echo (GRE) and positive signal enhancement (GRASP images) of the rabbit aorta (red arrow) prior to and 24 h after bolus administration of fractionated Feridex (< 20 nm in diameter) or Feridex (> 20 nm in diameter) at 4.8 mg Fe/kg. From Briley-Saebo et al., 2008, Magnetic Resonance in Medicine.

formulations up to 200 nm in diameter were able to enter the plaque. Gadolinium-loaded micelles[58] as big as 106 nm, were able to pass through a 25 nm pore filter *in vitro*. In another study, Gd-liposomes with a diameter of 203 nm were used to demonstrate the importance of the nature of phospholipids on macrophage uptake *in vitro*[59]. Both these agents were able to label atherosclerotic plaques in ApoE-/- mice, suggesting the potential of lipid-based nanoparticles to bend or squeeze through the fenestrae of leaky endothelium observed in atheroma lesions. Finally, studies in human patients using passive macrophage targeting by USPIO particles (Sinerem, Guerbet) showed a preferential accumulation in rupture-prone or ruptured atherosclerotic lesions[60], and the possibility to monitor statin-driven reduction in plaque macrophage content[61].

Advances in atherosclerosis research have revealed a wide number of molecular targets and/or metabolic process for imaging purposes and consequently supported the development of targeted MR contrast agents[62,63]. Targeted compounds are produced by chemical attachment of a MR contrast agent, such as gadolinium chelates or superparamagnetic particles, to an affinity ligand: a compound capable of specific recognition and binding to a target site such as peptides, proteins, or antibodies.

Molecular imaging of early markers of atherogenesis, including endothelial cell adhesion molecules, such as P- and E-selectin, vascular cell adhesion molecule-1 (VCAM-1) and intercellular adhesion molecule-1 (ICAM-1), has been at the forefront, because the upregulation of these molecules is a sign of an early event.

Vascular cell adhesion molecule (VCAM)-1 is expressed and upregulated endothelial cells but also on macrophages, and smooth muscle cells within atherosclerotic plaques. Based on this fact, Michalska et al.[64] have developed USPIOs (diameter ≈26 nm) conjugated to a cyclic peptide specifically recognizing VCAM-1 and demonstrated their capability to visualize atherosclerotic plaques thanks to MRI with ultra high magnetic field (17.6 T).

Fibrin as a molecular target has also been at the center of attention, and several generations of anti-fibrin probes were developed to image preclinical small and large animal models of carotid artery[65], coronary artery[66], atrial[67], and cerebral venous sinus thrombosis [68]. Makowski et al.[69] propose the use of a well-established gadolinium-based fibrin-binding contrast agent, FTCA (EP-2104R, EPIX Pharmaceuticals) to provide positive contrast enhancement of fibrin on the surface and in necrotic cores within the atheroma plaque where fibrin is highly represented. The same

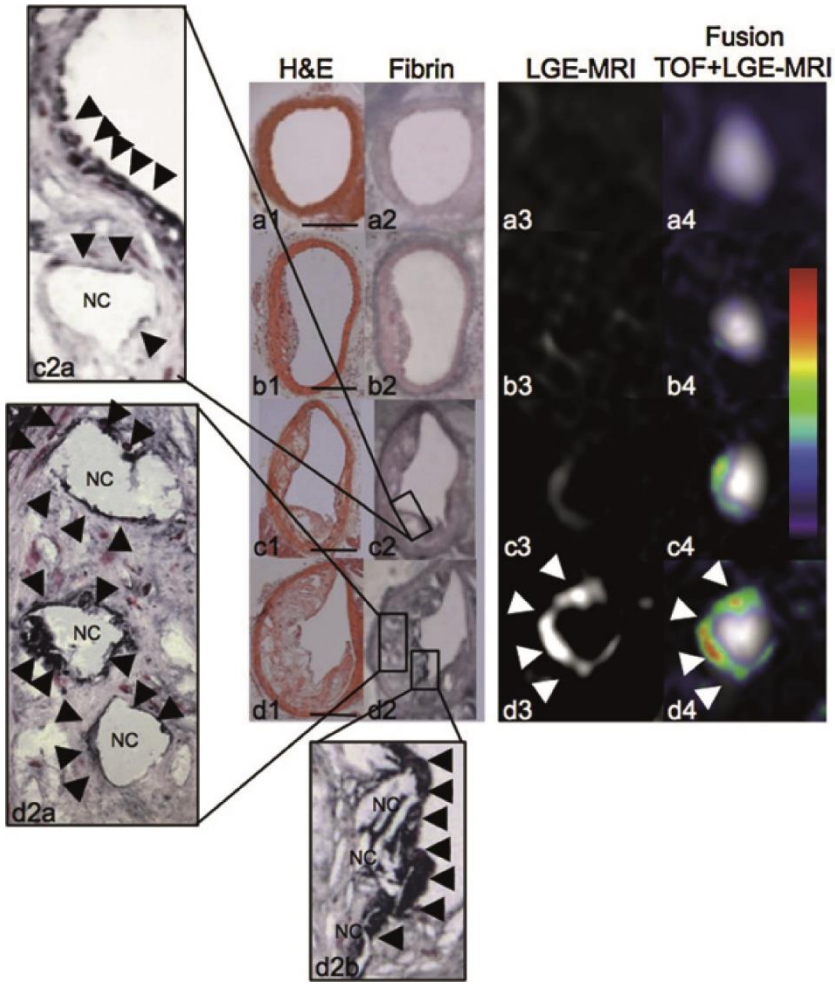

Figure 10: In vivo imaging after administration of Gd-FTCA and ex vivo immunohistochemistry/immunoblotting using a fibrin specific antibody: MRI was performed on the brachiocephalic artery of ApoE$^{-/-}$ mice fed a high fat diet (HFD) at one (b), two (c) and three (d) months, (a) control WT mice, prior to and 90 min after the administration of FTCA. Corresponding sections from histology (H and E stain (1), fibrin stain (2)) and late gadolinium enhancement (LGE)-MRI images after the administration of Gd-FTCA (3) fused with TOF images (4). A significant increase in vessel wall enhancement on LGE-MRI can be observed in the lateral part of the vessel wall (d3 and d4, white arrowheads) corresponding to increased fibrin deposition in atherosclerotic plaque after 3 months of HFD. Positive fibrin staining was associated with the necrotic core (Ac2a, Ad2a and b, black arrowheads) and endothelium (Ac2a, Ad2b, black arrowheads) NC: necrotic core. In vivo MRI measurements were in good agreement with ex vivo fibrin density measurements on immunohistological sections stained with a fibrin-specific antibody. From Makowski et al., 2012, Atherosclerosis.

agent was tested in humans for the molecular MR imaging of intracardiac thrombi[70], offering a tool for imaging thrombi potentially responsible for strokes. This emphasizes the opportunity to target fibrin at all atherogenesis steps, from early atherosclerosis imaging to rupture and luminal thrombosis. It highlights the potential value of FTCA in in vivo fibrin imaging during the course of plaque development, even before luminal thrombus formation [71] (Figure 10).

Besides their passive targeting using iron-oxide based nanoparticles, other macrophages targeting agents were constructed from physiologic ligands to provide both imaging and therapeutic modalities. A Gd-labeled statin-loaded reconstituted High-Density Lipoprotein (rHDL) nanoparticle, that facilitates the delivery of statins to atherosclerotic plaque, have been followed up over 12 weeks using typical T1-weighted MR images of the abdominal aortas of

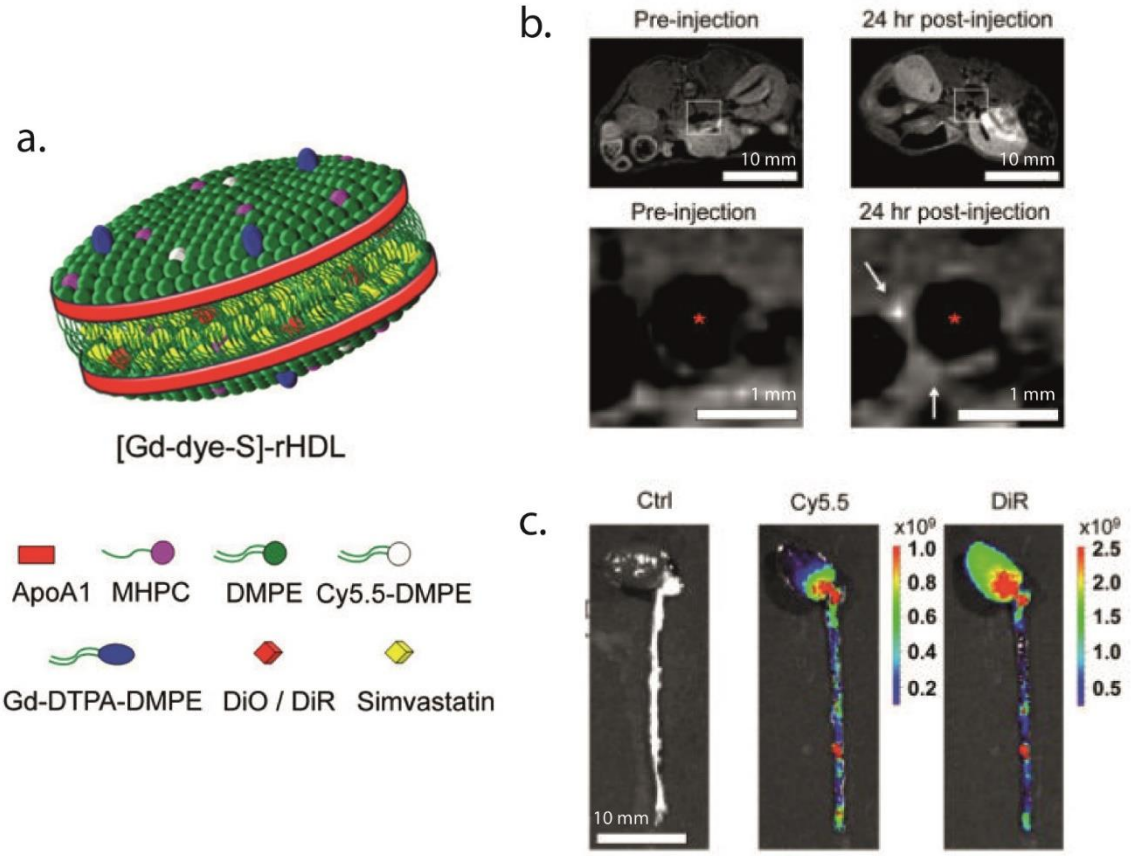

*Figure 11: (a) Schematic representation of dual gadolinium and fluorescent dye (Cy5.5, DiO, DiR) labeled statin-containing reconstituted high density lipoprotein ([Gd-dye-S]-rHDL); (b) Typical T1-weighted images of the abdominal aorta of an ApoE-/- mouse before and 24 hours after injection of [Gd-Dye-S]-rHDL. The lumen is indicated by *.The 24h post-injection image shows signal enhancement in the vessel wall (white arrows), indicative of nanoparticle infiltration and retention in the aortic plaques. (c) [S]-rHDL labeled with Cy5.5 (lipid monolayer) and DiR (hydrophobic core) was intravenously injected to ApoE-/- mice. NIRF shows that Cy5.5 and DiR preferentially accumulate in the areas rich with atherosclerotic lesions. From Duivenvoorden et al., 2014, Nature communications.*

mice[72] (Figure 11). In this study, ApoA1 lipoproteins, which structure the rHDL (see Figure 11, a), were used as targeting moieties to deliver the statin cargo into the plaque. However, ApoA1 is not specific to the macrophages colonizing the atheroma plaque. Thus, the key to bypassing liver accumulation and hepatotoxicity [73] relies on HDL functionalization with specific ligands in order to drive the nanocarrier to the site of interest.

Platelets have also been targeted using naturally-occuring ligands: the sulfated polysaccharide fucoidan presents a high affinity for P-selectin, a cell adhesion molecule highly expressed on the surface of activated platelets. In a recent study, Suzuki et al.[74] developed USPIO particles coated with fucoidan, and showed that MRI can detect platelet-rich thrombi from 15 min after injection, with a high spatial resolution, in a rat elastase aneurysm model. This could be of great interest for a fast and efficient detection of unstable plaques in clinics.

As presented before, antibodies are highly specific and affine ligands that can be used for the detection of cellular or molecular markers of atherogenesis and lesions evolution. A number of team have developed antibody-conjugated MR contrast agents, which should theoretically be able to reach their targets and accumulate at much higher concentrations on the site of injury than if the MR contrast agents were administered in free form. Logically, many studies have been devoted to the assessment of these potentially valuable tools for the noninvasive detection and monitoring of atherosclerosis using MRI.

As previously underlined, monocyte recruitment into vascular tissues is promoted by the overexpression of adhesion molecules, such as vascular cell adhesion molecule-1 (VCAM-1; CD106), intercellular adhesion molecule-1 (ICAM-1), E-selectin (CD62E), and P-selectin (CD62P), on the activated endothelium. The monocyte endothelial binding mechanism represents an opportunity to exploit both cell adhesion molecules and selectins on the activated endothelium as targets to directly report arterial endothelial activation and inflammation[75]. In a study by Paulis et al., a paramagnetic Gd-liposome (100 nm) contrast agent was functionalized with an Ab targeting ICAM-1. Its ability to bind endothelial cells relied on their ICAM-1-expression level in vitro, and was retained under physiological flow conditions. This contrast agent, presenting high longitudinal and transversal relaxivities should allow for a good contrast between inflamed and resting endothelial cells, even in the challenging environment encountered in the circulation[76]. Another strategy was to use a dual targeting against E-selectin and VCAM-1. Antibody-conjugated superparamagnetic particles of iron oxide (SPIO) were able to render activated arterial endothelium MR visible ex vivo in human carotid plaques. In this setting, symptomatic carotid plaques could be discriminated from asymptomatic ones based on the degree of inflammation[77]. Recent evidence suggests that endothelial CD81 (TAPA-1) is specifically upregulated in the endothelium of atherosclerotic plaques in human arteries[78]. Yan

et al. [79] proved the feasibility of using CD81-targeted microparticles (4.5 μm diameter) of iron oxide (CD81-MPIO) for magnetic resonance imaging in a murine atherosclerosis model *ex vivo*.

Another valuable target for atherosclerosis burden evaluation are leukocytes. Besides the possibilities of passive macrophage uptake described earlier, some authors have proposed molecular targeting of these actors using antibodies. In 2007, Amirbekian et al. assessed the ability of macrophage scavenger receptor (MSR, CD204)-targeted micelles to detect macrophages in atherosclerotic plaque by MRI *in vivo* in ApoE-/- mice. Immunomicelles (size = 107 nm) were loaded with Gadolinium which provided, 24h after their injection, an average aortic MRI signal enhancement of 79% compared to 34% when using untargeted micelles[80]. CD163 is also a typical marker of anti-inflammatory M2 macrophages subtype, which has been described at sites of inflammation, in association with hemorrhage or asymptomatic plaques, but not in healthy aortas. Using gold-coated iron oxide nanoparticles functionalized with an anti-CD163 murine anti-human antibody, Tarin et al. first demonstrated its specific binding to CD163+ macrophages only. Upon *in vivo* injection in ApoE-/- mice, a MR signal decrease was observed in the abdominal aorta that was maximal between 24 and 48 hours after injection[81]. Inflammation-associated myeloid-related protein 8/14 (Mrp-8/14) is another interesting target since it was shown to colocalize with rupture prone areas of plaque, in animal and human studies, typically with large necrotic cores and high macrophage content. Mrp-8/14-targeted Gd-containing liposomes (83 nm), injected to ApoE-/- mice were able to enter the plaque and be detected using T_1w weighted MR sequences. The signal enhancement at the abdominal aorta level was 5 fold superior to this of control muscle[82].

Activated platelets can be found in plaques at early asymptomatic inflammation stages (Jacobin-Valat et al, Nanomedicine), and during arterial thrombus formation after plaque rupture [83,84]; as such they represent a broad and valuable marker of atherosclerosis development. Platelet and endothelial P-selectin are both critical in the promotion of monocyte internalization, leading to plaque development. Consequently, Jacobin-Valat et al. developed versatile USPIO (VUSPIO) particles, labeled with rhodamine and coupled to an anti-human P-selectin antibody (VH10)[85] which was evaluated *ex vivo* an *in vivo* in aortas from atherosclerotic ApoE-/- mice.

Finally, elements from the lesions microenvironment can be similarly targeted for molecular imaging. Gd micelles (23 nm in size) were functionalized with a commercial rat antibody targeting the Neutrophil gelatinase-associated lipocalin (NGAL). NGAL is an effector molecule of the innate immune system, which associates with MMP9 to enhance its activity. As such, it is a marker of high risk plaques, since MMP9 is involved in matrix erosion. This agent was assessed in ApoE-/- mice, and showed a maximum micelles uptake 72h after injection, after an early and unspecific was observed at 24h[86]. Therefore the authors suggested that care should be taken

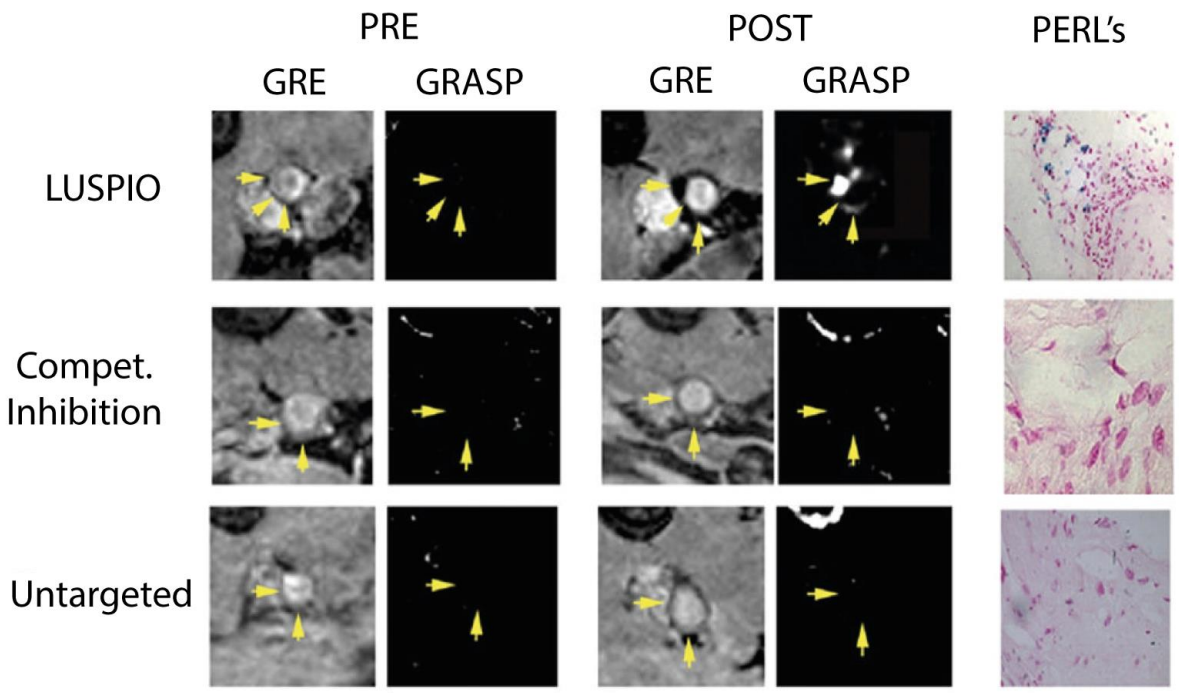

Figure 12: OxLDL epitopes targeting using lipid-coated ultrasmall iron oxide particles (LUSPIO). Representative magnetic resonance images obtained before (PRE) and 24 h after (POST) in vivo injection of a 3.9 mg Fe/kg dose in ApoE-/- mice. The yellow arrows indicate the position of the abdominal aorta lumen. Gradient echo (GRE) images were obtained with an echo time of 7 ms. Corresponding enhanced positive contrast (GRASP) images are also shown. Compet. Inhibition: ApoE-/- mice were administered unconjugated MDA2 antibody in excess before MDA2-labeled LUSPIO injection. Untargeted: untargeted LUSPIO were injected and imaged in the same conditions, as a control for irrelevant labelling. Matched histology sections stained with Perl's reagent (PERL's) show iron deposition (blue) within foam cells associated with the arterial wall. Modified from Briley-Saebo et al., 2011, JACC.

with respect to MRI timing, and carefully adapted for each nanoparticle-target combination, as well as confronted to a proper control with an irrelevant antibody.

Consecutively to their previous study [55], Briley-Saebo et al. have produced lipid-coated USPIOs (LUSPIO, size <20 nm), targeted to oxidized phospholipid (oxLDL) with human antibodies. If validated in humans, those should provide a valuable tool for atherosclerosis diagnosis[87].

As a conclusion, it should be pointed out that all antibodies used in these studies for functionalizing nanoparticles, micelles or liposomes, exception made of IK-17, an human anti-oxLDL Ab[87], are rodent antibodies specifically developed to recognize murine biomarkers. We would like to highlight that the originality of our project is linked to the human origin of the antibodies developed in-house that we used and thus to their potential for a **translational process from pre-clinical to clinical studies.** Two main advantages can indeed be pointed out: the inter-species cross-reactivity will theoretically allow a promising object to be tested in a variety of pre-clinical animal models or in human patients. Additionally, if the developed objects

were to reach the clinics, the use of human antibodies should limit the risk of immunogenicity, saving the time that would be required for humanization of murine antibodies.

References

1. Puri, R., Worthley, M. I. & Nicholls, S. J. Intravascular imaging of vulnerable coronary plaque: current and future concepts. *Nat. Rev. Cardiol.* **8,** 131–139 (2011).

2. Tarkin, J. M. *et al.* Imaging Atherosclerosis. *Circ. Res.* **118,** 750–769 (2016).

3. Taqueti, V. R. *et al.* Global Coronary Flow Reserve Is Associated With Adverse Cardiovascular Events Independently of Luminal Angiographic Severity and Modifies the Effect of Early RevascularizationCLINICAL PERSPECTIVE. *Circulation* **131,** 19–27 (2015).

4. Kaul, P. & Douglas, P. S. Atherosclerosis Imaging Prognostically Useful or Merely More of What We Know? *Circ. Cardiovasc. Imaging* **2,** 150–160 (2009).

5. DeMaria, A. N., Narula, J., Mahmud, E. & Tsimikas, S. Imaging Vulnerable Plaque by Ultrasound. *J. Am. Coll. Cardiol.* **47,** C32–C39 (2006).

6. Ma, T. *et al.* Multi-Frequency Intravascular Ultrasound (IVUS) Imaging. *IEEE Trans. Ultrason. Ferroelectr. Freq. Control* **62,** 97–107 (2015).

7. Yamagishi, M. *et al.* Morphology of vulnerable coronary plaque: insights from follow-up of patients examined by intravascular ultrasound before an acute coronary syndrome. *J. Am. Coll. Cardiol.* **35,** 106–111 (2000).

8. Kotani, J. *et al.* Intravascular Ultrasound Analysis of Infarct-Related and Non–Infarct-Related Arteries in Patients Who Presented With an Acute Myocardial Infarction. *Circulation* **107,** 2889–2893 (2003).

9. Ehara, S. *et al.* Spotty Calcification Typifies the Culprit Plaque in Patients With Acute Myocardial Infarction. *Circulation* **110,** 3424–3429 (2004).

10. Vancraeynest, D., Pasquet, A., Roelants, V., Gerber, B. L. & Vanoverschelde, J.-L. J. Imaging the Vulnerable Plaque. *J. Am. Coll. Cardiol.* **57,** 1961–1979 (2011).

11. Mehta, S. K., McCrary, J. R., Frutkin, A. D., Dolla, W. J. S. & Marso, S. P. Intravascular ultrasound radiofrequency analysis of coronary atherosclerosis: an emerging technology for the assessment of vulnerable plaque. *Eur. Heart J.* **28,** 1283–1288 (2007).

12. Schaar, J. A. *et al.* Current diagnostic modalities for vulnerable plaque detection. *Curr. Pharm. Des.* **13,** 995–1001 (2007).

13. Huang, D. *et al.* Optical Coherence Tomography. *Science* **254,** 1178–1181 (1991).

14. Suter, M. J. *et al.* Intravascular optical imaging technology for investigating the coronary artery. *JACC Cardiovasc. Imaging* **4,** 1022–1039 (2011).

15. Fercher, A. F., Drexler, W., Hitzenberger, C. K. & Lasser, T. Optical coherence tomography - principles and applications. *Rep. Prog. Phys.* **66,** 239 (2003).

16. Brezinski, M. E. *et al.* Optical Coherence Tomography for Optical Biopsy. *Circulation* **93,** 1206–1213 (1996).

17. Jang, I.-K. *et al.* Visualization of coronary atherosclerotic plaques in patients using optical coherence tomography: comparison with intravascular ultrasound. *J. Am. Coll. Cardiol.* **39,** 604–609 (2002).

18. van Soest, G. *et al.* Atherosclerotic tissue characterization in vivo by optical coherence tomography attenuation imaging. *J. Biomed. Opt.* **15,** 011105-011105-9 (2010).

19. Uemura, S. *et al.* Thin-cap fibroatheroma and microchannel findings in optical coherence tomography correlate with subsequent progression of coronary atheromatous plaques. *Eur. Heart J.* **33,** 78–85 (2012).

20. Insull Jr., W. The Pathology of Atherosclerosis: Plaque Development and Plaque Responses to Medical Treatment. *Am. J. Med.* **122,** S3–S14 (2009).

21. Quillard, T. & Libby, P. Molecular imaging of atherosclerosis for improving diagnostic and therapeutic development. *Circ. Res.* **111,** 231–244 (2012).

22. Zagaynova, E. V. *et al.* Contrasting properties of gold nanoparticles for optical coherence tomography: phantom, in vivo studies and Monte Carlo simulation. *Phys. Med. Biol.* **53,** 4995 (2008).

23. Kirillin, M. *et al.* Contrasting properties of gold nanoshells and titanium dioxide nanoparticles for optical coherence tomography imaging of skin: Monte Carlo simulations and in vivo study. *J. Biomed. Opt.* **14,** 021017-021017-11 (2009).

24. Jefferson, A. *et al.* Molecular imaging with optical coherence tomography using ligand-conjugated microparticles that detect activated endothelial cells: rational design through target quantification. *Atherosclerosis* **219,** 579–587 (2011).

25. Yoo, H. *et al.* Intra-arterial catheter for simultaneous microstructural and molecular imaging in vivo. *Nat. Med.* **17,** 1680–1684 (2011).

26. Ughi, G. J. *et al.* Clinical Characterization of Coronary Atherosclerosis With Dual-Modality OCT and Near-Infrared Autofluorescence Imaging. *JACC Cardiovasc. Imaging* (2016). doi:10.1016/j.jcmg.2015.11.020

27. Gallino, A. *et al.* 'In vivo' imaging of atherosclerosis. *Atherosclerosis* **224,** 25–36 (2012).

28. Kaur, S. *et al.* Recent trends in antibody-based oncologic imaging. *Cancer Lett.* **315,** 97–111 (2012).

29. Ferrante, E. A., Pickard, J. E., Rychak, J., Klibanov, A. & Ley, K. Dual targeting improves microbubble contrast agent adhesion to VCAM-1 and P-selectin under flow. *J. Control. Release Off. J. Control. Release Soc.* **140,** 100–107 (2009).

30. Chen, J. *et al.* In Vivo Imaging of Proteolytic Activity in Atherosclerosis. *Circulation* **105,** 2766–2771 (2002).

31. Jaffer, F. A., Libby, P. & Weissleder, R. Optical and Multimodality Molecular Imaging Insights Into Atherosclerosis. *Arterioscler. Thromb. Vasc. Biol.* **29,** 1017–1024 (2009).

32. Rudd, J. H. F. *et al.* Imaging Atherosclerotic Plaque Inflammation With [18F]-Fluorodeoxyglucose Positron Emission Tomography. *Circulation* **105,** 2708–2711 (2002).

33. Tatsumi, M., Cohade, C., Nakamoto, Y. & Wahl, R. L. Fluorodeoxyglucose Uptake in the Aortic Wall at PET/CT: Possible Finding for Active Atherosclerosis. *Radiology* **229,** 831–837 (2003).

34. Tahara, N. *et al.* Vascular Inflammation Evaluated by [18F]-Fluorodeoxyglucose Positron Emission Tomography Is Associated With the Metabolic Syndrome. *J. Am. Coll. Cardiol.* **49,** 1533–1539 (2007).

35. Hetterich, H. *et al.* Natural history of atherosclerotic disease progression as assessed by 18F-FDG PET/CT. *Int. J. Cardiovasc. Imaging* **32,** 49–59 (2015).

36. Mazurek, T. *et al.* PET/CT evaluation of 18F-FDG uptake in pericoronary adipose tissue in patients with stable coronary artery disease: Independent predictor of atherosclerotic lesions' formation? *J. Nucl. Cardiol.* 1–10 (2016). doi:10.1007/s12350-015-0370-6

37. Hartung, D. *et al.* Radiolabeled Monocyte Chemotactic Protein 1 for the Detection of Inflammation in Experimental Atherosclerosis. *J. Nucl. Med.* **48,** 1816–1821 (2007).

38. Sarai, M. *et al.* Broad and Specific Caspase Inhibitor-Induced Acute Repression of Apoptosis in Atherosclerotic Lesions Evaluated by Radiolabeled Annexin A5 Imaging. *J. Am. Coll. Cardiol.* **50,** 2305–2312 (2007).

39. Fujimoto, S. *et al.* Molecular Imaging of Matrix Metalloproteinase in Atherosclerotic LesionsResolution With Dietary Modification and Statin Therapy. *J. Am. Coll. Cardiol.* **52,** 1847–1857 (2008).

40. Hyafil, F. *et al.* Quantification of Inflammation Within Rabbit Atherosclerotic Plaques Using the Macrophage-Specific CT Contrast Agent N1177: A Comparison with 18F-FDG PET/CT and Histology. *J. Nucl. Med.* **50,** 959–965 (2009).

41. Laitinen, I. *et al.* Evaluation of v 3 Integrin-Targeted Positron Emission Tomography Tracer 18F-Galacto-RGD for Imaging of Vascular Inflammation in Atherosclerotic Mice. *Circ. Cardiovasc. Imaging* **2,** 331–338 (2009).

42. Beer, A. J. *et al.* PET/CT Imaging of Integrin αvβ3 Expression in Human Carotid Atherosclerosis. *JACC Cardiovasc. Imaging* **7,** 178–187 (2014).

43. Seo, J. W. *et al.* 64Cu-Labeled LyP-1-Dendrimer for PET-CT Imaging of Atherosclerotic Plaque. *Bioconjug. Chem.* **25,** 231–239 (2014).

44. Nahrendorf, M. *et al.* 18F-4V for PET–CT Imaging of VCAM-1 Expression in Atherosclerosis. *JACC Cardiovasc. Imaging* **2,** 1213–1222 (2009).

45. Torzewski, M. *et al.* Reduced In Vivo Aortic Uptake of Radiolabeled Oxidation-Specific Antibodies Reflects Changes in Plaque Composition Consistent With Plaque Stabilization. *Arterioscler. Thromb. Vasc. Biol.* **24,** 2307–2312 (2004).

46. Ardipradja, K. *et al.* Detection of activated platelets in a mouse model of carotid artery thrombosis with 18F-labeled single-chain antibodies. *Nucl. Med. Biol.* **41,** 229–237 (2014).

47. Phinikaridou, A. *et al.* Molecular MRI of Atherosclerosis. *Molecules* **18,** 14042–14069 (2013).

48. Chu, B. *et al.* MRI Features of the Disruption-Prone and the Disrupted Carotid Plaque: A Pictorial Essay. *JACC Cardiovasc. Imaging* **2,** 883–896 (2009).

49. Hatsukami, T. S. & Yuan, C. MRI in the early identification and classification of high-risk atherosclerotic carotid plaques. *Imaging Med.* **2,** 63–75 (2010).

50. Zhao, X.-Q. *et al.* MR Imaging of Carotid Plaque Composition During Lipid-Lowering Therapy. *JACC Cardiovasc. Imaging* **4,** 977–986 (2011).

51. Anderson, J. D. & Kramer, C. M. MRI of Atherosclerosis: Diagnosis and Monitoring Therapy. *Expert Rev. Cardiovasc. Ther.* **5,** 69–80 (2007).

52. Silvera, S. S. *et al.* Multimodality imaging of atherosclerotic plaque activity and composition using FDG-PET/CT and MRI in carotid and femoral arteries. *Atherosclerosis* **207,** 139–143 (2009).

53. Ripa, R. S. & Kjær, A. Imaging Atherosclerosis with Hybrid Positron Emission Tomography/Magnetic Resonance Imaging. *BioMed Res. Int.* **2015,** 1–8 (2015).

54. Petibon, Y. *et al.* Towards coronary plaque imaging using simultaneous PET-MR: a simulation study. *Phys. Med. Biol.* **59,** 1203–1222 (2014).

55. Briley-Saebo, K. C., Mani, V., Hyafil, F., Cornily, J.-C. & Fayad, Z. A. Fractionated feridex and positive contrast: In vivo MR imaging of atherosclerosis. *Magn. Reson. Med.* **59,** 721–730 (2008).

56. Terashima, M. *et al.* Human ferritin cages for imaging vascular macrophages. *Biomaterials* **32,** 1430–1437 (2011).

57. Kosuge, H. *et al.* FeCo/graphite nanocrystals for multi-modality imaging of experimental vascular inflammation. *PloS One* **6,** e14523 (2011).

58. Briley-Saebo, K. C. *et al.* Gadolinium mixed-micelles: Effect of the amphiphile on in vitro and in vivo efficacy in apolipoprotein E knockout mouse models of atherosclerosis. *Magn. Reson. Med.* **56,** 1336–1346 (2006).

59. Maiseyeu, A. *et al.* Gadolinium-containing phosphatidylserine liposomes for molecular imaging of atherosclerosis. *J. Lipid Res.* **50,** 2157–2163 (2009).

60. Kooi, M. E. *et al.* Accumulation of ultrasmall superparamagnetic particles of iron oxide in human atherosclerotic plaques can be detected by in vivo magnetic resonance imaging. *Circulation* **107,** 2453–2458 (2003).

61. Tang, T. Y. *et al.* The ATHEROMA (Atorvastatin Therapy: Effects on Reduction of Macrophage Activity) Study. Evaluation using ultrasmall superparamagnetic iron oxide-enhanced magnetic resonance imaging in carotid disease. *J. Am. Coll. Cardiol.* **53,** 2039–2050 (2009).

62. McAteer, M. A., Akhtar, A. M., von Zur Muhlen, C. & Choudhury, R. P. An approach to molecular imaging of atherosclerosis, thrombosis, and vascular inflammation using microparticles of iron oxide. *Atherosclerosis* **209,** 18–27 (2010).

63. Kanwar, R. K., Chaudhary, R., Tsuzuki, T. & Kanwar, J. R. Emerging engineered magnetic nanoparticulate probes for targeted MRI of atherosclerotic plaque macrophages. *Nanomed.* **7,** 735–749 (2012).

64. Michalska, M. *et al.* Visualization of Vascular Inflammation in the Atherosclerotic Mouse by Ultrasmall Superparamagnetic Iron Oxide Vascular Cell Adhesion Molecule-1-Specific Nanoparticles. *Arterioscler. Thromb. Vasc. Biol.* **32,** 2350–2357 (2012).

65. Sirol, M. Chronic Thrombus Detection With In Vivo Magnetic Resonance Imaging and a Fibrin-Targeted Contrast Agent. *Circulation* **112,** 1594–1600 (2005).

66. Spuentrup, E. *et al.* Molecular Magnetic Resonance Imaging of Coronary Thrombosis and Pulmonary Emboli With a Novel Fibrin-Targeted Contrast Agent. *Circulation* **111,** 1377–1382 (2005).

67. Spuentrup, E. *et al.* Molecular Magnetic Resonance Imaging of Atrial Clots in a Swine Model. *Circulation* **112,** 396–399 (2005).

68. Stracke, C. P. *et al.* Molecular MRI of cerebral venous sinus thrombosis using a new fibrin-specific MR contrast agent. *Stroke J. Cereb. Circ.* **38,** 1476–1481 (2007).

69. Makowski, M. R. *et al.* In vivo assessment of intraplaque and endothelial fibrin in ApoE−/− mice by molecular MRI. *Atherosclerosis* **222,** 43–49 (2012).

70. Spuentrup, E. *et al.* MR imaging of thrombi using EP-2104R, a fibrin-specific contrast agent: initial results in patients. *Eur. Radiol.* **18,** 1995–2005 (2008).

71. Clofent-Sanchez, G., Jacobin-Valat, M.-J. & Laroche-Traineau, J. The growing interest of fibrin imaging in atherosclerosis. *Atherosclerosis* **222,** 22–25 (2012).

72. Duivenvoorden, R. *et al.* A Statin-Loaded Reconstituted High-Density Lipoprotein Nanoparticle Inhibits Atherosclerotic Plaque Inflammation. *Nat. Commun.* **5,** 3065 (2014).

73. Tardif, J.-C. *et al.* Effects of reconstituted high-density lipoprotein infusions on coronary atherosclerosis: a randomized controlled trial. *JAMA* **297,** 1675–1682 (2007).

74. Suzuki, M. *et al.* Ultrasmall superparamagnetic iron oxide nanoparticles coated with fucoidan for molecular MRI of intraluminal thrombus. *Nanomed.* **10,** 73–87 (2015).

75. Mousa, S. A. Adhesion molecules: potential therapeutic and diagnostic implications. *Methods Mol. Biol. Clifton NJ* **663,** 261–276 (2010).

76. Paulis, L. E. *et al.* Targeting of ICAM-1 on vascular endothelium under static and shear stress conditions using a liposomal Gd-based MRI contrast agent. *J. Nanobiotechnology* **10,** 1 (2012).

77. Chan, J. M. S., Monaco, C., Wylezinska-Arridge, M., Tremoleda, J. L. & Gibbs, R. G. J. Imaging of the Vulnerable Carotid Plaque: Biological Targeting of Inflammation in Atherosclerosis using Iron Oxide Particles and MRI. *Eur. J. Vasc. Endovasc. Surg.* **47,** 462–469 (2014).

78. Rohlena, J. *et al.* Endothelial CD81 is a marker of early human atherosclerotic plaques and facilitates monocyte adhesion. *Cardiovasc. Res.* **81,** 187–196 (2009).

79. Yan, F. *et al.* Magnetic resonance imaging of atherosclerosis using CD81-targeted microparticles of iron oxide in mice. *BioMed Res. Int.* **2015,** (2015).

80. Amirbekian, V. *et al.* Detecting and assessing macrophages in vivo to evaluate atherosclerosis noninvasively using molecular MRI. *Proc. Natl. Acad. Sci.* **104,** 961–966 (2007).

81. Tarin, C. *et al.* Targeted gold-coated iron oxide nanoparticles for CD163 detection in atherosclerosis by MRI. *Sci. Rep.* **5,** 17135 (2015).

82. Maiseyeu, A. *et al.* In Vivo Targeting of Inflammation-Associated Myeloid-Related Protein 8/14 Via Gadolinium Immunonanoparticles. *Arterioscler. Thromb. Vasc. Biol.* **32,** 962–970 (2012).

83. Langer, H. F. & Gawaz, M. Platelet-vessel wall interactions in atherosclerotic disease. *Thromb. Haemost.* (2008). doi:10.1160/TH07-11-0685

84. Lievens, D. & von Hundelshausen, P. Platelets in atherosclerosis. *Thromb. Haemost.* **106,** 827–838 (2011).

85. Jacobin-Valat, M.-J. *et al.* MRI of inducible P-selectin expression in human activated platelets involved in the early stages of atherosclerosis. *NMR Biomed.* **24,** 413–424 (2011).

86. te Boekhorst, B. C. *et al.* Molecular MRI of murine atherosclerotic plaque targeting NGAL: a protein associated with unstable human plaque characteristics. *Cardiovasc. Res.* **89,** 680–688 (2011).

87. Briley-Saebo, K. C. *et al.* Targeted Iron Oxide Particles for In Vivo Magnetic Resonance Detection of Atherosclerotic Lesions With Antibodies Directed to Oxidation-Specific Epitopes. *J. Am. Coll. Cardiol.* **57,** 337–347 (2011).

4 Monoclonal antibodies

Although its empirical practice was reported early in Asia, the first “modern” vaccination by Edward Jenner, at the end of the XVIIIth century, is contemporary to the discovery of immunity. He proposes to inoculate a benign disease -the cow vaccine, hence the name vaccination- to humans, to protect them from the related and lethal smallpox [1]. When Louis Pasteur demonstrates the protective properties of attenuated cholera germs in chicken, he pays Jenner a tribute by calling the method “vaccination”. In 1885 he uses tissue extracts from rabies-deceased animals to cure humans exposed to the disease [2]: the famous case of the young Joseph Meister, supposedly cured from the rabies, caused so much enthusiasm that a fundraise was organized which allowed the creation of the globally-known Pasteur Institute in Paris.

Emile Roux, co-worker of Pasteur, shows in 1888 that diphtheria is due to a toxin produced by the bacteria rather than to the bacteria itself and that immunity can be acquired through vaccination with this compound. Two years later in Berlin, Emil Von Behring and Shibasaburo Kitasato hypothesize that the blood of immunized animals contains an antitoxin substance that can be transferred to another animal to specifically inactivate this toxin. The same conclusion was drawn about tetanus toxin, however the protection was specific to each toxin and immunization against one didn’t confer protection to the other. Immunity was hence shown to be specific and transferable [3]. In the following years, an efficient serotherapy is developed and used as a treatment for diphtheria in children, with outstanding results. This success grants Roux and von Behring a prize from the Paris medicine academy [4].

In 1895, Elie Metchnikoff describes phagocytosis, first stone in the wall of innate immunity. Five years later Paul Ehrlich theorizes “antibodies” able to recognize “antigens” as the key to Roux and von Behring observations. At the time he believes each lymphocyte bears on its surface receptors of different specificities that are specifically amplified upon contact with the antigen and released in the bloodstream[5,6]. Although their activity was well-described, the first structural studies of immunoglobulins were only carried out in the early 1960s [7,8], with Rodney Porter proposing the first structure for immunoglobulins[5,6,9] which will grant him a Nobel Prize. Ehrlich’s theory is only amended in 1975 by Georges Köhler and César Milstein who prove, with the hybridoma technology, the relationship “one lymphocyte, one receptor; one plasmocyte, one immunoglobulin”, and propose the first method to produce antibodies of defined specificity [10].

This breakthrough initiates the development of monoclonal antibodies and, in 1986, the first therapeutic antibody orthoclone OKT3 is approved as a preventive drug for kidney transplant rejection. The first chimeric monoclonal antibodies appear in the late 1990s, followed by humanized, then fully human antibodies: adalimumab is approved for treating rheumatoid arthritis in 2002[11].

Nowadays, the complex physiology of immunoglobulins has gained considerable understanding and modern biotechnology is able to synthetize and produce antibodies or fragments thereof in a controlled manner. As of November 10, 2014, forty-seven monoclonal antibody or Ab-based products had been approved in the US or Europe for various indications. With a mean approval rate of around four new products per year, roughly 70 monoclonal antibody-related drugs should be on the market by 2020, with overall global sales accounting for nearly $125 billion[12].

4.1 Origin of immunoglobulins

Immunity consists in two intertwined systems: innate immunity is the first line of response to pathogens entering the organism, immediately triggering inflammation; its principal actors are phagocytes (including dendritic cells and macrophages), granulocytes (including neutrophils), and natural killer (NK) cells. The second system is called adaptive immunity, it responds to longer term infections and coordinates a multiplicity of actors, including those involved in innate immunity. T and B lymphocytes are key players in adaptive immunity, by triggering complex cooperation they regulate the global immune response. B lymphocytes in particular, bear a unique role by defining the humoral response: B cell-derived plasmocytes secrete immunoglobulins (Ig) in the blood that specifically recognize pathogens and trigger a coordinated immune response (complement, phagocytes).

The maturation of B lymphocytes from the hematopoietic stem cell occurs along two different sequences, in different locations, as shown by Figure 14.

The first sequence is antigen-independent and occurs in the bone marrow, the evolution of the stem cell into an immature B cell involves the rearrangement of the Ig genes coding for the B cell receptor (BCR), which is a membrane Ig. This phenomenon occurs as follows: for the light chains, one of the variability V genes rearranges with one junction J gene. This recombination leads to the elimination of the other V and J genes. In a similar manner, for heavy chains, one diversity D region associates with a J gene, then the DJ combination rearranges with a V gene. This rearrangement occurs at the DNA level, so each B cell produces only BCR of defined specificity (recognizing the same epitope). Figure 13 is a schematic representation of the immunoglobulin germline genes before they undergo rearrangement.

In a second phase, the mature B cell, expressing both μ and δ heavy chains (membrane IgM and IgD), is released from the bone marrow and is taken up via the blood stream to the secondary lymphoid organs. There, the BCR can come in contact with its specific antigen, via a cooperation with T cells, which triggers B cell activation. This results into a proliferation, termed clonal expansion because each antigen activates only one B cell clone. Part of these clones differentiate into short-life plasmocytes able to secrete soluble immunoglobulins of IgM isotype, specific to the primary humoral response. Part of the activated B cells will transform into memory lymphocytes, forming a “database” of known antigens.

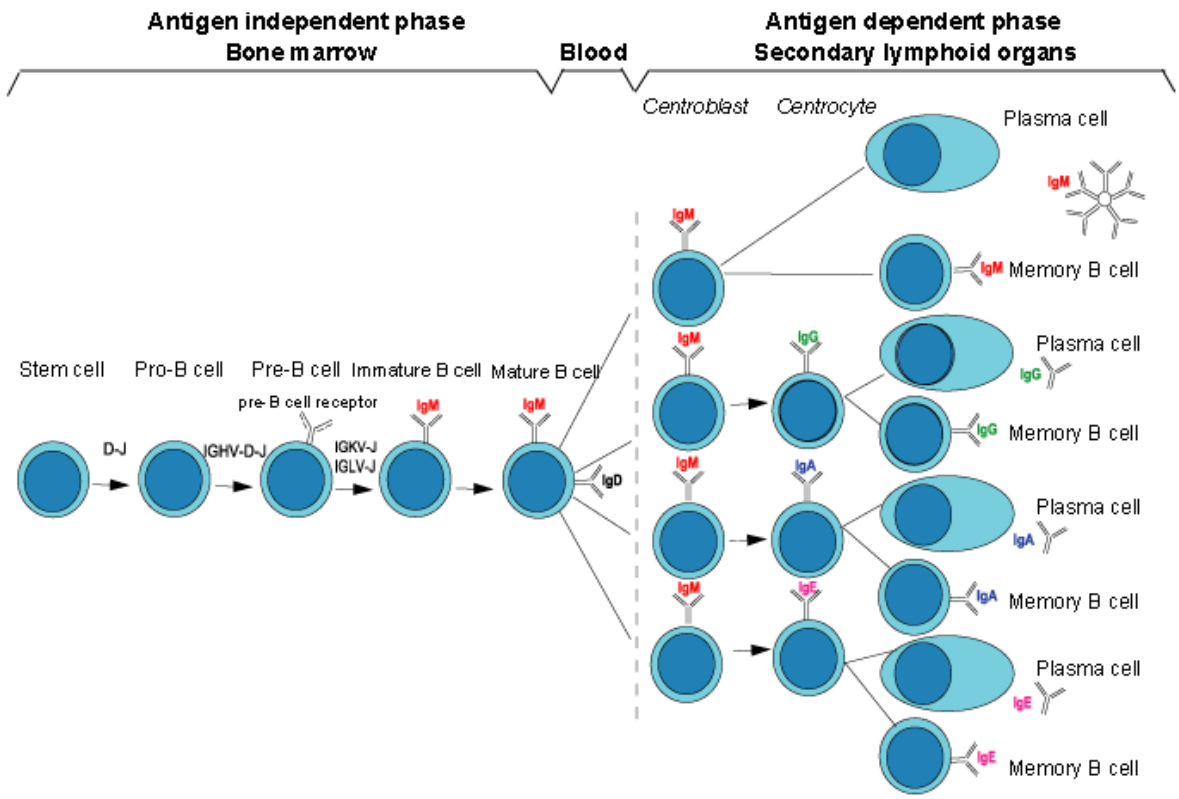

Figure 14: Lymphocyte B maturation process. From www.imgt.org.

Upon secondary antigen encounter, the corresponding memory B cell clones will be activated, differentiating into IgG-secreting plasmocytes, and producing a stronger and quicker humoral response. The memory B cells issued from this secondary response are able to persist several years in humans, they support the very principle of vaccination.

There are 5 types of heavy chains in human: γ, α, μ, ε and δ coding respectively for IgG, IgA, IgM, IgE and IgD isotypes; and only 2 types of light chains: κ or λ. Upon second antigen encounter, isotypic class switching occurs: the VJ or VDJ portion previously rearranged was associated "by default" with a constant C μ gene, specific of IgM isotype. This gene is

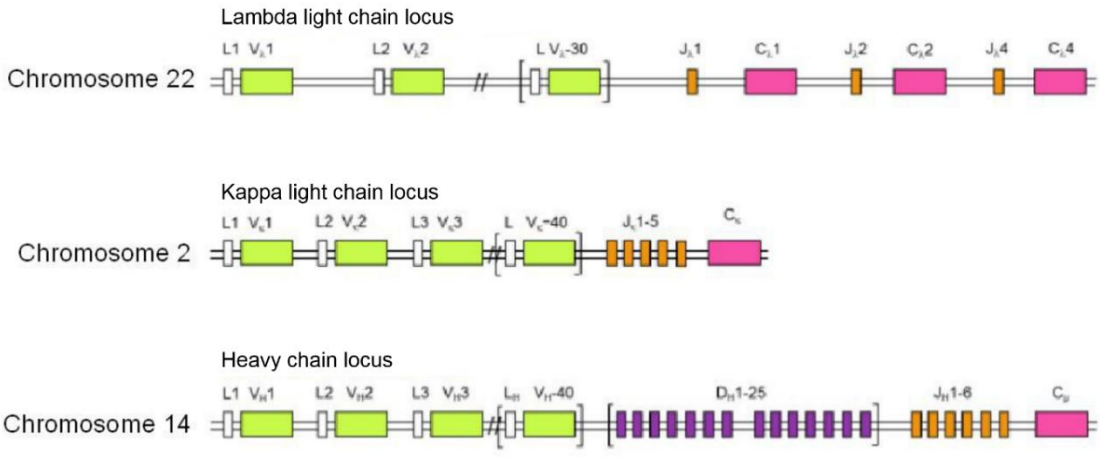

Figure 13: Human immunoglobuline germline genes and their loci on respective chromosomes. V: variability genes; J: junction genes; C: constant domain genes; D: diversity genes, supplementary repertoire carried by chromosome 14. Modified from www.imat.org.

replaced by another, further away on the chromosome that defines the new Ig isotype. The other C regions are then eliminated.

4.2 Structure

Immunoglobulins are heterodimeric glycoproteins of around 150 kDa. They comprise two heavy chains (50 kDa ≈ 450 aa) with 3 constant heavy (CH) and 1 variable heavy (VH) domains. Both heavy chains are bound by disulfide bonds that form the hinge which separate the fragment antigen binding (Fab) from the fragment cristalizable (Fc). Two light chains (25 kDa ≈ 220 aa) composed of one constant light (CL) and one variable light (VL) assemble on each side of the heavy chains. Their variable domains consist of β-sheet frameworks assembled by pairs to form two variable fragments (Fv), carrying the complementarity defining regions (CDRs) loops or hypervariable regions that bear the antibody specificity. The framework (FR) regions serve as a backbone for the correct folding of the binding pocket (Figure 15).

The amino-acids of the binding site interact with the antigen through many non-covalent interactions: hydrogen or hydrophobic bonds, Van der Waals forces; although they are "weak" bonds, their multiplicity allows for a very strong binding [13].

Schematically, the Fab fragments hold the specificity, while at the other end the Fc fragment is responsible for the functional properties of the Ig *in vivo*. Indeed, the Fc fragment of IgG can interact with receptors located on other cells to trigger antibody-dependent cellular cytotoxicity (ADCC) or complement-dependent cytotoxicity (CDC, also possible with IgM).

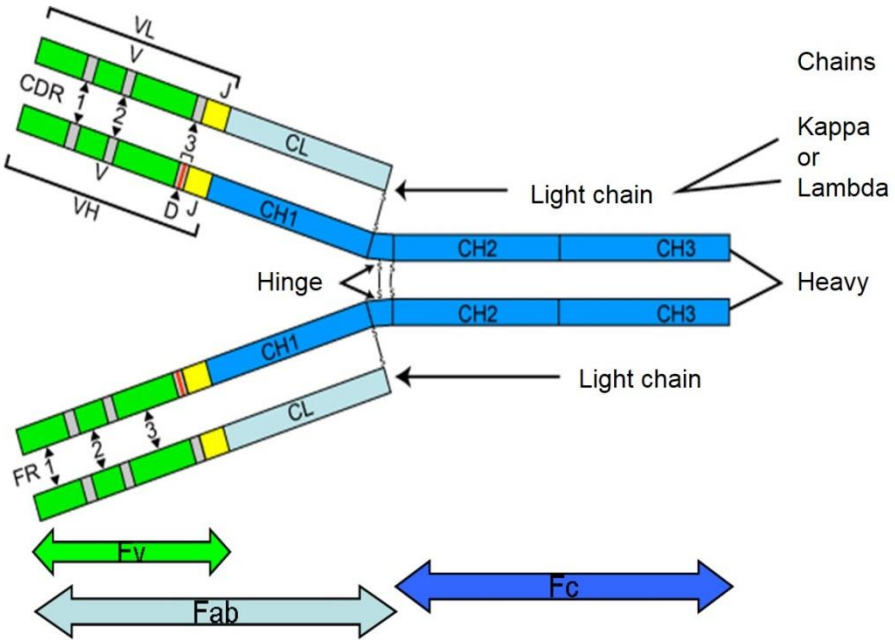

Figure 15: Typical immunoglobulin structure (modified from www.imgt.org). Fv: variable fragment; Fc: crystallizable fragment; Fab: fragment antigen binding; VL: variable domain of the light chain; VH: variable domain of the heavy chain; CDR 1, 2, 3: hypervariable domains; CL: constant domain of the light chain; CH 1, 2, 3 : constant domains of the heavy chain.

Additionally, Fcγ can bind to a receptor called FcRn (for neonate receptor) that originally serves to transfer immunity from the mother to its fetus through the placenta. In adults it transports IgG within and outside the cells, rescuing them from a default degradative pathway and allowing an extended serum half-life of IgGs, up to 3 weeks when IgM and IgA circulate for roughly a week.

The heavy and light chains of an Ig are assembled to one another by disulfide bonds, and each chain is further stabilized by intramolecular bonds[14]. This particular structure requires elaborate post-translation processing and an oxidizing environment to allow for the formation of these bonds.

As glycoproteins, immunoglobulins undergo post-translational glycosylation by the endoplasmic reticulum (ER). Glycan are attached to the heavy chain of antibodies: one conserved N-glycosylation on the asparagine 297 residue (Asp297 or N297) of the Fc fragment; a minority of Ig also bears a second N-linked glycosylation site in their variable region. They condition the Ab proper folding and structural properties[15]. Furthermore, although the Ig glycan are limited in size, their complexity and diversity support the Ab activity and pharmacokinetic properties, as shown in Figure 16[16,17].

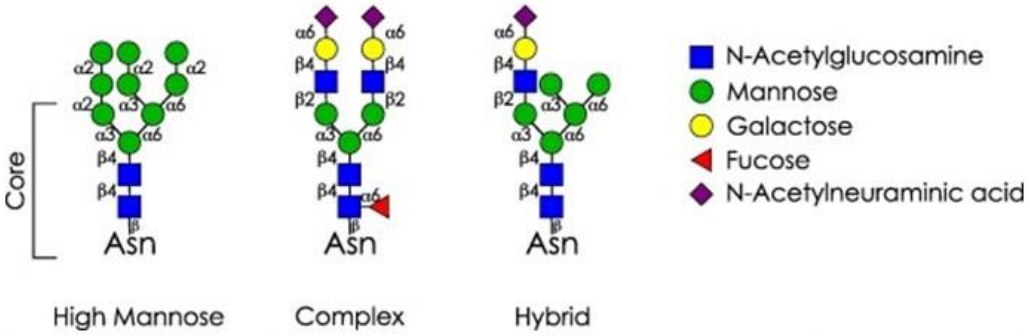

Glycan species	Safety/immunogenicity	Biologic activity/efficacy	Clearance (PK/PD)
Galactose	Unknown	+	Unknown
α1,3-galactose	––	Unknown	Unknown
Fucose	(–)	++	Unknown
Bisecting GlcNac	(–)	+	Unknown
High mannose	Unknown	+	––
NANA	Unknown	(–)	+
NGNA	––	(–)	+
β1,2-Xylose/α1,3-Fucose	––	Unknown	Unknown
NGHC	Unknown	–	(–)

+ Positive impact; – negative impact; ++ high positive impact; –– high negative impact; (+/–) potential impact.

Figure 16: Structure and impact of immunoglobulin glycosylation.Upper image: schematic representation of the 3 N-glycan types existing in antibodies. Bottom table: impact of Fc glycans on safety/immunogenicity, biologic activity/efficacy and clearance (PK/PD). Asn: asparagine; GlcNac: N-Acetylglucosamine; NANA: N-acetylneuraminic acid; NGNA: N-glycolylneuraminic acid; NGHC: nonglycosylated heavy chain. Modified from Higel et al., 2016, Eur. J. Pharmaceutics and Biopharmaceutics and Reusch et al., 2015, Glycobiology.

4.3 Methods for mAbs generation

4.3.1 The hybridoma method

The first method for "continuous cultures of fused cells secreting antibody of predefined specificity", called the hybridoma method, was proposed by Georges Köhler and Cesar Milstein in 1975 [10]. This innovation granted them a Nobel Prize in 1984.

The schematic method is summarized in Figure 17. Briefly, a mouse is immunized against an antigen by repeated injections. The mouse is sacrificed and plasmocytes isolated from its spleen. They are fused to myeloma cells, which cannot produce immunoglobulins and lack the HPRT enzyme (hypoxanthine-guanine phosphoribosyl transferase) involved in nucleotide synthesis. The selection of fused cells happens on a media containing hypoxanthine, aminopterin, and thymidine (HAT medium), forcing the cells to use the HPRT to survive, hence eliminating the unfused myeloma cells. On the other hand, the unfused plasmocytes only have a limited replication capacity and dye rapidly. This way, after a growth period on HAT medium, only hybridomas survive. They are then isolated to proceed to further screening tests and affinity maturation.

This technique is very efficient with mouse plasmocytes and has been widely used ever since. However, it is trickier with human plasmocytes. Despite the fact that immunization in humans is not ethically acceptable and the only available targets are naturally-occurring pathologies or auto-immune diseases [18], immortalization of human plasmocytes by Epstein-

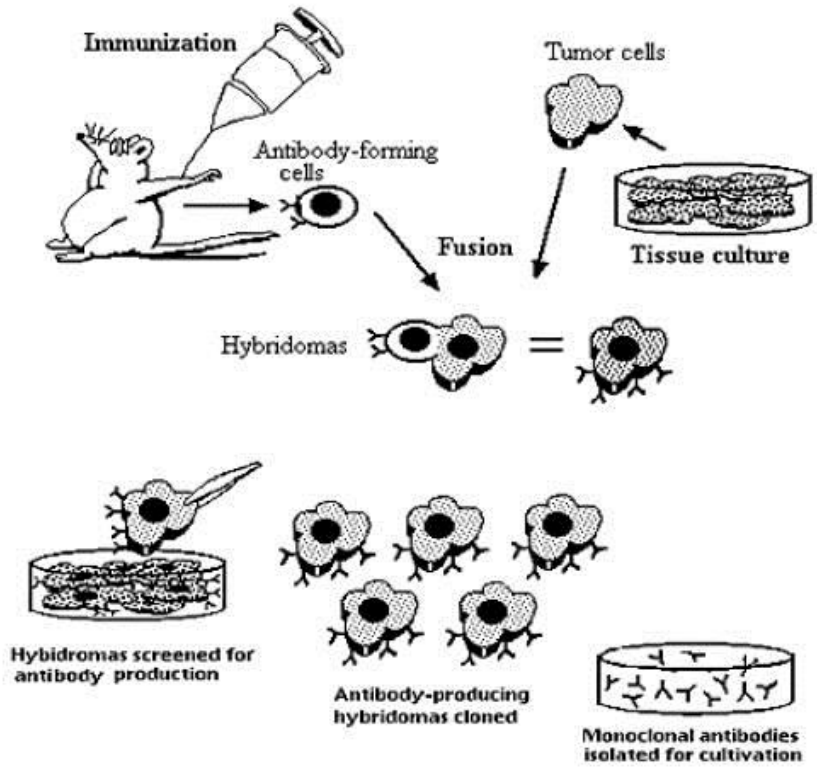

Figure 17: Hybridoma technology description. From Köhler and Milstein, Nature, 1975.

Barr virus (EBV) was very inefficient until better understanding of the molecular activation mechanisms of lymphocytes was gained. Nowadays, the use of CD40 or TLR9 ligands has allowed the cloning of naive or memory B lymphocytes [19]. Nonetheless, the need to address various targets limits the use of plasmocytes from human origin. Thus, to be able to propose human antibodies for the clinics, other methods have been described.

4.3.2 Phage display technology

One of the proposed method for the obtainment of antibodies from human origin is the phage display technology that was described by McCafferty and colleagues in 1990[20].

A bacteriophage, or phage, is a virus that specifically infects and replicates inside bacteria. Phages were discovered by microbiologists Felix Twort and Felix d'Hérelle in 1915 and 1917. A certain type of phages, called lytic phages because their replication involves a lytic cycle, and able to specifically kill one genre or specie of bacteria, bear a potential as therapeutic agents [21]; they have been early on used as such, and remain the best alternative for the treatment of antibiotic-resistant infections [21–23]. However, non-lytic phages can integrate in bacteria and use the cellular machinery to produce their own proteins. This was found responsible for the virulence of certain bacterial infections, e.g. in cholera, diphtheria, or dysentery, by coding for a toxin responsible for the symptoms[24,25].

The phage display technology takes advantage of the property of non-lytic-phages to have their proteins translated by the host. It relies on the expression of a peptide, protein or antibody fragment of interest, fused to a surface glycoprotein displayed at the surface of the

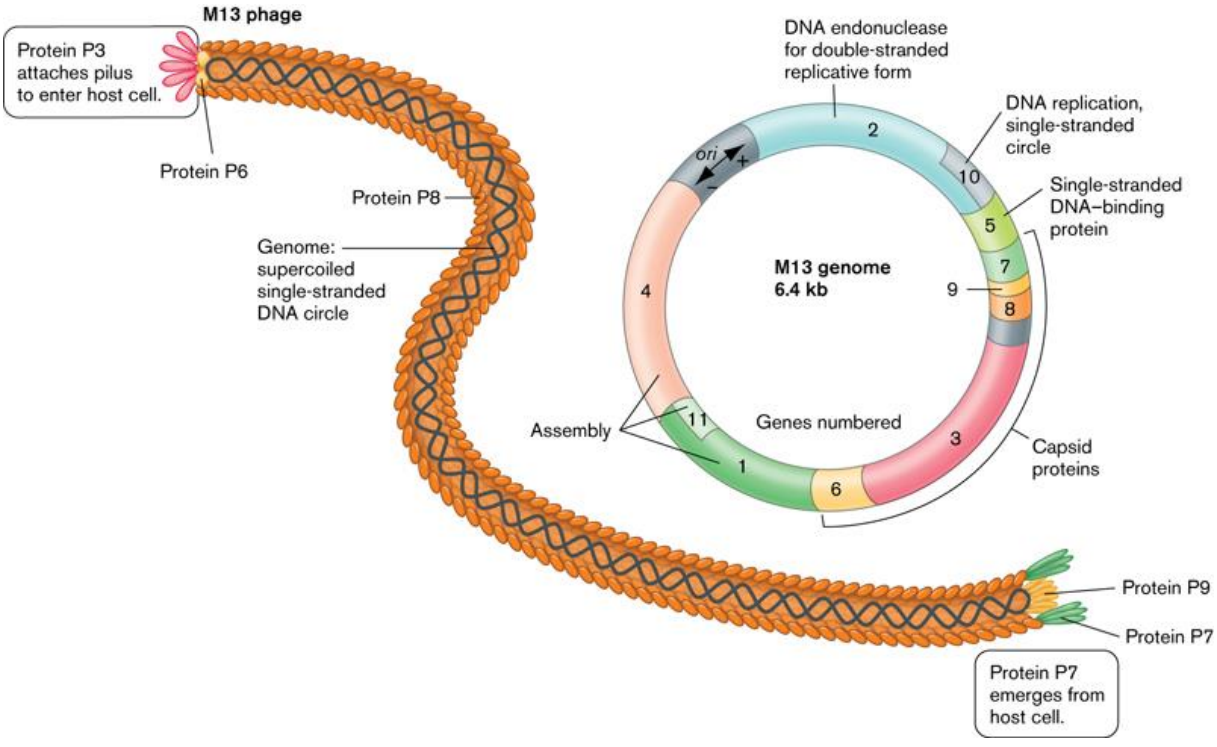

Figure 18: M13 filamentous phage structure and genome. The genome is color-coded according to the corresponding proteins. From www.wwnorton.com

virus. Its major strength consists in the preservation of the genetic information coding for the fusion protein inside the genome of the particle. This preserved link between pheno- and genotype allows performing functional screening followed by straightforward retrieval of the genetic information from the clones of interest.

Figure 18 presents the general structure of the phage. The phage genome is contained in a circular, single strand DNA molecule of 4.5 to 8kb encoding for capsid proteins (Figure 18, M13 genome).

The filamentous-phage-derived vector, called phagemid, **comprises a bacterial/plasmid) origin of replication (e.g. ColE1 Ori), and a phage origin of replication (e.g. M13 Ori). The gene of the fusion protein g3p-recombinant protein is under the control of a bacterial promoter, flanked by** restriction enzyme recognition sites, **and followed by tags for purification (e.g. 6His) or protein detection.**

Within the bacteria, the phagemid replicates like a normal plasmid, thanks to a bacterial origin of replication (e.g. ColE1 Ori). However, this phagemid is non-infectious because it doesn't possess the genes necessary to virions formation. Hence, the bacteria has to be further infected with a helper phage, which genome has a defective origin of replication but possesses the structural and functional proteins necessary to the replication cycle. The phagemid DNA is amplified and encapsidized in a phage particle instead of the helper phage DNA that is not replicated because of the defective Ori. The recombinant phage particle contains both the wild-type g3p and the fusion protein, but only one DNA molecule, which is preferentially the recombinant phagemid. This allows for the cloning of long DNA fragments and limits the number of fusion protein g3p at the surface of the particle, at the same time limiting the potential screening bias induced by an increased avidity.

Smith and colleagues [26] first described the technique of phage-display with peptides, then McCafferty and his team managed to clone and express an antibody fragment[20]. Both V regions of a known antibody, attached by a flexible linker, were fused to the gene III protein (g3p)(Figure 19). The fusion product retained the original antibody reactivity and specificity. This work paved the way to phage-antibody libraries generation and screening. The successful anti-TNFα antibody Adalimumab (Humira©) first authorized for marketing by the EMEA in 2003 originates from a phage display selection. Although this technology is traditionally used for *in vitro* selection on a known target of interest, Pasqualini and colleagues first proposed an *in vivo* selection strategy. After a synthetic peptide library was injected to an animal, then bound phages were extracted from organs of interest. This strategy should give access to a broader variety of markers [27]. Based on this work, our team used a human antibody library to perform an *in vivo* selection of atherosclerosis specific antibodies[28,29].

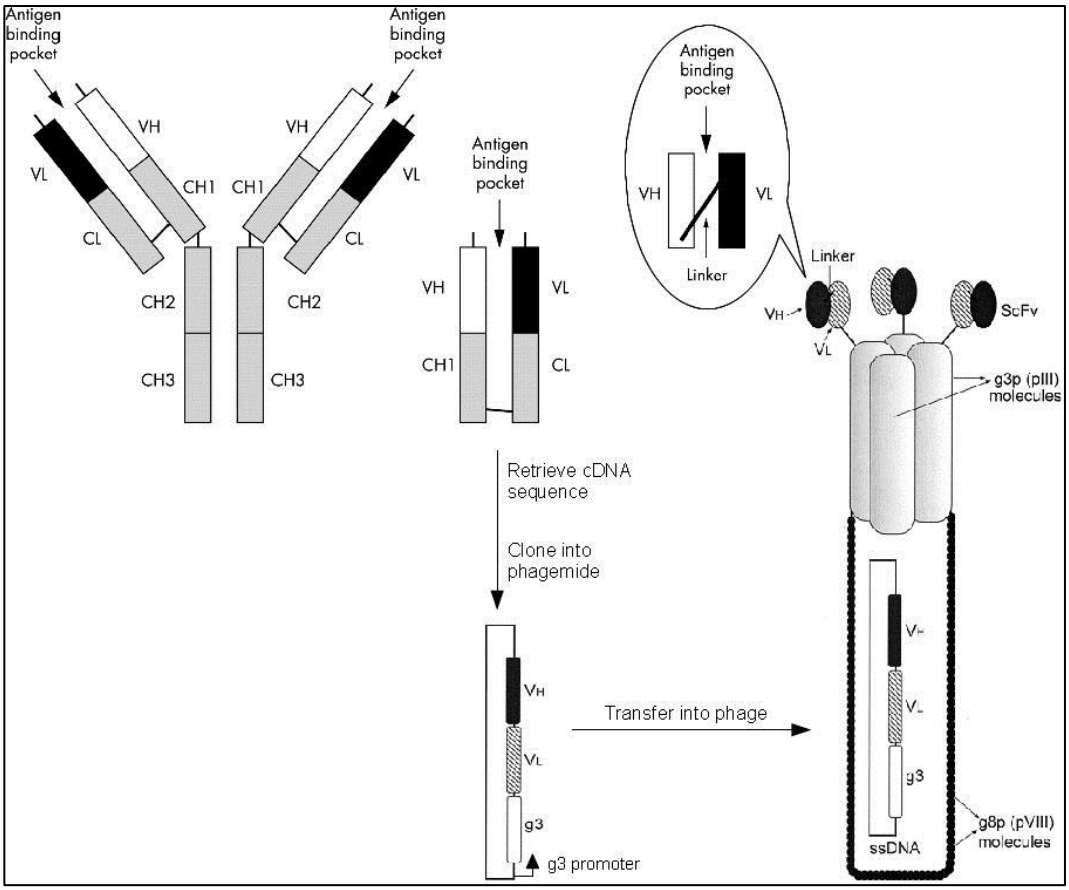

Figure 19: Principle of the phage display technology. g3p: gene 3 protein; g8p: gene 8 protein.

Antibody-phage display technology relies on the construction of combinatorial libraries, in which PCR-amplified immunoglobulin light and heavy chains DNA are randomly recombined into a vector, irrespective of their pairing *in vivo*.

To obtain libraries of V domain sequences, mRNA is isolated from B lymphocytes or spleen cells, and all expressed heavy and light chain V region genes are PCR-amplified, then cloned by using framework primers. Usually one library is constructed for the heavy chain variable domains and two sub-libraries for the κ and λ light chain domains. These libraries are genetically combined so that the VH are paired independently with both the κ and the λ VL, to increase the diversity. All the resulting constructs can be displayed on the surface of the phage as g3p fusion-proteins[30].

When considering human antibodies, different types of libraries can be used: naïve or immune; semi-synthetic or synthetic. Immune libraries can only be obtained from patients "naturally" immunized against a certain pathology[31]. V genes are then retrieved from IgG-expressing B cells, allowing access to rearranged immunoglobulins genes with a potential high affinity for their target. Naïve libraries, on the contrary, are issued from the rearranged IgM repertoire of non-immunized donors, and theoretically present less affinity maturation and a repertoire closer to the germline[32].

Synthetic and semi-synthetic libraries can originate from one antibody which structure is well-known. If mutations are introduced in one subset of CDR (VH and VL) at a time, such as this described by Philibert et al.[33,34], the library is considered semi-synthetic. In contrast, a synthetic library may introduce simultaneous replacement of multiple CDR[35].

4.3.3 Transgenic mice

To try and tackle the limitations of human hybridoma generation, and thanks to the tools of genetic engineering, transgenic mice have been generated that are able to express "human" antibodies.

The immunoglobulin genes in these mice are replaced by part of their human analog, which rearrange and mature in the mouse immune system. The resulting B cells are ready to be activated as a response to antigen stimulation [36]. This technology is interesting because mice B cells generate stable hybridomas, which produce good yields of immunoglobulins. It was initially limited by the available genetic tools, which only allowed for the transfer of small transgenes. Yet, five years after the initial description, two teams were able to propose an improved method by cloning larger portions of the human repertoire in mouse embryos. These human-Ig producing mice were further bred with mice which endogenous repertoire had been knocked-out to avoid the generation of murine Ig [37–40]. Figure 20 presents the

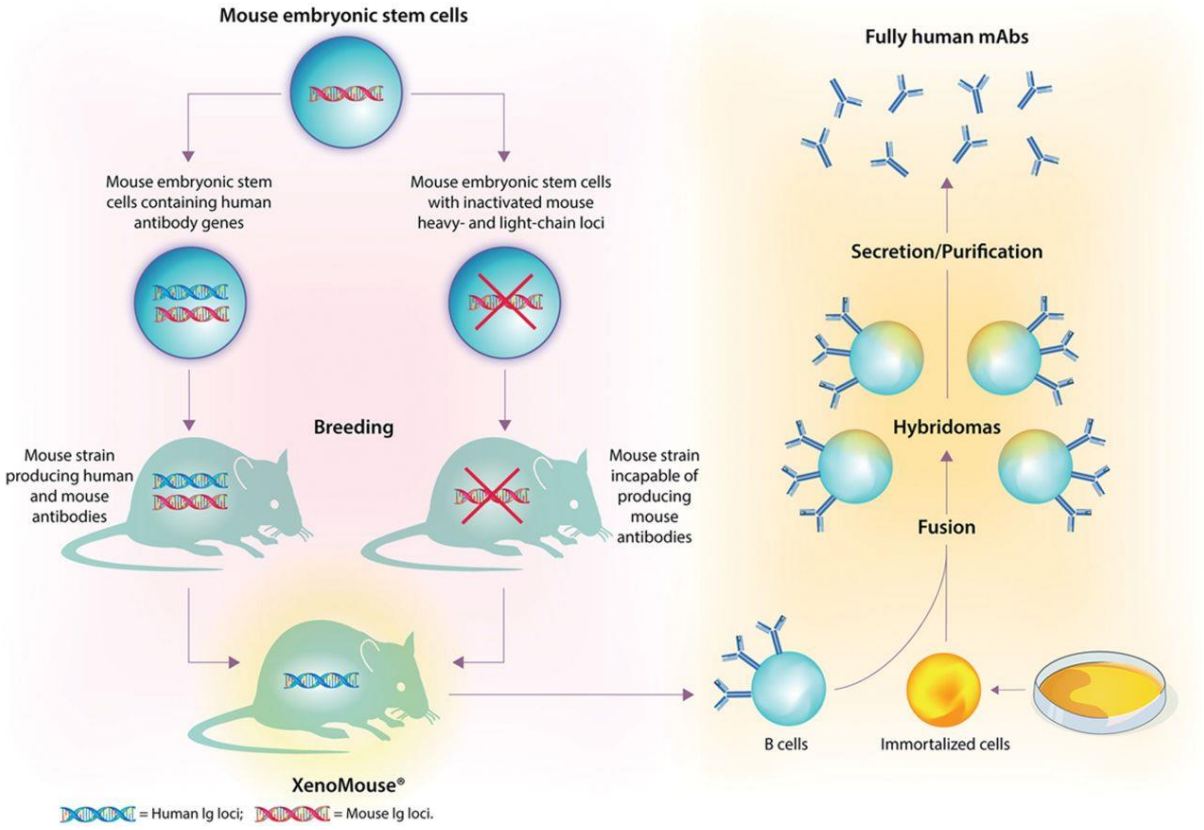

Figure 20: Transgenic mice producing human immunoglobulin, example of the Xenomouse®. Creation of transgenic mice from embryonic stem cells; breeding to obtain a "pure" transgenic line. Plasmocytes from the Xenomouse are then immortalized using the hybridoma technology to produce fully human monoclonal antibodies (mAbs). From Foltz et al., Circulation, 2013.

summarized procedure for the generation of human monoclonal antibodies (mAbs) from transgenic mice. As a result, several companies marketed transgenic mice systems for human antibodies generation: Medarex (UltiMab®), Abgenix (Xenomouse®), Regeneron (VelocImmune®), and Kymab (Kymouse®). The mAb panitumumab (Vectibix®), targeting the EGFR (epidermal growth factor receptor) and obtained by this technology, was marketed in 2006.

4.3.4 Conclusion

The evolution of the techniques has given rise to two major "sources" of human antibodies, as shown in Figure 21: a) *In vitro* constructed libraries are expressed using the phage display technology (other types of display exist that will not be presented here) and screened against the target of interest. The particles exhibiting sufficient affinity are amplified along the selection rounds and eventually expressed, using molecular biology tools. b) Transgenic mice expressing antibodies with human sequences, which obtainment is detailed above, are immunized with an antigen. The circulating plasmocytes are extracted from the animal and

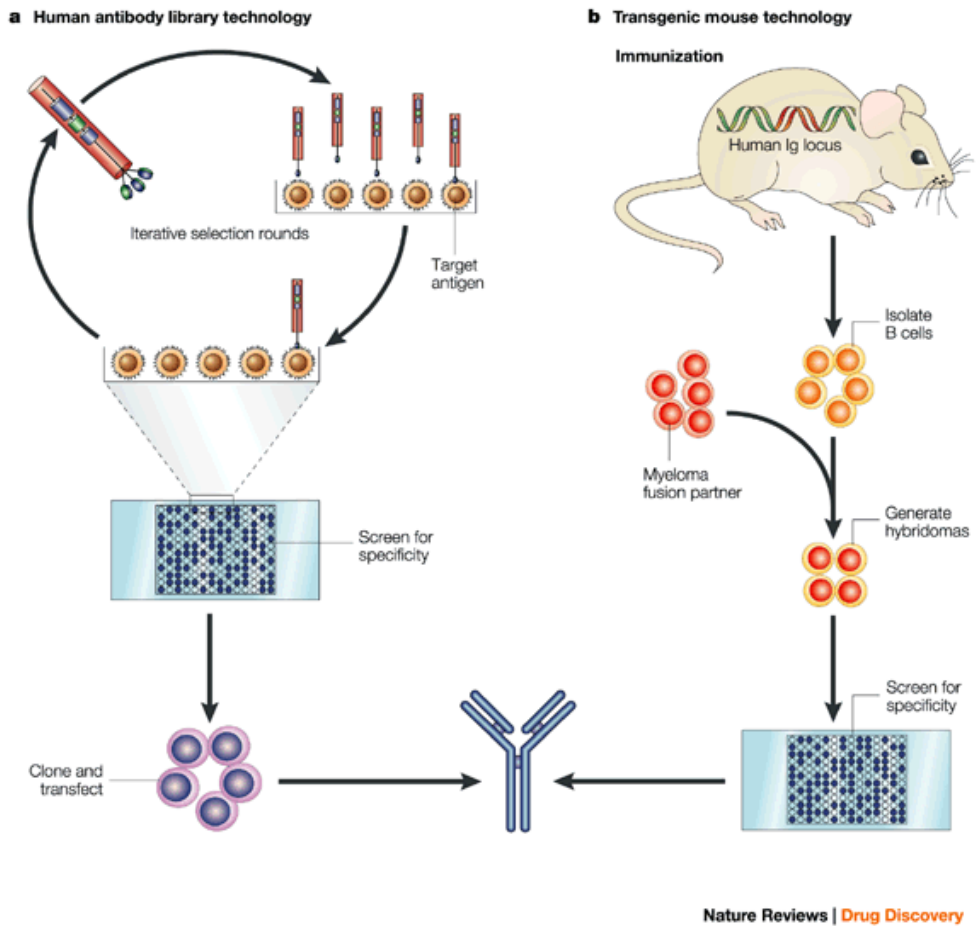

Figure 21: Representation of two main human antibody selection methods. a. screening of a vitro constructed library of antibody fragments and production of the best candidates. b. immunization of a transgenic mouse with an antigene and immortalization of its B lymphocytes with the hybridoma method. From Brekke and Sandlie, Nat. Rev. Drug Disc., 2003.

immortalized using the hybridoma method as described in the first paragraph. The produced immunoglobulins are screened for their affinity to the target. Among the mAbs on the market in 2013, 2 human IgG were issued from phage display: briakinumab and gantenerumab; 5 from transgenic mice: ipilimumab, nivolumab, sarilumab, zalutumumab, and zanolimumab[41].

4.4 Antibody formats and production systems

In the years 1980 – 90, as more recombinant antibodies became available for imaging or therapy, mouse monoclonal antibody rapidly revealed unsuitable as their recognition by the host immune system leads to a short serum half-life and the generation of human anti-mouse antibodies (HAMA)[30]; furthermore, their Fc fragment is unable to trigger human effector functions. Hence, new methods emerged to gradually replace the murine sequences with human ones.

This evolution led from the fully murine antibodies, ("-momab"), to chimeric antibodies in which all constant regions are human ("-ximab"), to humanized antibodies containing only the CDRs from murine origin ("-zumab"), to the most recent fully human antibodies selected through phage display or recombinant mice, for example ("-mumab"). Figure 22 presents their schematic structure and principal production methods, presented in 4.3. The genetic engineering methods will be treated in paragraph 4.4.1.

Nowadays, amongst marketed antibodies, most are humanized or fully human. As an example, out of the seven therapeutic antibodies newly approved in the EU and US in 2015, 6 were humanized or human, and only one was chimeric; 6 were IgGs and one was a Fab. Among the 53 Ab in phase 3 evaluation, 47 are humanized or human, 4 are chimeric or murine, and 10 are engineered formats: antibody fragments, bispecific antibodies or

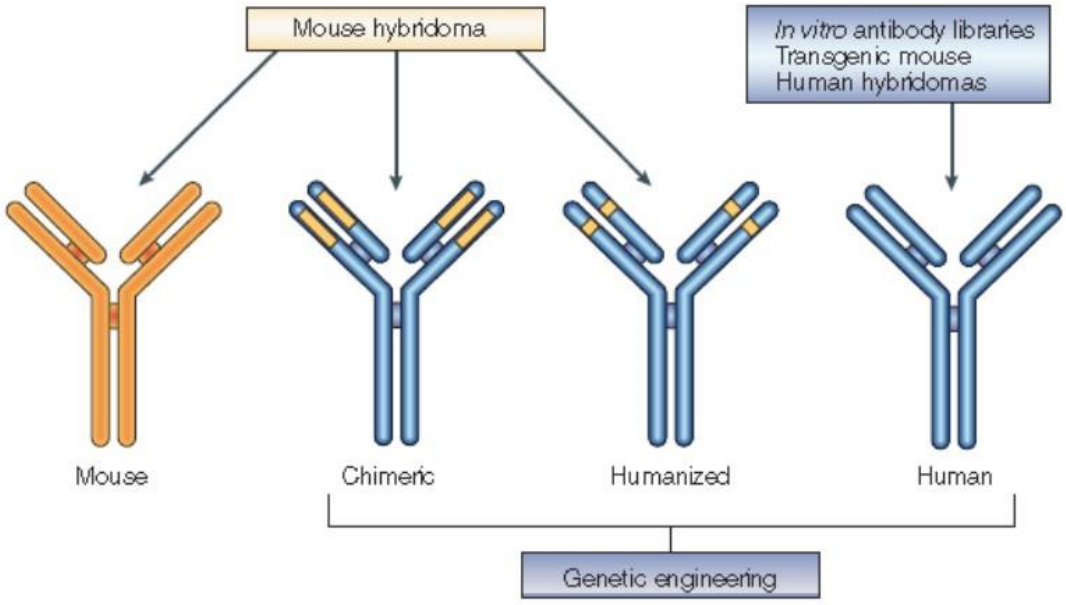

Figure 22: Towards fully human antibodies. The different antibody natures and their methods of generation. From Brekke and Sandlie, Nat. Rev. Drug Disc., 2003.

antibody-drug conjugates [42]. As a conclusion, evolutions in the technique allow for the generation of antibodies with various properties, which meet the needs of diagnosis and therapy.

4.4.1 Engineering

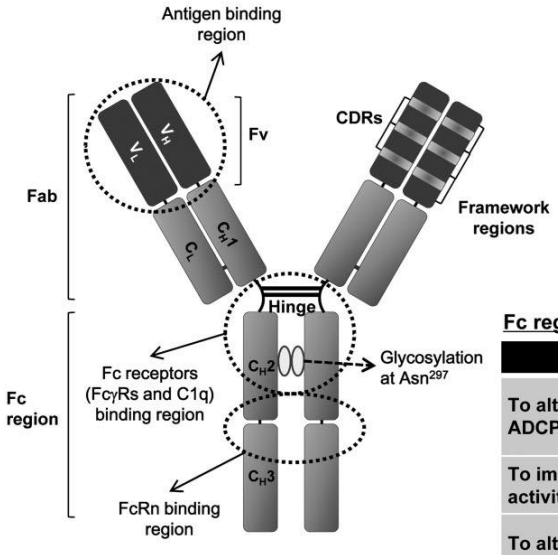

Variable region

Objectives of Engineering	Strategies of Engineering
To modulate Antigen binding affinity or specificity	• Random mutation in CDRs and high throughput screening • Rationale design in CDRs
To reduce immunogenicity	• Humanization or dehumanization of framework regions
To decrease elimination of IgG	• Mutation of variable region to lower the isoelectric point

Fc region

Objectives of Engineering	Strategies of Engineering
To alter effector functions (ADCC, ADCP and CDC)	• Sequence alteration in Fc region • Modified glycosylation (non fucosylation, Aglycosylation)
To improve an anti-inflammatory activity	• Introduction of sialylated glycans
To alter half-life (pharmacokinetic)	• Sequence alteration in Fc regions (FcRn binding region)
To construct antibody based drugs or toxins To label a radioisotope	• Fc fusion to target molecules • Introduction of Cys residue

Figure 23: Structure of an immunoglobulin G and the different engineering strategies for each region. From Jeong et al., 2011, Biotechnology Journal.

Figure 23 summarizes the different antibody engineering strategies; they mainly concern either the Fv regions or the Fc fragment.

Genetic engineering of the variable regions permits to transfer one antibody specificity into the structure of another: it is the principle of chimerization, where Fv regions of a mouse antibody of known specificity are combined to a human structure. Similarly, humanization can be operated by grafting only the hypervariable regions of interest inside the framework sequence[43,44]. Resurfacing subsequently allows to refine the process by replacing the solvent-accessible amino acids of the structure by “more human” ones[45,46], potentially decreasing immunogenicity and tuning pharmacokinetic properties. It has also been observed that the immunogenicity of human antibodies can be reduced by mutating potentially reactive typical B-cell or T-cell epitopes[47]. Finally, random mutagenesis of the hypervariable regions can be used as a way to tune the antibody affinity.

Alternatively, or concurrently, Fc fragment engineering can be used to alter the Ab pharmacokinetic properties or effector functions. These diverse functions, mediated by residues located in the hinge region and CH2 constant domain of an Ab, can be tuned by modifying the Fc structure, its aa sequence or its glycosylation motifs[48]. Indeed, the Fc fragment of an IgG is responsible for highly specific binding to Fc γ receptors (FcγR) that mediate antibody-dependent cellular cytotoxicity (ADCC). It has been proven that FcγR

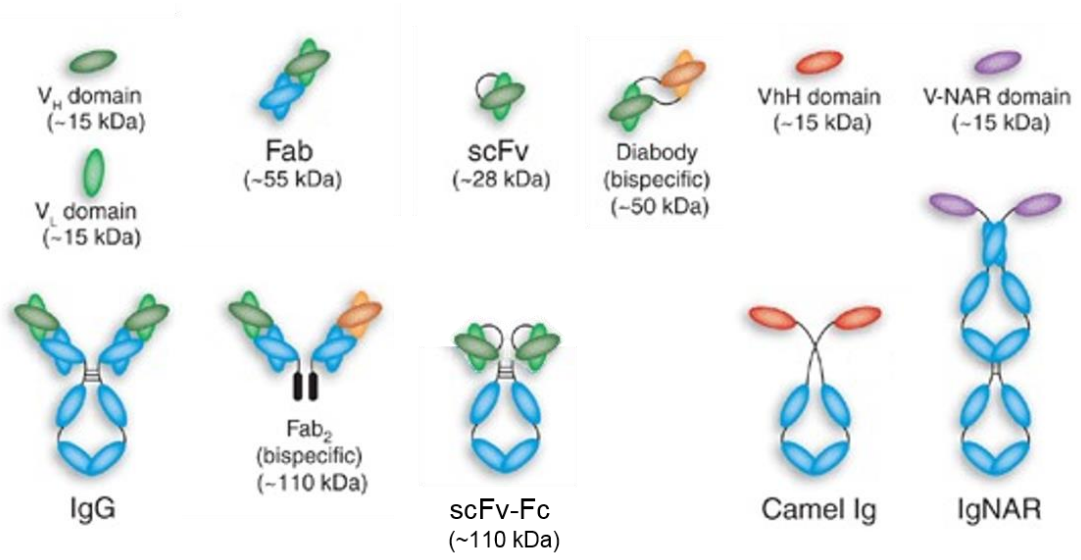

Figure 24: Common antibody formats used for imaging or therapy. Ig: immunoglobuline; VH: variable heavy domain; VL: variable light domain; Fab: fragment antigen binding; scFv: single chain fragment variable; Fc: fragment cristalizable; IgNA : Ig nurse shark antigen receptor; kDa: kiloDaltons. Modified from Holliger and Hudson, Nature Biotech. 2005.

polymorphisms can influence the therapeutic activity of IgG[49]. Because patients receptors cannot be modified indeed, the idea was to tune the Fc fragment to improve its affinity for FcγR and enhance its ADCC activity[50–52], or to the complement components (notably C1q), triggering complement-dependent cytotoxicity (CDC), or both[53]. Because the neonate receptor FcRn is responsible for the recycling of IgG, prolongs their serum half-life, and their transcytosis-mediated tissular distribution[54], it can also be modified to tune Ab elimination rate[55]. The Fc fragment has also been used to attach exogenous compounds: cytotoxic drugs for cancer therapy[56], or tracers for imaging[57].

Finally, the Ab sequence can be adapted to the production system to improve the production efficiency. The genetic code is redundant: there are 64 different codons (including 3 stop codons) but only 20 different translated amino acids. This degeneration allows a biased codon use: different organisms will preferentially use one of the codons encoding one same amino acid over the others. This means the sequence of a protein can be adapted to include the preferred codons corresponding to each aa in a given production system. This technique improves the production yield and folding.

4.4.2 Antibody formats

Although for most therapeutic applications the Fc fragment is needed to trigger the effector function of the Ab, for other applications such as imaging the Fc function is not desirable. Indeed a long serum half-life results in poor signal-to-noise ratio[57]. Worse, inappropriate activation of Fc receptor–expressing cells can lead to massive cytokine release and associated toxic effects.

In addition, effective antibody targeting involves that the antibodies should be able to enter the tissues of interest. Small antibody fragments do better than full antibodies in this respect

as they exhibit higher diffusion and tissue penetration and ability to access sites with high steric bulk that prevent massive molecules from entering[47]. Furthermore, due to their small size and non-glycosylated structure, they are also easier and less expensive to produce.

In this perspective, Fab and F(ab')2 fragments have been obtained by enzymatic digestion (respectively by papain and pepsin) of a full IgG. The era of genetic engineering has subsequently unveiled a whole world of possible antibody fragments, each with different advantages.

Single chain fragment variable (scFv) are composed of the VH and VL domains of an immunoglobulin, with the three CDRs and framework regions. It does not include the CH1 region with disulfide bounds and is instead joined by a flexible polypeptide linker typically composed of glycines and serines. It retains the specific, monovalent, antigen-binding affinity of the corresponding Fab, while showing improved pharmacokinetics for tissue penetration [44].

In 1989, Ward et al. proposed an even smaller fragment, the mouse single variable (V) domains, which because of their smaller size, could potentially target cryptic epitopes [58]. They were shown to be functional, unfortunately their affinity was hardly as high as it of the parental antibody, certainly because mouse antibodies are matured as an association of VH and VL. On the contrary, naturally-occuring heavy chain immunoglobulins were then described in camelids (camels and llamas) and cartilaginous fish (wobbegong and nurse sharks), and respectively called VHH and V-NAR. They are high-affinity single V-like domains mounted on an Fc equivalent constant domain framework [59]. In addition, VHH and V-NAR domains display long surface loops, often larger than their murine and human counterpart, that are able to penetrate cavities in target antigens, such as enzyme active sites and canyons in viral and infectious disease biomarkers. “Camelized” human VH domains were engineered for this application [60]. Due to their extremely small size, they exhibit a quick, mainly renal clearance.

The main drawback of synthetic monovalent fragments is the decrease in their avidity (global particle affinity) compared to a bivalent IgG. To circumvent this loss, it is possible to associate antibody fragments into dimers, trimers or more to generate oligovalent antibody fragments with increased avidity and the ability to crosslink target molecules. The diabodies, described in 1993, are scFv fragments with two different antigen specificities, one directed against the target and one directed against effector molecules such as complement or Fc receptors. Hence, they are able to display the effector functions of complete antibodies [61].

As a conclusion, each different antibody format displays specific pharmacokinetics and pharmacodynamics as well as activity. Table 4 recapitulates the major properties for each format.

Table 4: Pros and cons of common antibody formats. Modified from Kaur et al., 2012, Cancer Letters.

	Full IgG	**Fab**	**F(ab)'$_2$**	**Diabodies**	**scFv**	**scFv-Fc**
Reactivity / affinity	+++	+	++	+++	+	++
Pharmacokinetics	Long circulation time	High tissue penetration Fast blood clearance	Good tissue penetration Fast blood clearance	Good tissue penetration and longer retention	High tissue penetration Fast blood clearance	High tissue uptake Slow clearance
Imaging contrast	- (high background)	+++	+	++	+++	+
Immunogenicity	+ (HAMA response)	--	-	-	--	+
Remarks	High cost	Renal clearance	Renal clearance		Renal and hepatic clearance	Better therapeutic efficacy

4.4.3 Production systems

To efficiently produce an immunoglobulin, transcription and translation are the key points: an appropriately designed expression vector will ensure efficient transcription of the antibody genes; on the other hand, a cell line competent in translating antibody mRNAs, assembling and modifying the antibody at high rates with minimal accumulation of incorrect proteins, and having sufficient secretory capacity, will achieve good production yields. The necessity of post-translational processing of the recombinant antibodies may be another argument [62].

4.4.3.1 Prokaryotic

Bacterial expression systems are wildly used for their fast growth, inexpensive and straightforward culture conditions. Among them, *Escherichia coli* is a host of choice because of its well-studied genetics. It has become the most important production system for recombinant proteins, notably thanks to the improvement of extracellular production capacity, allowing for a marked increase in the yields in the gram per liter range [63–65].

However, because antibodies are large, dimeric proteins, their post-translational assembly requires favorable conditions. One of the earliest attempts by Cabilly et al.[66] reported the production of an anti-carcinoembryonic antigen (CEA) Fab fragment as separate heavy and light chains. Both polypeptides accumulated as insoluble inclusion bodies in *E. coli*, before subsequent assembly *in vitro*. However, previous experiments in our team[67] showed that biological activity could not be recovered from inclusion bodies-processed fragments. Despite improvements in the production system, only a small proportion of active scFv, produced in the cytoplasm of cells, could be retrieved.

In 1988, Better and colleagues[68], and Skerra and Pluckthun[69] proposed the production in *E. coli* of antibody fragments, respectively a chimeric human carcinoma cell line-reactive Fab, and a phosphorylcholine-binding scFv. The heavy and light –or single- chains of the Ab fragments were co-/expressed and secreted into the periplasmic space which oxidizing environment would allow for a correct folding and assembly. The scFv proved as active as the parent IgG it was derived from; while the Fab produced by this method had a preserved activity compared to its enzymatic digestion-derived counterpart.

The optimization of the signal sequence to trigger the secretion of the products greatly simplified their purification by affinity chromatography; along with improvements in the culture conditions, it permitted to increase the active Ab fragments yields in *E. coli* [70]. However, the major drawback of this expression system remains the risk of protein misfolding or aggregation[71]. The overall yields in E. coli ranged from the microgram to a few grams per liter.

Because of their lack of outer membrane, Gram positive bacteria have been proposed as an alternative production system. Members of the *Bacillus* genre were able to produce active antibody fragments: for example *B. brevis*[72,73], *B. subtilis*[74,75], and *B. megaterium*[76,77]. Lactobacilli are another genre of interest for antibody production; indeed, their generally regarded as safe (GRAS) status allows for *in situ* delivery of antibodies of interest for antibacterial[78–80] or antiviral therapy[79,80].

Despite their low cost and uncomplicated culture, bacterial systems conserve the major disadvantage of their prokaryotic nature: they are unable to produce elaborate post-translational modifications, such as glycosylation, which may impair the antibody activity.

4.4.3.2 Monocellular eukaryotes: yeasts

Yeasts combine the advantages of unicellular organisms with those of eukaryotes: short generation time, simple nutritional requirements, and ease of genetic manipulation, yet an elaborate protein production machinery allowing for correct folding, post-translational processing and excretion of complicated products including full IgGs. Additionally, because they have been used in human alimentation throughout history and are well-known, they benefit from the GRAS status [70].

P. pastoris is the most used production system in this category. It presents indeed a number of valuable features: it can grow to high cell densities, allowing for good production yields; it does not massively secrete its own proteins, yet has efficient secretion pathways that can be used for the recombinant protein, which simplifies the subsequent purification steps[81]; it is also able to use methanol as a carbon source, permitting to use this substrate as a production inducer via the strong promoter alcohol oxidase 1 (AOX1). Additionally, *P. pastoris* generates glycosylation profiles that resemble those seen in human [48,70], as opposed to other yeasts, notably *S. cerevisiae*, that tend to introduce hypermannosylated structures, including in sites non glycosylated in the native mammalian protein, which is at risk of

increasing immunogenicity or triggering adverse reactions in human [82]. Usual yields in this production system range from a few milligrams to a gram per liter.

To further improve this process, glyco-engineered *P. pastoris* strains have been generated which produce humanized glycosylation patterns[83,84], allowing for the production of IgG with preserved Fc effector function[85,86]. However, most antibodies produced in this system are small fragments for which glycosylation is not pivotal of their function.

4.4.3.3 Insect cells

Recombinant protein production in insect cells relies on their transfection with viruses from the *Baculoviridae* family. Baculoviruses are arthropod-specific viruses with a restricted host range and are considered safe for humans and mammalians in general.

Non-essential genes involved in the late viral replication cycle are replaced by constructs of interest via a homologous recombination. Large heterologous genes of more than 20 kb can be inserted by this method and generate stable recombinant viruses. These are then used to infect an insect cell line, the most frequently used being Sf-9 and Sf-21 of *Spodoptera frugiperda*, DS2 cells of *Drosophila melanogaster*, or High Five cells (BTI-TN-5B1-4) of *Trichopulsia ni* [70,87]. Insect cells generally produce milligrams to dozens of milligrams of antibodies per liter of culture.

Although full IgGs were generated that were able to trigger proper CDC[88,89] and ADCC function[90], the Lepidopteran glycosylation motifs differ from the mammalian ones. Indeed, they express lower levels of various transferase enzymes, leading to shorter mannose motifs and partially fucosylated glycans compared to mammals. Additionally, a potentially allergenic epitope (α1,3-branched fucose), characteristic of several insect cell lines, may pose a threat to clinical use[91]. To circumvent these, “humanization” was proposed either by integrating the cDNA for the missing glycosyltransferases into the cellular or the viral genome[92].

4.4.3.4 Mammalian cells

As of November 2014, over 90% of recombinant antibodies on the market were produced in mammalian cells [12]. Gold-standard for the production of functional recombinant human proteins are Chinese hamster ovary (CHO) or human embryonic kidney (HEK293) cell line[93]. Both of them, plus mouse myeloma-derived (NS0), baby hamster kidney (BHK), and human retinal cells, have obtained regulatory approval for recombinant protein production [94]. Despite their relatively high cost and exigent handling, the elaborate cellular apparatus for folding, secretion and post-translational modifications of mammalian cells results in high quality product, minimizing the subsequent need for downstream processing. Additionally, the once-concerning risks of contamination by pathogens or bovine spongiform encephalopathy agents have been well-controlled by the implementation of Good Manufacturing Practice (GMP)[70].

When considering protein production for research purposes, transient transfection of HEK293 cells is an adequate choice because of its rapid establishment and sufficient production yield. However, it requires high amounts of purified DNA, which make it difficult to scale-up. For larger production purposes, the generation of a stable recombinant cell line is preferable although more time-consuming[95]. Amongst the available cell lines for stable expression, HEK293 and CHO, adapted to suspension and serum-free cultivation, are the most commonly used. Other lines such as HeLa (Henrietta Lacks), baby hamster kidney (BHK), and human PER.C6 can also be used for stable recombinant cell line generation. However, in this regard, CHO seems to be superior for large-scale protein production[95] and much efforts have been deployed to enhance their productivity[96].

Various elements influence the expression levels of a transgene: the promoter used, the choice of the selection agent, the existence of splicing sites, and the adaptation of the sequence to the host codon use bias (see 4.4.1). In stably transfected clones, the transgene insertion site, the culture medium composition, and genetic cell line engineering modulate the recombinant protein productivity[94]. The production levels in mammalian cells are highly disparate, but generally range from milligrams to hundreds of milligrams per liter.

4.4.3.5 Alternative

Transgenic plants have been proposed as an alternative for the production of recombinant proteins. Despite the relatively low productivity (from microgram to a hundred milligram per kilo) exhibited so far by this system, the method is easy to scale up, which lowers the relative production cost for large quantities. Furthermore, expression in leaves or seeds could theoretically permit short- or long-term storage in harvested material pending purification[97]. The technology consists in transforming dicotyledonous plants with a gene contained in the tumor-inducing plasmid of the plant pathogen *Agrobacterium tumefaciens*. Under the action of virulence (vir) genes contained in the vector, the transgene is integrated into the plant genome by non-homologous recombination. Tobacco plants like *Nicotiana tabacum* or *N. benthamiana* are most commonly used for Ab production[70]. Antibody fragments were produced in this plant either via transient[98] or stable[99] expression. Other options include production of Ab fragments in *Arabidopsis thaliana*[98], or full IgG in maize[100].

Numerous studies have proposed transgenic mice for the production of chimeric, humanized, or human immunoglobulins. Besides these, other species were assessed for the large scale production of polyclonal antibody serum with reduced immunogenicity, for example in cattle [101], or rabbit [102]. Other approaches relied on a tissue-specific transgene expression to produce immunoglobulins. For example in eggs [103] because of its advantages as a production system: up-scalable, potential high productivity; or in milk, where the direct secretion of anti-viral antibodies would be a valuable clinical tool for the treatment of gastro-enteric infections in neonates for example[104,105]. However promising, to date none of these approaches has yet reached the market.

References

1. Berche, P. *L'histoire des microbes*. (John Libbey Eurotext, 2007).

2. Darmon, P. *Pasteur*. (Fayard, 1995).

3. Behring, null & Kitasato, null. [On the development of immunity to diphtheria and tetanus in animals]. *Dtsch. Med. Wochenschr. 1946* **90,** 2183 (1965).

4. Kourislky, P. BEHRING EMIL ADOLF VON - (1854-1917). *Encyclopædia Universalis [en ligne]* Available at: http://www.universalis.fr/encyclopedie/emil-adolf-von-behring/. (Accessed: 17th October 2016)

5. Fougereau, M. Les anticorps monoclonaux : un fantastique arsenal thérapeutique en plein devenir. *médecine/sciences* **25,** 997–998 (2009).

6. Watier, H. De la sérothérapie aux anticorps recombinants « nus »: Plus d'un siècle de succès en thérapie ciblée. *médecine/sciences* **25,** 999–1009 (2009).

7. Edelman, G. M., Benacerraf, B., Ovary, Z. & Poulik, M. D. Structural differences among antibodies of different specificities. *Proc. Natl. Acad. Sci.* **47,** 1751–1758 (1961).

8. Porter, R. R. Chemical structure of γ-globulin and antibodies. *Br. Med. Bull.* **19,** 197–201 (1963).

9. Cohen, S. & Porter, R. R. in *Advances in Immunology* (ed. Humphrey, F. J. D. and J. H.) **4,** 287–349 (Academic Press, 1964).

10. Köhler, G. & Milstein, C. Continuous cultures of fused cells secreting antibody of predefined specificity. *Nature* **256,** 495–497 (1975).

11. Beck, A., Wurch, T., Bailly, C. & Corvaia, N. Strategies and challenges for the next generation of therapeutic antibodies. *Nat. Rev. Immunol.* **10,** 345–352 (2010).

12. Ecker, D. M., Jones, S. D. & Levine, H. L. The therapeutic monoclonal antibody market. *mAbs* **7,** 9–14 (2015).

13. Hornick, C. L. & Karuch, F. Antibody affinity. 3. The role of multivalance. *Immunochemistry* **9,** 325–340 (1972).

14. Edelman, G. M. Antibody Structure and Molecular Immunology. *Science* **180,** 830–840 (1973).

15. Krapp, S., Mimura, Y., Jefferis, R., Huber, R. & Sondermann, P. Structural Analysis of Human IgG-Fc Glycoforms Reveals a Correlation Between Glycosylation and Structural Integrity. *J. Mol. Biol.* **325,** 979–989 (2003).

16. Reusch, D. & Tejada, M. L. Fc glycans of therapeutic antibodies as critical quality attributes. *Glycobiology* **25,** 1325–1334 (2015).

17. Higel, F., Seidl, A., Sörgel, F. & Friess, W. N-glycosylation heterogeneity and the influence on structure, function and pharmacokinetics of monoclonal antibodies and Fc fusion proteins. *Eur. J. Pharm. Biopharm.* **100,** 94–100 (2016).

18. Lanzavecchia, A., Corti, D. & Sallusto, F. Human monoclonal antibodies by immortalization of memory B cells. *Curr. Opin. Biotechnol.* **18,** 523–528 (2007).

19. Guillot-Chene, P., Lebecque, S. & Rigal, D. Vers une maîtrise industrielle du clonage des lymphocytes B humains pour la fabrication des anticorps monoclonaux issus du répertoire humain. *Ann. Pharm. Fr.* **67,** 182–186 (2009).

20. McCafferty, J., Griffiths, A. D., Winter, G. & Chiswell, D. J. Phage antibodies: filamentous phage displaying antibody variable domains. *Nature* **348,** 552–554 (1990).

21. Carlton, R. M. Phage therapy: past history and future prospects. *Arch. Immunol. Ther. Exp.-Engl. Ed.-* **47,** 267–274 (1999).

22. Brüssow, H. Phage therapy: the Escherichia coli experience. *Microbiology* **151,** 2133–2140 (2005).

23. Nobrega, F. L., Costa, A. R., Kluskens, L. D. & Azeredo, J. Revisiting phage therapy: new applications for old resources. *Trends Microbiol.* **23,** 185–191 (2015).

24. Wagner, P. L. & Waldor, M. K. Bacteriophage Control of Bacterial Virulence. *Infect. Immun.* **70,** 3985–3993 (2002).

25. Brüssow, H., Canchaya, C. & Hardt, W.-D. Phages and the Evolution of Bacterial Pathogens: from Genomic Rearrangements to Lysogenic Conversion. *Microbiol. Mol. Biol. Rev.* **68,** 560–602 (2004).

26. Smith, G. P. Filamentous fusion phage: novel expression vectors that display cloned antigens on the virion surface. *Science* **228,** 1315–1317 (1985).

27. Pasqualini, R. & Ruoslahti, E. Organ targeting In vivo using phage display peptide libraries. *Nature* **380,** 364–366 (1996).

28. Deramchia, K. *Interrogation de la plaque d'athérome par phage---display in vivo : une approche pour un ciblage moléculaire à l'aide d'anticorps humains armés pour l'imagerie et la thérapie*. (Bordeaux 2, 2010).

29. Deramchia, K. *et al.* In Vivo Phage Display to Identify New Human Antibody Fragments Homing to Atherosclerotic Endothelial and Subendothelial Tissues. *Am. J. Pathol.* **180,** 2576–2589 (2012).

30. Owens, R. J. & Young, R. J. The genetic engineering of monoclonal antibodies. *J. Immunol. Methods* **168,** 149–165 (1994).

31. Jacobin, M.-J. *et al.* Human IgG monoclonal anti-alpha(IIb)beta(3)-binding fragments derived from immunized donors using phage display. *J. Immunol. Baltim. Md 1950* **168,** 2035–2045 (2002).

32. Gram, H. *et al.* In vitro selection and affinity maturation of antibodies from a naive combinatorial immunoglobulin library. *Proc. Natl. Acad. Sci.* **89,** 3576–3580 (1992).

33. Barbas, C. F., Bain, J. D., Hoekstra, D. M. & Lerner, R. A. Semisynthetic combinatorial antibody libraries: a chemical solution to the diversity problem. *Proc. Natl. Acad. Sci. U. S. A.* **89,** 4457–4461 (1992).

34. Philibert, P. *et al.* A focused antibody library for selecting scFvs expressed at high levels in the cytoplasm. *BMC Biotechnol.* **7,** 81 (2007).

35. Chen, G. & Sidhu, S. S. Design and generation of synthetic antibody libraries for phage display. *Methods Mol. Biol. Clifton NJ* **1131,** 113–131 (2014).

36. Brüggemann, M. *et al.* A repertoire of monoclonal antibodies with human heavy chains from transgenic mice. *Proc. Natl. Acad. Sci. U. S. A.* **86,** 6709–6713 (1989).

37. Taylor, L. D. *et al.* A transgenic mouse that expresses a diversity of human sequence heavy and light chain immunoglobulins. *Nucleic Acids Res.* **20,** 6287–6295 (1992).

38. Taylor, L. D. *et al.* Human immunoglobulin transgenes undergo rearrangement, somatic mutation and class switching in mice that lack endogenous IgM. *Int. Immunol.* **6,** 579–591 (1994).

39. Green, L. L. *et al.* Antigen–specific human monoclonal antibodies from mice engineered with human Ig heavy and light chain YACs. *Nat. Genet.* **7,** 13–21 (1994).

40. Lonberg, N. *et al.* Antigen-specific human antibodies from mice comprising four distinct genetic modifications. *Nature* **368,** 856–859 (1994).

41. Larivière, M. Les anticorps monoclonaux dans le domaine de la santé. (2013).

42. Reichert, J. M. Antibodies to watch in 2016. *mAbs* **8,** 197–204 (2016).

43. Jones, P. T., Dear, P. H., Foote, J., Neuberger, M. S. & Winter, G. Replacing the complementarity-determining regions in a human antibody with those from a mouse. *Nature* **321,** 522–525 (1986).

44. Peterson, N. C. Advances in Monoclonal Antibody Technology: Genetic Engineering of Mice, Cells, and Immunoglobulins. *ILAR J.* **46,** 314–319 (2005).

45. Novotný, J. *et al.* Antigenic determinants in proteins coincide with surface regions accessible to large probes (antibody domains). *Proc. Natl. Acad. Sci. U. S. A.* **83,** 226–230 (1986).

46. Staelens, S. *et al.* Humanization by variable domain resurfacing and grafting on a human IgG4, using a new approach for determination of non-human like surface accessible framework residues based on homology modelling of variable domains. *Mol. Immunol.* **43,** 1243–1257 (2006).

47. Brekke, O. H. & Sandlie, I. Therapeutic antibodies for human diseases at the dawn of the twenty-first century. *Nat. Rev. Drug Discov.* **2,** 52–62 (2003).

48. Jeong, K. J., Jang, S. H. & Velmurugan, N. Recombinant antibodies: Engineering and production in yeast and bacterial hosts. *Biotechnol. J.* **6,** 16–27 (2011).

49. Cartron, G. *et al.* Therapeutic activity of humanized anti-CD20 monoclonal antibody and polymorphism in IgG Fc receptor FcγRIIIa gene. *Blood* **99,** 754–758 (2002).

50. Stavenhagen, J. & Koenig, S. Engineering fc antibody regions to confer effector function. (2007).

51. Umana, P. Glycosylation engineering of antibodies for improving antibody-dependent cellular cytotoxicity. (2011).

52. Beliard, R. *et al.* Monoclonal antibodies with enhanced adcc function. (2012).

53. Dall'acqua, W., Wu, H., Damschroder, M. & Casa-Finet, J. Modulation of antibody effector function by hinge domain engineering. (2008).

54. Magdelaine-Beuzelin, C., Ohresser, M. & Watier, H. FcRn, un récepteur d'IgG aux multiples facettes. *médecine/sciences* **25,** 1053–1056 (2009).

55. Igawa, T., Ishii, S., Maeda, A. & Nakai, T. Antibodies with modified affinity to fcrn that promote antigen clearance. (2011).

56. Beck, A. & Reichert, J. M. Antibody-drug conjugates. *mAbs* **6,** 15–17 (2014).

57. Kaur, S. *et al.* Recent Trends in Antibody-based Oncologic Imaging. *Cancer Lett.* **315,** 97–111 (2012).

58. Ward, E. S., Güssow, D., Griffiths, A. D., Jones, P. T. & Winter, G. Binding activities of a repertoire of single immunoglobulin variable domains secreted from Escherichia coli. *Nature* **341,** 544–546 (1989).

59. Hamers-Casterman, C. *et al.* Naturally occurring antibodies devoid of light chains. *Nature* **363,** 446–448 (1993).

60. Riechmann, L. & Muyldermans, S. Single domain antibodies: comparison of camel VH and camelised human VH domains. *J. Immunol. Methods* **231,** 25–38 (1999).

61. Holliger, P., Prospero, T. & Winter, G. 'Diabodies': small bivalent and bispecific antibody fragments. *Proc. Natl. Acad. Sci. U. S. A.* **90,** 6444–6448 (1993).

62. Birch, J. R. & Racher, A. J. Antibody production. *Adv. Drug Deliv. Rev.* **58,** 671–685 (2006).

63. Schmidt, F. R. Recombinant expression systems in the pharmaceutical industry. *Appl. Microbiol. Biotechnol.* **65,** 363–372 (2004).

64. Terpe, K. Overview of bacterial expression systems for heterologous protein production: from molecular and biochemical fundamentals to commercial systems. *Appl. Microbiol. Biotechnol.* **72,** 211 (2006).

65. Ni, Y. & Chen, R. Extracellular recombinant protein production from Escherichia coli. *Biotechnol. Lett.* **31,** 1661–1670 (2009).

66. Cabilly, S. *et al.* Generation of antibody activity from immunoglobulin polypeptide chains produced in Escherichia coli. *Proc. Natl. Acad. Sci. U. S. A.* **81,** 3273–3277 (1984).

67. Robert, R., Noubhani, A., Jacobin, M., Santarelli, X. & Clofent-Sanchez, G. Improvement in production and purification bioprocesses of bacterially expressed anti-alphaIIbbeta3 human single-chain FV antibodies. *J. Chromatogr. B Analyt. Technol. Biomed. Life. Sci.* **818,** 43–51 (2005).

68. Better, M., Chang, C. P., Robinson, R. R. & Horwitz, A. H. Escherichia coli secretion of an active chimeric antibody fragment. *Science* **240,** 1041–1043 (1988).

69. Skerra, A. & Pluckthun, A. Assembly of a functional immunoglobulin Fv fragment in Escherichia coli. *Science* **240,** 1038–1041 (1988).

70. Frenzel, A., Hust, M. & Schirrmann, T. Expression of Recombinant Antibodies. *Front. Immunol.* **4,** (2013).

71. Makrides, S. C. Strategies for achieving high-level expression of genes in Escherichia coli. *Microbiol. Rev.* **60,** 512–538 (1996).

72. Inoue, Y. *et al.* Efficient production of a functional mouse/human chimeric Fab' against human urokinase-type plasminogen activator by Bacillus brevis. *Appl. Microbiol. Biotechnol.* **48,** 487–492 (1997).

73. Shiroza, T. *et al.* Production of a single-chain variable fraction capable of inhibiting the Streptococcus mutans glucosyltransferase in Bacillus brevis: construction of a chimeric shuttle plasmid secreting its gene product. *Biochim. Biophys. Acta BBA - Gene Struct. Expr.* **1626,** 57–64 (2003).

74. Wu, S.-C., Ye, R., Wu, X.-C., Ng, S.-C. & Wong, S.-L. Enhanced Secretory Production of a Single-Chain Antibody Fragment from Bacillus subtilis by Coproduction of Molecular Chaperones. *J. Bacteriol.* **180,** 2830–2835 (1998).

75. Wu, S.-C. *et al.* Functional Production and Characterization of a Fibrin-Specific Single-Chain Antibody Fragment from Bacillus subtilis: Effects of Molecular Chaperones and a Wall-Bound Protease on Antibody Fragment Production. *Appl. Environ. Microbiol.* **68,** 3261–3269 (2002).

76. Jordan, E., Al-Halabi, L., Schirrmann, T., Hust, M. & Dübel, S. Production of single chain Fab (scFab) fragments in Bacillus megaterium. *Microb. Cell Factories* **6,** 38 (2007).

77. David, F. *et al.* Antibody production in Bacillus megaterium: Strategies and physiological implications of scaling from microtiter plates to industrial bioreactors. *Biotechnol. J.* **6,** 1516–1531 (2011).

78. Krüger, C. *et al.* In situ delivery of passive immunity by lactobacilli producing single-chain antibodies. *Nat. Biotechnol.* **20,** 702–706 (2002).

79. Chancey, C. J. *et al.* Lactobacilli-Expressed Single-Chain Variable Fragment (scFv) Specific for Intercellular Adhesion Molecule 1 (ICAM-1) Blocks Cell-Associated HIV-1 Transmission across a Cervical Epithelial Monolayer. *J. Immunol.* **176,** 5627–5636 (2006).

80. Pant, N. *et al.* Lactobacilli Expressing Variable Domain of Llama Heavy-Chain Antibody Fragments (Lactobodies) Confer Protection against Rotavirus-Induced Diarrhea. *J. Infect. Dis.* **194,** 1580–1588 (2006).

81. Vallet-Courbin, A. *et al.* A Recombinant Human Anti-platelet scFv Antibody Produced in Pichia Pastoris for Atheroma Targeting. *submitted*

82. Grinna, L. S. & Tschopp, J. F. Size distribution and general structural features of N-linked oligosaccharides from the methylotrophic yeast, Pichia pastoris. *Yeast Chichester Engl.* **5,** 107–115 (1989).

83. Choi, B.-K. *et al.* Use of combinatorial genetic libraries to humanize N-linked glycosylation in the yeast Pichia pastoris. *Proc. Natl. Acad. Sci. U. S. A.* **100,** 5022–5027 (2003).

84. Hamilton, S. R. *et al.* Humanization of Yeast to Produce Complex Terminally Sialylated Glycoproteins. *Science* **313,** 1441–1443 (2006).

85. Li, H. *et al.* Optimization of humanized IgGs in glycoengineered Pichia pastoris. *Nat. Biotechnol.* **24,** 210–215 (2006).

86. Potgieter, T. I. *et al.* Production of monoclonal antibodies by glycoengineered Pichia pastoris. *J. Biotechnol.* **139,** 318–325 (2009).

87. Juliant, S. *et al.* Engineering the baculovirus genome to produce galactosylated antibodies in lepidopteran cells. *Methods Mol. Biol. Clifton NJ* **988,** 59–77 (2013).

88. zu Putlitz, J. *et al.* Antibody Production in Baculovirus-Infected Insect Cells. *Nat. Biotechnol.* **8,** 651–654 (1990).

89. Rae Jin, B., Jeih Ryu, C., Kwon Kang, S., Hi Han, M. & Jeong Hong, H. Characterization of a murine-human chimeric antibody with specificity for the pre-S2 surface antigen of hepatitis B virus expressed in baculovirus-infected insect cells. *Virus Res.* **38,** 269–277 (1995).

90. Edelman, L. *et al.* Obtaining a functional recombinant anti-rhesus (D) antibody using the baculovirus–insect cell expression system. *Immunology* **91,** 13–19 (1997).

91. Hsu, T.-A. *et al.* Differential N-Glycan Patterns of Secreted and Intracellular IgG Produced in Trichoplusia ni Cells. *J. Biol. Chem.* **272,** 9062–9070 (1997).

92. Cérutti, M. & Golay, J. Lepidopteran cells, an alternative for the production of recombinant antibodies? *mAbs* **4,** 294–309 (2012).

93. Fath, S. *et al.* Multiparameter RNA and Codon Optimization: A Standardized Tool to Assess and Enhance Autologous Mammalian Gene Expression. *PLOS ONE* **6,** e17596 (2011).

94. Wurm, F. M. Production of recombinant protein therapeutics in cultivated mammalian cells. *Nat. Biotechnol.* **22,** 1393–1398 (2004).

95. Hacker, D. L. & Balasubramanian, S. Recombinant protein production from stable mammalian cell lines and pools. *Curr. Opin. Struct. Biol.* **38,** 129–136 (2016).

96. Xiao, S., Shiloach, J. & Betenbaugh, M. J. Engineering cells to improve protein expression. *Curr. Opin. Struct. Biol.* **26,** 32–38 (2014).

97. Fiedler, U., Phillips, J., Artsaenko, O. & Conrad, U. Optimization of scFv antibody production in transgenic plants. *Immunotechnology* **3,** 205–216 (1997).

98. De Buck, S. *et al.* Production of camel-like antibodies in plants. *Methods Mol. Biol. Clifton NJ* **911,** 305–324 (2012).

99. McCormick, A. A. *et al.* Individualized human scFv vaccines produced in plants: humoral anti-idiotype responses in vaccinated mice confirm relevance to the tumor Ig. *J. Immunol. Methods* **278,** 95–104 (2003).

100. Rademacher, T. *et al.* Recombinant antibody 2G12 produced in maize endosperm efficiently neutralizes HIV-1 and contains predominantly single-GlcNAc N-glycans. *Plant Biotechnol. J.* **6,** 189–201 (2008).

101. Matsushita, H. *et al.* Triple Immunoglobulin Gene Knockout Transchromosomic Cattle: Bovine Lambda Cluster Deletion and Its Effect on Fully Human Polyclonal Antibody Production. *PLOS ONE* **9,** e90383 (2014).

102. Flisikowska, T. *et al.* Efficient Immunoglobulin Gene Disruption and Targeted Replacement in Rabbit Using Zinc Finger Nucleases. *PLOS ONE* **6,** e21045 (2011).

103. Zhu, L. *et al.* Production of human monoclonal antibody in eggs of chimeric chickens. *Nat. Biotechnol.* **23,** 1159–1169 (2005).

104. Castilla, J., Pintado, B., Sola, I., Sánchez-Morgado, J. M. & Enjuanes, L. Engineering passive immunity in transgenic mice secreting virus-neutralizing antibodies in milk. *Nat. Biotechnol.* **16,** 349–354 (1998).

105. Castilla, J., Sola, I., Pintado, B., Sánchez-Morgado, J. M. & Enjuanes, L. in *Coronaviruses and Arteriviruses* (eds. Enjuanes, L., Siddell, S. G. & Spaan, W.) 675–686 (Springer US, 1998).

Section 2

Research project

Foreword

The project presented in this section has started many years ago and will continue after I leave, for it is complex and mobilizes a broad set of expertise and know-how. In order to maintain a coherence in the description I present some of the results that were obtained either before I joined the team or with my help, but not as the main purpose of my PhD, along with the results of my project *per se*. To help the reader I will detail the situations here.

The library screening and antibody selection performed by Marie-Josée Jacobin-Valat[1] and Kamel Deramchia[2] during their respective PhD (*cf. infra*) provided me with a set of antibodies of interest for *in vitro* and *in vivo* screening.

The project of MRI imaging with functionalized VUSPIO nanoparticles had also started before I joined the team. At the time it concerned full IgG antibodies, conjugated in a non site-specific manner to the VUSPIO. It served as my training with the various techniques I had to master, and I performed *in vitro* validations and results analysis on this project, hence I am associated to the resulting publication in Nanomedicine[3].

My project involved the use of antibody fragments: scFv-Fc were conjugated to fluorescent dyes before injection, as a proof of concept for *in vivo* targeting of atheroma with these antibodies, and for fluorescent imaging. Then scFv fragments were produced[4] and used for site-specific grafting by two strategies, leading to *in vitro* validation and even *in vivo* injection. The use of targeted VUSPIO, multi-functionalized by this method, showed significant improvement in target detection *in vitro*, and was also assessed *in vivo*, in a bimodal imaging setting. These results were submitted for publication.

5 Design of the project

5.1 Uncovering and targeting molecular markers

The team I joined for this project had previous knowledge and know-how with phage display selection of antibodies. Over the years, they have constructed and screened human libraries of different types (immune or semi-synthetic), discovering several antibodies of interest in the field of cardiovascular pathologies. Two of the selections will be presented here.

5.1.1 Phage display selection

A first selection was operated *in vitro* from an immune library on a known target: platelets. The idea at the time was to target thrombus, it later revealed more powerful for atheroma detection. A second setting searched for new markers of atheroma, proceeding to *in vivo* selection on animal models from a semi-synthetic library with broad specificity.

5.1.1.1 In vitro selection of TEG4 [1]

The main antibody for this project, called TEG4, was selected for specific platelet binding; it targets the integrin αIIbβ3 which plays a critical role in platelet aggregation. The function of

αIIbβ3 in platelet aggregation depends upon its capacity to undergo activation, a transition from a low to a high affinity state for its ligands. This transformation allows αIIbβ3 to bind fibrinogen and von Willebrand factor (VWF), ligands that can bridge platelets together[5].

The immune library used was constructed from platelet-autoreactive patients. Briefly, the B cells of a polytransfused patient with autoimmune thrombocytopenic purpura (AITP) and possessing serum IgG Abs against αIIbβ3 were used to build a combinatorial library of single-chain Abs. Indeed, these patients having developed an immune response against human platelets are likely to possess Abs against a whole range of epitopes on αIIbβ3.

Spleen tissue from the patient was used as a source of mRNA for the generation of IgG libraries. The mRNA was retrotranscripted into cDNA and amplified using primers for the V regions. VH and VL (κ and λ) genes were separately cloned into the phagemid display vector pSEX81 and amplified in bacteria. Then, combinatorial phagemids were constructed by ligating H chain genes into κ- and λ L chain sublibraries. This generated two primary libraries, κ and λ, with diversities of $1.5\ 10^7$ and $2.7\ 10^7$, respectively. The final constructs were electroporated in *E. coli* XL-1 blue. Phagemid libraries containing both chains of recombinant scFv were then rescued by infection with M13KO7 helper phage.

The human anti-αIIbβ3 binding fragments went through a sequential selection on both activated platelets and Chinese hamster ovary (CHO) cells expressing αIIbβ3 locked in a high affinity state. Two rounds of panning were performed against activated platelets. A third round included a negative selection against resting αIIbβ3-expressing CHO cells, before positive selection of the remaining phages, against activated αIIbβ3-expressing CHO. This process allowed for the selection of several candidates.

Among them, the selected TEG4 phage Ab was found to compete with fibrinogen, the physiologic ligand of αIIbβ3, and to have a Kd value for its target of 2.6×10^{-6} M.

5.1.1.2 In vivo selection [2]

In order to address new markers, a different approach was used: a semi-synthetic library with a broad diversity was selected *in vivo* in animal models of the atherosclerotic condition.

This semi-synthetic scFv-fragment library was designed and constructed by P. Philibert and al. [6]. It was created using a single optimized framework from a very stable human scFv (named 13R4), by introducing CDR3 amino acid distribution similar to those naturally observed in human CDR3 loops. The library was constructed in the phagemide vector pCANTAB6, in fusion with the N-terminus of the minor pIII protein. Its diversity was about 1.5×10^9 different variants.

To select human phage-scFvs able to selectively home to atherosclerotic plaques, ApoE-/- mice were used. This model, maintained on a high cholesterol “western diet”, displays advanced lesion development mimicking the physiological aspects of the human coronary artery disease [7].

Three continuous flows were injected into the tail vein of an ApoE-/- mouse for 5 min, after which the animal was sacrificed and PBS was perfused via the heart to ensure phage clearance from the blood. Using three successive perfusions for each round should promote the chance for phages of interest not to be unspecifically adsorbed either on the luminal surface of endothelial cells or circulating proteins, and to avoid their clearance from the blood by the reticuloendothelial system [8]. Furthermore, during *in vivo* circulation a subtractive selection of non-specific fragments takes place naturally at the unaffected sites.

The aorta was then recovered from the aortic arch to the iliac bifurcation. Three different fractions were recovered: 1/ endothelium cell surface bound phages (F1 fraction), 2/ intra-tissular phage (F2 fraction) and 3/ internalized phages (F3 fraction), were separately rescued by infection of XL1-blue *E.coli*. The phage libraries were produced following super-infection with M13KO7 helper phage. Two additional rounds of selection and amplification into subsequent mice were performed in order to enrich the pool with specific antibodies.

The selected phage-Abs were then produced as scFv fragments and their reactivity confirmed via homogeneous time-resolved fluorescence (HTRF) assay for atheromatous protein binding and IHC on rabbit and human pathological aorta sections.

Two Abs issued from this selection were used in this work, H2.1 and C3.3. When first assessed by IHC, H2.1 stained areas rich in macrophage- and smooth muscle cell-derived foam cells, under the endothelium, and rich in necrotic cells adjacent to the internal elastic lamina in the advanced lesion. C3.3 scFv staining appeared much more localized beneath the endothelium, especially in lipid and necrotic cores.

5.2 Expression of selected fragments

Although the TEG4 Ab has been more extensively investigated and proven to be a good candidate for atheroma imaging, other selected clones also show great promises in this application and have been tested as well in the course of this work. Depending on the method used, the selected Abs were expressed in different formats and production systems, as summarized in Table 5.

Table 5: Antibody formats and expression systems used for this project. Our collaborators are acknowledged and corresponding publications stated for reference.

Clone	Format	Gross size	Structure	System	Collaborator	Published
TEG4	IgG4	150 kDa	Full IgG	Baculovirus, insect cells	Martine Cérutti, CNRS UPS3044, St Christol-Les-Alez	[3] See 6.1.2.1
TEG4	scFv-Fc	110 kDa	Two scFv fragments linked by a Fc "tail"	Baculovirus, insect cells	Martine Cérutti, CNRS UPS3044, St Christol-Les-Alez	

TEG4, C3	scFv-Fc	110 kDa	Two scFv fragments linked by a Fc "tail"	HEK free style, suspension	Alexandre Fontayne, LFB Biotechnologies, Lille	
TEG4	scFv 2C	30 kDa	2 cysteines residues at the N terminal end	Pichia pastoris	Majid Noubhani, Xavier Santarelli, ENSTBB, Bordeaux	[4] See 7.1.2.1
TEG4, C3, H2	scFv-Fc	110 kDa	Two scFv fragments linked by a Fc "tail"	E.coli, HEK adherent	Jeanny Laroche-Traineau, CNRS UMR5536, Bordeaux	See 6.2.2.1
TEG4, C3, H2	scFv-LPETG	30 kDa	scFv modified with an LPETG tag for Sortase conjugation	HEK free style, suspension	Shweta Jagdale, ACBD, Monash University, Melbourne Gilles Joucla, CBMN UMR 5248, Bordeaux	See 7.2.2.2

6 “Classical” probe-antibody conjugation

Antibodies contain amine side chains, mainly Lysine amino-acids, able to form covalent bonds with a variety of reactive groups. This process is often taken advantage of for functionalizing Ab.

6.1 Thiol – maleimide

This chapter describes the functionalization of ultrasmall iron nanoparticles called VUSPIO (described below) with the TEG4 Ab expressed under a full IgG4 format. The detailed methods and results are available in the article *Nanoparticles functionalized with an anti-platelet human antibody for in vivo detection of atherosclerotic plaque by magnetic resonance imaging*, published in *Nanomedicine* in 2015[3] and online supplementary data.

6.1.1 Principle

Maleimides possess a double bond able to react with sulfhydryl groups to form stable thioether bonds. This is an alkylation reaction, specific for thiols in the pH range of 6.5 to 7.5. For higher pH values, cross-reactivity with amino groups may take place [9]. Both the maleimide and subsequent thioether functions are also subject to hydrolysis, which typically happens faster when the pH rises.

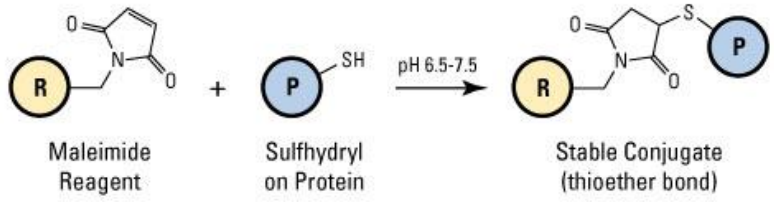

Figure 25: General outline for the thiol - maleimide conjugation reaction. From www.thermofisher.com.

6.1.2 Material and methods

6.1.2.1 TEG4 rIg4 antibody

For this study, TEG4 Ab was produced under a recombinant IgG4 format, produced with the Baculovirus technology in Sf9 insect cells by Dr Martine Cérutti in St Christol-Les-Alez.

Specific baculovirus cassettes have been designed to express the heavy and light chains of an antibody which consist of (i) a strong viral promoter, (ii) a sequence encoding an immunoglobulin signal peptide, (iii) two unique restriction sites for heavy or light chain expression cassette to allow the insertion of the VH or VL sequences of the TEG4 anti-αIIbβ3 antibody in frame with the upstream signal peptide sequence, and (iv) a downstream sequence that encodes the human heavy (γ4) or light chain (λ) constant region. These cassettes are flanked by viral sequences that direct the integration by specific recombination of the foreign genes into a specific non-essential locus. Recombinant IgG4 TEG4 was

produced from Sf9 cells infected with the recombinant baculovirus coexpressing the TEG4 heavy and light chains. Recombinant IgG4 TEG4 was further purified on Protein A column.

6.1.2.2 VUSPIO platform and TEG4 IgG4 grafting

TEG4 IgG4 was grafted to iron oxide nanoparticles called Versatile UltraSmall SuperParamagnetic Iron Oxide (VUSPIO). The VUSPIO platform is the expertise of Dr Stéphane Mornet in ICMCB, Pessac[10,11], it is based on 7.5 nm-sized magnetic cores of maghemite γ-Fe2O3 embedded in a dextran corona. Their surface is functionalized with long heterobifunctional poly(ethylene oxide) chains serving as cross linkers for derivatization. The primary amine terminal groups are converted into maleimide functions by using SM(PEG) as a coupling agent to conjugate the rIgG4 TEG4 antibody.

Briefly, a desired quantity of VUSPIO nanoparticles was incubated with SM(PEG)24 in 50 mM HEPES buffer pH 7.4 for 1 h 30 at room temperature on a rotating shaker. The reaction was then loaded on a magnetic column (MACS, Miltenyi Biotec, Lyon, France) equilibrated with 100 mM HEPES buffer pH 7.4 and the activated VUSPIO were eluted in 100 mM HEPES buffer pH 7.4.

In parallel, a thiolation of TEG4 is performed with 2-Iminothiolane-HCL (Traut's Reagent): the primary amines inside the Ab structure (for example lysine aa side chain) were thiolated with Traut's Reagent so as to introduce sulfhydryl (—SH) groups while maintaining charge properties similar to the original amino group. A thiolation of TEG4 was performed with 2-Iminothiolane-HCL (Traut's Reagent, Thermo Scientific), for 1 h 30 at room temperature. The reaction was terminated by loading the sample on PD-10 desalting columns, previously equilibrated and further eluted with 100 mM HEPES buffer pH 7.4. The activated VUSPIO were added to rIgG4 TEG4 and the conjugation reaction was completed by incubation for 12 h on a rotating shaker at 4 °C. During that time the maleimide groups of VUSPIO react with the sulfhydryl groups of the antibody to form stable thioether bonds. A magnetic separation column (MACS, Miltenyi Biotec) was used to separate the unbound rIgG4 TEG4 from the magnetic conjugates.

The same experiment was performed with polyclonal IgG from human serum and with human IgG4 isotypic control to obtain IgG cont-VUSPIO and human IgG4 cont-VUSPIO respectively, which served as negative controls for unspecific binding.

6.1.2.3 IHC

Binding of the rIgG4 TEG4 Ab to activated platelets was first confirmed by IHC, and flow cytometry. For flow cytometry method and results please refer to the full article.

All animal studies were approved under the No. 50120192-A by the Animal Care and Use Committee of Bordeaux, France. ApoE−/− mice were fed a high-cholesterol diet for 21 weeks. Human coronary arteries were harvested from patients with end-stage heart failure having undergone heart transplantation. All of the clinical interventions took place at Haut-

Lévèque Hospital (Pessac, France). Human tissue specimens were collected after informed consent. They were immediately processed and embedded in paraffin.

Paraffin-embedded sections of arterial tissue from mouse or human were deparaffinized, rehydrated, and heat mediated antigen retrieval was performed with Tris-EDTA pH 9 buffer following the specifications of Abcam, Paris, France (www.abcam.com/ps/pdf/protocols/ihc_p.pdf). Endogenous peroxidase was then blocked with 3 % H_2O_2 in water, for 15 min. After washing in PBS 1X + 0.025 % Triton (PBST), nonspecific binding was blocked with PBS 1X + 0.2 % Triton + 2 % bovine serum albumin (BSA) for 1 h at room temperature.

Afterwards, either unconjugated rIgG4 TEG4 human antibody or VUSPIO conjugated antibodies (TEG4-VUSPIO or IgG cont-VUSPIO) were applied overnight at 4 °C, diluted at 10 µg/ml in PBS 1X + 1 % BSA. AP-2 mouse antibody (courtesy of Dr Alan Nurden) targeting integrin αIIbβ3[12] was used as a positive control, at the same concentration. When the AP-2 mouse antibody was used on mouse tissue, blocking of endogenous immunoglobulins was performed with an anti-mouse IgG (Beckman Coulter, France) at 100 µg/mL.

Following the first incubation and after three washes with PBST, diluted peroxydase-labelled antibodies specific to (1) human IgG H+L (Beckman Coulter) for TEG4, TEG4-VUSPIO and IgG cont-VUSPIO (working dilution 1/200); (2) mouse IgG H+L (Beckman Coulter) for AP-2 (working dilution 1/500), were applied to the sections for 1 h at room temperature. After a further three washes with PBST, staining was performed by adding the peroxidase substrate diaminobenzidine (DAB substrate kit, Eurobio/ABCys, Les Ulis, France) with H_2O_2. It yielded a yellow brown deposit within 10 min at room temperature. After a wash in dH2O to stop the enzymatic reaction, slides were counterstained in hematoxylin, dehydrated and mounted.

6.1.3 Results

6.1.3.1 Grafting

The concentration of antibody in the conjugate was determined by ELISA. Briefly, a standard curve was obtained using rIgG4 TEG4 antibody at concentrations ranging from 0.025 to 0.1 µg/mL. Samples of diluted TEG4-VUSPIO, IgG cont-VUSPIO and antibody-free VUSPIO solutions were incubated on anti-human IgG antibody-coated wells. An HRP-conjugated anti-human IgG was added to recognize bound analytes, and revealed with ABTS (2,2'-Azinobis [3-ethylbenzothiazoline-6-sulfonic acid]-diammonium salt). The absorbance was read at 405 nm and the TEG4 concentration in each sample calculated by equivalence with the standard curve.

In parallel, the absorbance of iron in the VUSPIO samples was measured at 480 nm using a spectrophotometer. This value was converted to a VUSPIO concentration equivalent following the formula given by Dr Mornet[13]:

$$C_{VUSPIO} = C_{Fe2O3} / {}^{4}/_{3}\,\pi \times r^3 \times m_p \times 20$$

Where C_{VUSPIO} and C_{Fe2O3} are the calculated VUSPIO and measured Fe_2O_3 concentrations, respectively. $r = 3.75 \times 10^{-7}$ is the radius; $m_p = 4.87$ is the weight of one Fe_2O_3 core, and 20 is the number of cores per VUSPIO particle.

The calculation of both VUSPIO and TEG4 molarities led to an overall estimated ratio of one antibody per VUSPIO.

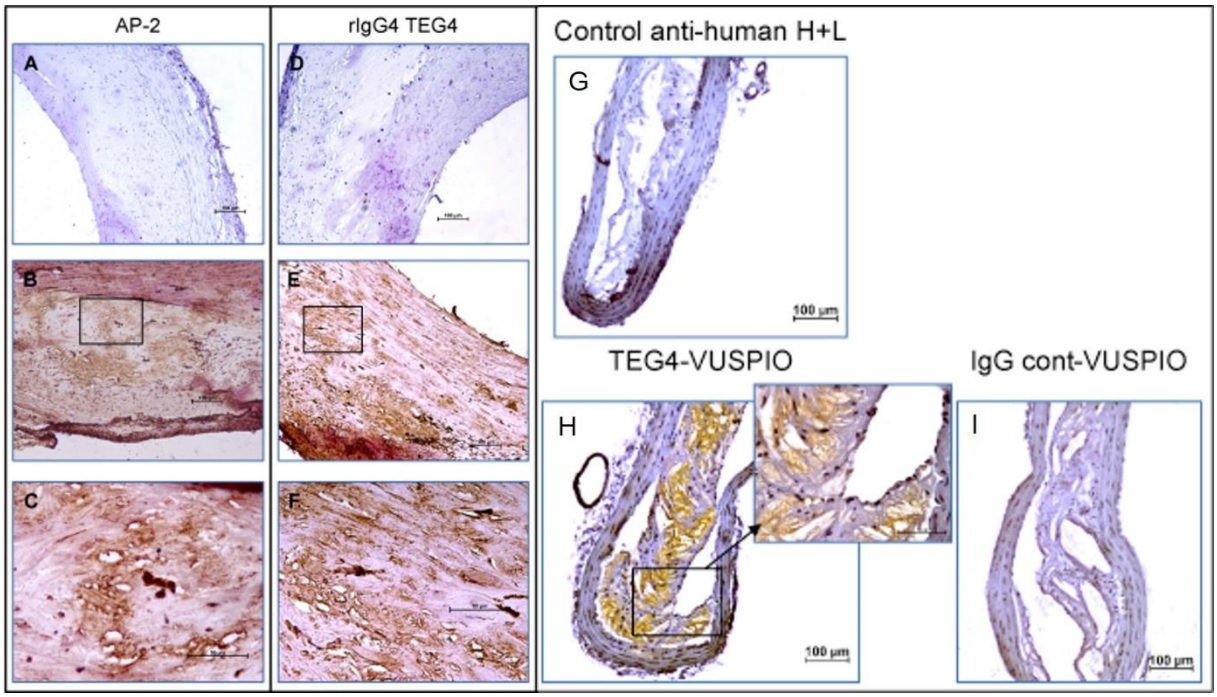

Figure 26: Immunohistochemical detection of integrin αIIbβ3 on coronary human sections and mouse aorta sections. Left panels: the presence of platelets was shown on human sections using the mouse anti-αIIbβ3 antibody AP-2 (B, C) and the human antibody rIgG4 TEG4 (E, F). (C, F) are enlarged views of (B, E). Controls were performed with secondary HRP-labelled anti-mouse IgG antibody (A) or HRP-labelled anti-human H + L antibody (D). Right panel: TEG4-VUSPIO (H) or control IgG-VUSPIO (I) were incubated on mouse aorta sections. Control (G) was performed using the secondary HRP-labelled anti-human H+L antibody. Bars: 100 µm and 50 µm for enlarged views.

6.1.3.2 IHC

Immunohistochemistry on human atheroma sections for coronary arteries showed a similar staining pattern for the anti-platelet murine AP-2 antibody and human TEG4 antibody, confirming the presence of platelets in distinct areas of the plaque. Additionally, the reactivity of VUSPIO-conjugated Ab was confirmed by the staining of mouse aorta sections (Figure 26).

6.2 Fluorescent labelling

As shown previously, several Ab candidates selected through phage display *in vivo* (5.1.1.2) have shown good reactivity and specificity for atherosclerosis *in vitro*. To assess the feasibility of *in vivo* targeting with these antibodies, they were produced under the slightly

smaller (110 kDa) but bivalent scFv-Fc format (see Table 1), and conjugated to fluorochromes using commercial kits designed for this use.

6.2.1 Principle

NHS ester reagents react with primary amines of Ab according to the reaction described in Figure 27.

N-hydroxysuccinimide (NHS) ester is one of the most common activation chemistry for creating reactive acylating agents. NHS ester-activated crosslinkers and labeling compounds react with primary amines in physiologic to slightly alkaline conditions (pH 7.2 to 9) to yield stable amide bonds. In the presence of amine nucleophiles that can attack at the electron deficient carbonyl of the active ester, the sulfo-NHS group rapidly leaves, creating a stable amide linkage with the amine compound. The protein concentration must be sufficient to prevent hydrolysis of the NHS ester to compete with the primary amine reaction, and maintain a good conjugation efficiency[9].

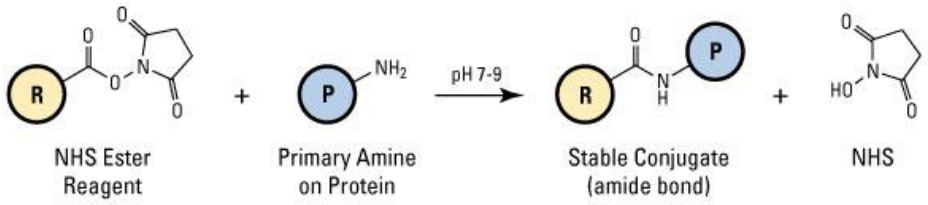

Figure 27: Overview of the reaction of the NHS ester-probe with the Ab primary amine. From www.thermofisher.com

6.2.2 Material and methods

6.2.2.1 Antibody production

Following the phage display selection of atheroma-reactive human scFv fragments by Kamel Deramchia, the coding sequences for variable heavy and light chains were introduced in the pFUSE-hFc. This vector, designed by Franck Perez and colleagues[14], allows for the obtention of two scFvs each fused to a hinge fragment, followed by constant domains CH2 and CH3 of a human IgG2, which assemble into an Fc tail. The construct was stably expressed in HEK293 cell line and purified using affinity chromatography on protein G.

In more details, the recombinant phagemide pCANTAB6 containing the scFv DNA sequence was digested with *NcoI* and *NotI* restriction enzymes (New England BioLabs, Evry, France). The scFv DNA fragments were separated on an agarose gel, purified, and subsequently ligated into a *NcoI*/*NotI* digested pFuse-hIgG-Fc2 vector. XL-1 blue *Escherichia coli* bacteria (Agilent Technologies, Massy, France) transfected with the recombinant pFuse-hIgG-Fc2 were grown on Low Salt LB Medium agar plates containing 50 µg/mL of Zeocin (Life Technologies, Saint Aubin, France).

Clones were tested for the presence of correct scFv sequences by digestion with *EcoRV*/*BglII*. The digestion products were analyzed by electrophoresis on a 1.2 % agarose gel. Then the

clones showing DNA fragments with the expected size (800 bp) were sequenced at GATC Biotech, Marseille, France.

HEK 293 cells were cultivated onto 75 cm² tissue culture flasks (Dominique Dutscher, Brumath, France) into complete medium (DMEM 10 % SVF, Glutamine 1 mM , penicillin-streptomycin mixture 400µg/mL). After 48 h, when the cells reached 90% confluence, 5.10^6 HEK 293 cells were transfected by electroporation using 30 µg of recombinant plasmid DNA (pFuse-hIgG-Fc2 containing the scFv construct) into 400 µl medium with NaCl 23 mM. After transfection, the cells were plated onto 25 cm² tissue culture flasks at 37 °C in complete medium for 48 hours. Then, medium was removed and fresh selective medium with Zeocin (600 µg/mL) was added. We replenished the selective medium every other day for 10 days. Then the medium was gradually replaced with serum free AIM-V medium with Zeocin. Maintaining the selection pressure allows transfected cells to pass the recombinant DNA to their progeny. This way a stable transfection is achieved, allowing for longer production times. Cells supernatants were harvested every week, aliquoted and stored at -20°C pending purification, and the cells split in fresh medium.

After protein G-affinity chromatography purification, the concentration of antibody into culture supernatant was determined by ELISA. Microtiter plates (Nunc) were coated with 100 µL of goat anti-human IgG, Fc fragment antibody (5 µg/mL, Jackson ImmunoResearch) overnight at 4°C. Each well was blocked with 200 µL of 5% (w/v) powdered milk in PBS for 1 h at room temperature. Duplicate samples of diluted supernatants were added to antibody-coated wells and incubated at room temperature for 2 h. A standard curve was obtained using IgG2 antibody at concentrations ranging from 0.025 to 0.1 µg/mL. The wells were then washed with PBS and incubated with 100 µL of a 1/10 000 dilution of HRP-conjugated anti-human IgG(H+L) antibody (Immunotech, Marseille, France) for 1 h, washed in PBS and incubated with 100 µL of ABTS (Sigma-Aldrich). The absorbance was read at 405 nm using an Emax precision microplate reader (Molecular Devices, Sunnyvale, CA).

6.2.2.2 Conjugation

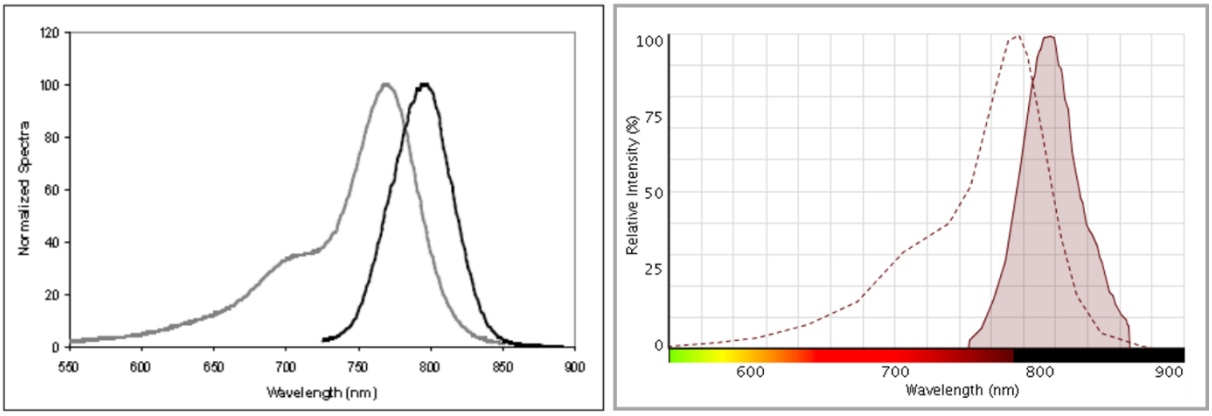

XenoLight CF 770 Alexa Fluor 790

Figure 28: Absorption and emission spectra of two near-infrared dyes Xenolight CF770 on the left, and AlexaFluor790 on the right.

The conjugation was carried out according to the manufacturer's instructions. Two kits were used: IVIS XenoLight CF770 Rapid Antibody Labeling kit (Perkin Elmer, Courtaboeuf, France) and DyLight Antibody Labeling kit (Life Technologies, Courtaboeuf, France) for comparison. Spectra for both dyes are presented by Figure 28, they may roughly be superimposed. Labelling was based on the same chemical reaction: fluorochromes containing a NHS ester terminus reacted with primary amines of the Ab structure, generally Lysine side-chain.

Briefly, the Ab was mixed with the reactive fluorochrome in an appropriate buffer and left to react at room temperature. To separate the conjugated Ab from the remaining free dye, a centrifugation column was used, that either retained the conjugated Ab at the top of the column (XenoLight kit) or let it flow through while retaining the free dye (DyLight kit).

After the purification step, the conjugation ratio and final antibody concentration were assessed by absorbance spectrophotometry at 280 nm (Ab λ_{max}) or 770 nm (dye λ_{max}), following the formulas provided in each kit.

6.2.3 Results

6.2.3.1 Conjugation

The conjugation reactions were carried out using 50 to 100 µg of each scFv-Fc. After purification, at least 80% of the initial quantity could be retrieved and the calculated ratio was on average 1.5 mole of dye per mole of Ab. As a control for free dye binding in vivo, a mock conjugation was carried out using only PBS instead of the Ab.

The results of injection to ApoE-/- mice will be presented in the next chapter, with the other imaging data.

7 Site specific conjugation

As described earlier, usual conjugation strategies involve the amine side chains of the Ab, which may be a good strategy for full IgG but presents the risk to degrade the binding sites of smaller Ab fragments and impede their reactivity. Furthermore the number of probes conjugated to an Ab is not well-controlled. To avoid loss of reactivity and obtain homogenous conjugation ratio, protein engineering has been applied that both reduces the probe size and allows for site-specific conjugation. Compared to full IgGs (150 kDa), scFv fragments (30 kDa), present an increased tissue penetration. This reduced size also makes them more suitable for functionalizing relatively small nanoparticles. Moreover, this recombinant form can be generated with tags for purification and site-specific attachment to improve reaction yields while avoiding loss of bioactivity.

7.1 Cysteine – maleimide

7.1.1 Principle

A scFv protein composed of the variable heavy (VH) and light (VL) chains of an antibody linked with a flexible peptide has been constructed by recombinant DNA technology. Two cysteines (amino acids containing thiol functions) were added in the sequence to allow for site-specific conjugation to a maleimide residue. TEG4 HuAb was here processed as scFv fragments in the yeast *Pichia pastoris*.

The thiol – maleimide conjugation occurs as described in 6.1.1.

7.1.2 Method

7.1.2.1 TEG4-2C scFv production [4]

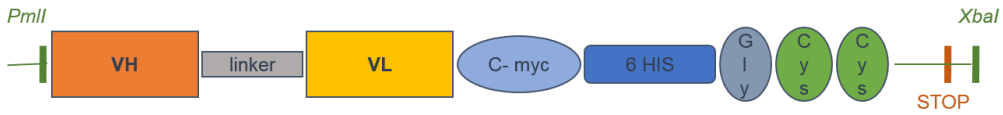

Figure 29: Sequence of TEG4 scFv 2C.PmlI and XbaI: restriction sites. VH – linker – VL: template scFv sequence. 6 His –Gly – Cys – Cys: PCR-introduced sequence.

The TEG4 scFv DNA fragment was used as a template to generate a new scFv format containing 2 cysteines into the C-terminal end. The coding sequence was PCR-amplified: the primers were used to introduce the 6 HisTag – Gly – Cyc – Cys – Stop amino acid sequence flanked by *PmlI* and *XbaI* restriction sites, as shown by Figure 29. After control by sequencing, the TEG4 – 6His – Gly – Cys – Cys DNA fragment was digested by *PmlI* and *XbaI*, ligated into the expression vector pPICZαA containing a Zeocin resistance cassette and transformed in bacteria for amplification. After extraction the plasmid was linearized and transformed into competent *P. pastoris* X-33 cells by electroporation. Transformed yeasts that exhibited high resistance to Zeocin were primarily grown in shake flasks before inoculation in a 5L bioreactor. After 120 h (5 days) of induction, the supernatant was

harvested and the expressed recombinant TEG4-2C scFv purified using IMAC. The elution fraction was dialyzed against PBS.

7.1.2.2 Site specific multivalent grafting onto VUSPIO

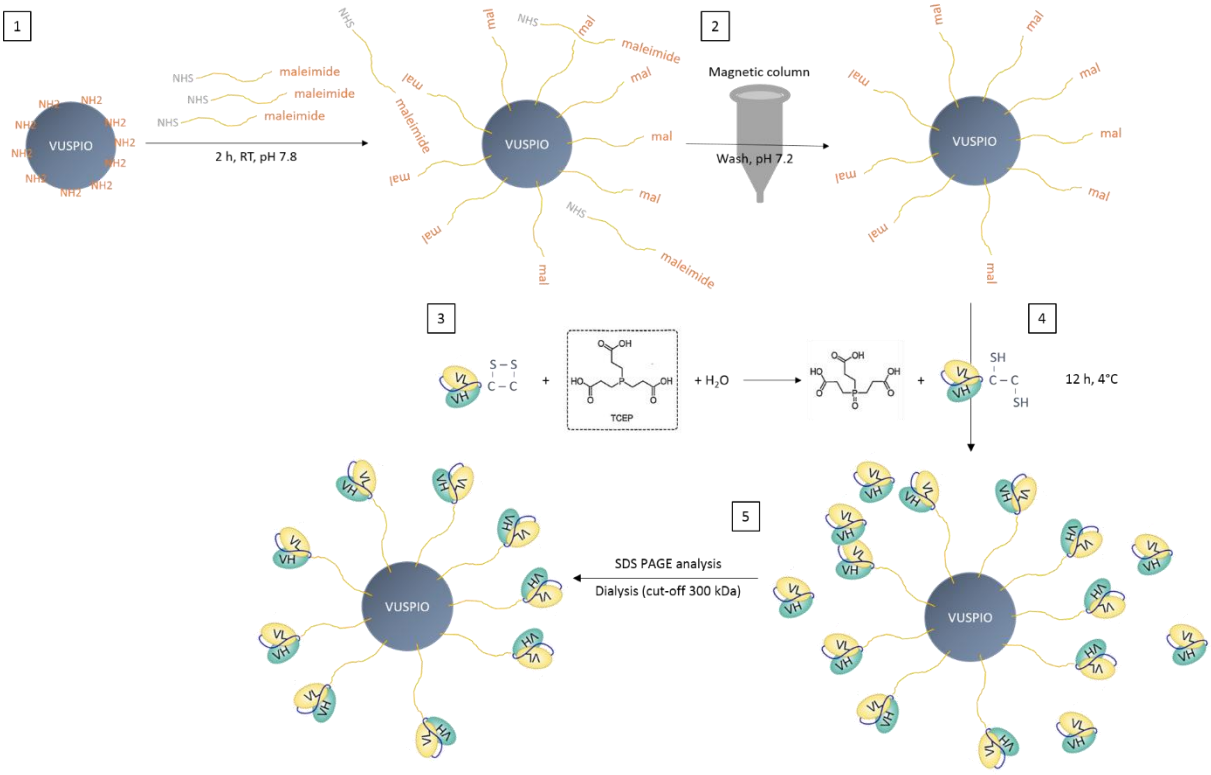

Figure 30: Schematic workflow for the conjugation process. 1: an excess NHS – PEG – mal is reacted onto the surface amines of the particle, 2: the VUSPIOs are washed on a magnetic column to remove the unreacted PEG and stop the reaction, 3: scFvs are activated by reduction with TCEP, 4: activated scFv react with the surface maleimide of the VUSPIO for 12 h, 5: the grafting yield is determined via a gel analysis while the excess scFv are cleaned by dialysis.

VUSPIO nanoparticles synthesis was performed as described previously in 6.1.2.2. After surface functionalization with heterobifunctional poly(ethylene oxide) chains, derivatization with a near-infrared-emitting dye was carried out in the same team by Laurent Adumeau[13]. The remaining primary amine terminal groups were then converted into maleimide functions to allow Ab grafting.

Figure 30 provides an overview of the workflow for this conjugation. An excess of the VUSPIO stock solution is diluted in 1/10 of HEPES buffer 200 mM, pH 7.8, so as to obtain a solution of desired iron concentration in HEPES 20 mM final. Then a heterobifunctional NHS – PEG – maleimide spacer arm is grafted on the surface amines of the VUSPIO nanoparticle. The quantity of NHS ester – PEG3400 – maleimide (MW = 3400 $g.mol^{-1}$, Laysan Bio, Arab, USA) used is 10 times superior to the number of amine functions on the surface of the VUSPIO, which was around 400 NH2 / VUSPIO for the batch we used. The corresponding PEG quantity is directly solubilized in the VUSPIO suspension, in HEPES buffer 20 mM pH 7.8, and left to react for 2 h at room temperature. At the end of the reaction time, the suspension is

washed on a magnetic column (MACS, Miltenyi Biotec, Paris) with a large volume of HEPES buffer 10 mM, pH 7.2 to remove the excess PEG and stop the reaction. The reaction of thiols with maleimides being both oxidation and pH sensitive, a 10 mM pH 7.2 HEPES buffer is vacuum degassed beforehand for at least one hour and saturated with argon gas for this step. In the meantime, the scFv is "activated" by reduction of the N terminal cysteines to make the thiols reactive. A solution of TCEP 10 mM is made fresh and added to the scFv so as to obtain a ratio n(TCEP) / n(scFv) = 20. The reduction is carried out for 30 min at 4°C. TCEP is preferred to other reducing agents because it is known to reduce only the outermost disulfide bonds and has low reactivity (contrary to β-mercaptoethanol for example) for the maleimide present in the next step [13].

Following the reaction of the surface amines of the VUSPIO with the NHS ester end of a heterobifunctional NHS – PEG – maleimide molecule, the maleimide function is displayed on the surface of the NP. After washing, the VUSPIO concentration is assessed by spectrophotometry at 480 nm and mixed with scFv in respective quantities calculated to obtain different Ab to particle ratios: R3, R6 and R14. The grafting reaction processes 12 h at 4°C. The conjugated-NP are finally dialyzed (cut-off 100 kDa, Spectra-Por Float-A-Lyzer G2, 1 mL, MWCO 100 kDa, Sigma Aldrich, St Quentin Fallavier, France) against PBS to remove excess scFv. Before this last step a small sample of the reaction medium is analyzed by SDS-PAGE to evaluate the conjugation yield: while the unconjugated scFv is able to migrate freely through the gel, the VUSPIO are retained on top of it by their important size. Each ratio of scFv/VUSPIO is loaded in a way that the initial scFv quantity is equivalent; after migration, the unconjugated scFv quantity is assessed by comparison to an equal amount of free scFv loaded on the same gel. The quantification is performed by image analysis as described in the next paragraph.

7.1.2.3 Conjugation yield calculation

The conjugation yield was calculated from the gels using the open source image processing program *ImageJ* (https://imagej.nih.gov/ij/ or http://imagej.net).

The Coomassie blue – stained gels were scanned at high resolution (600 dpi) using a Sharp multifunctional printer and saved as a high quality PDF file. A screenshot was captured and converted from 32 to 8 bits with ImageJ. The contrast was enhanced to facilitate visualization. The consecutive bands of interest were selected and plotted to convert their intensity into a measurable area. The box below recapitulates the sequential ImageJ commands. Figure 31 represents a screenshot of the gel analysis procedure in ImageJ software and an example of conjugation yield calculation using Excel (Microsoft office). Noteworthy, whenever it was possible, two lanes of the gel were loaded with the unreacted scFv to serve as a reference for quantification. The table presents the results using each of them, and the mean of both.

The sequence of commands in the ImageJ software are as follows:

> Image > Type > 8-bit
> Image > Adjust > Brightness/Contrast > Auto
[select bands]
> Analyze > Gels > Select First Lane [then] > Plot Lanes
> Wand (tracing) tool

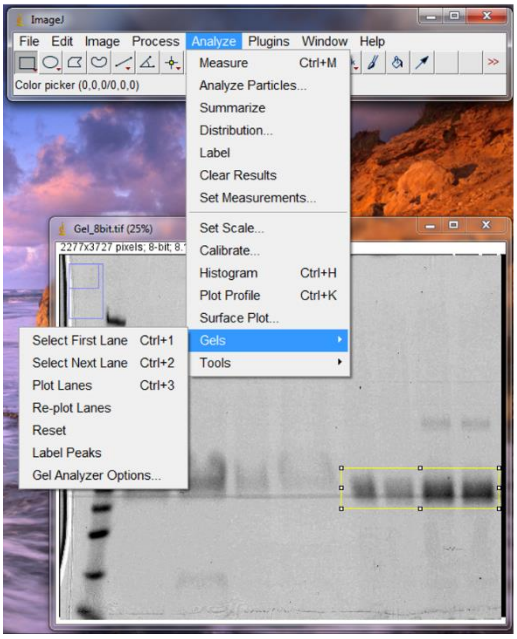

Sample	Peak area	Loaded quantity	Calculated quantity	Percent conjugated	Calculated number of scFv / particle	Mean
VUSPIO scFv PBS 16	21186,811		0,74 µg	50,64	8,10	**8,12**
VUSPIO scFv PBS 32	19371,782		0,68 µg	54,87	17,56	**17,59**
scFv PBS 1	42920,196	1,50 µg	1,50 µg			
scFv PBS 2	43115,317		1,51 µg			
VUSPIO scFv PBS 16	21186,811		0,74 µg	50,86	8,14	
VUSPIO scFv PBS 32	19371,782		0,67 µg	55,07	17,62	
scFv PBS 1	42920,196		1,49 µg			
scFv PBS 2	43115,317	1,50 µg	1,50 µg			

Figure 31: Conjugation yield calculation. Left panel: screenshot of the ImageJ procedure; right panel: representative Excel datasheet of the calculations.

7.1.2.4 Avidity measurement

The avidity of the TEG4-2C scFv before and after grafting to the VUSPIO was assessed by surface plasmon resonance (SPR) sensing on purified αIIbβ3 integrin (Enzyme Research Laboratories, Swansea, UK). The experiments were carried out according to the manufacturer's instructions by Laëtitia Minder and Carmelo Di Primo, at the European Chemistry and Biology Institute (IECB, Pessac, France) using the BIAcoreTM 3000 (GE Healthcare Europe GmbH, Velizy-Villacoublay, France) equipped with research-grade CM5 sensor chips. HBS-P buffer (0.01 M HEPES, pH 7.4, 0.15 M NaCl, 0.005% v/v Surfactant P20) (GE Healthcare, Aulnais-/s-bois, France) with 2 mM Ca2+ was used as a running buffer. Calcium ions were added to allow the good folding of the αIIbβ3 integrin complex.

First the surface of the sensor chip was activated using the Biacore amine coupling kit (GE Healthcare, Aulnais-/s-bois, France), following the reaction described in Figure 32.

Briefly, the carboxylic acid group is attacked by the EDC crosslinker leading to an active o-Acylisourea intermediate. The latter is unstable in aqueous solutions: it can be hydrolyzed

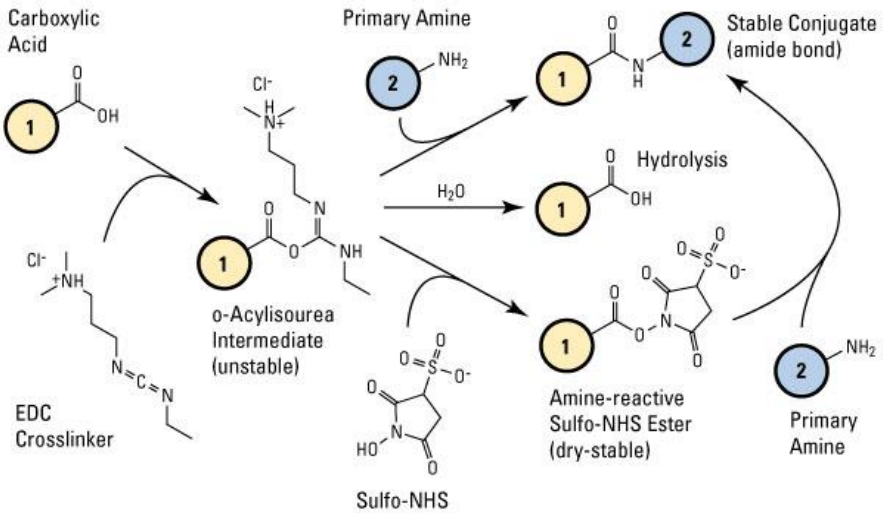

Figure 32: Principle of the EDC/NHS-mediated cross-linking. From www.thermofisher.com.

with regeneration of the carboxyls. To avoid this, Sulfo-N-hydroxysuccinimide (Sulfo-NHS) is added to the reaction media to create dry-stable (amine-reactive) intermediates. This NHS ester is considerably more stable than the O-acylisourea intermediate while allowing for efficient conjugation to primary amines by nucleophilic attack at physiologic pH. The primary amine forms an amide bond with the original carboxyl group [9].

Afterwards, the purified αIIbβ3 was first dialysed in running buffer, then diluted in acetate buffer 10 mM, pH 4.5 (GE Healthcare, Aulnais-/s-bois, France) to a 30 µg/mL concentration, and finally attached on the surface of the chip following this reaction. The EDC/NHS reaction was stopped using ethanolamine hydrochloride 1 M, pH 8.5. The chip was finally washed using Glycine buffer pH 2.5, followed by NaOH then HBS-Ca running buffer. The common unit for SPR is the resonance unit (RU), which represents 1 pg protein per mm².

The scFv and VUSPIO-scFv samples were dialyzed in running buffer, which also served to record the baseline. The chip was regenerated between each sample with NaOH followed by HBS-P Ca.

The scFv alone was flown on the chip at 33, 100, and 300 µg/mL as a control for its affinity to αIIbβ3. The following dilutions of VUSPIO R3, R6, and R14 were assessed: 1/54 for R6 and R14; 1/18, 1/6, ½ for R3, R6, and R14.

7.1.2.5 Reactivity assessment

The reactivity of TEG4-2C scFv alone, and after grafting to the VUSPIO was confirmed by IHC on paraffin-embedded sections of arterial tissue from mouse, rabbit or human.

All animal studies were approved under the N° 50120192-A by the Animal Care and Use Committee of Bordeaux, France. All work with tissues from human subjects had been approved by the CPP committee (Comité de Protection des Personnes Sud-Ouest et Outre Mer) of Bordeaux and from the Research Ministry in France (Authorization number DC - 2016- 2724).

ApoE-/- mice were obtained from Charles River Laboratories and fed a high-cholesterol diet (0.15% cholesterol, Avogadro Western diet, Safe, Augy, France) for 21 weeks to allow for the development of atherosclerotic lesions. Wild-type control C57BL6 mice were used as a negative control (Charles River Laboratories, St Germain sur l'Arbresle, France).

Adult male New Zealand rabbits (NZW) were obtained from Charles Rivers Laboratories, fed a fat atherogenic diet including 0.3% cholesterol for 8 months and subjected to surgeries to trigger the formation of complex plaques with intramural thrombi. Aortas from control untreated rabbits and balloon-injured aortas from hypercholesterolemic rabbits were extracted from the aortic arch to the iliac bifurcation.

Human coronary arteries were harvested from patients with end-stage heart failure having undergone heart transplantation at Haut-Lévèque Hospital (Pessac, France). Human carotid tissue was obtained from patients with life-threatening carotid stenosis receiving endarterectomy surgery at Pellegrin Hospital (Bordeaux, France). Human tissue specimens were collected after informed consent to use surgical waste for investigational purposes.

All tissues were immediately fixed in paraformaldehyde (PFA) 4% (Eurobio, Les Ulis, France) and embedded in paraffin.

To perform immunohistochemistry, the paraffin blocks were thinly sliced (7 µm) and adhered on glass slides. The sections were deparaffinized, rehydrated, and heat mediated antigen retrieval was performed with Tris-EDTA pH 9 buffer following the specifications of Abcam, Paris, France (www.abcam.com/ps/pdf/protocols/ihc_p.pdf). Endogenous peroxidase was then blocked with 3 % H_2O_2 in water, for 15 min. After washing in PBS 1X + 0.025 % Triton (PBST), nonspecific binding was blocked with PBS 1X + 0.2 % Triton + 2 % bovine serum albumin (BSA) for 1 h at room temperature.

Afterwards, VUSPIO alone or antibody-conjugated VUSPIO corresponding to R3, R6 and R14 ratios were applied to the slides, diluted to the same iron concentration so as to compare the avidity of the VUSPIO in each batch. TEG4 Ab alone was applied to the slides in concentrations matching the theoretical Ab content in each VUSPIO dilution to compare their reactivity.

The incubation was carried out overnight at 4 °C, diluted in PBS 1X + 1 % BSA. The following day, three washes with PBST were performed. To detect TEG4-2c scFv fragments, a HRP-conjugated antibody specific to 6His (working dilutions 1:250) was applied to the sections for 1 h at room temperature.

After a further three washes with PBST, staining was performed by adding the peroxidase substrate diaminobenzidine (DAB substrate kit, Eurobio/ABCys, Les Ulis, France) with H_2O_2. It yielded a yellow brown deposit within 10 min at room temperature. After a wash in dH_2O to stop the enzymatic reaction, slides were counterstained in hematoxylin, dehydrated and mounted.

7.1.3 Results

7.1.3.1 TEG4-2C scFv production

An average of 30 mg of TEG4-2C scFv were produced and secreted by *P. pastoris* into 1L broth medium after 5 days of growth. After IMAC purification, the yield was around 22 mg TEG4-2C scFv per liter of culture, with a purity superior to 80%.

The eluted fractions were analyzed by SDS-PAGE (Figure 33), which revealed a major band of 35 kDa from the elution step fractions, corresponding to the expected molecular mass of recombinant TEG4-2C scFv. A weaker band of 75 kDa was also present in this lane, but the mass spectroscopy analysis revealed that TEG4-2C scFv was the only protein present in this fraction (data not shown). This data strongly suggests that the higher molecular weight protein was indeed TEG4-2C scFv dimer.

The SDS-PAGE (Figure 33) shows the purified TEG4-2C scFv as a single thick band with an estimated purity higher than 80%. The profile of TEG4-2C scFv into PBS buffer is similar to the elution fraction (E) obtained at the end of IMAC. Noteworthy, SDS-PAGE analysis shows that some of the protein of interest was lost in the flowthrough and wash fractions.

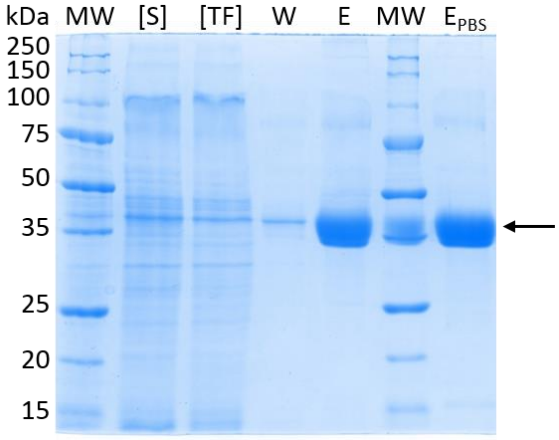

Figure 33: SDS PAGE analysis of the purification fractions. Molecular Weight (MW) markers in kiloDaltons (kDa) are indicated on the left. [S] is the supernatant, [TF] the flowthrough and W the wash fraction. E is the eluted fraction at the end of IMAC purification, and E_{PBS} is the eluted fraction after dialysis in PBS buffer. The arrow shows the expected scFv size at 35 kDa.

7.1.3.2 Site specific multivalent grafting

TEG4-2C scFv dialyzed in PBS or MES buffer (Figure 34) were reacted with the VUSPIO in different ratios (from 4 to 32 scFv fragments per VUSPIO, as shown on the graph, Figure 34), and the end product loaded on a gel before dialysis. The unconjugated scFv could then be stained, visualized and quantified by comparison with the scFv alone, loaded in the same amount as theoretically available in the reaction mix. Hence, the VUSPIO-conjugated scFv would be retained at the top of the gel by the massive size of the NPs, while the free TEG4

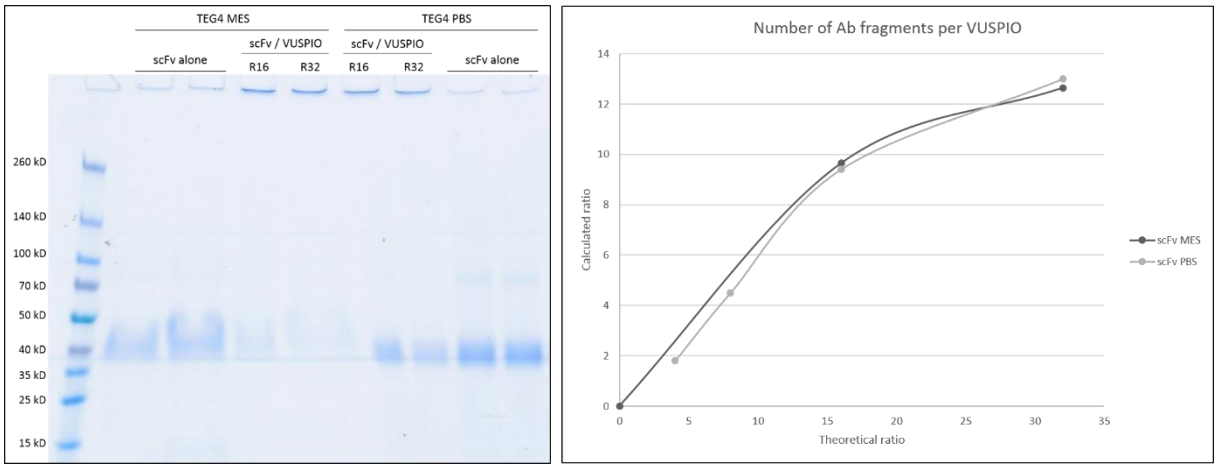

Figure 34: Conjugation yield of the VUSPIO functionalization. Left: SDS-PAGE analysis for quantification. Right: Number of fragments actually grafted on the particles versus theoretical ratio.

could migrate freely. Figure 34 shows a typical Coomassie-stained SDS-PAGE analysis after the conjugation reaction (left panel). Two scFv/VUSPIO ratios (16 and 32) and two different buffers (MES and PBS) were used in that case. MES buffer disrupts the Ab migration in SDS, showing a spread, blurry band. Right panel curves compares the calculated and theoretical grafting ratios for each buffer. The profiles are similar, roughly linear with a bend from 15 fragments per particle.

7.1.3.3 Avidity measurements and reactivity validation

The final immobilized αIIbβ3 density on the surface of the SPR chip was 2200 RU.

SPR analysis of the scFv alone and grafted to the VUSPIO nanoparticles showed indeed that TEG4-2C scFv retained its binding capacity to the integrin αIIbβ3 in both settings.

Table 6: TEG4-conjugated VUSPIO data. Iron concentration, VUSPIO equivalent, and scFv concentrations are given for each ratio. VUSPIO molarity is calculated using the formula in 6.1.3.1.

scFv/VUSPIO	**R3**	**R6**	**R14**
Fe3+ (M)	0.04	0.04	0.03
VUSPIO (M)	2.72E-7	2.47E-7	1.68E-7
scFv (g/L)	0.0241	0.0469	0.0768
scFv (M)	7.52E-7	1.47E-6	2.40E-6

ScFv alone being monovalent, they are known to have a lower affinity compared to their full IgG counterpart. Because of this, increasing the valence by grafting several fragments should benefit to the avidity of the nanoparticle. To confirm this, each scFv/VUSPIO sample was diluted according to its iron content, in order to assess the avidity of each ratio. Dilutions 1/18, 1/6, and ½ yielded similar results. The representative curves obtained for the 1/6 dilution are shown by Figure 35: SPR sensing confirmed that the VUSPIO binding avidity increases with the number of grafted scFv. The association/dissociation curves represent a quicker association and higher maximum bound analyte for the R14 compared to the R6,

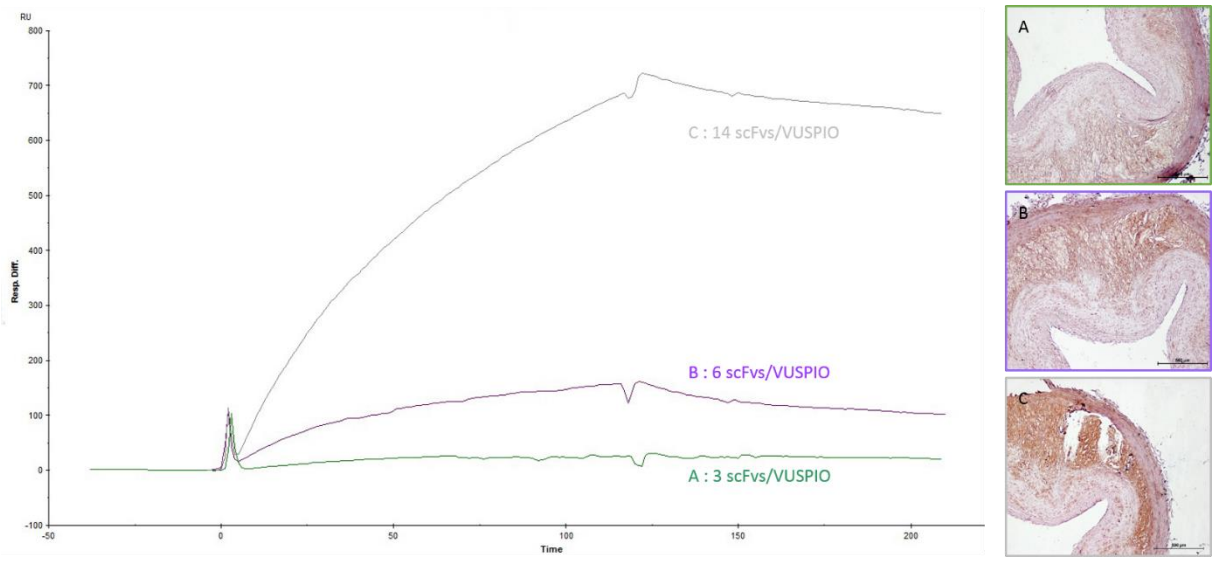

Figure 35: Affinity and reactivity evaluation of VUSPIO conjugated to increasing scFv ratios. Left: SPR avidity measurement; right: immunohistochemistry on atherosclerotic rabbit aortas sections. A: 3 scFv/VUSPIO; B: 6 scFv/VUSPIO; C: 14 scFv/VUSPIO;

itself superior to the R3. However, a Kd couldn't be calculated from these experiments because no sufficient dissociation was measured.

In parallel, immunohistochemistry on rabbit aorta slices showed a specific staining of the areas of platelets accumulation in the atheroma plaque, similar between the scFv fragment alone and its VUSPIO-grafted counterpart as shown by Figure 25, right panel. Interestingly, while the quantity of VUSPIO incubated on the slices was constant, the staining intensity increased with the valence of the particles: A: R3; B: R6, C: R14, consistent with the increased avidity measured by SPR.

7.2 Sortase

The Sortase conjugation is the expertise of Dr Christoph Hagemeyer's team in the Australian Center for Blood Diseases (ACBD) in Melbourne, Australia. I have Shweta Jagdale to thank for teaching me all the molecular biology and protein production steps, Dr Karen Alt for her expertise on the conjugation chemistry, and all the team for their help and support.

7.2.1 Principle

Sortases are expressed by staphylococci and other Gram-positive bacteria. They are essential in cell wall biosynthesis and covalent attachment of surface proteins to its peptidoglycans. These proteins are often virulence factors that interact with extracellular matrices, molecules or cells from the infected organism to mediate bacterial adherence to tissues, invasion of target cells or evasion from the immune system. [15–17]

This mechanism requires a C-terminal 35-aa cell wall sorting signal: an LPXTG motif (leucine, proline, X: any aa, threonine and glycine), followed by a hydrophobic region and a tail of positively charged residues. When the protein is secreted it is retained in the cytoplasmic membrane by the hydrophobic domain and charged region which allows the membrane-

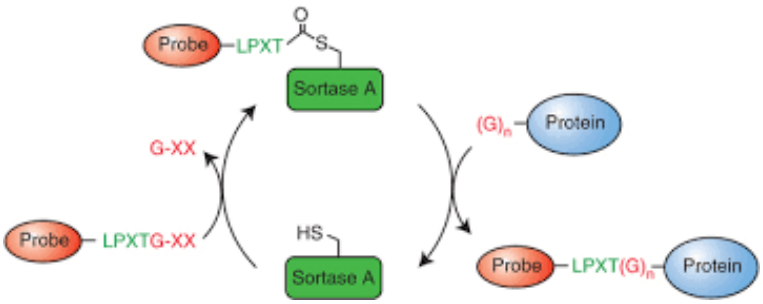

Figure 36: Principle of the Sortase conjugation. The LPXTG (X being any amino-acid) forms an intermediate with the enzyme that is resolved upon reaction with the poly-G labeled protein. From Theile et al., Nat Protoc, 2013.

bound enzyme to recognize the LPXTG motif and bind the protein to the cell wall. This two-step reaction involving cleavage and transpeptidation can be performed in vitro [18]. Figure 36 recapitulates the conjugation steps.

After recognition of the sortase A LPXTG motif, the catalytic site of the enzyme serves as a nucleophile to cleave the peptide bond between the threonine and glycine aa. A thioacyl intermediate is formed, which is resolved when the N terminus of an (oligo)glycine nucleophile reacts with it, ultimately creating a stable peptide bond between the substrate and nucleophile. In the absence of this nucleophile the intermediate resolves with water, resulting in hydrolysis of the LPXTG motif. Hence when carrying out the reaction it must be ensured that the nucleophile is in large excess [19].

The sortase A enzyme used in this study originates from *Staphylococcus aureus*, its sequence is 206 aa long for a 17.9 kDa protein.

7.2.2 Method

7.2.2.1 Gene sub-cloning and amplification

The annotated sequence of each scFv of interest served as a template for the introduction of the LPETG tag. The synthetic gene was ordered from GeneArt (Thermo Fisher Scientific), and delivered in frame with their proprietary plasmide.

On top of the LPETG introduction, the gene was adapted for the production in human HEK293F cells. Indeed, the proprietary GeneOptimizer software processes the sequence so as to fulfill the following claims: “Identification of the best way to incorporate [the] requested sequence elements; elimination of cryptic splice sites and RNA destabilizing sequence elements for increased RNA stability; addition of RNA stabilizing sequence elements; codon optimization and G/C content adaptation for [the chosen] expression system; intron removal, and avoidance of stable RNA secondary structures.” (https://www.thermofisher.com/fr/fr/home/life-science/cloning/gene-synthesis/geneart-gene-synthesis/geneoptimizer.html). This process is meant to improve mRNA stability and translation efficiency, leading to higher production yields. Figure 37 recapitulates the sub-cloning procedure of the construct from the GeneArt plasmid to the expression vector.

In more details, the gene-containing commercial plasmid was mixed with KCM 1X buffer (0.1 M KCl, 0.03 M $CaCl_2$, 0.05 M $MgCl_2$) to a volume of 100 µL, another 100 µL MEB competent bacteria were added and the mix left to react on ice for 30 minutes, after what it was heat shocked at 42°C for 1.5 min using a Thermomixer (Eppendorf) and immediately put back on ice. Warm LB (lysogeny broth) broth (37°C) was added to the bacteria to a final volume of 1 mL and mixed gently, before a 15min incubation at 37°C with gentle horizontal shaking to allow recovery. Finally the bacteria were plated on selective LB ampicilin agar plates and left in the incubator at 37°C overnight.

The next day single colonies were transferred in 10 mL LB broth plus ampicilin (100 µg/mL) and again grown overnight at 37°C for the subsequent plasmid purification step.

After 10 min centrifugation at 4000 rpm, the supernatant was discarded and the pellets treated with the QIAprep™ Spin Miniprep kit (Qiagen) following the manufacturer's instructions. The purified DNA concentration was measured using a NanoDrop 2000 UV-Vis Spectrophotometer (NanoDrop) against a blank of Milli-Q water, making sure the max absorbance was around 260 and the A260/280 ratio between 1,8 and 2 to check for the absence of contaminants, either RNA or proteins. DNA was kept at RT for short-term use or frozen at -20°C or below for long-term storage.

The Geneart construct and pSecTag destination plasmid are separately digested with *NotI*

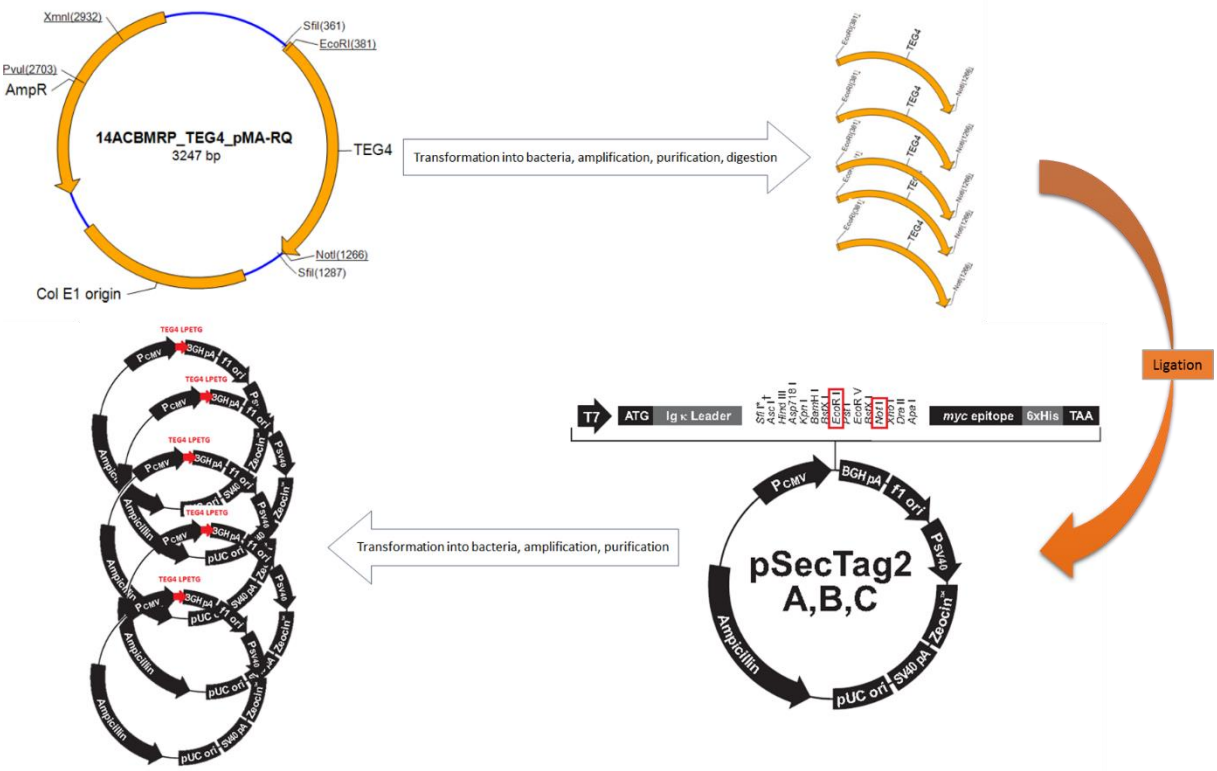

Figure 37: Summarized sub-cloning procedure from the GeneArt proprietary plasmid to the pSecTag expression vector. The construct was first transformed into competent bacteria, amplified, purified and digested. The scFv gene was ligated into the pSecTag vector, transformed into bacteria and amplified. The presence of the construct was checked by PCR amplification, then sequenced and compared to the original sequence. Selected clones for each construct were further amplified and purified for subsequent transfection into HEK cells.

and *EcoRI* for 3h at 37°C. The fragments are then ran on a 0,8 % agarose gel with RedSafe DNA marker in 1X TAE buffer for 30 min at 135 V. Bands of interest are then excised on a Gel Doc UV trans-illuminator (Bio-Rad) and frozen at -20°C until the next day.

The Wizard SV Gel and PCR Clean-Up System (Promega) was used as per manufacturer's instruction to retrieve the DNA, which concentration was measured using the Nanodrop. Ligation of the construct into the pSecTag vector was processed in 1:3 and 1:6 vector to construct ratio and for 1h at RT and overnight at 16°C. A mock ligation of the plasmid, i.e. with no construct and religated on itself, was used as a control.

The ligation products were used to transform MEB bacteria as previously described and grown overnight on ampicillin plates. Bacteria containing the pSecTag without an insert grew much fewer colonies than the clones of interest. These latter were screened via PCR amplification (Initial denaturation 95°C – 2 min, denaturation 95°C – 30 sec, annealing 50°C – 30 sec, extension 72°C – 60 sec, final extension 72°C – 5 min), 10 colonies for each construct, with the universal T7 Forward Primer-TAATACGACTCACTATAGGG and Rev Primer-TAGAAGGCACAGTCGAGG, flanking the construct in the pSecTag. The amplification products were again ran on agarose.

Three clones for each construct were grown from the master plate in LB broth plus ampicillin, overnight at 37°C, their DNA purified, amplified for sequencing and sent out to the AGRF sequencing platform (http://www.agrf.org.au/). The result files were compared to the original GeneArt sequences for length (approx.. 1000 bp) and AA sequence after translation using ExPASy online tool (http://web.expasy.org/translate/).

One positive clone for each construct was grown from the master plate in 250 mL culture for subsequent plasmid purification using a Maxiprep kit (Qiagen) according to the manufacturer's instructions. The purified plasmid as well as aliquots of the bacteria in 50% glycerol were stored at -80°C.

7.2.2.2 scFv LPETG production and purification

HEK293F cells were cultured as a suspension in serum free medium (Freestyle 293, Thermo Fisher Scientific, Illkirch, France) in a horizontal shaking incubator at 37°C with 8% CO_2. They were split every other day and transfected between passage 5 and 30.

Cells were grown to an optimal density of 2 million cells per mL, checked to have a viability greater than 95% and transfected using linear polyethylenimine (PEI) (Polyscience Inc., Germany) at 1 mg/mL. The transfection ratio was 1 µg DNA:3 µg PEI:1 mL transfection volume, made up in warm PBS (37°C) to reach 10% of the final transfection volume. This mix was incubated for 15 min at RT then added to the cell culture and the final glucose concentration adjusted to 6 g/L. The culture was maintained for 5 to 7 days while monitoring that cell viability didn't go under 40% and glucose concentration was adjusted every other day. On days 1 and 5, Lupin peptone solution (Solabia, Beauvais, France) was added to a concentration of 5 g/L as an AA supplement; on days 3, 5 and 7, the medium was

supplement with 2 mM L-Glutamine (Sigma-Aldrich, Saint-Quentin Fallavier, France). A sample of the culture was collected, centrifuged and the supernatant kept at 4°C to follow the protein expression and excretion.

At the end of the culture, the cells were centrifuged at 40000 G, 15 min at RT and the supernatant filtered on a 0.45 µm vaccum filter to remove impurities before IMAC (immobilized metal ion affinity chromatography) purification on either a Bio-Rad Biologic Duo Flow FPLC system in Melbourne or an ÄKTA purifier (GE Healthcare, Uppsala, Sweden) chromatography system in Bordeaux. The supernatant was loaded on Ni-NTA cartridges or Ni Sepharose HisTrap Excel 5 mL column (GE Healthcare, Uppsala, Sweden), respectively, rinsed with running buffer (NaCl 0,5 M, Tris base 50 mM, pH 7.4), washed with 5% elution buffer (same as running uffer plus 0,5 M imidazole) or 25 mM imidazole, and finally eluted in 80 to 100% elution buffer (0.4 to 0.5 M imidazole).

7.2.2.3 Sortase conjugation

The protocol was adapted from Hagemeyer and colleagues [19]. The Sortase enzyme was produced in-house in *E.coli*[20]. The reaction was carried out in a buffer containing 50 mM Tris-HCl, 150 mM NaCl, pH 8.0. The components were added in this order: 1/ buffer, so as to be at least 1/2 but no more than 4/5 of the final volume; 2/ scFv; 3/ peptide (nucleophile); 4/ sortase and 5/ CaCl2 to a 0.5 mM final. The quantities were calculated to reach molar ratios of 1:3:3 corresponding to scFv, enzyme and peptide (nucleophile), respectively. Those could be adapted depending on the reaction outcome. The reaction was carried out at 37°C with horizontal stirring for 4 to 6h.

In the scFv sequence, the 6His tag is placed closer to the C-terminus than the LPETG sequence. This way, it is cleaved by the enzyme during conjugation, and to eliminate the unreacted scFv and Sortase from the final product, the affinity of 6His for metal ions (Ni or Co) is taken advantage of.

Cobalt beads are used to remove these unwanted products from the reaction media. 500 µL beads (Talon His Tag Purification Resin, Clontech) were used per 1 mg scFv in Sortase reaction. Beads were first rinsed in ten times their volume of wash buffer (NaCl 0,5 M, Tris base 50 mM, pH 7.4) to remove the preservatives used by the manufacturer. They were left to settle or slowly spun on a tabletop centrifuge, the supernatant was discarded and new buffer added. This operation was repeated thrice. The beads were then introduced in the Sortase reaction mix and gently mixed on a roller for 2 to 3 h at 4°C. Afterwards, the beads were left to settle again and the supernatant retrieved. To remove the small remaining peptides a spin column was used (Millipore, cut-off 10 kDa).

Following each step of the reaction and cleaning process a small sample of the reaction media was removed, mixed with 5X Laemmli buffer with β_mercaptoethanol, heated at 95°C for 15 min and finally loaded on a gel for SDS-PAGE analysis. After migration, the gel was

stained with Coomassie brilliant blue (Bio-Rad). After destaining the gel was scanned on an Odyssey scanner (Li-Cor).

The SCE5 antibody targeting the integrin α2bβ3, previously described by Schwarz and colleagues [21], and produced in-house was used as a control for all the conjugation steps.

7.2.2.4 Reactivity evaluation in vitro

Immunohistochemistry was performed as described previously in 7.1.2.4. Atherosclerotic sections from atherosclerotic rabbits were used to assess the activity maintenance of biotin-conjugated antibodies.

Briefly, the sections were prepared as described previously, incubated overnight with the conjugated antibodies at 50 µg/mL each; rinsed, further incubated with a HRP-conjugated Streptavidin (Abcam, Paris, France)(working dilution 1/1000), rinsed again, then revealed with DAB.

7.2.3 Results

7.2.3.1 scFv LPETG production

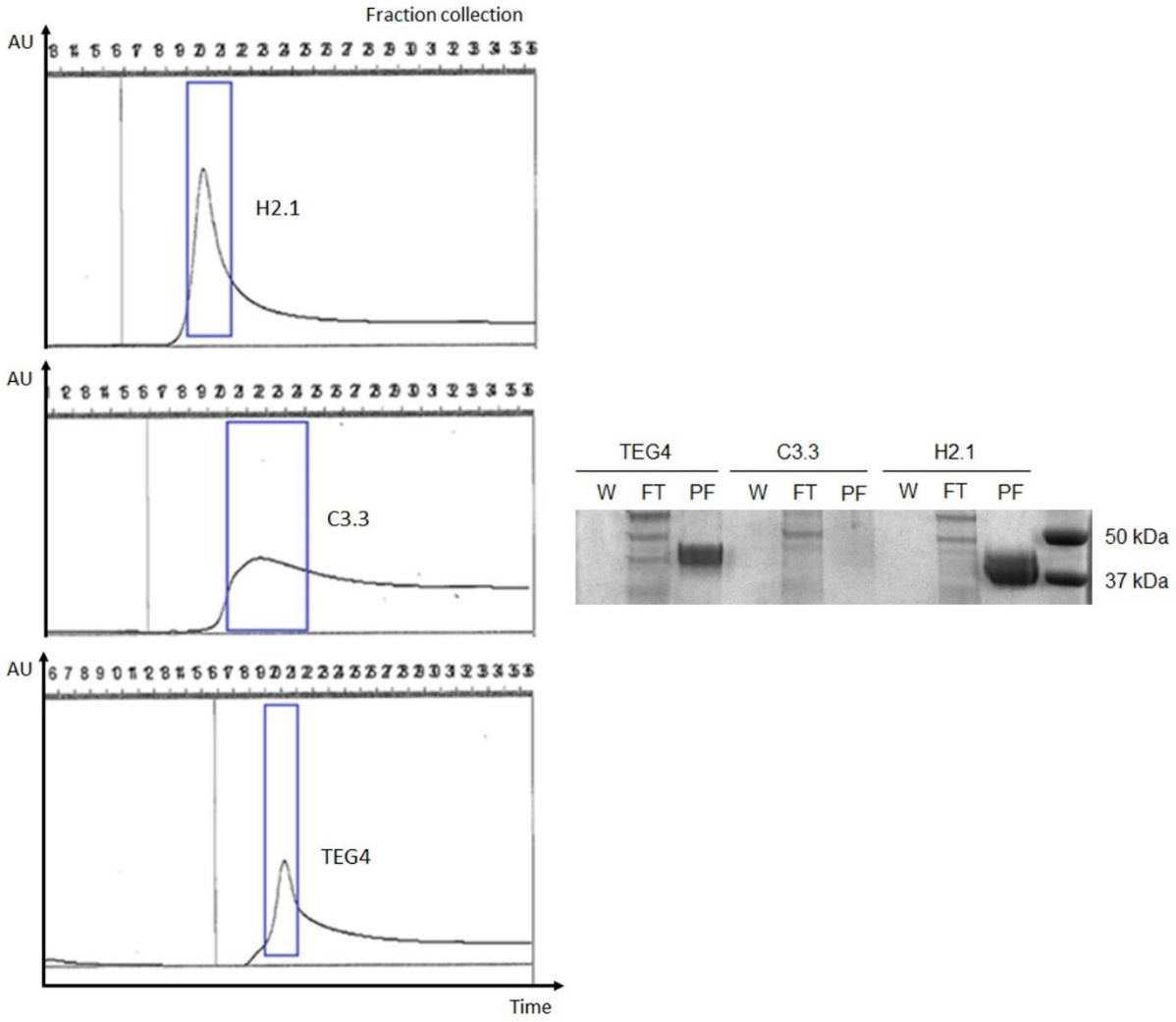

Figure 38: Purification of three scFv LPETG constructs H2.1, C3.3, TEG4. Left: purification reports showing the protein peak during elution; AU: absorbance units. Right: SDS-PAGE analysis of the purified fraction (PF) consisting of the antibody; flowthrough (FT) containing the impurities; wash (W) fraction showing no contaminant or unwanted protein elution.

After 7 days of culture (5 days if the cell viability dropped), the supernatant was harvested as described in the methods section, purified by IMAC and 1 mL fractions were collected. Figure 38 shows the purification report and SDS-PAGE analysis for 3 constructs: H2.1, C3.3 and TEG4. H2.1 and TEG4 purifications yielded a narrow protein peak whereas C3.3 was broader and slumped. H2.1 and TEG4 both yielded a 2 mL purified fraction with concentrations of 0.7 and 0.5 mg/mL, respectively. C3.3 gave a 5 mL fraction at 0.1 mg/mL. All three batches originating from a 250 mL culture volume, the overall yield for this production was 5.6, 4 and 2 mg per liter of culture for H2.1, TEG4 and C3.3, respectively. The gel electrophoresis shows that most impurities went to the flowthrough, and that the washing didn't elute the antibody, which seems collected into the purified fraction.

7.2.3.2 Sortase conjugation

A ratio of scFv/Sortase enzyme/nucleophile of 1/3/3 was generally used as a start and adapted to the nucleophile substrate, if necessary, to improve the conjugation yields. The fluorochrome Cyanine 7 (Cy7; λEx=750 nm; λEm=775 nm) was used as a first intention substrate because it could be revealed rapidly on a gel stained with Coomassie and read on the Odyssey scanner: protein bands appeared red in the 700 nm channel and the NIR fluorochrome green in the 800 nm channel. Figure 39 shows a typical analysis for scFv conjugation: in the upper gel, the scFv alone was loaded as a control for size around 37 kDa, showing in the red channel; the 1/3/3 lane shows the Ab, more or less NIR-labelled (red and green); the sortase enzyme below, around 25 kDa; and finally the unconjugated Cy7 around 10 kDa in green. Interestingly, the SCE5 Ab presents two distinct bands of very close size; after reaction with the Sortase, the same two bands remain but their size drops. This phenomenon, although extremely reproducible, doesn't seem to affect the Ab reactivity and remains unexplained.

The 1/0/3 ratio, with no enzyme, was used as a negative control to show that the

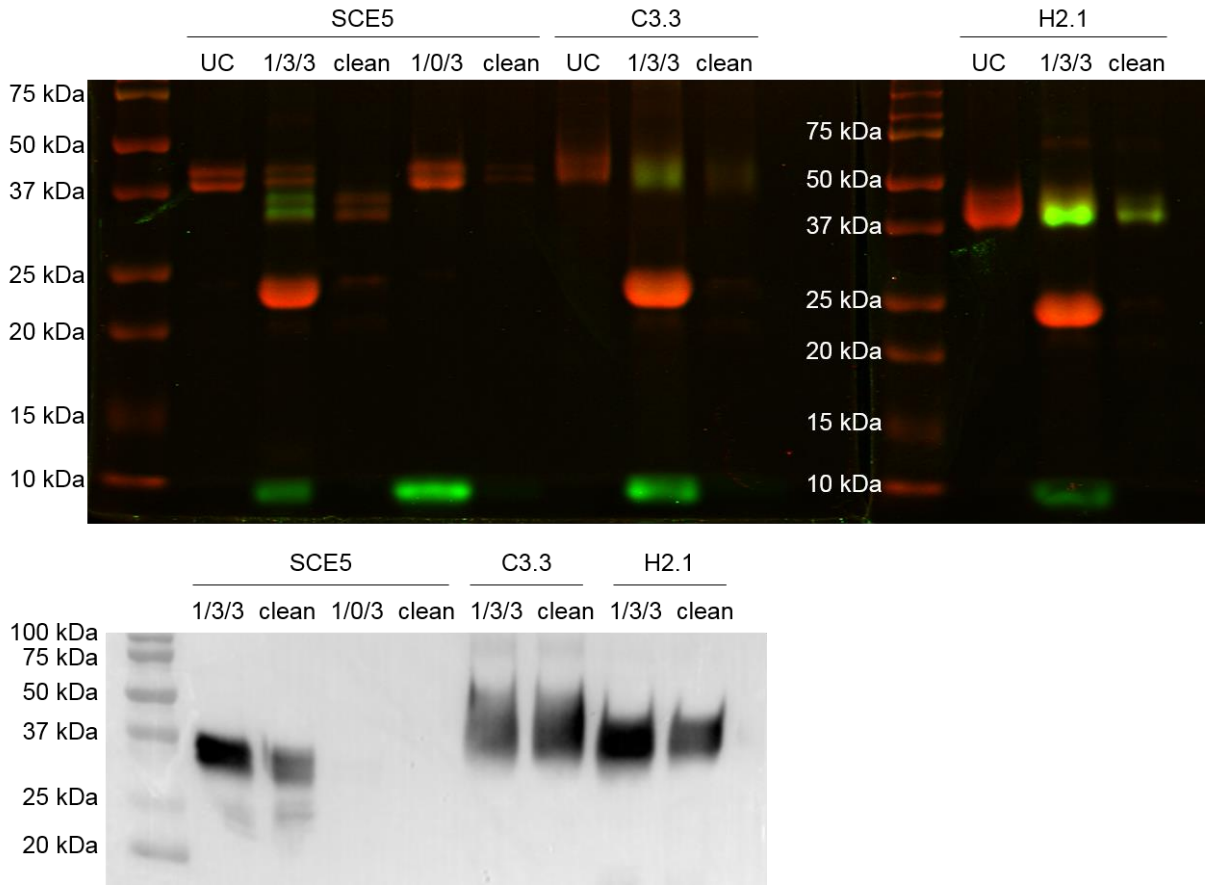

Figure 39: Sortase conjugation of Abs to different substrates. Top: conjugation of SE control scFv, C3.3 and H2.1 scFv to the fluorochrome Cyanine 7, readout on the Odyssey scanner at 700 nm (red) and 800 nm (green). Bottom: conjugation of SE control scFv, C3.3 and H2.1 scFv to Biotine, revealed by Western blotting with a HRP-labelled Streptavidin and using a chemiluminescent substrate. UC: unconjugated is the scFv alone; 1/3/3: is the scFV/enzyme/nucleophile ratio, 1/0/3 being the negative control reaction with no enzyme; clean: after the cleaning procedure with MAC beads and spin column purification.

conjugation was indeed specific. The clean lane is the result of a two-step process involving incubation with cobalt beads that specifically bind the 6His protein label, both on the Ab and the enzyme; in a second step the supernatant is span on a column with a 10 kDa cut-off to get rid of the nucleophile. Noteworthy, none of the components' size -compared to the protein ladder- accurately reflects its theoretical molecular size. This may be due to uncomplete denaturation or impaired migration in SDS. The bottom part of the figure is the Western blot analysis of a scFv – Biotin conjugation, further incubated with HRP-Streptavidin and revealed with chemiluminescent substrate.

In each case, the 1/3/3 lane indeed shows a conjugation of the substrate to the scFv, either revealed by fluorescence or Western blotting. After cleaning, the signal decreases, indicating that some of the conjugated-scFv is lost, most likely adsorbed on the column during the spinning process. In the case of the SCE5, the clean product is seemingly not fluorescent (red/yellow signal), which would mean the conjugation didn't work well. The Western blot readout on the biotin conjugation mitigates this conclusion as there is a strong signal in the 1/3/3 lane, which decreases dramatically after cleaning, but still exists. SCE5 conjugate appears more sensitive to non-specific binding to Talon beads or spin column than C3.3 and H2.1 that only show a slight signal diminution. This difference between both techniques may either be due to the conjugation itself, through different reactivity of the nucleophile groups, or to the sensitivity of the readout method.

7.2.3.3 IHC

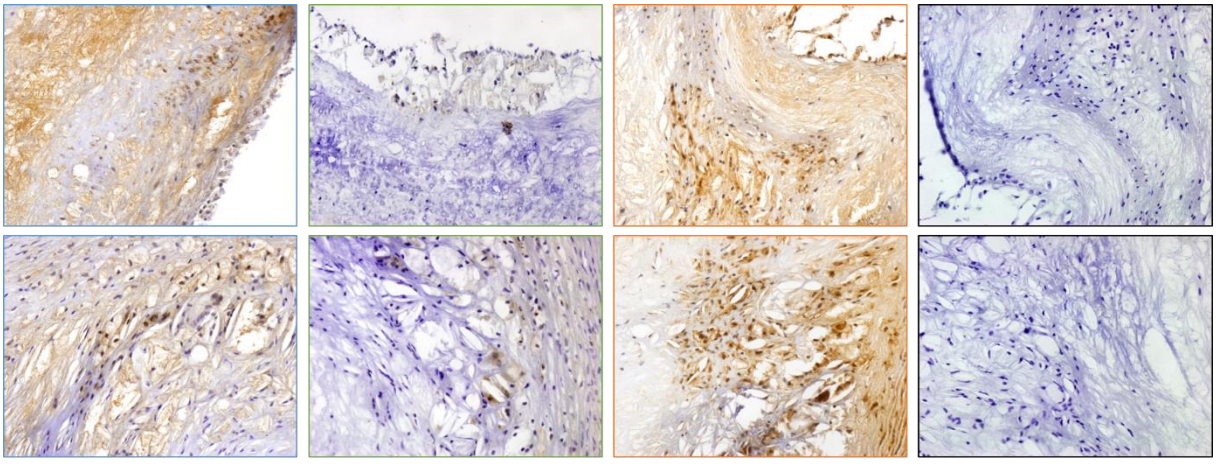

Figure 40: Immunohistochemistry staining of rabbit atherosclerotic plaques using biotin-labelled scFvs. Top row images show the luminal area while bottom row images focus on the lipid-rich core (as shown by the vacuoles). Streptavidin-HRP is used to reveal the biotin-labelled Ab and alone as a control for endogenous biotin content of the tissue.

Immunohistochemistry was used as a way to monitor the scFv reactivity against atherosclerotic plaque content. The SCE5 Ab, specific for activated platelets [21], was used as a positive control. Biotin-labelled C3.3, H2.1, and SCE5 were incubated on atherosclerotic rabbit lesions at a concentration of 50 µg/mL, and revealed with HRP-labelled Streptavidin.

In presence of DAB, the HRP-conjugated Ab-biotin-streptavidin complex yielded a brown deposit.

Both C3.3 and H2.1 targets are unknown, but show different staining patterns, as shown by Figure 40. C3.3 yields a diffuse signal towards the outer plaque area and more distinct in the lipid-rich core, which resembles this of SCE5. In contrast, H2.1 is fairly limited to sparse cellular structures.

References

1. Jacobin, M.-J. *et al.* Human IgG monoclonal anti-alpha(IIb)beta(3)-binding fragments derived from immunized donors using phage display. *J. Immunol. Baltim. Md 1950* **168,** 2035–2045 (2002).

2. Deramchia, K. *et al.* In Vivo Phage Display to Identify New Human Antibody Fragments Homing to Atherosclerotic Endothelial and Subendothelial Tissues. *Am. J. Pathol.* **180,** 2576–2589 (2012).

3. Jacobin-Valat, M.-J. *et al.* Nanoparticles functionalised with an anti-platelet human antibody for in vivo detection of atherosclerotic plaque by magnetic resonance imaging. *Nanomedicine Nanotechnol. Biol. Med.* **11,** 927–937 (2015).

4. Vallet-Courbin, A. *et al.* A Recombinant Human Anti-Platelet scFv Antibody Produced in Pichia pastoris for Atheroma Targeting. *PloS One* **12,** e0170305 (2017).

5. Ma, Y.-Q., Qin, J. & Plow, E. F. Platelet integrin alpha(IIb)beta(3): activation mechanisms. *J. Thromb. Haemost. JTH* **5,** 1345–1352 (2007).

6. Philibert, P. *et al.* A focused antibody library for selecting scFvs expressed at high levels in the cytoplasm. *BMC Biotechnol.* **7,** 81 (2007).

7. Curtiss, L. K. & Boisvert, W. A. Apolipoprotein E and atherosclerosis. *Curr. Opin. Lipidol.* **11,** 243–251 (2000).

8. Zou, J., Dickerson, M. T., Owen, N. K., Landon, L. A. & Deutscher, S. L. Biodistribution of filamentous phage peptide libraries in mice. *Mol. Biol. Rep.* **31,** 121–129 (2004).

9. Hermanson, G. T. in *Bioconjugate Techniques (Third edition)* 229–258 (Academic Press, 2013).

10. Mornet, S. Synthèse et modification chimique de la surface de nanoparticules de maghémite à des fins d'applications biomédicales. (Université Sciences et Technologies - Bordeaux I, 2002).

11. Mornet, S., Portier, J. & Duguet, E. A method for synthesis and functionalization of ultrasmall superparamagnetic covalent carriers based on maghemite and dextran. *J. Magn. Magn. Mater.* **293,** 127–134 (2005).

12. Pidard, D., Montgomery, R. R., Bennett, J. S. & Kunicki, T. J. Interaction of AP-2, a monoclonal antibody specific for the human platelet glycoprotein IIb-IIIa complex, with intact platelets. *J. Biol. Chem.* **258,** 12582–12586 (1983).

13. Adumeau, L. *Développement de stratégies de biofonctionnalisation de surface de nano-objets pour des applications biologiques*. (Bordeaux, 2015).

14. Moutel, S. *et al.* A multi-Fc-species system for recombinant antibody production. *BMC Biotechnol.* **9,** 14 (2009).

15. Schneewind, O., Model, P. & Fischetti, V. A. Sorting of protein a to the staphylococcal cell wall. *Cell* **70,** 267–281 (1992).

16. Mazmanian, S. K., Liu, G., Ton-That, H. & Schneewind, O. Staphylococcus aureus sortase, an enzyme that anchors surface proteins to the cell wall. *Science* **285,** 760–763 (1999).

17. Marraffini, L. A. & Schneewind, O. Anchor Structure of Staphylococcal Surface Proteins V. ANCHOR STRUCTURE OF THE SORTASE B SUBSTRATE IsdC. *J. Biol. Chem.* **280,** 16263–16271 (2005).

18. Paterson, G. K. & Mitchell, T. J. The biology of Gram-positive sortase enzymes. *Trends Microbiol.* **12,** 89–95 (2004).

19. Hagemeyer, C. E. *et al.* Particle generation, functionalization and sortase A–mediated modification with targeting of single-chain antibodies for diagnostic and therapeutic use. *Nat. Protoc.* **10,** 90–105 (2015).

20. Alt, K. *et al.* A versatile approach for the site-specific modification of recombinant antibodies using a combination of enzyme-mediated bioconjugation and click chemistry. *Angew. Chem. Int. Ed Engl.* **54,** 7515–7519 (2015).

21. Schwarz, M. *et al.* Single-chain antibodies for the conformation-specific blockade of activated platelet integrin αIIbβ3 designed by subtractive selection from naive human phage libraries. *FASEB J.* **18,** 1704–1706 (2004).

8 Imaging

8.1 Targeted Magnetic Resonance Imaging

The detailed methods and results for this chapter are available in the article *Nanoparticles functionalized with an anti-platelet human antibody for in vivo detection of atherosclerotic plaque by magnetic resonance imaging*[1] and online supplementary data.

8.1.1 Introduction interest of study

This study provided a proof of concept for platelet targeting as a relevant marker for atherosclerosis, as shown by IHC, flow cytometry, confocal microscopy and electron microscopy. It also demonstrated the feasibility of targeted nanoparticles imaging in MRI, *ex vivo* on atherosclerotic mice aorta, and as a potential tool for *in vivo* imaging. The ligand used for functionalizing nanoparticles is the recombinant TEG4 human anti-platelet antibody under IgG4 format (rIgG4 TEG4).

8.1.2 Material and methods

8.1.2.1 Confocal microscopy, TEM

Preserved targeting capacity of the rIgG4 TEG4-VUSPIO nanoparticles was further assessed by confocal microscopy, transmission electron microscopy (TEM) and MRI. For confocal microscopy results please refer to the full article.

8.1.2.1.1 TEM

Aliquots of 10^8 human platelets activated with 0.5 U/ml thrombin were fixed with 0.1 % (v/v) glutaraldehyde / 1.5 % (v/v) paraformaldehyde for 30 min at room temperature, washed in 0.1 M phosphate buffer (pH 7.4) and mixed with rIgG4 TEG4-VUSPIO and IgG cont-VUSPIO in 0.1 M phosphate buffer.

After overnight incubation, the platelets were washed in 0.1 M phosphate buffer (pH 7.4) and then post-fixed in 1% (v/v) osmium tetroxide in 0.1 M phosphate buffer for 1 h 45 at room temperature. After washing in 0.1 M phosphate buffer, the platelets were embedded in 1 % agarose (m/v) and sectioned in small pieces (1 mm3). Samples were dehydrated through a series of graded ethanol and propylene oxide baths. Specimens were embedded in a mixture of propylene oxide and epoxy resin (Epon 812; EMS, Hatfield, PA) (v/v) for 2 hours and then in 100 % resin overnight. The resin was polymerized at 60°C for 48 h. The samples were sectioned using a diamond knife on an ultra-microtome (Ultracut-E, Leica Microsystems). Thin sections (70 nm) were picked up on copper grids and then stained with uranyl acetate and lead citrate. The grids were examined with a transmission electron microscope at 80 kV (H7650, Hitachi, Tokyo, Japan), Mode High Resolution equipped with a camera GATAN Orius 11Mpixel.

In parallel, drops of nanoparticles were adsorbed to carbon film copper grids and were examined without contrast.

8.1.2.2 MRI

8.1.2.2.1 Ex vivo MRI

ApoE−/− mice fed a high fat diet or control C57BL/6 wild-type mice were terminally anaesthetized by inhalation of isoflurane. The aorta was exposed and washed by intra-cardiac injection of PBS heparin, then PBS alone. Then a solution of either rIgG4 TEG4-VUSPIO, IgG cont-VUSPIO or PBS was incubated for 20 min before rinsing and fixing in paraformaldehyde (PFA). The aorta was then removed and embedded in agarose in a glass tube. *Ex vivo* MR imaging was performed using FAST sequence on a 9.4 Tesla MRI system (Bruker). The use of iron oxide agents in MRI imposes to use a T2* weighted imaging sequence, showing a local "negative contrast" enhancement.

8.1.2.2.2 In vivo MRI

In vivo MRI was performed using a 4.7 Tesla system (Bruker BIOSPEC 47/50; Ettlingen, Germany) prior and 24 h after injection in the tail vein of rIgG4 TEG4-VUSPIO sample diluted in 200 µL physiological serum. Four milligram Fe3+ per kilo of body weight (n=3) or 15 mg/kg Fe3+ body weight (n=3) doses were administrated. Atherosclerotic ApoE-/- mice were anesthetized using 2.5 % isoflurane before imaging. Pre-contrast and post-contrast T2*-weighted MR imaging of the atherosclerotic ApoE-/- mice thoracic aorta were acquired with a Flash 2D sequence (TE= 3.8 ms; TR= 22 ms; 32 scans, 2 slices, thickness 1 mm, resolution 0.146 x 0.146 mm2, FOV 28 x 28 mm^2).

A mouse that received a dose of 4 mg/kg Fe3+ was euthanized after the final MRI scan. The aorta was removed and embedded in a glass MR tube containing 0.8 % m/v high-grade, low melting-point agarose. MR imaging was performed using a 9.4 Tesla MRI system as described above.

8.1.3 Results

8.1.3.1 TEM

TEM images clearly showed the presence of contrast agents distributed all around the platelets, especially in the pseudopodia developed in activated platelets: Figure 42. The

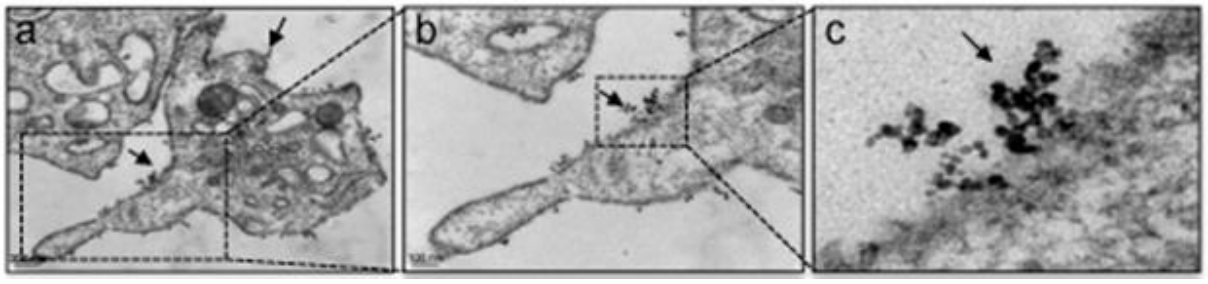

Figure 41: TEM images of rIgG4 TEG4-VUSPIO incubated with activated platelets. The arrowheads point to the localization of the contrast agent, seen as black dots on the images. b and c are magnified views of image a (zoom indicated by dashed line).

same platelets incubated with IgG cont-VUSPIO showed no VUSPIO labelling (See full article).

8.1.3.2 Ex vivo MRI

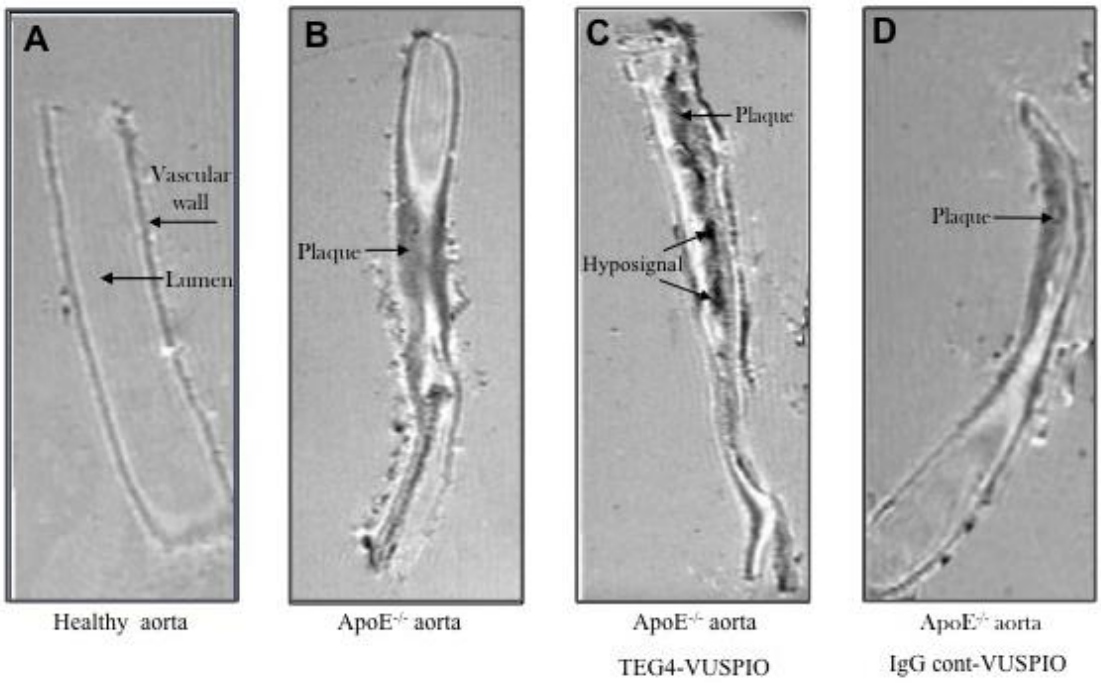

Figure 42: Ex vivo MRI at 9.4 Tesla. The healthy (A) or atherosclerotic ApoE aorta (B, C, D) were perfused ex vivo with PBS (A, B), rIgG4 TEG4-VUSPIO (C), IgG-cont VUSPIO (D). No atherosclerotic plaque was visible in healthy aorta (A). Panel C shows an intense hyposignal due to iron deposition within atherosclerotic plaque. In contrast, no loss of signal was observed when IgG cont-VUSPIO was administered (D).

Aortas from control C57BL/6 wild-type or ApoE−/− mice fed a high fat diet and perfused with PBS allowed for plaque localization on the MRI images at 9.4 Tesla. When incubated with rIgG4 TEG4-targeted VUSPIO, ApoE-/- mice aorta showed vascular wall nanoparticles take-up, shown by a local negative contrast enhancement or hyposignal, compared to control irrelevant IgG-VUSPIO (Figure 42).

8.1.3.3 In vivo MRI

Previous studies have reported the accumulation of superparamagnetic iron oxide particles in the aorta of atherosclerotic rabbits. Therefore we injected antibody-free VUSPIO in ApoE-/- mice and failed to observe differences between uninjected and antibody-free VUSPIO injected atherosclerotic ApoE-/- mice (data not shown). rIgG4 TEG4-VUSPIO contrast agent was then injected in ApoE-/- mice. rIgG4 TEG4-VUSPIO nanoparticles were well-tolerated *in vivo*. There were no clinical signs indicative of toxicity during or after iron oxide administration.

Representative *in vivo* MR images obtained before and 24 h after injection of rIgG4 TEG4-VUSPIO are shown in Figure 43. Axial T2-weighted images of two ApoE-/- mice, realized before (Figure 43, A, D) and 24 h after injection of 4 mg/kg Fe3+ (Figure 43, B, C) or 15 mg/kg Fe3+ (Figure 43, E, F) showed an hyposignal (Figure 43, B, C, E, F) compared to pre-contrast

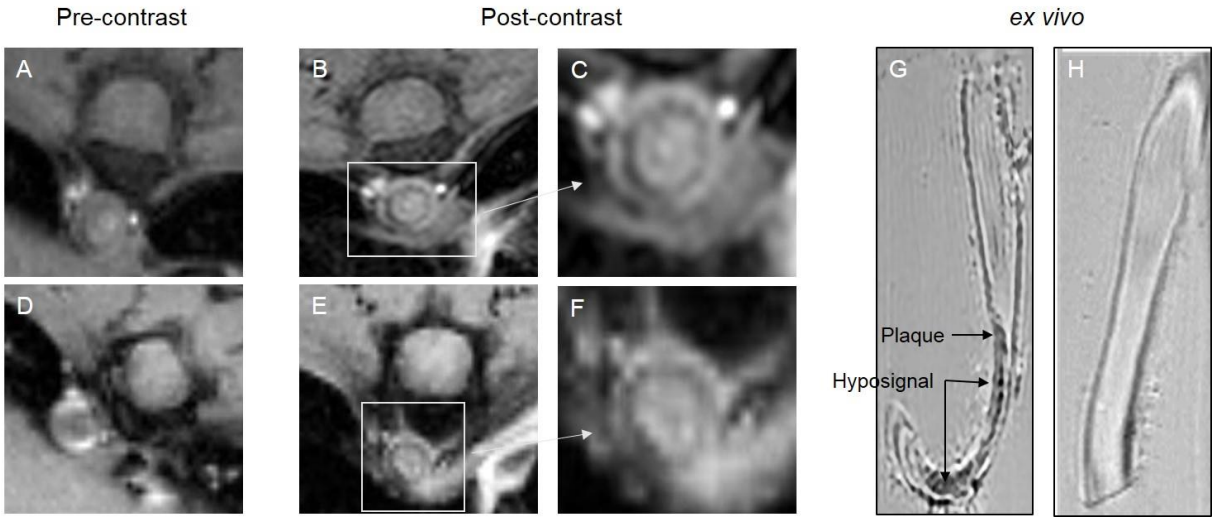

Figure 43: In vivo MRI at 4.7 Tesla. The aorta was imaged in vivo by IRM before (Pre-contrast) and 24 h after (Post-contrast) the administration of doses of 4 mg/kg Fe3+ and 15 mg/kg Fe3+ of rIgG4 TEG4-VUSPIO to atherosclerotic ApoE mice. Panels B, C (4 mg/kg Fe3+) and E, F (15 mg/kg Fe3+) show a signal loss in the arterial wall (white arrow). Ex vivo MRI performed at 9.4 Tesla shows hyposignals (G) in atherosclerotic plaques developed in the lower part of thoracic aorta whereas no hyposignal was detected in the upper part, which was without intimal thickening (H).

images (Figure 43, A, D). No significant difference in hyposignal was observed between both doses. These preliminary *in vivo* studies tend to show a loss of MR signal generated by iron oxide accumulation in the atherosclerotic vessel wall of ApoE-/- mice 24 h after administration of the rIgG4 TEG4-VUSPIO contrast agent. This was confirmed by *ex vivo MRI* performed on the atherosclerotic aorta extracted from an *in vivo imaged* ApoE-/- mouse that received the 4 mg/kg Fe3+ dose. A focal signal loss was observed in atherosclerotic plaques located in the lower part of the thoracic aorta (Figure 43, G). No hyposignal was detected in the upper part of the thoracic aorta, which was without intimal thickening (Figure 43, H).

8.1.4 Discussion

In this study, we were able to demonstrate the targeting of activated platelets within the aorta lesions both *in vitro* and *ex vivo*, with a full IgG4 Ab produced with the Baculovirus technology. The conjugation ratio didn't exceed one Ab per nanoparticle, probably due to the steric bulk of a full IgG. Preliminary results also indicate the potential of these targeted nanoparticles for *in vivo* atheroma imaging in an animal model.

In further studies the chosen Ab formats were small-size fragments scFv or scFv-Fc (5.2) and the conjugation method was improved to be site specific so as to graft multiple fragments to improve nanoparticle avidity and avoid Ab binding site disruption (6.1).

The grafting of antibodies to nanoparticles being too time consuming for primary screening, fluorescent imaging was preferred as a first intention. It was also used as a tool for further validation of nanoparticles biodistribution and to confirm potential plaque targeting observed in MRI.

8.2 Targeted fluorescent imaging

Ab candidates selected through phage display *in vivo* and produced under the scFv-Fc format were assessed for their *in vivo* targeting capacity. To this end they were conjugated to fluorochromes emitting in the near infrared range (see 6.2.2). Indeed, fluorescent imaging is known to be very sensitive and presents the advantage to be easy to set up. Near infra-red fluorescence (NIRF) was used because atheroma plaque is rich in autofluorescent content[2]; additionally, it provides increased imaging depth compared to shorter wavelengths.

8.2.1 Material and methods

8.2.1.1 In vivo injection

ApoE−/− mice fed a high fat diet or control C57BL/6 wild-type mice were gas – anaesthetized (induction with 5% isoflurane in a flow of 1.5 mL air per min for a couple minutes then maintenance at 0.5% isoflurane). Basal images were acquired before injection, then immediately after (T0) and again after 24 hours (T24).

Two fluorescent imaging apparatus were used in the VivOptic imaging facility led by Dr Franck Couillaud in Bordeaux University, France. The Fluobeam (Fluoptics, Grenoble, France) is a real-time intraoperative 2D camera system coupled with a 780 nm excitation laser and emission filters at 820 nm. The fluorescence molecular tomography system FMT 4000 apparatus (Perkin Elmer Inc., Boston, MA, USA) is a small-animal imaging system for preclinical research. A calibrated quantitative tomographic image is reconstructed from the signal collected within the depth of the animal tissues. The apparatus has four near-infrared channels excited at 635, 670, 746 and 790 nm, and emitting at 660, 700, 775 and 805 nm, respectively. Our experiments used the farthest channel: λ_{Ex} 790 nm – λ_{Em} 805 nm. The images were reconstructed using the TrueQuant software.

After 24 h the animals were humanely killed, dissected, and biodistribution images in various organs and the aorta were immediately acquired.

8.2.1.2 Fluorescent microscopy

As a control for *in vivo* targeting, immunofluorescence was considered.

Fluorescent microscopy was carried out at the Bordeaux imaging center (BIC), on a confocal microscope (Leica, DMI6000). Unfortunately, the excitation and detection wavelengths of the system didn't match those of the fluorochrome, which impaired the signal detection. The main problem encountered at the time with this method was that no laser/filter system was available in the right excitation/emission wavelengths. No sufficient signal could be gathered from the sections to either confirm or disprove the fluorescent Ab binding.

As a perspective for this method, a new filter block in the desired wavelength was acquired by Dr Frederic Bringaud in collaboration with the VivOptic platform that should help for this

validation. Furthermore, Dr Florence Ottones who recently joined our team has an expertise in fluorescent histology and will be able to assist with protocol troubleshooting.

8.2.2 Results

8.2.2.1 Standardization

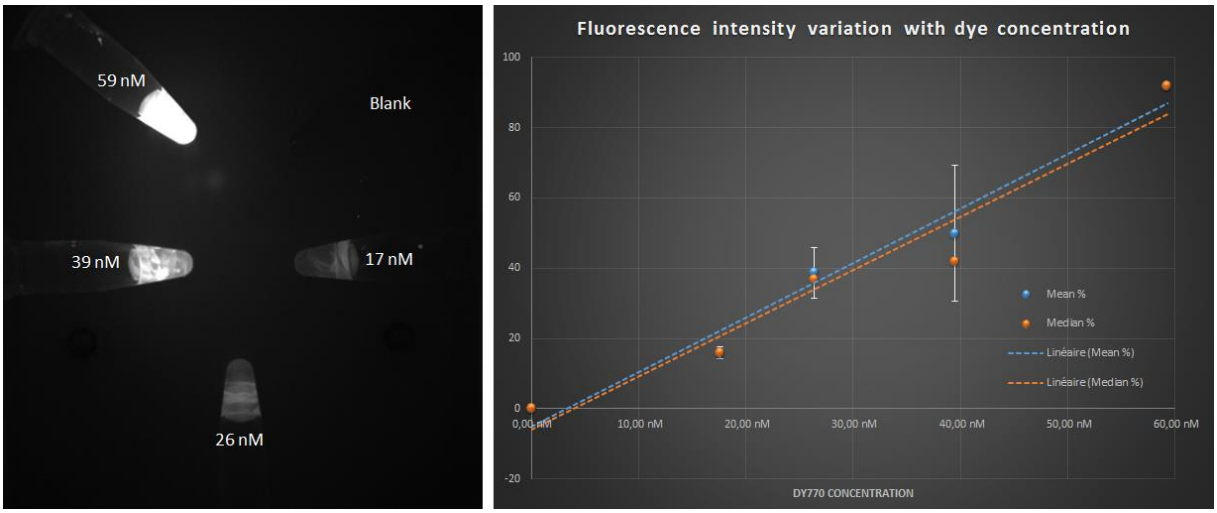

Figure 44: Serial dilutions and standardization curve for the Dy770 dye. Left: fluorescent image of the dye dilution range captured using the Fluobeam camera at 1000 ms exposure; right: plotted fluorescence intensity values acquired with ImageJ software.

To standardize the data obtained with the Fluobeam, an image of serial dilutions was acquired, and the signal quantified using ImageJ. Briefly, the Threshold function (Image > Adjust > Threshold) was used to 1/ measure the tube or aorta fluorescence level (Analyze > Measure); 2/ measure the image background. ImageJ Threshold function allows eliminating all the pixel values below or above a set threshold in the image measurement. The Measure function permits to perform analysis such as measuring the Area, calculating the Mean pixel values, the Standard Deviation, and recording the Max and Min pixel values. By plotting the Mean pixel values in the tubes we were able to establish a standardization curve: Fluorescence Intensity = f[dye]. When comparing the aorta fluorescence levels, each image was standardized against its own background using the ImageJ Math function (Process > Math > Divide).

Before FMT imaging, the dyes were loaded in the calibration cassette and calibration was performed according to the manufacturer instructions.

8.2.2.2 In vivo imaging and biodistribution

All conjugated Ab was usually injected to ApoE-/- mice, without exceeding 200 µL. The same antibody was injected to a wild-type C57BL/6 mouse, or PBS injected to an ApoE-/- mouse, as controls. *In vivo* imaging by Fluobeam or FMT yielded the same images, showing a massive take-up of the fluorescence by the liver, consistent with the preferential elimination pathway. The same was observed with the wild-type mouse, but the dye alone was mainly eliminated by the urinary pathway as expected from its small size. After 24 h, all mice

showed a decrease in liver fluorescence and the mock injected mouse was back to its fluorescent baseline.

After sacrifice and dissection, a similar pattern was observed since the liver was making up most of the observed signal. Upon removal and dissection of the other organs, fluorescence could be detected in kidneys, heart and aorta, inconstantly in spleen, but not in abdominal fat, lungs or thigh muscle which were used as controls (data not shown, similar as VUSPIO-Dye distribution: Figure 48). Also, to assess the baseline autofluorescence in ApoE mice for biodistribution interpretation, an uninjected ApoE mouse was also imaged as a control. FMT imaging couldn't be successfully used with dissected mice because a different interface was then present in the imaging cassette that prevented the TrueQuant software algorithm from correctly reconstructing the fluorescent area.

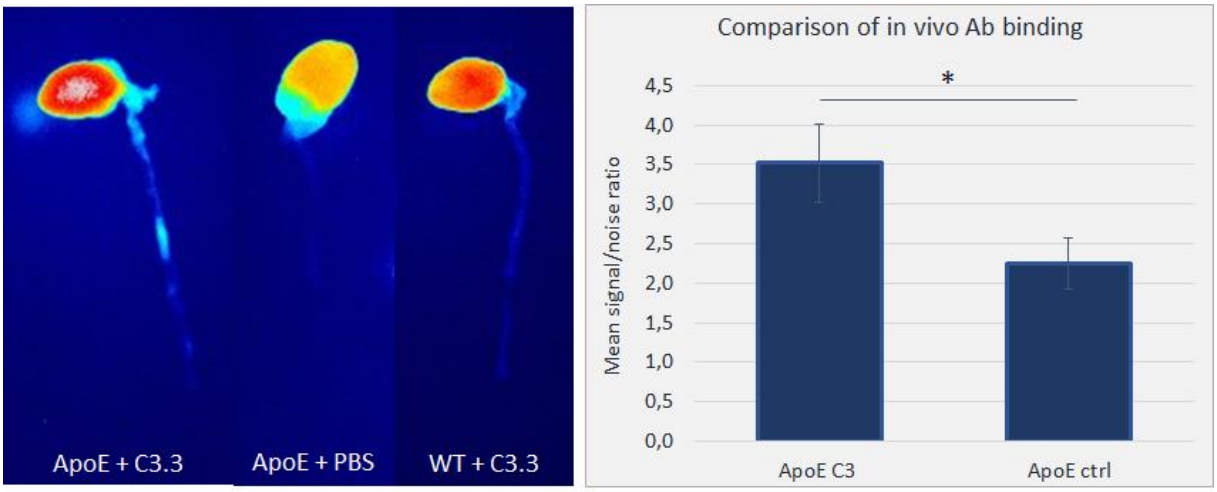

*Figure 45: In vivo binding of fluorescent Ab to mouse aorta. Left: images from mouse aortas captured with the Fluobeam camera at 1000 ms exposure and color-enhanced using ImageJ software, aortas from ApoE mice fed a high fat diet or a wild-type (WT) mouse, injected with C3.3-dye or with PBS. Right: ImageJ quantification of the fluorescent signal in aortas from ApoE mice injected with dye-conjugated C3.3 (C3) or with PBS (ctrl), N=3 in each group, *p=0.1.*

Aortas from mice injected *in vivo* with C3.3-dye showed a greater fluorescent signal than their non-injected counterparts (Figure 45, right). The pattern of fluorescence distribution followed this of lesion areas, as confirmed by the absence of brighter "spots" on the wild-type aorta (Figure 45, left). Interestingly, the heart possesses a strong auto-fluorescence that is further enhanced by the fluorochrome injection, possibly because it is unspecifically trapped in the terminal branches of coronary arteries. Another explanation, supported by the apparent stronger fluorescence enhancement in the heart of ApoE-/- mice, is that coronary atherosclerotic lesions, although too small to be imaged with sufficient resolution, are indeed present and retain the targeted fluorochrome.

8.2.3 Discussion

NIRF imaging clearly demonstrated its usefulness to assess the reactivity of selected Ab fragments *in vivo*. It proved easy to set up, sensitive, and, with a correct protocol set up and image analysis procedure, should allow to compare the candidates in a semi-quantitative way.

Unfortunately, *in vivo* imaging of the aorta couldn't be realized because of its depth, small size, and relative low signal compared to other organs. Overall, fluorescence appears like a good method for proof-of-concept demonstration, but inherently lacks resolution.

8.3 Bimodal NIRF – MRI imaging

8.3.1 Introduction

We previously demonstrated that TEG4 monoclonal human antibody, obtained from phage display *in vitro*, can target platelets in atheroma lesions both *in vitro* and *ex vivo.* We also showed that iron nanoparticles (VUSPIO) functionalized with TEG4 were still able to bind platelets both *in vitro* and *ex vivo*, and could be detected by TEM and MRI[1].

In this study, we investigated the effect of multivalent, site-specific grafting of antibody fragments on the reactivity of VUSPIO nanoparticles: at least 6 scFv fragments were attached to the surface of the nanoparticles, for all experiments presented in this chapter. In addition, fluorochromes were attached to the surface of the VUSPIO to allow for a multimodal NIRF – MRI detection.

The same activated platelet – reactive TEG4 antibody was produced as a scFv fragment in the yeast *Pichia pastoris* (see 7.1.2.1). This Ab was further engineered to possess 2 terminal cysteines that allowed for site directed grafting on the surface of the nanoparticle.

Avidity and reactivity were assessed as previously described (7.1.2) and atheroma imaging was performed in the mouse model ApoE-/-.

Ex vivo binding was first studied via NIRF measurements and MRI, then the functionalized carrier was injected to evaluate its reactivity *in vivo* and its usefulness as an atheroma-specific diagnosis agent.

8.3.2 Material and methods

8.3.2.1 Imaging

All animal studies were approved under the N° 50120192-A by the Animal Care and Use Committee of Bordeaux, France. ApoE-/- mice were obtained from Charles River Laboratories and fed a high-cholesterol diet (0.15% cholesterol, Avogadro Western diet, Safe, Augy, France) for 21 weeks. Wild-type control C57BL6 mice were used as a negative control (Charles River Laboratories, St Germain sur l'Arbresle, France).

8.3.2.1.1 Ex vivo

ApoE−/− mice fed a high fat diet or control C57BL/6 wild-type mice were terminally anaesthetized by inhalation of isoflurane. The aorta was exposed and washed by intra-cardiac injection of PBS heparin, then PBS alone. Then a solution of either multivalent TEG4-VUSPIO, IgG cont-VUSPIO or PBS was incubated for 20 min before rinsing and fixing in paraformaldehyde (PFA). The heart and aorta were then removed and embedded in agarose in a glass tube. *Ex vivo* high resolution MR imaging was performed on a horizontal 7 T Biospec system (Bruker, Ettlingen, Germany). T2* maps were calculated from a RF-spoiled multi gradient echo (MGE) images (repetition time TR = 1000 ms, first echo time TE = 3.2 ms, ΔTE = 3.6 ms, number of echoes = 8, α = 30°, FOV = 32 x 12 mm², NEx = 32), using the Paravision software (Bruker). Fluorescent images were then acquired on the aforementioned imaging device Fluobeam.

8.3.2.1.2 In vivo

Animals were anaesthetized with 2% isoflurane (Belamont, Nicholas Piramal Limited, London, UK) in air for all imaging procedures.

Multivalent TEG4-VUSPIO-Dylight800 particles were injected to ApoE-/- mice, in a quantity corresponding to 4 mg Fe /kg and imaged by MRI and fluorescence imaging. Basal images before injection were acquired for each *in vivo* technique. Non-injected and irrelevant-Ab injected mice served as controls.

MRI was carried out on a horizontal 4.7 T Biospec system (Bruker, Ettlingen, Germany), equipped with a 12 cm gradient insert capable of 200 mT/m maximum strength. T2* weighted multi gradient echo (MGE) MR sequence were acquired (repetition time TR = 1000 ms, first echo time TE = 3.5 ms, ΔTE = 4.5 ms, α = 60°, NEx = 3). The images were acquired before, immediately after injection and 24 h later.

A section corresponding to the abdominal aorta was imaged using T2star (T2*) map MGE sequences. Before and after injection, Black blood procedure was used to delineate the luminal border of the atheroma plaque, and Bright blood procedure to optimize the MR contrast between blood and iron oxide-labelled plaque. Comparison of MR signal before and after injection was helped by the calculation of a R2* map (=1/T2*) for each voxel, which was done as described previously using the Paravision software.

After the last image was acquired, the animals were humanely killed and dissected, while fluorescence imaging was performed at the Vivoptic facility in Bordeaux, using the Fluobeam imager. A blood sample was immediately retrieved from the cava vein and all remaining blood washed from the circulatory system and organs with a 3 mL PBS heparin (50 U/mL), followed by a 10 mL PBS intracardiac perfusion.

The aorta was removed and embedded in a glass MR tube containing 0.8 % m/v high-grade, low melting-point agarose. MR imaging was performed using a 7 Tesla MRI system as described above.

8.3.3 Results

8.3.3.1 Ex vivo imaging

Taking advantage of the bimodal imaging agents injected, both fluorescent and MR images of the aortas were acquired and compared. Fluorescent images were standardized for their respective background using ImageJ software. Successive echo images were used to establish a T2* map of the signal. While the presence of fluorescent particles in the aortic wall is noted by an increased pixel value (color-coded from black to white); the presence of VUSPIO is noted by a decrease in the T2* values (color-coded from cyan to purple). Figure 46 shows ApoE-/- mice aortas either uninjected (Figure 46, a, b) or multivalent TEG4-VUSPIO-injected (Figure 46, c, d, e). The intimal thickening (white arrows) characteristic of atherosclerotic plaque is present in both mice, although it doesn't yield a fluorescent signal, it provokes a decrease of the T2* values (T2* = 11.2 ± 0.7 ms). In the multivalent TEG4-VUSPIO injected mouse, a strong T2* shortening (T2* = 7.0 ± 0.9 ms; Figure 46, e, dashed arrows) also corresponds to an increase in fluorescence (Figure 46, d, dashed arrows), characteristic of plaque labelling.

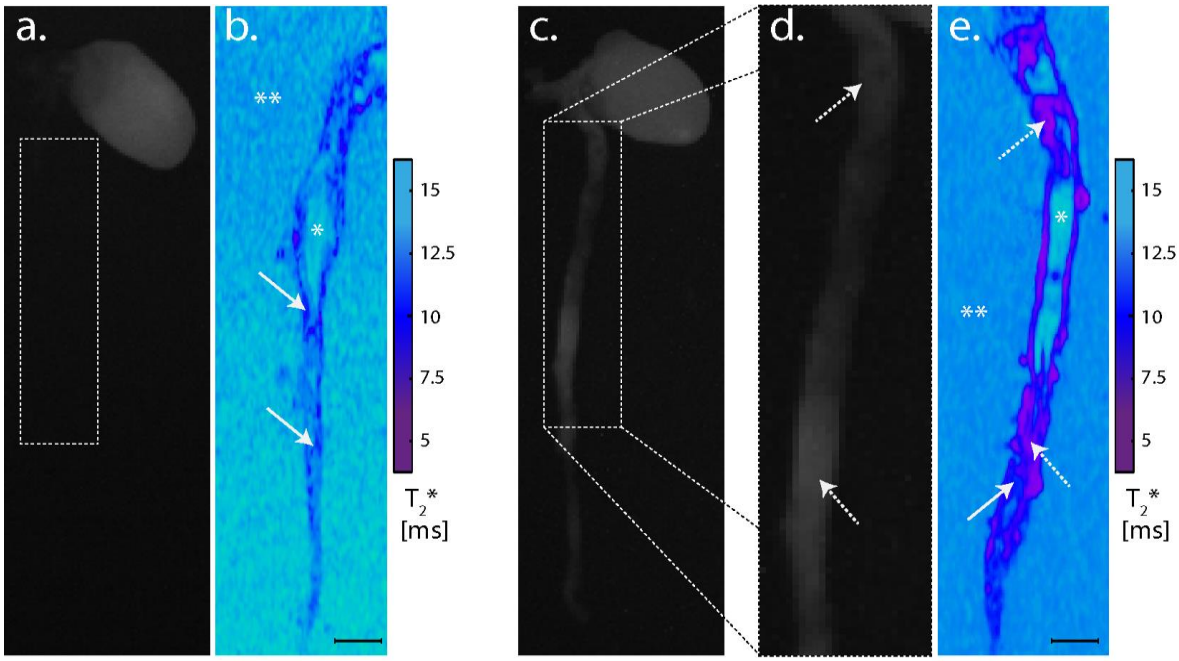

Figure 46: Ex vivo multimodal MRI-NIRF imaging. Fluobeam images 1000 ms exposure and their corresponding T2 maps. Uninjected ApoE, a: fluorescence image, b: T2* map. Multifunctionalized TEG4-VUSPIO injected ApoE, c: fluorescence image, d: fluorescence, magnified dashed line area, e: T2* map. White arrows: atherosclerotic plaques, dashed arrows: T2* shortening (VUSPIO Particles). * arterial lumen, ** agarose bed, white arrows, dashed arrows, scale bar = 1 mm.*

8.3.3.2 *In vivo imaging*

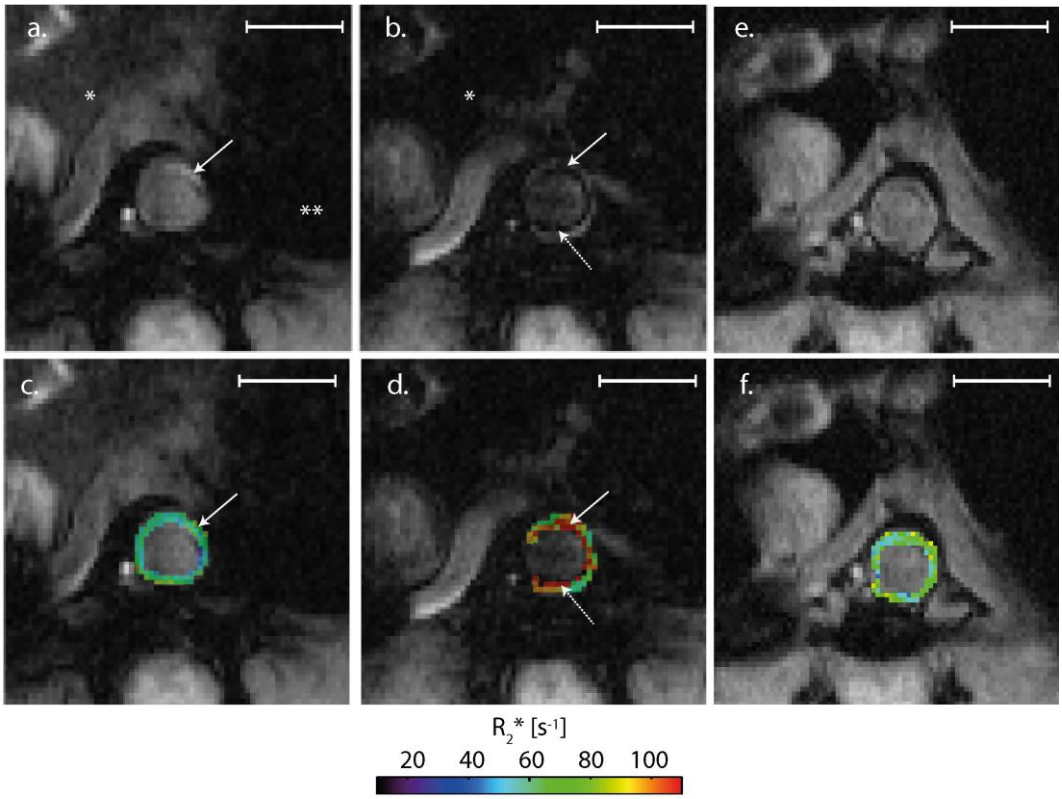

Figure 48:: In vivo MR imaging in a multivalent TEG4-VUSPIO injected ApoE mouse. The thoracic aorta region was imaged using a T2 weighted MR sequence. a, c: before injection, bright blood, echo 4 (TE 17 ms); b, d: 15 min after injection, bright blood, echo 4 (TE 17 ms); e, f: 24 h after injection, bright blood, echo 4 (TE 17 ms); c, d, f: same images overlaid with R2* map. * liver, ** stomach, White Arrows = Atherosclerotic plaques, Dashed Arrows = Hypo signal (VUSPIO Particles), scale bar = 1.5 mm.*

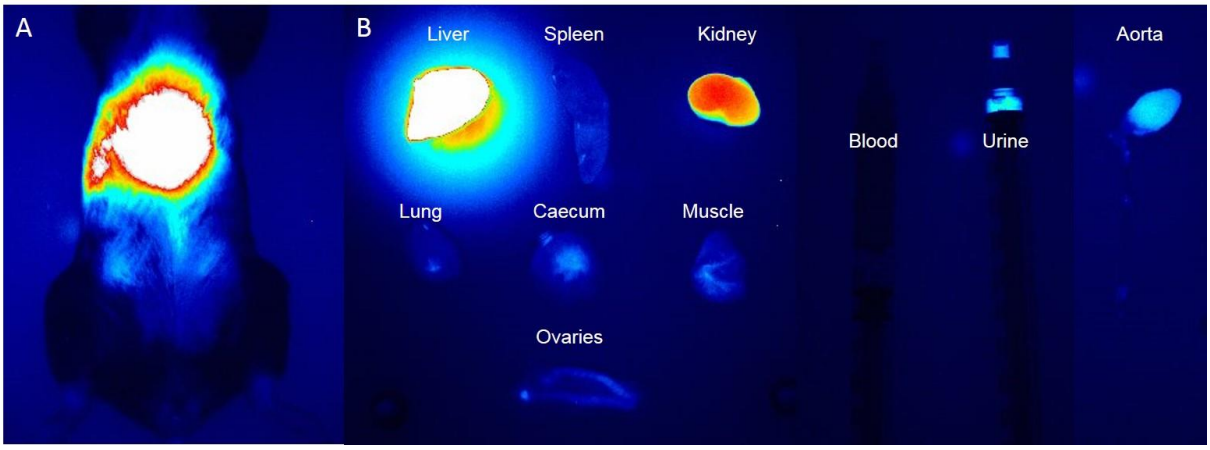

Figure 48: Nanoparticles fluorescence biodistribution imaging. 24 h after in vivo injection of targeted VUSPIO in ApoE mice, images were acquired using the Fluobeam. A: in vivo imaging; B: fluorescence biodistribution in dissected organs. All images are the result of 1000 ms exposure, normalized for background and color enhanced using ImageJ software.

Given the satisfying results obtained *ex vivo*, we decided to inject the nanoparticles to ApoE-/- mice to perform *in vivo* imaging. Immediately after multivalent TEG4-VUSPIO injection, Bright blood images showed a negative contrast in the vessel wall of the atherosclerotic mice which was not observed before injection (**Erreur ! Source du renvoi introuvable.**, b and a, respectively), confirmed by an increase on the R2* map (**Erreur ! Source du renvoi introuvable.**, c and d). Unfortunately, the MR images acquired after 24 h didn't show such a strong negative contrast, and R2* maps were inconclusive (Figure 50, e and f).

Fluorescent biodistribution images didn't show a clear advantage in the take up of multivalent targeted VUSPIO versus untargeted ones. Figure 48 represents a typical fluorescence distribution after 24 h in a multivalent TEG4-VUSPIO-injected ApoE-/- mice. *In vivo* (Figure 48, A), the visualization of the aorta is rendered impossible by the tremendous signal displayed by the liver. The kidneys are the only other organs that can be lightly distinguished. *Ex vivo* (Figure 48, B), the most important signal is displayed by the liver, kidneys, and urine, which is relevant with elimination pathways. All particles have been cleared from the blood and didn't distribute into lungs or muscles. Interestingly, the extremely strong signal in the liver creates a halo that impedes correct signal detection from the other organs, so the biodistribution image was acquired again without the liver sample and showed similar results (data not shown).

8.3.4 Discussion

In the previous chapter, we were able to demonstrate the influence of multifunctionalization on the contrast agent avidity and atheroma plaque recognition *in vitro*. To further assess these objects, on top of the iron oxide cores detectable by MR imaging, NIR fluorochromes were added to the VUSPIO platform to allow for fluorescence imaging as a confirmation method. Additionally, Cyril Lorenzato, who recently joined our team as a post-doc, established a MRI protocol using multi-gradient echo sequence parameters to permit the quantification (T2* map) of signal modulation by the VUSPIO nanoparticles.

Using these sequence parameters, combined with NIRF imaging, *ex vivo* reactivity was evaluated in the ApoE-/- mouse model. A specific contrast agent-driven enhancement of the atheroma plaques was detected by MRI at 7 T. Furthermore, NIRF imaging revealed a matching lesion distribution and specific enhancement.

Subsequently, *in vivo* targeting was assessed. NIRF imaging revealed unable to discriminate between the strong unspecific signal due to the accumulation of nanoparticles in the liver, and the signal from the aorta. Biodistribution studies performed on these *in vivo*-injected animals failed to prove a real benefit from VUSPIO multivalent functionalization on plaque recognition. Furthermore, MR imaging yielded mitigate results, as a local negative contrast could be observed in the plaque immediately after injection which wasn't confirmed after 24 h.

Noteworthy, comparison with the previously obtained images[1] was not possible because of the different sequence parameters used. It also seemed that nanoparticles elimination by liver take up was quicker than previously observed.

References

1. Jacobin-Valat, M.-J. *et al.* Nanoparticles functionalised with an anti-platelet human antibody for in vivo detection of atherosclerotic plaque by magnetic resonance imaging. *Nanomedicine Nanotechnol. Biol. Med.* **11,** 927–937 (2015).

2. Sartori, M. *et al.* Laser-Induced Autofluorescence of Human Arteries. *Circ. Res.* **63,** 1053–1059 (1988).

9 Discussion and perspectives

9.1 Proteomics / molecular targeting

Atherosclerosis is a complex, multifactorial disease that has not yet revealed all of its secrets. By interrogating the atheroma plaque *in vivo* with a phage display library, we propose to address highly relevant markers that may not be yet known. Furthermore, as underlined before (see 5.1.1.2), our phage display selection method, using several injections and relatively long circulation times, should operate a negative selection *in situ* of phages recognizing physiologic endothelium components, typically avoiding the selection of phage-Ab binding to highly represented vascular tree proteins which would not be specific for atherosclerosis. Thus, this method gives access to phage-Abs characteristically recognizing atheroma components.

Immunoprecipitation experiments are under way in order to identify these markers, with selected scFv antibodies, which have not been successful so far for the H2 and C3 scFvs here described. Proteomics studies are currently carried out in the team to help identify potentially relevant proteins that could be further used for screening. So far we found that the most represented proteins where those of the cytoskeleton which are common to physiologic arteries, proving the interest of the negative *in situ* selection described before. It has been previously noted that the proteins of interest for atheroma are feebly represented in extracts from atherosclerotic plaques[1], and methods to specifically enrich the proteins present in minority in these extracts as described by Malaud et al.[2] will be tested. Furthermore, it is likely that the atheroma plaque lysates which were used for immunoprecipitation contain a majority of proteins which conformation does not reflect this of the native proteins in the pathophysiological microenvironment targeted by the atheroma-specific phage-Abs.

Alternatively, an interesting method of ribosome-displayed ORF libraries, called PLATO (ParalleL Analysis of Translated ORFs), is described in Figure 48. It was recently presented by Zhu et al. [3,4] and allowed for screening potential partners of a target of interest. This method could be valuable in our case to help with epitopes identification.

9.2 Fluorescent imaging

In order to rapidly assess the usefulness of antibodies previously selected by phage-display for imaging, a straightforward conjugation to fluorochrome was carried out. To address targeting and biodistribution by fluorescence approaches, NIRF probes were preferred because autofluorescence has been largely described in atherosclerotic plaques, as a result of fibrous and lipid content, and inflammation[5,6]. Notably, the UV-excited fluorophores collagen, elastin and NADH, highly represented in the plaque, are shown on Figure 49, which represents the excitation and emission spectra of the principle contributors to tissues autofluorescence.

After conjugation of the Ab of interest to the NIRF probe, three different apparatus were used for *ex vivo* and *in vivo* evaluation of their relevance as targeting agents. Dye-conjugated antibodies were either injected *in vivo* in a living animal or *ex vivo* perfused in the heart ventricle after having killed the animal.

For *in vivo* readout, the FMT 4000 apparatus and associated TrueQuant software are meant to provide fluorescence quantification, and have been successfully used for prostate tumor imaging in a mouse model at the Vivoptic facility[7]. Unfortunately we were unable to detect the mouse aorta *in vivo*, mainly because the unspecific take up by the liver was yielding a strong signal that impaired the detection of other signals, and also because the aorta was at the same time too deep, too small, and its labelling not strong enough to be observed from outside.

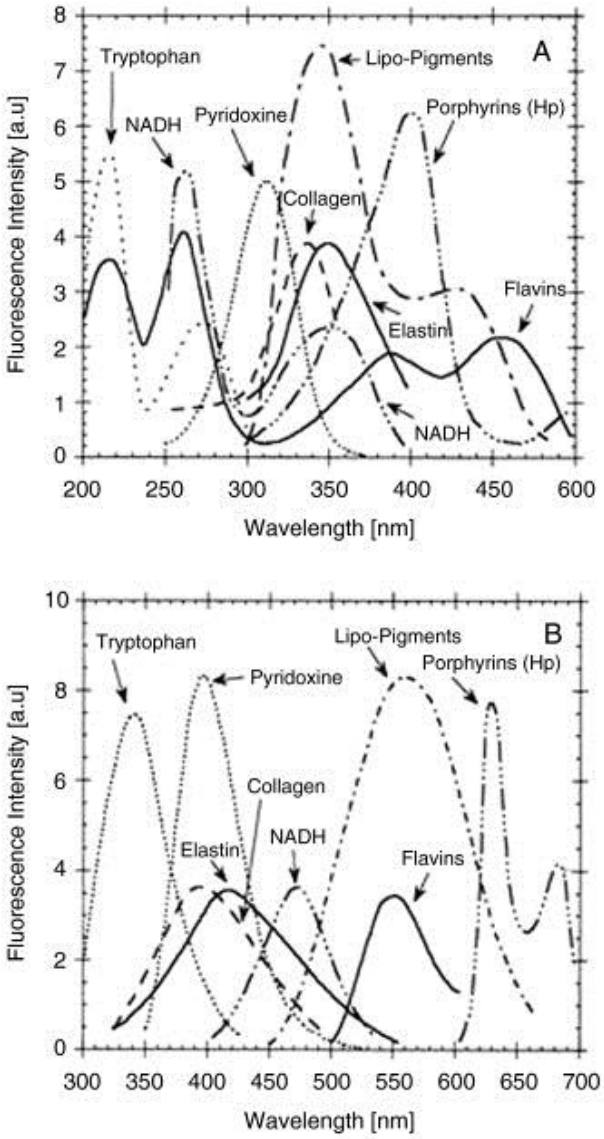

Figure 50: Fluorescence spectra of the main components contributing to tissues autofluorescence. A: excitation spectra, B: emission spectra. From Monici, 2005, Biotechnology Annual Review.

Thus, *ex vivo* imaging of the aortas using the Fluobeam 2D fluorescent imager was carried out. A post-treatment procedure was established within the ImageJ software to normalize for background variations, and we were able to analyze our results in a semi-quantitative way. These biodistribution studies showed positive results.

The same *ex vivo* biodistribution experiments were tried with the FMT apparatus. However, the True Quant software reconstruction algorithm is optimized for whole animals filling the imaging cassette, and doesn't accurately measure the fluorescence in isolated tissue. We recently tested whether agarose was a suitable embedding media to allow for this reconstruction. The first results indicate that fluorescent discs could be reconstructed, but this is an ongoing work and several parameters need to be tuned before a proper quantification can be performed.

A third apparatus was used for *ex vivo* fluorescence imaging: the Odyssey scanner (Li-Cor), with the principle advantages to exhibit a higher resolution (up to 20 µm), and to be able to record 2 wavelengths at the same time (700 and 800 nm excitation lasers). On this system, background fluorescence from uninjected aortas proved hard to discriminate from the dye-Ab specific signal.

Indeed, it is usually considered that the near-infrared (NIR) range is devoid of autofluorescence, leading our choice of NIR fluorochromes for atheroma imaging. However, recent studies in the team of Guillermo Tearney in Boston explored the possibility to record NIR fluorescence as a marker of plaque instability, in a bimodal setting of intravascular imaging (OCT-NIRAF)[8].

There are several hypotheses about the source of near infrared autofluorescence (NIRAF) in atherosclerotic plaques[9]. First, plaques with intraplaque hemorrhage show an accumulation in the necrotic core of cholesterol crystals, foam cells, erythrocyte fragments, and iron deposits; the accumulation of erythrocytes leads to hemoglobin and heme degradation product buildup, a major source of NIR autofluorescence. Second, lipid-soluble carotenoid, especially beta carotene, often colocalize with lipid deposition in the vascular wall. Although beta carotene by itself does not emit autofluorescence, its association with cholesterol and cholesterol ester (themselves non fluorescent either), has been reported to be NIR fluorescent. Third, lipid pigments of the plaque which exhibit strong autofluorescence in the visible range could contribute to NIRAF. Ceroid is one of these pigments, which formation is associated with the presence of lipid, LDL peroxidation products, and hemoglobin. Ceroid being initially present in the cytoplasm of macrophages, it is logically found again in large extracellular deposits in the necrotic core. Finally, NIRAF could be a result of protein modification caused by the combination of inflammation and oxidative stress. Tyrosine oxidation was identified as a promising candidate to explain high NIRAF signal in atherosclerotic plaques, where was reported to be higher than in normal arterial tissue[9].

As a conclusion, there is a need for finer wavelengths separation in the NIR range that would help discriminate plaque components and NIRF-labelled antibodies. In the meantime, proper controls with irrelevant antibodies should not be overlooked.

9.3 Magnetic resonance molecular imaging

9.3.1 Interest of multivalence

While we were able to demonstrate the benefit of multivalent grafting *in vitro*, a systematic study of different grafting ratios would allow for evaluating the actual impact of *ex vivo* homing to atherosclerotic lesions.

In vivo experiments with the TEG4-VUSPIO nanoparticles yielded mitigate results, depending on the TEG4 IgG4-VUSPIO or multivalent TEG4 scFv-VUSPIO targeting agent used, or on the conjugated-nanoparticle batch, also depending on acquisition times, immediately after

injection or 24 h after. But various reasons could impair *in vivo* the efficient targeting observed *in vitro*.

9.3.2 In vivo targeting

First, the size of our particles should be taken into account. Indeed, in 2008, a study by Briley-Saebo et al.[10] hypothesized that, in order to enter the plaque, rigid objects like USPIO (ultrasmall paramagnetic iron oxide nanoparticles) had to be small enough to fit through the vascular fenestrae of the impaired endothelium. The estimated maximum size was reported to be this of native lipoproteins, up to 25 nm. Of course this could vary from one specie to another, and it is not clear whether 25 nm is a suitable size for mice studies.

This first study took advantage of the passive accumulation in macrophages of dextran-coated nanoparticles. In 2011, lipid-coated USPIO (LUSPIO), inferior to 20 nm in size, and functionalized with antibodies targeting oxidation specific epitopes, showed a superior accumulation in plaque macrophages than their non-targeted counterpart. They also showed a superior MR signal attenuation than either targeted or untargeted LSPIO, theoretically more potent but displaying a size between 35 and 40 nm which was hypothesized to impair their accumulation in the plaque. Accordingly, the VUSPIO having a size of approximately 90 nm before functionalization, they may not be able to enter through the vascular fenestrae. Yet, in the case of our studies with TEG4 targeting activated platelets, the particle, if not internalized, could bind to the arterial wall of atheroma lesions. However, it is likely that the stringency of arterial blood flow disturbs the particles binding. To overcome these issues, improvements should work at 1/ further increasing the affinity and avidity, 2/ exhibit longer circulation times, and 3/ be able to enter and be retained within the plaque.

This third option has been explored thanks to Gd-loaded micelles. Although superior to 100 nm in size, they were able to squeeze through 25 nm diameter pores and be taken up by macrophages[11,12]. Additionally, the formulation of such lipid-based particles may be a key in achieving long circulation times.

In this prospect, a collaboration was recently started with Dr Sylvie Crauste-Manciet, in Bordeaux, for the formulation of nanoemulsions containing iron oxide and their functionalization with atheroma-specific antibodies.

9.4 PET imaging

Even smaller than 20 nm, dye-conjugated antibodies proved efficient for *in vivo* binding assessment. Unluckily, fluorescent detection *in vivo* couldn't be achieved with the available apparatus, but another method using small contrast agents was considered.

Indeed, positron emission tomography (PET) tracers are small molecules that don't impair Ab penetration in the tissues. Furthermore, compared to fluorescent imaging, PET sensitivity is high and imaging depth is increased.

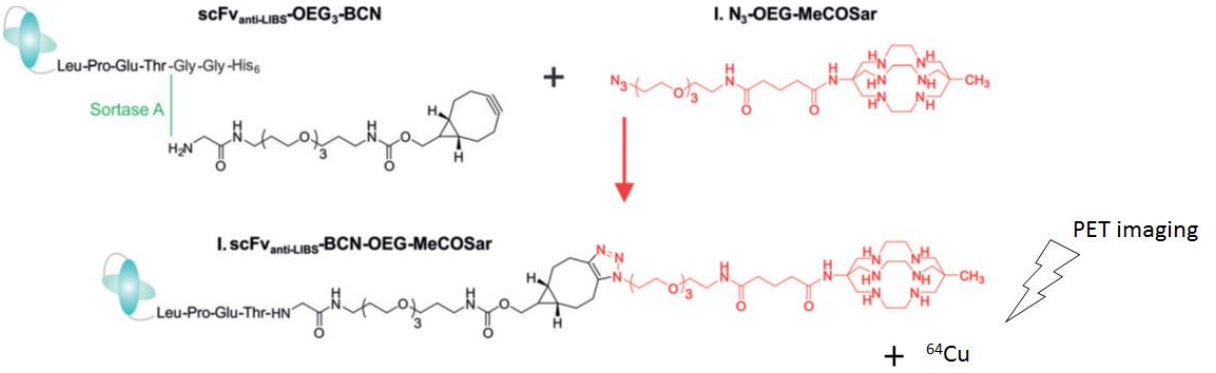

Figure 51: Overview of the two-step bio-click site-specific modification of scFv anti-LIBS-LPETGG-His6 with Gly-OEG3-BCN followed by the macrobicyclic cage amine sarcophagine ligand N3-OEG-MeCOSar. The scFv anti-LIBS (Hagemeyer et al., 2007, Semin Thromb Hemost) binds selectively to activated platelets by targeting ligand-induced binding sites (LIBS) on the glycoprotein IIb/IIIa (αIIbβ3, CD41/CD61) receptor. From Alt et al., 2015, Ang. Chem.

Nuclear imaging is the expertise of Dr Hagemeyer and Dr Alt in Melbourne. A metal affinity chelator, called the MeCoSAR cage, has been conjugated to Ab of various specificities to serve as an imaging tool for various conditions. This approach was considered as an alternative to MRI for atheroma imaging and was one of the reasons to organize the exchange with ACBD in Australia.

Following the sortase reaction (see 7.2.2.3), cleanup on metallic ions is not possible with the MeCoSAR cage chelator because of its affinity for them: it would load with Co or Ni and prevent the 64Cu radiotracer from entering. To overcome this problem, a Sortase conjugation followed by a Copper-free “click” chemistry approach based on the method described by (Alt et al. 2015) was tested, as described by Figure 50.

As described previously, the scFv LPETG generation and sortase conjugation tuning represented a lot of work. Additionally, during my stay, a certain number of problems prevented the continuation of these experiments, i.e. lab moves and restricted access to material, plus a breakdown on the apparatus that took several months to repair.

For these reasons, only preliminary biodistribution experiments were carried out, which didn’t show the expected preferential binding of the Ab to the aorta of ApoE-/- mice. Hence, there is still a need for tuning the conjugation protocol and imaging procedure, but PET imaging could be a good alternative to MRI in order to assess the usefulness of our antibody candidates in atheroma detection.

9.5 ApoE-/- mouse model of atherosclerosis

Finally, atherosclerotic lesions in the ApoE-/- mouse model take several months to develop, and it is not well characterized yet if unstable plaques resembling those observed in humans can be found in mice. To try and circumvent this, Chen et al.[13] proposed a surgical model, called tandem stenosis, which reproduces in the carotid artery different flow conditions. After only 7 weeks, different sections of the carotid artery showed distinct protein expression patterns, and exhibited 4 different phenotypes, shown by Figure 51, which were

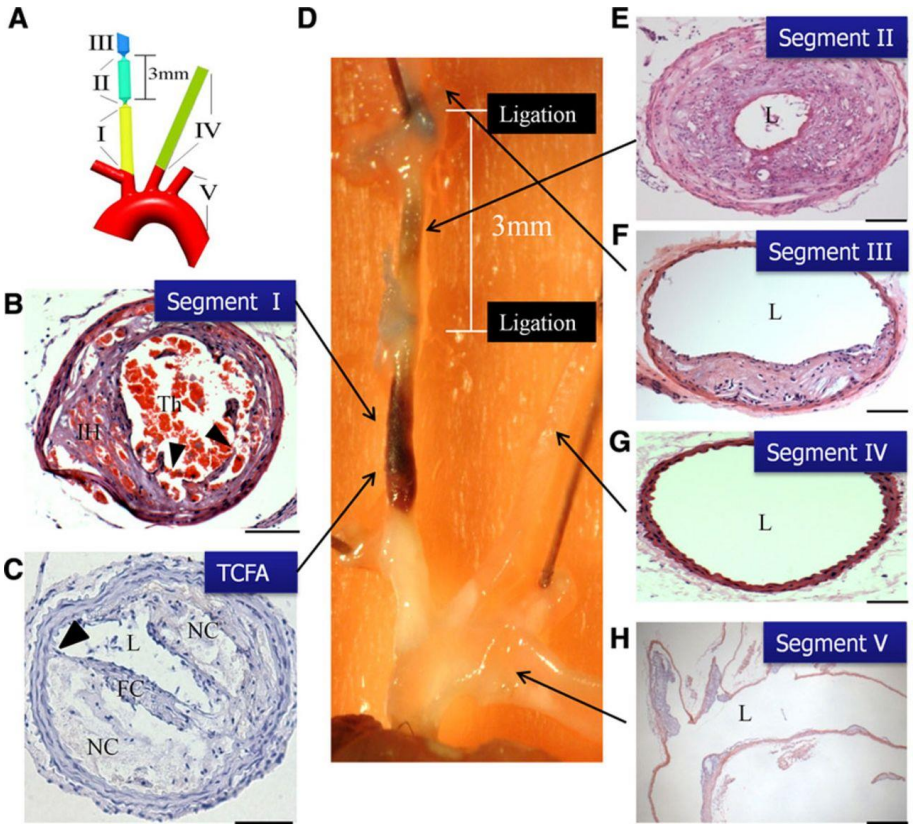

Figure 52: Cross-section of different vessel segments representing healthy, nonatherosclerotic areas and areas of stable and unstable atherosclerosis. A, Schematic drawing of the different vessel segments investigated in the described tandem stenosis (TS) model. B, Vessel segment I represents unstable/rupture-prone atherosclerotic plaques characterized by disruption of fibrous caps and luminal thrombosis. C, Representative thin cap fibroatheroma (TCFA) prone to rupture as typically seen in vessel segment I. D, Representative gross anatomy after 7 weeks after TS surgery at the depicted vessel segments. The ligation suture is blue. E, Vessel segment II often contains intact thin fibrous caps with highly cellular content. F, Vessel segment III exhibits a stable atherosclerotic phenotype containing thick fibrous caps and small necrotic cores. G, Vessel segment IV represents plaque-free healthy vasculature. H, Vessel segment V contains the aortic arch and adjacent vessel segments. The plaque phenotype shows a stable atherosclerotic plaque characterized by thick caps, which consist of fibrous tissue and smooth muscle cells. Luminal thrombi were not found in this segment. Bars indicate 100 µm in B, C, and E–G, and 1000 µm in H. All histological pictures depict hematoxylin and eosin staining, except C which depicts hematoxylin staining. FC indicates fibrous cap; IH, intraplaque hemorrhage; L, lumen; NC, necrotic core; and Th, thrombus. From Chen et al., 2013, Circulation research.

relevant with those observed in humans. Hence, this would reveal a helpful model for further antibody candidates screening, or for a new *in vivo* selection.

9.6 Clinical imaging of atheroma

As a conclusion, it is interesting to note that despite the important number of teams involved in atheroma imaging research, and the wide number of studies realized over the years, no satisfying, let alone ideal, contrast agent has arisen. A few modalities were assessed as preliminary studies in humans[14–16], yet to date none of them has reached the clinics, proving the global difficulty of transferring promising animal studies into human patients.

Yet, currently, the severity of carotid stenosis and presence of symptoms determines the indication for revascularization. The carotid surgery or stent implantation is associated with a significant risk of death or subsequent restenosis, therefore benefits should be carefully evaluated. It is now commonly accepted that a stenosis > 70% associated with symptoms is an indication for surgery. However, in more controversial cases, were stenotic lesions occupy 50 to 69% of the vascular lumen, the benefit – risk ratio is uncertain, yet molecular imaging could address these limitations. In the case of coronary atheroma, PET imaging using the ^{18}FDG radioactive glucose analog has already yielded promising results in humans, although the exploration of the entire coronary bed is still hindered by cardiac and respiratory motion, and an insufficient resolution[17].

Considering that there is a major need for molecular imaging, which remains unaddressed, we proposed the use of antibodies from human origin, selected to specifically target molecular markers of atherosclerosis. These antibodies were used to functionalized a wealth of contrast agents, imaged with different devices possessing their own strengths and weaknesses. Interestingly, our antibodies cross-react on different species, allowing to perform pre-clinical studies in animal models of the pathology. Thus, a proven ideal combination between contrast agent and affinity ligand could be easily transferred to human patients with a minimal risk of adverse reaction and no need for further antibody engineering.

References

1. Malaud, E. *et al.* Carotid atherosclerotic plaques: Proteomics study after a low-abundance protein enrichment step. *ELECTROPHORESIS* **33,** 470–482 (2012).

2. Malaud, E. *et al.* Local carotid atherosclerotic plaque proteins for the identification of circulating biomarkers in coronary patients. *Atherosclerosis* **233,** 551–558 (2014).

3. Zhu, J. *et al.* Protein interaction discovery using parallel analysis of translated ORFs (PLATO). *Nat. Biotechnol.* **31,** 331–334 (2013).

4. Zhu, J. *et al.* Protein interaction mapping with ribosome-displayed using PLATO ORF libraries. *Nat. Protoc.* **9,** 90–103 (2014).

5. Sartori, M. *et al.* Laser-Induced Autofluorescence of Human Arteries. *Circ. Res.* **63,** 1053–1059 (1988).

6. Monici, M. in (ed. Review, B.-B. A.) **11,** 227–256 (Elsevier, 2005).

7. Mazzocco, C. *et al.* In vivo imaging of prostate cancer using an anti-PSMA scFv fragment as a probe. *Sci. Rep.* **6,** 23314 (2016).

8. Ughi, G. J. *et al.* Clinical Characterization of Coronary Atherosclerosis With Dual-Modality OCT and Near-Infrared Autofluorescence Imaging. *JACC Cardiovasc. Imaging* (2016). doi:10.1016/j.jcmg.2015.11.020

9. Wang, H. NEAR INFRARED AUTOFLUORESCENCE AUGMENTATION OF OPTICAL COHERENCE TOMOGRAPHY FOR DIAGNOSIS OF CORONARY ATHEROSCLEROSIS. (2014).

10. Briley-Saebo, K. C., Mani, V., Hyafil, F., Cornily, J.-C. & Fayad, Z. A. Fractionated feridex and positive contrast: In vivo MR imaging of atherosclerosis. *Magn. Reson. Med.* **59,** 721–730 (2008).

11. Briley-Saebo, K. C. *et al.* Gadolinium mixed-micelles: Effect of the amphiphile on in vitro and in vivo efficacy in apolipoprotein E knockout mouse models of atherosclerosis. *Magn. Reson. Med.* **56,** 1336–1346 (2006).

12. Maiseyeu, A. *et al.* Gadolinium-containing phosphatidylserine liposomes for molecular imaging of atherosclerosis. *J. Lipid Res.* **50,** 2157–2163 (2009).

13. Chen, Y.-C. *et al.* A Novel Mouse Model of Atherosclerotic Plaque Instability for Drug Testing and Mechanistic/Therapeutic Discoveries Using Gene and MicroRNA Expression Profiling. [Miscellaneous Article]. *Circ. Res. July 19 2013* **113,** 252–265 (2013).

14. Kooi, M. E. *et al.* Accumulation of ultrasmall superparamagnetic particles of iron oxide in human atherosclerotic plaques can be detected by in vivo magnetic resonance imaging. *Circulation* **107,** 2453–2458 (2003).

15. Spuentrup, E. *et al.* MR imaging of thrombi using EP-2104R, a fibrin-specific contrast agent: initial results in patients. *Eur. Radiol.* **18,** 1995–2005 (2008).

16. Tang, T. Y. *et al.* The ATHEROMA (Atorvastatin Therapy: Effects on Reduction of Macrophage Activity) Study. Evaluation using ultrasmall superparamagnetic iron oxide-enhanced magnetic resonance imaging in carotid disease. *J. Am. Coll. Cardiol.* **53,** 2039–2050 (2009).

17. Jaffer, F. A. & Verjans, J. W. Molecular Imaging of Atherosclerosis: Clinical State-of-the-Art. *Heart Br. Card. Soc.* **100,** 1469–1477 (2014).

Section 3

Annexes

Liste des Annexes

- Liste des publications, communications et posters
- Curriculum vitae
- Scientific articles

Nanoparticles functionalised with an anti-platelet human antibody for in vivo detection of atherosclerotic plaque by magnetic resonance imaging

A Recombinant Human Anti-platelet scFv Antibody Produced in Pichia pastoris for Atheroma Targeting

Targeted nanoparticles for multimodal molecular imaging in a mouse model of atherosclerosis

- Résumé français

Liste des publications, communications et posters

PUBLICATIONS

Manuscrit en préparation

Sortase site-specific conjugation of detection devices to human antibody fragments for atherosclerosis imaging purpose

M. Larivière, S. Jagdale, K. Alt, G. Clofent-Sanchez, C.E. Hagemeyer

2016

Manuscrit en voie de soumission (Nanomaterial)

Magnetic particle imaging dedicated Oil-in-Water nanoemulsion platform for atherosclerosis diagnosis

G. Prévot, T. Kauss*, C. Lorenzato*, A. Gaubert, M. Larivière, J. Baillet, M-J. Jacobin-Valat, S. Mornet, P. Barthélémy, G. Clofent-Sanchez*, S. Crauste-Manciet* (* equivalent positions of authors)

2016

Manuscrit en voie de soumission (PlosOne)

Targeted nanoparticles for multimodal molecular imaging in a mouse model of atherosclerosis

M. Larivière*, C. Lorenzato*, L. Adumeau, A. Hémadou, M-J. Jacobin-Valat, A. Noubhani, X. Santarelli, S. Mornet, J. Laroche-Traineau*, G. Clofent-Sanchez* (* equivalent positions of authors)

2016

PlosOne

A Recombinant Human Anti-platelet scFv Antibody Produced in Pichia pastoris for Atheroma Targeting

A. Vallet-Courbin, M. Larivière, A. Hocquellet, A. Hemadou, Sarjapura-Nagaraja P., J. Traineau, A. Vonarburg, X. Santarelli, G. Clofent-Sanchez, M-J. Jacobin-Valat* and A. Noubhani* (* equivalent position of authors)

2015

Nanomedicine: Nanotechnology, Biology and Medicine 11 (4), 927-937

Nanoparticles functionalised with an anti-platelet human antibody for in vivo detection of atherosclerotic plaque by magnetic resonance imaging

M-J. Jacobin-Valat*, J. Laroche-Traineau*, M. Larivière, S. Mornet, S. Sanchez, M. Biran, C. Lebaron, J. Boudon, S. Lacomme, M. Cérutti, G. Clofent-Sanchez (* equivalent position of authors)

2013

Presses Académiques Francophones

Les anticorps monoclonaux dans le domaine de la santé

M. Larivière

COMMUNICATIONS

2016

10th International Conference on Nanomedicine and Nanotechnology in Health Care, Bangkok, Thaïlande

et

9th Young Scientists Symposium, IECB, Pessac

Targeted nanoparticles for multimodal molecular imaging in a mouse model of atherosclerosis

M. Larivière, C. Lorenzato, A. Hémadou, L. Adumeau, A. Noubhani, X. Santarelli, M-J. Jacobin-Valat, S. Mornet, J. Laroche-Traineau, G. Clofent-Sanchez

2013

Meeting automnal du GDR ACCITH (Anticorps et ciblage thérapeutique), Montpellier

Imagerie moléculaire des plaques d'athérome vulnérables avec des fragments d'anticorps humains

M. Larivière, J. Laroche-Traineau, M-J. Jacobin-Valat, G. Clofent-Sanchez

POSTERS

2016

Journée scientifique du LabEx TRAIL (Translational Research and Advanced Imaging Laboratory), Bordeaux

Multimodal molecular imaging of the atheroma plaque

M. Larivière, C. Lorenzato, A. Hémadou, L. Adumeau, A. Noubhani, X. Santarelli, M-J. Jacobin-Valat, S. Mornet, J. Laroche-Traineau, G. Clofent-Sanchez

2014

10ème congrès de la NSFA (Nouvelle Société Française d'Athérosclérose), Biarritz

New developments on nanoparticles functionalized with human antibodies for molecular imaging of vulnerable atheroma plaques

M. Larivière, M-J. Jacobin-Valat, J. Laroche-Traineau, L. Adumeau, A. Noubhani, S. Sanchez, C. Mazzocco, F. Couillaud, X. Santarelli, S. Mornet, G. Clofent-Sanchez

Mélusine LARIVIÈRE

PharmD, PhD (2016)

+33(0)651518955

melusinelariviere@gmail.com

LinkedIn: Melusine Lariviere

30 years-old, female, French

Languages:

French (native)

English (full capacity)

3 months in Finland, 1 year in Australia

German (basic)

RESUME

As a pharmacist, my education includes Cellular and Molecular Biology, Chemistry and general Health Sciences. I am also trained to various *in vitro* techniques, as well as Animal handling and *in vivo* methods. Going through diverse work environments on transversal projects I developed my adaptability and troubleshooting ability. Creative, rigorous, honest, I am a team player as well as an independent worker.

RESEARCH

2013 – 2016

PhD student – Biotechnology, imaging, vascular biology (Bordeaux University, France / Monash University, Australia)

- Project: *in vivo* imaging of atheroma plaques with nanoparticles functionalized using human antibody fragments
- Co-funded through a French "Investment for the Future program" ANR grant and an Australian NHMRC grant
- Antibody production (HEK cells) and *in vitro* validation (immunohistochemistry)
- Site-specific conjugation to fluorochromes and nanoparticles
- Transgenic mouse model handling
- Imaging: Fluorescent Molecular Tomography, Magnetic Resonance Imaging

2012 – 6 months

Research assistant – Biotechnology, oncology (France)

- Project: identification of partner proteins involved in the mechanism of action of an anti-cancer antibody
- Proteome analysis and mechanistic studies
- Flow cytometry, immunoprecipitation

2011 – 3 months

Research assistant – Pharmacology, neurology (Finland)

- Project: study of the different internalization pathways in an *in vitro* model of human blood-brain barrier
- siRNA transfection, Western blot

2010 – 6 weeks

Research internship – Pharmacology, neurology (France)

- Project: effects of vine polyphenols on an in vitro model of Alzheimer's disease
- Cell line culture, pharmacology of chemical compounds, *in vitro* oxydative stress assays

Authorized for **animal experiments** design and conduct (2014)

Certified for working with **radioactive material** (for PET imaging) (2015)

EDUCATION

2013

Doctor of Pharmacy (PharmD), with Honours (Faculty of Pharmacy, Bordeaux University, France)

> Pharmacy thesis « Monoclonal antibodies and human health » (in French)
> Awarded Best Thesis (2013) by the Bordeaux Pharmaceutical Sciences Society
> Published by the Academic Francophone Press

2011-2012

Master degree (MSc) in Biotechnology, with Honours (Faculty of Sciences and Technics, Limoges University, France)

> Cellular and molecular biology, genetics, immunology, bioengineering
> Intellectual and Industrial property, project management

2005 - 2013

Pharmaceutical sciences (Faculty of Pharmacy, Bordeaux University, France)

> Pharmacology, chemistry, physics
> Laboratory know-how
> General knowledge about drug development and legislation

PUBLICATIONS

2016
PLoS ONE 12(1), e0170305

A Recombinant Human Anti-Platelet scFv Antibody Produced in Pichia pastoris for Atheroma Targeting

A. Vallet-Courbin, M. Larivière, A. Hocquellet, A. Hemadou, Sarjapura-Nagaraja P., J. Laroche-Traineau, X. Santarelli, G. Clofent-Sanchez, M-J. Jacobin-Valat, A. Noubhani

2015
Nanomedicine: Nanotechnology, Biology and Medicine 11 (4), 927-937

Nanoparticles functionalised with an anti-platelet human antibody for in vivo detection of atherosclerotic plaque by magnetic resonance imaging

M-J. Jacobin-Valat, J. Laroche-Traineau, M. Larivière, S. Mornet, S. Sanchez, M. Biran, C. Lebaron, J. Boudon, S. Lacomme, M. Cérutti, G. Clofent-Sanchez

2013
Presses Académiques Francophones

[Monoclonal antibodies and human health] (FR)

M. Larivière

COMMUNICATIONS

2016

10th International Conference on Nanomedicine and Nanotechnology in Health Care
and
9th Young Scientists Symposium

Targeted nanoparticles for multimodal molecular imaging in a mouse model of atherosclerosis

M. Larivière, C. Lorenzato, A. Hémadou, L. Adumeau, A. Noubhani, X. Santarelli, M-J. Jacobin-Valat, S. Mornet, J. Laroche-Traineau, G. Clofent-Sanchez

2016

3 Minute Thesis Competition – french version "MT180"

[Molecular imaging of vulnerable atheroma plaques with human antibody fragments] (FR)

Youtube: youtu.be/VP-GI3jYkyw

POSTERS

2016

Translational Research and Advanced Imaging Laboratory (TRAIL) scientific day

Multimodal molecular imaging of the atheroma plaque

M. Larivière, C. Lorenzato, A. Hémadou, L. Adumeau, A. Noubhani, X. Santarelli, M-J. Jacobin-Valat, S. Mornet, J. Laroche-Traineau, G. Clofent-Sanchez

2014

10th Congres of the New Atherosclerosis French Society (NSFA)

New developments on nanoparticles functionalized with human antibodies for molecular imaging of vulnerable atheroma plaques

M. Larivière, M-J. Jacobin-Valat, J. Laroche-Traineau, L. Adumeau, A. Noubhani, S. Sanchez, C. Mazzocco, F. Couillaud, X. Santarelli, S. Mornet, G. Clofent-Sanchez

POTENTIAL CLINICAL SIGNIFICANCE

Nanomedicine: Nanotechnology, Biology, and Medicine
11 (2015) 927–937

Original Article

nanomedjournal.com

Nanoparticles functionalised with an anti-platelet human antibody for *in vivo* detection of atherosclerotic plaque by magnetic resonance imaging

Marie-Josée Jacobin-Valat, PhD[a,b,1], Jeanny Laroche-Traineau, PhD[a,b,1], Mélusine Larivière[a,b], Stéphane Mornet, PhD[c], Stéphane Sanchez[a,b], Marc Biran, PhD[a], Caroline Lebaron[d], Julien Boudon, PhD[c], Sabrina Lacomme[e], Martine Cérutti, PhD[d], Gisèle Clofent-Sanchez, PhD[a,b,*]

[a]*CNRS, UMR5536, CRMSB, Centre de Résonance Magnétique des Systèmes Biologiques, Université Bordeaux, Bordeaux, France*
[b]*Plateforme Technologique et d'Innovation Biomédicale, Pessac, France*
[c]*CNRS, UPR9048, Université de Bordeaux, Institut de Chimie de la Matière Condensée de Bordeaux, Pessac, France*
[d]*CNRS, UPS3044, "Baculovirus et thérapie", St Christol-Les-Alez, France*
[e]*Bordeaux Imaging Center, Université Bordeaux, Bordeaux, France*

Received 4 April 2014; accepted 4 December 2014

Abstract

Atherosclerosis is an inflammatory disease associated with the formation of atheroma plaques likely to rupture in which platelets are involved both in atherogenesis and atherothrombosis. The rupture is linked to the molecular composition of vulnerable plaques, causing acute cardiovascular events. In this study we propose an original targeted contrast agent for molecular imaging of atherosclerosis. Versatile USPIO (VUSPIO) nanoparticles, enhancing contrast in MR imaging, were functionalised with a recombinant human IgG4 antibody, rIgG4 TEG4, targeting human activated platelets. The maintenance of immunoreactivity of the targeted VUSPIO against platelets was confirmed *in vitro* by flow cytometry, transmission electronic and optical microscopy. In the atherosclerotic ApoE$^{-/-}$ mouse model, high-resolution *ex vivo* MRI demonstrated the selective binding of TEG4-VUSPIO on atheroma plaques. It is noteworthy that the rationale for targeting platelets within atherosclerotic lesions is highlighted by our targeted contrast agent using a human anti-αIIbβ3 antibody as a targeting moiety.

From the Clinical Editor: Current clinical assessment of atherosclerotic plagues is suboptimal. The authors in the article designed functionalized superparamagnetic iron oxide nanoparticles with TEG4, a recombinant human antibody, to target activated platelets. By using MRI, these nanoparticles can be utilized to study the process of atheroma pathogenesis.

Key words: MRI contrast agents; Atherosclerosis; Nanoparticles; Platelets; Human antibody

Atherosclerosis is a systemic disorder affecting arterial beds throughout the body, potentially resulting in acute atherothrombotic events such as coronary artery disease (CAD), cerebrovascular disease (CVD), peripheral arterial disease (PAD) or a combination of all (polyvascular or diffuse vascular disease). These cardiovascular diseases cause 19 million deaths per year in the world. They are expected to be the main cause of death globally within the next 10 years owing to their rapidly increasing prevalence in developing countries, due to population aging and other factors, including the increase in unhealthy dietary patterns, physical inactivity, obesity and diabetes mellitus.[1] Thus, the clinical burdent of atherosclerosis is likely to present enormous challenges in the future.

The current opinion is that atherosclerosis is an immune/inflammatory response of the intima to endothelial injury, mainly initiated by the transport of oxidised low-density lipoprotein (Ox-LDL) across the endothelium.[2,3] Several lines of evidence have shown that platelet interactions with modified lipoproteins seem to be quite important in triggering their transfer to the vessel wall.[4] Platelets are by themselves inflammatory cells[5] which can greatly influence monocyte and lymphocyte

Sources of funding: This study was supported by two public grants from the French "Agence Nationale de la Recherche" within the context of the Investments for the Future Program, referenced ANR-10-LABX-0057, named IdEx and TRAIL MIMATHUMAB and by public grants from the French "Agence Nationale de la Recherche" within the context of PCV programme, named IMATHABIO and SVSE5 programme, named ATHERANOS.

*Corresponding author at: CNRS, UMR5536, CRMSB, Centre de Résonance Magnétique des systèmes Biologiques, Université Bordeaux, Bordeaux, France.
E-mail address: gisele.clofent-sanchez@rmsb.u-bordeaux2.fr (G. Clofent-Sanchez).

[1] Contributed equally to this work.

http://dx.doi.org/10.1016/j.nano.2014.12.006
1549-9634/

recruitment through interactions with the dysfunctional endothelium in a well-controlled process involving selectins and integrins.[6-8] P-selectin-dependent formation of platelet-leucocyte aggregates (PLAs) further induces the release of a wealth of adhesive and pro-inflammatory substances.[9,10] The process continues in a vicious circle-like fashion and blood cells involved in adaptive immunity may play important roles in the self-perpetuating inflammatory process.[11,12] Monocytes further differentiate into activated macrophages expressing scavenger receptors which bind different forms of OxLDL, leading to lipid-laden foam cells.[13,14] Platelets also act on the stability and vulnerability of lipid-rich plaques, through αIIbβ3-mediated platelet-endothelium firm adhesion, CD40L expression and cytokine secretion[15] which coordinate extracellular matrix proteins lysis by matrix metallo-proteases (MMPs), well-known to degrade and fragilize the fibromuscular cap.[16,17]

Thus, platelets foster an inflammatory environment that influences atherosclerotic plaque development and vulnerability, in addition to their role in acute thrombus formation.[7]

Traditionally, the degree of luminal stenosis has been used as a marker of the stage of atherosclerosis and as an indication for surgical intervention. Coronary angiography is the gold standard technique for lumenography, but unfortunately provides no information about the functional and molecular events leading to plaque rupture.[18] Hence, imaging modalities with more pronostic value are highly desirable.

MRI approaches have successfully characterised carotid arteries, thanks to its high spatial resolution.[19] However, up to now, the tortuosity and size of the coronary arteries added to the respiratory and cardiac motion hinder the *in vivo* imaging of coronary plaque. To overcome these problems and provide information on the molecular and cellular events leading to plaque rupture, we must rely on molecular imaging modalities, capable of reporting on the molecular content of the arterial wall.

In recent years, considerable efforts have been spent in the development of targeted magnetic contrast agents for biomedical imaging in MRI.[20] These must be designed to have no toxicity and selective binding to desired epitopes such as cell surface receptors.[21] With affinities classically in the nanomolar range, antibodies offer binding properties advantages over bio-mimetics and peptides. In order to ensure safety for medical purposes, human antibodies are preferred over murine antibodies (see limitation sections). Moreover, the choice of the targeted biomarker is of fundamental importance because it has to fulfil two criteria: (1) it must sign a pathological state and (2) it should be highly represented.

In light of the above arguments, we believe molecular targeting of platelets is relevant due to their important involvement into every stage of atheroma pathogenesis.

The remaining question concerns their localization and representativity: due to the variety of mecanisms allowing their internalisation – in addition to haemorrhage and thrombi – platelets are certainly retained within the plaque, providing novel means of discriminating atheroma plaques at high risk of rupture.

We thus developed a recombinant human antibody, rIgG4 TEG4, targeting human activated platelets, to be used as a targeting moiety. TEG4 human antibody was obtained through phage-display technology by biopanning on activated platelets.[22] We now produced TEG4 in IgG4 format thanks to the baculovirus-insect cell system, in quantity sufficient to perform biofunctionalisation of nanoparticles. We then designed an original superparamagnetic iron oxide nanoparticle (VUSPIO for Versatile Ultra Small SuperParamagnetic Iron Oxide)[23] (patent FR 2855315 (also published as EP 1627395 and WO 2004107368)) chosen as the contrast agent moiety to covalently couple rIgG4 TEG4 human antibody in order to ensure safety if inoculated in humans.

Methods

Production of TEG4 antibody as a recombinant IgG_4 in baculovirus system

The general principle is to replace a non-essential gene with a DNA sequence encoding a foreign protein of interest. This replacement is promoted by homologous recombination between DNA purified from a replication-defective baculovirus[24,25] and a plasmid called "transfer vector" (pVT). Specific baculovirus cassettes have been designed[26] to express the heavy and light chains of an antibody. These cassettes consist of (i) a strong very late viral promoter (P10 or polyedrin (PH)), (ii) a sequence encoding an immunoglobulin signal peptide, (iii) two unique restriction sites (AflII-NheI for heavy chain expression cassette and BssHII-AvrII for light chain expression cassette) to allow the insertion of the VH or VL sequences of the TEG4 anti-αIIbβ3 antibody[22,27], in frame with the upstream signal peptide sequence, and (iv) a downstream sequence that encodes the human heavy (γ4) or light chain (λ) constant region. These cassettes are flanked by viral sequences that direct the integration of the foreign genes into a specific P10 or PH locus.

Recombinant IgG4 TEG4 was produced from *Sf*9 cells infected with the recombinant baculovirus coexpressing the TEG4 heavy and light chains. Recombinant IgG4 TEG4 was further purified on Protein A column (GE HealthCare Life Science,Velizy-Villacoublay, France). Details of cloning into transfer vectors, generation of recombinant viruses and purification of recombinant antibody are provided in online Supplementary Materials.

Synthesis of TEG4-VUSPIO and control-VUSPIO conjugates

The Versatile UltraSmall SuperParamagnetic Iron Oxide (VUSPIO) platform is based on 7.5 nm-sized magnetic cores (maghemite γ-Fe_2O_3) functionalised by an aminated polysiloxane film grafted on their surface and embedded in a dextran corona. VUSPIO particles differ from USPIO contrast agents by its chemical stability thanks to strong covalent bonds established between magnetic cores and dextran macromolecules. Moreover, their surface is functionalised with long heterobifunctional poly(ethylene oxide) chains serving as cross linkers for derivatisation by fluorochromes and targeting agents.[28,29]

The rIgG4 TEG4 antibody conjugation to VUSPIO contrast agent is achieved by using $SM(PEG)_{24}$ (Thermo Scientific, Courtaboeuf, France) as coupling agent by converting the remaining primary amine terminal groups into maleimide functions. In parallel, a thiolation of TEG4 is performed with

2-Iminothiolane-HCL (Traut's Reagent), in order to introduce sulfhydryl groups. Detail of TEG4-VUSPIO is provided in online Supplementary Materials. Then the maleimide groups of VUSPIO react with the sulfhydryl groups of the antibody to form stable thioether bonds. A magnetic separation column (MACS, Miltenyi Biotec) was used to separate the unbound rIgG4 TEG4 from the magnetic conjugates.

The same experiments were performed with polyclonal IgG from human serum (Jackson Immunoresearch Laboratories, West Grove, PA, USA) and with human IgG4 isotypic control (kindly provided by M. Cérutti) to obtain IgG cont-VUSPIO and human IgG4 cont-VUSPIO respectively which served as negative controls for unspecific binding.

Flow cytometry and optical microscopy imaging

Aliquots of 10^8 PFA-fixed-activated-platelets (100 μL)[27] were mixed with 25 μg/mL of rIgG4 TEG4 human antibody, AP-2 murine monoclonal antibody (courtesy of Dr Alan Nurden[30]) and other commercial antibodies (see online Supplementary Materials) targeting the αIIbβ3 integrin or with specified dilutions of TEG4-VUSPIO (48 μg/mL rIgG4 TEG4; 58 mM Fe^{3+}), IgG cont-VUSPIO (50 μg/mL IgG cont; 31 mM Fe^{3+}) and antibody-free VUSPIO (12 mM Fe^{3+}) overnight at 4 °C to obtain in fine 10 μg/mL of antibody and a minimum of 6.2 mM Fe^{3+}. See online Supplementary Materials for the quantification of antibody conjugated to VUSPIO. After two washes in PBS, mixtures were re-suspended in appropriate volumes to perform flow cytometry (10^6 platelets) and confocal microscopy studies (10^8 platelets).

In flow cytometry experiments, aliquots of the cell samples were further incubated 30 minutes with secondary Alexa Fluor 488 goat anti-human H + L (Jackson Immuno Research Laboratories) (1/20), goat anti-mouse H + L (Life Technologies, Saint-Aubin, France) (1/20) and fluorescein isothiocyanate (FITC) mouse anti-dextran antibodies (Stem-Cell Technologies, Grenoble, France) (1/5) for detection of respectively, the functionalising primary antibody (rIgG4 TEG4), murine AP-2 antibody and the dextran coating of antibody-conjugated VUSPIO nanoparticles.

For confocal experiments, aliquots of human platelets were re-suspended in 15 μL anti-fading solution (Mowiol® 4-88, Polysciences, Eppelheim, Germany). The digital microscope was a NIKON ECLIPSE 80i. The fluorescence emission was collected between 465 and 555 nm.

Immunohistochemical (IHC) analysis on murine and human atherosclerotic sections

All animal studies were approved under the No. 50120192-A by the Animal Care and Use Committee of Bordeaux, France. $ApoE^{-/-}$ mice were fed a high-cholesterol diet for 21 weeks. Human coronary arteries were harvested from patients with end-stage heart failure having undergone heart transplantation. All of the clinical interventions took place at Haut-Lévèque Hospital (Pessac, France). Human tissue specimens were collected after informed consent. They were immediately processed and embedded in paraffin.

Paraffin-embedded sections of arterial tissue from mouse or human were used in IHC experiments with unconjugated antibodies (rIgG4 TEG4, AP-2, anti-CD41 (αIIb) (Abcam)), PAC-1 antibody[31] (a murine antibody that binds to activated platelets, BD Biosciences), anti-CD68 (an antibody targeting macrophages, Dako, Les Ulis, France) or VUSPIO conjugated antibodies (TEG4-VUSPIO, IgG cont-VUSPIO) tested at 10 μg/mL. See Supplementary Materials for details of the IHC experiment.

Transmission electron microscopy

TEG4-VUSPIO bound to activated platelets was visually analysed by using transmission electron microscopy. An electron microscopy study was conducted at BIC (Bordeaux Imaging Center, University Victor Segalen Bordeaux). Aliquots of 10^8 human platelets activated with thrombin were fixed with 0.1% (v/v) glutaraldehyde/1.5% (v/v) paraformaldehyde and mixed with TEG4-VUSPIO and IgG cont-VUSPIO in 0.1 M phosphate buffer. See online Supplementary Materials for details of the experiment.

Magnetic resonance imaging

In vitro MR imaging for relaxivity measurement and for quantification of TEG4-VUSPIO nanoparticles per platelet is described in online Supplementary Materials.

Ex vivo MR imaging was performed using a 9.4 Tesla MRI system (Bruker) (inner coil diameter, 10 mm) on healthy or atherosclerotic aorta, respectively from C57BL/6 wild-type or $ApoE^{-/-}$ mice (n = 3) terminally anaesthesised by inhalation of isoflurane. The chest was opened by thoracotomy, the heart exposed and the right atrium cut. A 30-gauge needle was inserted in the left ventricle. PBS-heparin (50 UI/mL; 2.5 mL (Sanofi Aventis, Vitry-sur-Seine, France)) was inoculated followed by 10 mL PBS. Perfusion was continued with 2 mL of PBS containing a formulation of either TEG4-VUSPIO (20 μL; 58 mM Fe^{3+}) or IgG cont-VUSPIO (38 μL; 31 mM Fe^{3+}) or PBS. After 20 min, mice were again perfused with 10 mL PBS followed by 5 mL of 4% v/v paraformaldehyde (PFA). The aorta was then removed and embedded in a glass MR tube containing 0.8% p/v high-grade, low melting-point agarose. Imaging parameters (FAST low-angle shot three-dimensional sequence) included the following: TE = 8 ms; TR = 27 ms; field of view 10 × 10 × 10 mm^3; image resolution 0.039 × 0.067 × 0.067 mm^3/pixel; acquisition time: overnight; 48 scans.

Results

Production of TEG4 antibody as a recombinant IgG_4 in baculovirus system

After purification on Protein A, silver-stained SDS-PAGE under reducing and non-reducing conditions revealed proteins corresponding to the expected size of a correctly processed IgG4 and no major additional band (data not shown). Five milligrams of purified recombinant TEG4 (rIgG4 TEG4) was produced and the specificity of the recombinant molecules was controlled by ELISA on the αIIbβ3 integrin (data not shown).

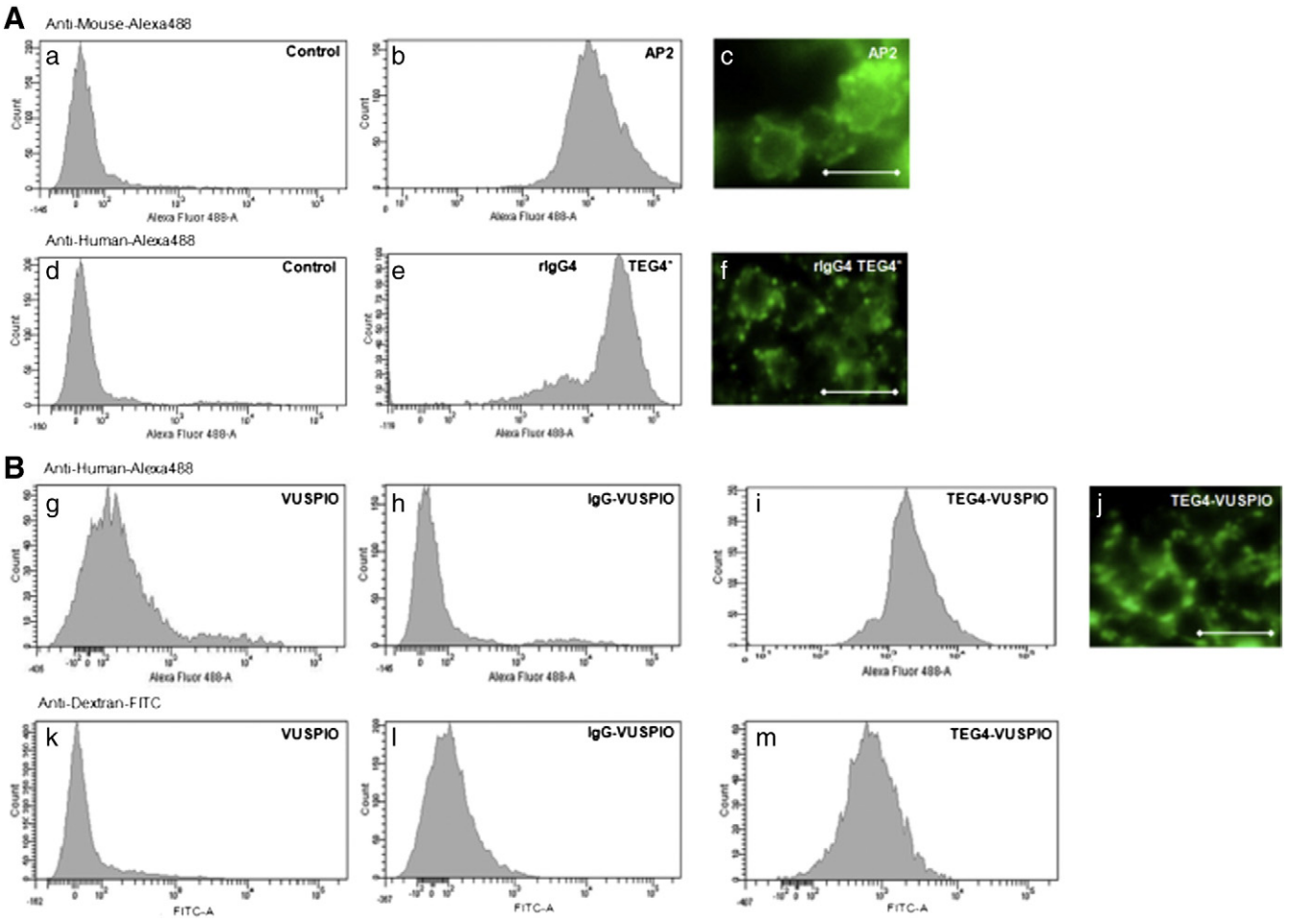

Figure 1. Flow cytometry and optical fluorescence microscopy assays performed on PFA-activated platelets. Incubations with AP-2 murine monoclonal antibody or rIgG4 TEG4 human monoclonal antibody **(A)**, and TEG4-VUSPIO contrast agent or IgG cont-VUSPIO **(B)** were followed by a second incubation with species-specific secondary antibodies labelled with Alexa Fluor 488 or anti-dextran antibodies labelled with FITC.The labelling of platelets in flow cytometry (**B, i, m**) and optical microscopy (**B, j**) with the TEG4-VUSPIO conjugate is similar to the labelling with rIgG4 TEG4 human antibody (**A, e, f**). Bar: 5 μm.

Comparison of rIgG4 TEG4 and AP-2 binding against human platelets and atheroma

The murine monoclonal antibody, designated AP-2, reacts specifically with the complex formed by the human platelet membrane glycoproteins αIIb and β3. The human antibody TEG4 was previously obtained through phage-display biopanning against activated platelets, and characterised as an anti-αIIbβ3 antibody.[22]

AP-2 and rIgG4 TEG4 were first tested in flow cytometry and optical microscopy experiments against human thrombin-activated platelets (Figure 1, *A*). Due to the high number (50,000 copies) of αIIbβ3 integrins on the surface of activated platelets, this specificity results in a significant shift of fluorescence when aliquots of 10^6 PFA-fixed-activated platelets were incubated with AP-2 antibody (Figure 1, *A*, *b*; Table 1 (geometric mean: 13,270; median: 12,180)). The same shift of fluorescence was observed with the rIgG4 TEG4 human antibody (Figure 1, *A*, *e*; Table 1 (geometric mean: 17,390; median: 25,340)). Activated platelets incubated with either AP-2 or rIgG4 TEG4 showed a fine labelling in optical microscopy (Figure 1, *A*, *c*, *f*).

Number of human antibodies per nanoparticle

The absorbance of the VUSPIO samples was measured at 480 nm using a spectrophotometer (U-2800A spectrophotometer, Hitachi). The iron content of samples of conjugated and unconjugated VUSPIO was deduced from the concentration of γ-Fe_2O_3 calculated as described.[28] The iron content of the TEG4-VUSPIO conjugate was 3.25 g/L Fe^{3+} (Fe^{3+} = 58 mM) and the antibody concentration calculated from ELISA curves was 48 μg/mL, leading to a ratio of one antibody per VUSPIO.

Analysis of TEG4-VUSPIO reactivity against platelets by fluorescence

The human recombinant monoclonal antibody rIgG4 TEG4 and polyclonal IgG conjugated to VUSPIO nanoparticles (TEG4-VUSPIO and IgG cont-VUSPIO) were incubated with aliquots of PFA-fixed-activated platelets (Figure 1, *B*). Unconjugated rIgG4 TEG4 antibody at 10 μg/mL and antibody free-VUSPIO at 12 mM Fe^{3+} (Figure 1, *B*, *g*, *k*) were used as positive and negative controls respectively. For flow cytometry detection of antibody-VUSPIO, aliquots of the cell samples were

Table 1
Results of cytometry.

Antibody	Flow cytometry results					
	Anti mouse Antibody		Anti human Antibody		Anti dextran Antibody	
	Geometric mean	Median	Geometric mean	Median	Geometric mean	Median
Unconjugated AP-2[#]	13,270	12,181				
Unconjugated TEG4[#]			17,386	25,338		
Unconjugated TEG4 *			4038	2258		
IgG cont-VUSPIO*			273	229	142	142
TEG4-VUSPIO *			2086	1966	744	740
Ab-free VUSPIO			154	73	209	166

The reactivity of TEG4 antibody is similar to AP-2, a mouse antibody targeting activated platelets.
TEG4-VUSPIO revealed anti-platelet target recognition as compared to antibody-free VUSPIO particles and IgG cont-VUSPIO particles.
* 10 μg/mL
[#] 25 μg/mL

further treated with Alexa Fluor 488 goat anti-human H + L or FITC anti-dextran antibodies. The first method indirectly detects targeted contrast agents accumulated all around platelets by staining the targeting ligand (e.g. the functionalising primary antibody) with a secondary antibody (anti-human H + L) recognising the primary human antibody. The second method, using an anti-dextran antibody, is useful to detect the nanoparticle by itself.

Flow cytometry using both secondary antibody systems revealed a distinct fluorescence shift of platelets incubated with TEG4-VUSPIO compared to antibody-free VUSPIO and IgG cont-VUSPIO controls (Figure 1, *B*). Using anti-human H + L and anti-dextran antibodies, a 7.6 and 5.2 enhancement in targeting was observed respectively for the geometric mean between the contrast agent functionalised with rIgG4 TEG4 and the same agent functionalised with an irrelevant antibody (Figure 1, *B*, *i*, *m*, *h*, *l*; Table 1). Moreover, quite the same platelet recognition was shown with free rIgG4 TEG4 at 10 μg/mL and rIgG4 TEG4 grafted on VUSPIO nanoparticles (4040 versus 2090 for the geometric mean and 2260 versus 1970 for the median (Table 1)).

Geometric mean and median values in flow cytometry corroborate the high fluorescence labelling of free rIgG4 TEG4 and TEG4-VUSPIO on activated platelets in optical microscopy.

Analysis of TEG4-VUSPIO reactivity against platelets by TEM and in vitro MRI

Another way to obtain a direct representation of the active targeting of the nanoparticle by itself is to perform TEM analysis on activated platelets. Binding experiments were performed with thrombin-activated platelets using either TEG4-VUSPIO or IgG cont-VUSPIO. TEG4-VUSPIO targeted contrast agent was particularly visible at the platelet periphery, along the plasma membrane (Figure 2, *A*, blacks arrowheads). Of particular interest was the binding of TEG4-VUSPIO to activated platelets characterised by irregular forms with many irradiating pseudopodes projecting from their surface. In contrast, no labelling was evidenced at the plasma membrane when IgG cont-VUSPIO was used (Figure 2, *A*, (*g*, *h*)). Figure 2, *A*, *i* is a TEM analysis of TEG4-VUSPIO nanoparticles.

Figure 2, *B* describes *in vitro* MRI platelet experiments assessing the binding of targeted and untargeted VUSPIO to activated platelets. In comparison to the signal obtained with platelets only, T2-weighted MR imaging of platelet phantoms incubated with TEG4-VUSPIO (Figure 2, *B*, *a*) revealed a significant signal loss, in the same order of VUSPIO nanoparticles at 250 μM Fe^{3+} (Figure 2, *B*, *b*). A minor signal loss was observed for platelets incubated with antibody-free VUSPIO particles and IgG4 cont-VUSPIO (Figure 2, *B*,(*e*, *c*)) when compared with platelet alone without any VUSPIO (Figure 2, *B*, g). Fewer VUSPIO nanoparticles remain trapped after two washes using IgG4 cont-VUSPIO (Figure 2, *B*, *c*) compared with antibody-free VUSPIO (Figure 2, *B*, *e*). These results suggest that −NH2 functional groups in antibody-free VUSPIOs are involved in residual nonspecific uptake, compared with nanoparticles whose amine groups were shielded by conjugated control antibodies. R2 relaxation rates of cell pellets treated with TEG4-VUSPIO, IgG4 cont-VUSPIO, unconjugated VUSPIO and with PBS only were 47.7 ± 3.5 s^{-1}, 7.8 ± 2.1 s^{-1}, 10.9 ± 1.9 s^{-1} and 4.4 ± 1.2 s^{-1} respectively.

These values and the curve correlating the 1/T2 values measured at 4.7 Tesla with Fe^{3+} concentrations were used to estimate the number of TEG4-VUSPIO nanoparticles bound per platelet. We found approximately 170 TEG4-VUSPIO per platelet which corroborates the number of counted targeted nanoparticles on TEM images.

Analysis of TEG4-VUSPIO reactivity against human and murine atheroma by immunohistochemistry

The presence of platelets within the atheroma plaque of $ApoE^{-/-}$ and human coronary specimens was tested using murine (AP-2) and human (rIgG4 TEG4) antibodies targeting the αIIbβ3 integrin and confirmed by commercial antibodies (anti-CD41 and PAC-1, respectively). Arterial sections from $ApoE^{-/-}$ mice showed a strong labelling of the intima in atheroma with both anti-platelet antibodies (Figure 3, *D*, *F*). The same staining was obtained with a commercial antibody (Figure 3, *B*) and controls were performed with appropriate secondary antibodies (Figure 3, *A*, *C*, *E*). The same strong labelling was observed when sections of human coronary specimens were incubated either with AP-2 or rIgG4 TEG4 antibodies (Figure 4, *B*, *C* and *E*, *F*, respectively). This result was confirmed by the

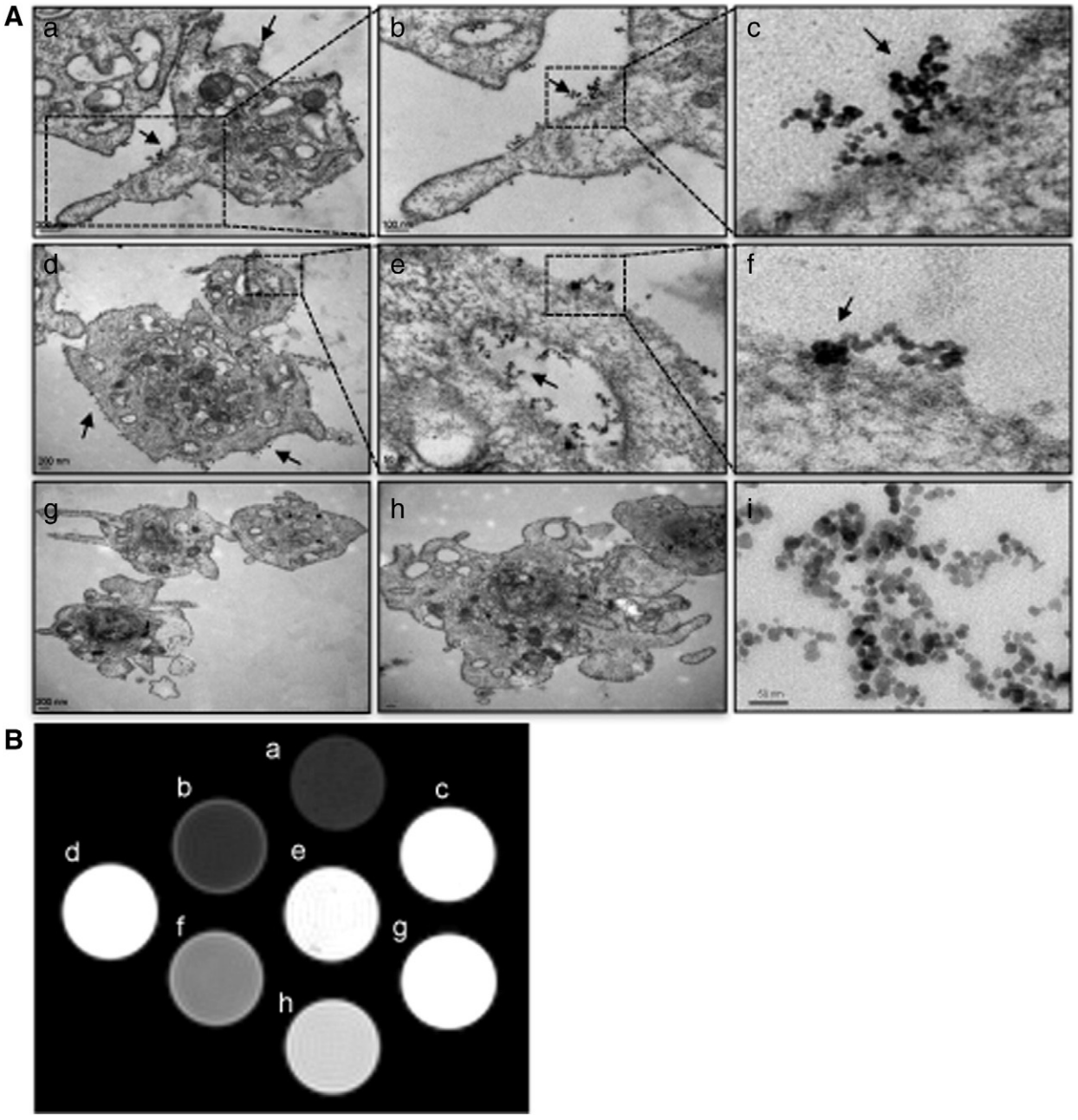

Figure 2. *In vitro* validation of platelet targeting by transmission electron microscopy (TEM) and T2-weighted MRI on phantoms. (**A**) TEM images of TEG4-VUSPIO nanoparticles targeting activated platelets. TEM images clearly show the presence of contrast agents as dots distributed all around the platelets (arrowheads), especially in the pseudopodia developed in activated platelets (**a**, **b**, **c**). **b**, **c** and **e**, **f** are zoomed frames of a and d respectively, indicated by dashed lines. The same platelets incubated with IgG cont-VUSPIO showed no VUSPIO labelling (**g**, **h**). (**i**) illustrated the TEG4-VUSPIO preparation at 48 mM Fe^{3+}. **(B)** T2 MR images of activated platelets targeted by TEG4-VUSPIO (**a**) shows the MRI signal obtained with TEG4-VUSPIO compared with the MRI signal of different concentrations of VUSPIO (0 μM Fe^{3+} (**d**), 62.5 μM Fe^{3+} (**h**), 125 μM Fe^{3+} (**f**), 250 μM Fe^{3+} (**b**)) in agarose gel, untargeted VUSPIOs (**e**), IgG4 cont-VUSPIO (**c**), platelets only (**g**). The TEG4-VUSPIO signal loss was in the same range of free VUSPIOs at 250 μM Fe^{3+} (**b**), indicating the efficiency of targeting.

commercial antibody PAC-1 (Figure 4, *H*, *I*). Enlarged views (Figure 4, *C*, *F*, *I*) showed the targeting of small neovessels located within the intima, in the desorganized media. The staining of macrophages by anti-CD68 antibody (Figure 4, *K*, *L*) matches some of the regions where platelets are found (Figure 4, *E*, *H*), suggesting the localisation of platelets in areas of foam cells and platelet-leucocytes-aggregates (PLA) accumulation. No labelling was observed with controls performed with appropriate secondary antibodies (Figure 4, *A*, *D*, *G*, *J*).

The targeted contrast agent TEG4-VUSPIO was tested on sections of $ApoE^{-/-}$ (Figure 3, *G*) and wild-type C57BL/6J mice (Supplementary data, Figure S3, *C*), showing a high labelling of

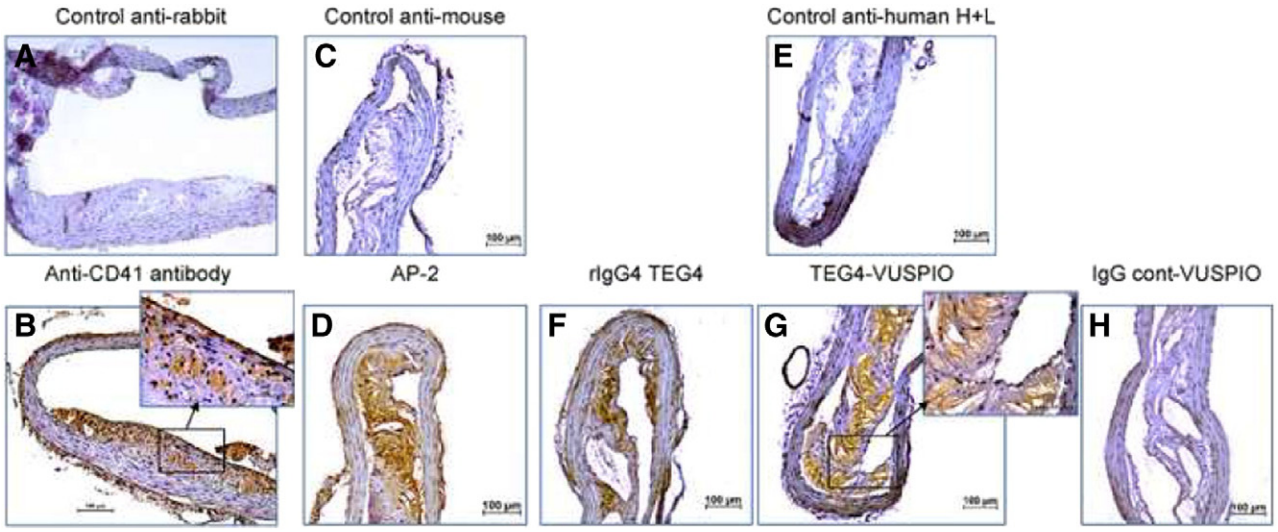

Figure 3. Immunohistochemical detection of integrin αIIbβ3 on aorta sections from ApoE$^{-/-}$ mice. The presence of platelets was shown using two different mouse antibodies: a commercial anti-CD41 (αIIb) antibody **(B)** and an antibody (AP-2) specific to the complex αIIbβ3 **(D)**. Controls were performed with secondary HRP-labelled anti-rabbit and anti-mouse antibodies **(A, C)**. The human antibody rIgG4 TEG4 **(F)** recognises platelets at the same level as both murine anti-αIIbβ3 antibodies. The conjugate TEG4-VUSPIO shows a high labelling of platelets within the intima **(G)** contrary to IgG cont-VUSPIO **(H)**. Controls were performed with a secondary HRP-labelled anti-human H + L antibody **(E)**. Bar: 100 μm and 50 μm for enlarged views.

platelets within the intima of ApoE$^{-/-}$ mouse (Figure 3, *G*) contrary to IgG cont-VUSPIO (Figure 3, *H*). VUSPIO conjugates tested on wild-type C57BL/6J mice (Supplementary data, Figure S3, *B*, *C*) and appropriate secondary antibody (Supplementary data, Figure S3, *A*) showed no labelling.

These *in vitro* results confirm the maintenance of TEG4 specificity after coupling to VUSPIO nanoparticles.

Ex vivo characterisation of the targeted-contrast agent nanoparticle

Atherosclerotic plaques in ApoE$^{-/-}$ mice thoracic aorta are clearly visible at 9.4 Tesla (Figure 5, *B*) when compared with healthy aorta of C57BL/6 wild type mice (Figure 5, *A*). The aorta from atherosclerotic ApoE$^{-/-}$ mice exposed *ex vivo* to TEG4-VUSPIO preparation shows an intense hypo-signal (black arrows) (Figure 5, *C*). In contrast, no hypo-signal was observed in the thoracic aorta of ApoE$^{-/-}$ mice that did not receive VUSPIO (Figure 5, *B*) or did receive IgG cont-VUSPIO (Figure 5, *D*). Thus, representative *ex vivo* MRI studies at 9.4 Tesla showed that TEG4-VUSPIO could induce a loss of MRI signal generated by VUSPIO accumulation in the atherosclerotic vessel wall of ApoE$^{-/-}$ mice, due to antibody targeting.

Discussion

This study demonstrates the interest of non invasive imaging of platelets recruited within atherosclerotic lesions by an αIIbβ3-targeted VUSPIO molecular imaging probe. The presence and effects of platelets inside the atherosclerotic plaque are relatively underexplored and this probe could give insight into intraplaque haemorrhage (IPH), neovasculature and vascular wall inflammation which constitute key plaque features underlying atherosclerosis.

The rationale for molecular imaging is to propose an accurate diagnosis method. Prospective clinical trials have shown that measurement of stenosis underestimates carotid plaque burden[18] and that the majority of patients with a history of recent transient ischemic attack (TIA) or stroke have mild-to moderate carotid stenosis. Debates still exist on how stenosis severity is related to the unstability of the culprit lesions.[32] However, data from the PROSPECT (Providing Regional Observations to Study Predictors of Events in the Coronary Tree) study have concluded that a small luminal area is independently associated with the 3-year risk of acute coronary events.[33] It is now admitted that looking beyond the lumen with functionalised contrast agents is needed to identify the high-risk plaques across a range of stenoses issuing from both carotid and coronary beds.

Compared to previous approaches using rodent antibodies, the use of a human antibody to functionalise nanoparticles is of particular interest for direct transfer into the clinic, considering the need of repeated injections to follow the progression of the disease. Using human antibodies may reduce immunogenicity by avoiding the development of anti-species antibodies usually described when murine antibodies were injected in humans.[34] (see Limitations section)

Recombinant IgG4 TEG4 antibody is able to target activated platelets in the same level as the murine AP-2 and anti-CD41 antibodies as demonstrated by fluorescence experiments. Our *in vitro* experiments conducted with the targeted contrast agent TEG4-VUSPIO confirmed maintenance of specificity against activated platelets using fluorescence and TEM. *In vitro* MRI results also showed that the activated platelets targeted with TEG4-VUSPIO have the highest signal reduction (R2 relaxation rate of 47.7 ± 3.5 s^{-1}) when compared with IgG4-cont VUSPIO, unconjugated VUSPIO and with PBS only (R2 relaxation rates of 7.8 ± 2.1 s^{-1}, 10.9 ± 1.9 s^{-1} and 4.4 ± 1.2 s^{-1} respectively), highlighting the added value of targeting versus

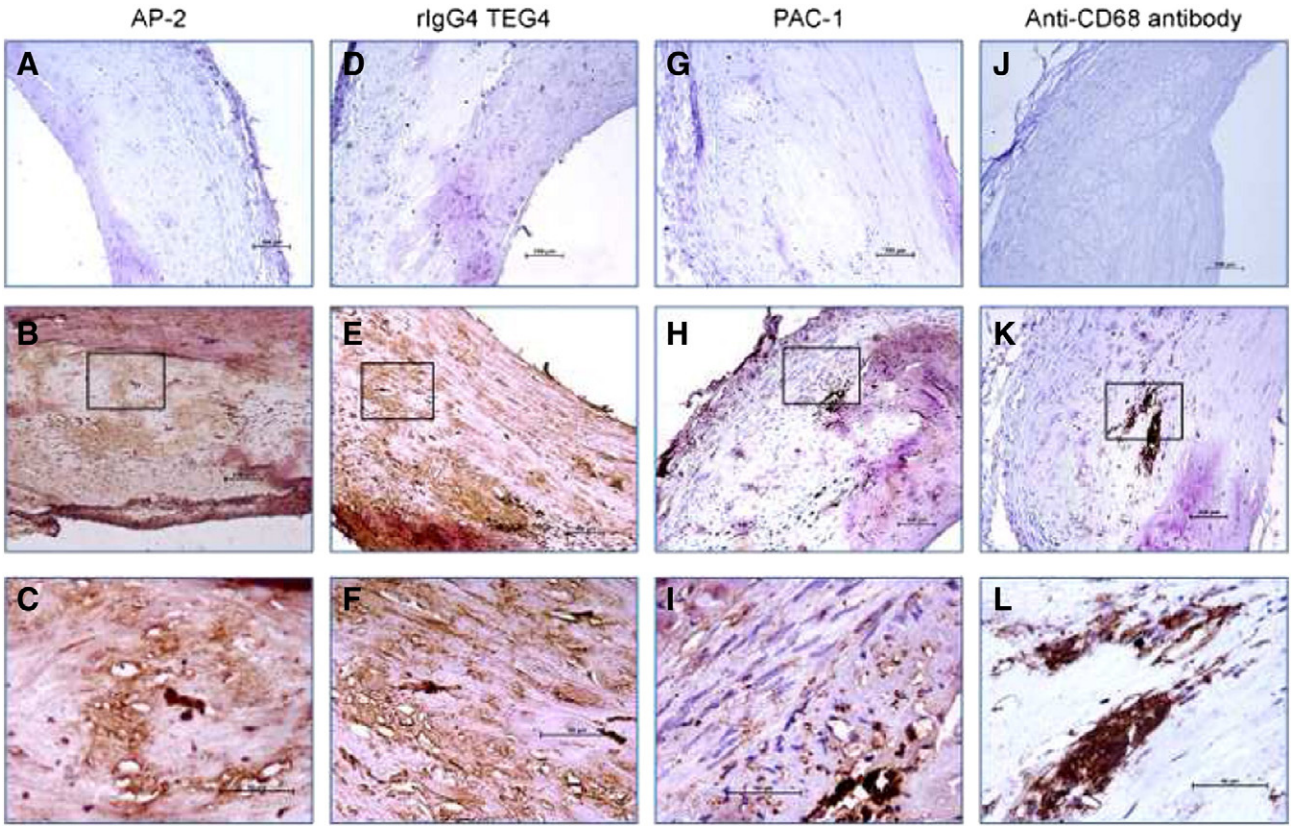

Figure 4. Immunohistochemical detection of integrin αIIbβ3 on coronary human sections. AP-2 and rIgG4 TEG4 panels: the presence of platelets was shown using the mouse anti-αIIbβ3 antibody AP-2 **(B, C)** and the human antibody rIgG4 TEG4 **(E, F)**. PAC-1 panel: the presence of platelets was confirmed with a commercially available mouse antibody specific to human activated αIIbβ3 **(H, I)**. Anti-CD68 panel: foam cells were detected with a commercially available mouse antibody specific to human CD68. **(C, F, I, L)** are enlerged views of **(B, E, H, K)**. Controls were performed with secondary HRP-labelled anti-mouse IgG antibody **(A, J)**, HRP-labelled anti-human H + L antibody **(D)** and HRP-labelled anti-mouse IgM antibody **(G)**. Bars: 100 μm and 50 μm for enlarged views.

passive take up of nanoparticles. All these results demonstrate that TEG4-VUSPIO can selectively accumulate around activated platelets. Recombinant IgG4 TEG4 antibody and TEG4-VUSPIO contrast agent were also shown to highly label atherosclerotic sections of murine and human specimens as demonstrated by IHC studies.

The rationale for targeting platelets within atherosclerotic lesions is that they are highly represented not only in thrombi and intraplaque haemorrhage (IPH) but also in atheroma burden, around necrotic areas and neovessels (see Figures 3 and 4). A pioneer study performed by Massberg et al[6] showed, by *intravital* videofluorescence microscopy, that platelets adhering at the carotid bifurcation (lesion-prone-site) in *ApoE*$^{-/-}$ mice, directly coincided with inflammatory gene expression and preceded atherosclerotic plaque invasion by leukocytes. Platelet-endothelial interactions linked to increased inflammatory activation and prothrombotic state in atherosclerosis are mediated, in part, by platelet glycoprotein (GP) Ibα. Jonathan Lindner's group[35] used recombinant GPIb as a targeting moiety on microbubble contrast agents to perform contrast-enhanced ultrasound molecular imaging of activated von Willebrand factor (vWF) and thus demonstrated widespread platelet-endothelial interaction in LDLR$^{-/-}$/ApoBec-1$^{-/-}$ mice.

Since then, many studies indicate that platelets not only contribute to endothelial dysfunction but also modulate various inflammatory responses by platelet-monocyte complex formation (PMA: platelet-monocyte aggregates)[36,37] or platelet-CD4^{+} T cell cross-talk[38], facilitating leucocyte transmigration and thus act on plaque vulnerability. Platelets themselves – like monocytes/macrophages – are able to bind, take up via scavenger receptors (CD36, LOX-1, SR-B1) and transport modified lipoproteins into the intima, thus contributing indirectly and directly to foam cell formation in atherogenesis.[4] Inside the plaque they are in close contact with macrophages and phagocytosis of platelets by macrophages was already proposed as an alternative mechanism of foam cell formation 53 years ago by Chandler et al.[39] Four decades later, De Meyer et al[40] confirmed *in vitro* that platelet phagocytosis by murine macrophages results in the formation of lipid-laden macrophages. The authors concluded that uptake of modified LDL by platelets and phagocytosis of LDL-laden platelets by macrophages may be critical steps for the development of lipid-rich plaques. Daub et al[41] more recently showed that platelet oxLDL contributes significantly to vascular inflammation and is able to promote atherosclerosis. Platelet-induced lipid accumulation in monocytes thus provides a novel mechanism for how platelets

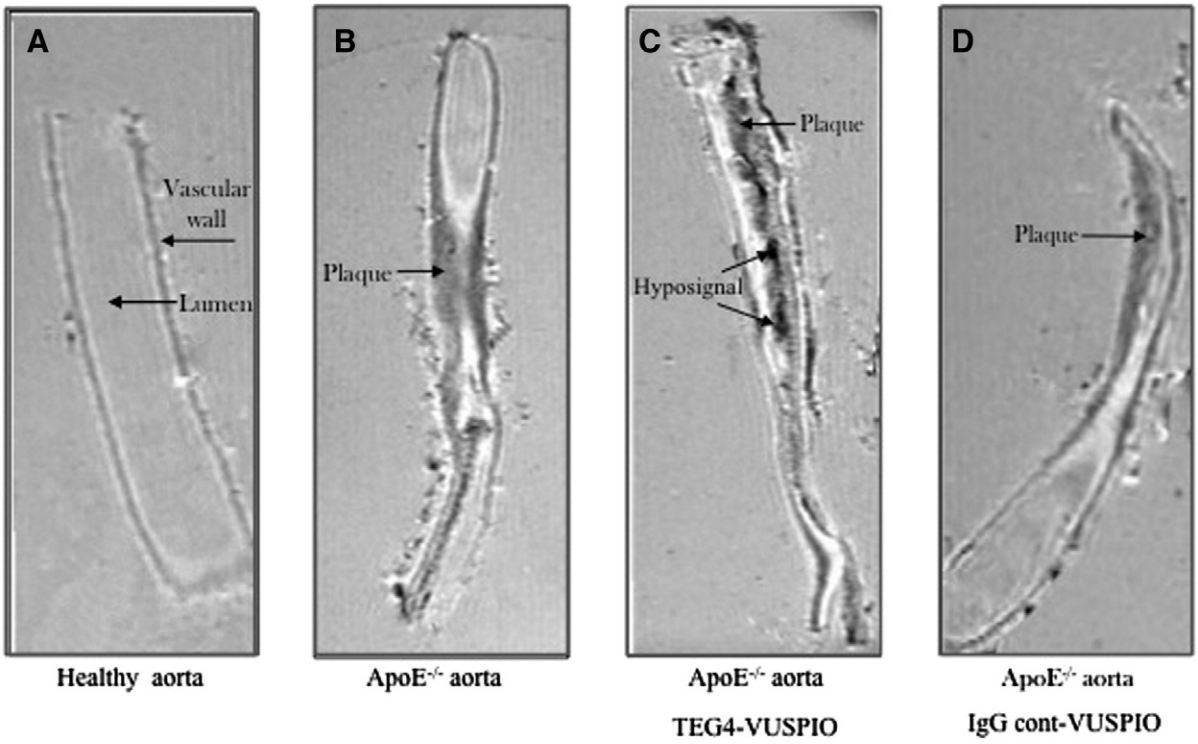

Figure 5. *Ex vivo* MRI at 9.4 Tesla. The healthy **(A)** or atherosclerotic ApoE$^{-/-}$ aorta (**B, C, D**) were perfused *ex vivo* with PBS (**A, B**), TEG4-VUSPIO **(C)**, IgG-cont VUSPIO **(D)**. No atherosclerotic plaque was visible in healthy aorta **(A)**. Panel C shows an intense hyposignal due to iron deposition within atherosclerotic plaque. In contrast, no loss of signal was observed when IgG cont-VUSPIO was administered **(D)**.

negatively regulate plaque stability.[8] Furthermore, platelets are contained in large amounts in early-calcified human atherosclerotic plaques as the results of plaque neovascularisation by leaky vessels, blood extravasation and haemorrhage. They have been involved in the release of osteocalcin in atherosclerotic lesions.[42] Thus, results from the literature and the high labelling shown in Figures 3 and 4 of this study prove that platelets are not only present on plaque surfaces or in IPH. They may play, outside thrombi formation, an important role in inflammation, necrotic core formation, release of factors like osteocalcin and matrix metalloproteinases[43] involved in plaque destabilisation.

So far, the proof of entry of platelets into atherosclerotic lesions has only been given in human atheroma and it was correlated with intraplaque microvascular leakage and IPH.[44] Mice atheroma does not typically develop IPH. This means that the different antibodies (TEG4, AP-2, anti-CD41 antibody) used in IHC recognise platelets within *ApoE*$^{-/-}$ mice atheroma which are not involved in intraplaque thrombi but are rather in interaction with other cells as reported in platelet-leucocyte aggregates (PLA). That is why our study is important from a fundamental point of view because it sheds light into the significant presence of platelets both within mouse and human atheroma as demonstrated in Figures 3 and 4 by IHC on sections of *ApoE*$^{-/-}$ aorta and human coronary arteries.

Moreover, MRI approaches have shown that complex plaque features, such as the necrotic core and intraplaque haemorrhage are prevalent in carotid arteries with minimal stenosis, including those with angiographically normal appearing arteries.[45] Thus, the development of probes that package MRI contrast agents with ligands targeting platelets might show great promise for providing a direct measure of plaque activity and function at the cellular and molecular level. In the current study, the *ex vivo* results highlighted an accumulation of the targeted contrast agent in the atherosclerotic vessel wall of ApoE$^{-/-}$ mice.

Cheruvu and colleagues showed that plaque composition varies depending on the anatomical site with striking heterogeneity even within the same individual.[46] Therefore, the finding of a focal distribution of suspected precursor lesions supports the efforts to develop reliable non-invasive imaging tools to identify the molecular and cellular composition of these structures that may occur at sites with and without flow-limiting stenoses.

This manuscript describes the development of a new targeted contrast agent for MRI, from the conception of the targeting moiety, a fully human antibody, to *ex vivo* MRI images.

Limitations

Today, most therapeutic mAbs in the clinic are humanised or fully human meaning that, theoretically, only a minimal immunogenic potential remains (as compared to murine mAbs).[47] However, evolution of recombinant technologies to produce fully human antibodies has only partially solved this historic obstacle of antibodies. Immunogenicity induced by injected proteins is a serious issue because it is directly related to the patient's safety. A risk assessment should be conducted for every biotherapeutic under

development to address the occurrence of immunogenicity, as well as the severity of the adverse effects caused. An induced antibody response against human antibodies, called human anti-human antibody (HAHA) response, must always be thoroughly tested in clinical studies.[48] In regard of that, the present study has limitations inherent to potential immunogenicity against the injected targeted contrast agent. Even if we have been careful to develop fully human antibodies to serve as the ligand moiety, it is impossible to guarantee, before clinical assays in a cohort of individuals, that anti-idiotypic antibodies will not arise. Moreover, the development of immunogenicity during treatment is highly dependent, not only of the individual status, but also of the pathology treated (immune disorders, chronic illnesses are more at risk to induce auto-antibodies formation) and of the target protein and mechanism of action.[49,50]

Appendix A. Supplementary data

Supplementary data to this article can be found online at http://dx.doi.org/10.1016/j.nano.2014.12.006.

References

1. Psarros C, Lee R, Margaritis M, Antoniades C. Nanomedicine for the prevention, treatment and imaging of atherosclerosis. *Nanomedicine* 2012;**8**(Suppl 1):S59-68.
2. Siegel-Axel DI, Gawaz M. Platelets and endothelial cells. *Semin Thromb Hemost* 2007;**33**:128-35.
3. Madamanchi NR, Vendrov A, Runge MS. Oxidative stress and vascular disease. *Arterioscler Thromb Vasc Biol* 2005;**25**:29-38.
4. Siegel-Axel D, Daub K, Seizer P, Lindemann S, Gawaz M. Platelet lipoprotein interplay: trigger of foam cell formation and driver of atherosclerosis. *Cardiovasc Res* 2008;**78**:8-17.
5. May AE, Seizer P, Gawaz M. Platelets: inflammatory firebugs of vascular walls. *Arterioscler Thromb Vasc Biol* 2008;**28**:s5-s10.
6. Massberg S, Brand K, Gruner S, Page S, Muller E, Muller I, et al. A critical role of platelet adhesion in the initiation of atherosclerotic lesion formation. *J Exp Med* 2002;**196**:887-96.
7. Gawaz M, Langer H, May AE. Platelets in inflammation and atherogenesis. *J Clin Invest* 2005;**115**:3378-84.
8. Badrnya S, Schrottmaier WC, Kral JB, Yaiw KC, Volf I, Schabbauer G, et al. Platelets mediate oxidized low-density lipoprotein-induced monocyte extravasation and foam cell formation. *Arterioscler Thromb Vasc Biol* 2014;**34**:571-80.
9. Pitsilos S, Hunt J, Mohler ER, Prabhakar AM, Poncz M, Dawicki J, et al. Platelet factor 4 localization in carotid atherosclerotic plaques: correlation with clinical parameters. *Thromb Haemost* 2003;**90**:1112-20.
10. Coppinger JA, Cagney G, Toomey S, Kislinger T, Belton O, McRedmond JP, et al. Characterization of the proteins released from activated platelets leads to localization of novel platelet proteins in human atherosclerotic lesions. *Blood* 2004;**103**:2096-104.
11. Yilmaz A, Lipfert B, Cicha I, Schubert K, Klein M, Raithel D, et al. Accumulation of immune cells and high expression of chemokines/chemokine receptors in the upstream shoulder of atherosclerotic carotid plaques. *Exp Mol Pathol* 2007;**82**:245-55.
12. Libby P, Ridker PM, Hansson GK, Leducq Transatlantic Network on A. Inflammation in atherosclerosis: from pathophysiology to practice. *J Am Coll Cardiol* 2009;**54**:2129-38.
13. Stephen SL, Freestone K, Dunn S, Twigg MW, Homer-Vanniasinkam S, Walker JH, et al. Scavenger receptors and their potential as therapeutic targets in the treatment of cardiovascular disease. *Int J Hypertens* 2010:646929.
14. Stary HC, Chandler AB, Glagov S, Guyton JR, Insull Jr W, Rosenfeld ME, et al. A definition of initial, fatty streak, and intermediate lesions of atherosclerosis. A report from the Committee on Vascular Lesions of the Council on Arteriosclerosis, American Heart Association. *Circulation* 1994;**89**:2462-78.
15. Tedgui A, Mallat Z. Cytokines in atherosclerosis: pathogenic and regulatory pathways. *Physiol Rev* 2006;**86**:515-81.
16. Sluijter JP, Pulskens WP, Schoneveld AH, Velema E, Strijder CF, Moll F, et al. Matrix metalloproteinase 2 is associated with stable and matrix metalloproteinases 8 and 9 with vulnerable carotid atherosclerotic lesions: a study in human endarterectomy specimen pointing to a role for different extracellular matrix metalloproteinase inducer glycosylation forms. *Stroke* 2006;**37**:235-9.
17. Schulz C, Massberg S. Platelets in atherosclerosis and thrombosis. *Handb Exp Pharmacol* 2012:111-33.
18. Wasserman BA, Wityk RJ, Trout III HH, Virmani R. Low-grade carotid stenosis: looking beyond the lumen with MRI. *Stroke* 2005;**36**:2504-13.
19. Saam T, Hatsukami TS, Takaya N, Chu B, Underhill H, Kerwin WS, et al. The vulnerable, or high-risk, atherosclerotic plaque: noninvasive MR imaging for characterization and assessment. *Radiology* 2007;**244**:64-77.
20. Klostergaard J, Seeney CE. Magnetic nanovectors for drug delivery. *Nanomedicine* 2012;**8**(Suppl 1):S37-50.
21. Choi HS, Frangioni JV. Nanoparticles for biomedical imaging: fundamentals of clinical translation. *Mol Imaging* 2010;**9**:291-310.
22. Jacobin MJ, Laroche-Traineau J, Little M, Keller A, Peter K, Welschof M, et al. Human IgG monoclonal anti-alpha(IIb)beta(3)-binding fragments derived from immunized donors using phage display. *J Immunol* 2002;**168**:2035-45.
23. Mornet S, Portier J, Duguet E. A method for synthesis and functionalisation of ultrasmall superparamagnetic covalent carriers based on maghemite and dextran. *J Magn Magn Mater* 2005;**293**:127-34.
24. Kitts PA, Possee RD. A method for producing recombinant baculovirus expression vectors at high frequency. *Biotechniques* 1993;**14**:810-7.
25. Luckow VA, Lee SC, Barry GF, Olins PO. Efficient generation of infectious recombinant baculoviruses by site-specific transposon-mediated insertion of foreign genes into a baculovirus genome propagated in Escherichia coli. *J Virol* 1993;**67**:4566-79.
26. Juliant S, Leveque M, Cerutti P, Ozil A, Choblet S, Violet ML, et al. Engineering the baculovirus genome to produce galactosylated antibodies in lepidopteran cells. *Methods Mol Biol* 2013;**988**:59-77.
27. Robert R, Clofent-Sanchez G, Hocquellet A, Jacobin-Valat MJ, Daret D, Noubhani AM, et al. Large-scale production, bacterial localization assessment and immobilized metal affinity chromatography purification of a human single-chain Fv antibody against alphaIIb-beta3 integrin. *Int J Biol Macromol* 2006;**39**:51-9.
28. Jacobin-Valat MJ, Deramchia K, Mornet S, Hagemeyer CE, Bonetto S, Robert R, et al. MRI of inducible P-selectin expression in human activated platelets involved in the early stages of atherosclerosis. *NMR Biomed* 2011;**24**:413-24.
29. Sonvico F, Mornet S, Vasseur S, Dubernet C, Jaillard D, Degrouard J, et al. Folate-conjugated iron oxide nanoparticles for solid tumor targeting as potential specific magnetic hyperthermia mediators: synthesis, physico-chemical characterization, and in vitro experiments. *Bioconjug Chem* 2005;**16**:1181-8.
30. Pidard D, Montgomery RR, Bennett JS, Kunicki TJ. Interaction of AP-2, a monoclonal antibody specific for the human platelet glycoprotein IIb-IIIa complex, with intact platelets. *J Biol Chem* 1983;**258**:12582-6.
31. Shattil SJ, Hoxie JA, Cunningham M, Brass LF. Changes in the platelet membrane glycoprotein IIb.IIIa complex during platelet activation. *J Biol Chem* 1985;**260**:11107-14.
32. Niccoli G, Stefanini GG, Capodanno D, Crea F, Ambrose JA, Berg R. Are the culprit lesions severely stenotic? *JACC Cardiovasc Imaging* 2013;**6**:1108-14.
33. Stone GW, Maehara A, Lansky AJ, de Bruyne B, Cristea E, Mintz GS, et al. A prospective natural-history study of coronary atherosclerosis. *N Engl J Med* 2011;**364**:226-35.

34. Lajus S, Clofent-Sanchez G, Jais C, Coste P, Nurden P, Nurden A. Thrombocytopenia after abciximab use results from different mechanisms. *Thromb Haemost* 2010;**103**:651-61.
35. McCarty OJ, Conley RB, Shentu W, Tormoen GW, Zha D, Xie A, et al. Molecular imaging of activated von Willebrand factor to detect high-risk atherosclerotic phenotype. *JACC Cardiovasc Imaging* 2010;**3**:947-55.
36. Postea O, Vasina EM, Cauwenberghs S, Projahn D, Liehn EA, Lievens D, et al. Contribution of platelet CX(3)CR1 to platelet-monocyte complex formation and vascular recruitment during hyperlipidemia. *Arterioscler Thromb Vasc Biol* 2012;**32**:1186-93.
37. Czepluch FS, Kuschicke H, Dellas C, Riggert J, Hasenfuss G, Schafer K. Increased proatherogenic monocyte-platelet cross-talk in monocyte subpopulations of patients with stable coronary artery disease. *J Intern Med* 2014;**275**:144-54.
38. Li N. CD4+ T cells in atherosclerosis: regulation by platelets. *Thromb Haemost* 2013;**109**:980-90.
39. Chandler AB, Hand RA. Phagocytized platelets: a source of lipids in human thrombi and atherosclerotic plaques. *Science* 1961;**134**:946-7.
40. De Meyer GR, De Cleen DM, Cooper S, Knaapen MW, Jans DM, Martinet W, et al. Platelet phagocytosis and processing of beta-amyloid precursor protein as a mechanism of macrophage activation in atherosclerosis. *Circ Res* 2002;**90**:1197-204.
41. Daub K, Seizer P, Stellos K, Kramer BF, Bigalke B, Schaller M, et al. Oxidized LDL-activated platelets induce vascular inflammation. *Semin Thromb Hemost* 2010;**36**:146-56.
42. Foresta C, Strapazzon G, De Toni L, Fabris F, Grego F, Gerosa G, et al. Platelets express and release osteocalcin and co-localize in human calcified atherosclerotic plaques. *J Thromb Haemost* 2013;**11**:357-65.
43. Seizer P, Schonberger T, Schott M, Lang MR, Langer HF, Bigalke B, et al. EMMPRIN and its ligand cyclophilin A regulate MT1-MMP, MMP-9 and M-CSF during foam cell formation. *Atherosclerosis* 2010;**209**:51-7.
44. van Lammeren GW, Pasterkamp G, de Vries JP, Bosch L, de Haan JJ, de Kleijn DP, et al. Platelets enter atherosclerotic plaque via intraplaque microvascular leakage and intraplaque hemorrhage: a histopathological study in carotid plaques. *Atherosclerosis* 2012;**222**:355-9.
45. Hatsukami TS, Yuan C. MRI in the early identification and classification of high-risk atherosclerotic carotid plaques. *Imaging Med* 2010;**2**:63-75.
46. Cheruvu PK, Finn AV, Gardner C, Caplan J, Goldstein J, Stone GW, et al. Frequency and distribution of thin-cap fibroatheroma and ruptured plaques in human coronary arteries: a pathologic study. *J Am Coll Cardiol* 2007;**50**:940-9.
47. Pavlou AK, Reichert JM. Recombinant protein therapeutics—success rates, market trends and values to 2010. *Nat Biotechnol* 2004;**22**:1513-9.
48. Reichert JM. Antibodies to watch in 2014. *MAbs* 2014;**6**:5-14.
49. Stas P, Lasters I. Immunogenicity of therapeutic antibodies. *Med Sci (Paris)* 2009;**25**:1070-7.
50. Chan AC, Carter PJ. Therapeutic antibodies for autoimmunity and inflammation. *Nat Rev Immunol* 2010;**10**:301-16.

Full title:

A Recombinant Human Anti-platelet scFv Antibody Produced in *Pichia pastoris* for Atheroma Targeting.

Amelie Vallet-Courbin[1], Mélusine Larivière[2], Agnès Hocquellet[1], Audrey Hemadou[2], Sarjapura-Nagaraja Parimala[1], Jeanny Laroche-Traineau[2], Xavier Santarelli[1], Gisèle Clofent-Sanchez[2], Marie-Josée Jacobin-Valat[2*] and Abdelmajid Noubhani[1*].

1 Bordeaux-INP, CBMN, UMR5248, F-33600, Pessac, France, **2** Centre de Résonance Magnétique de Systèmes Biologiques, Centre Nationale de Recherche Scientifique et Université de Bordeaux, Bordeaux, France.

***** Equivalent position of authors

Short title:

Production of Human scFv Antibody for Atheroma Targeting.

Correspondence to: Dr. Abdelmajid Noubhani,

Structure and activity of biological macromolecules. Institute of Chemistry and Biology of Membranes and Nano-objects. CBMN-CNRS UMR-5248.

Allée Geoffroy Saint Hilaire, B 14. 33600 PESSAC. France.

Phone : +33 557571722

Mail : noubhani@bordeaux-inp.fr

Abstract

Cells of the innate and adaptive immune system are key factors in the progression of atherosclerotic plaque, leading to plaque instability and rupture, potentially resulting in acute atherothrombotic events such as coronary artery disease, cerebrovascular disease and peripheral arterial disease. Here, we describe the cloning, expression, purification, and immunoreactivity assessment of a recombinant single-chain variable fragment (scFv) derived from a human anti-αIIbβ3 antibody (HuAb) selected to target atheromatous lesions for the presence of platelets. Indeed, platelets within atheroma plaques have been shown to play a role in inflammation, in platelet-leucocyte aggregates and in thrombi formation and might thus be considered as relevant biomarkers of atherosclerotic progression. The DNA sequence that encodes the anti-αIIbβ3 TEG4 scFv previously obtained from a phage-display selection on activated platelets, was inserted into the eukaryote vector (pPICZαA) in fusion with a tag sequence encoding 2 cysteines useable for specific probes grafting experiments. The recombinant protein was expressed at high yields in *Pichia pastoris* (30 mg/L culture). The advantage of *P. pastoris* as an expression system is the production and secretion of recombinant proteins in the supernatant, ruling out the difficulties encountered when scFv are produced in the cytoplasm of bacteria (low yield, low solubility and reduced affinity). The improved conditions allowed for the recovery of highly purified and biologically active scFv fragments ready to be grafted in a site-directed way to nanoparticles for the imaging of atherosclerotic plaques involving inflammatory processes and thus at high risk of instability.

Key words:

Cardiovascular disease. Atherosclerosis. Recombinant human antibody fragment, scFv. *Pichia pastoris*. Recombinant protein production. Immobilized metal affinity chromatography. Immunohistochemistry.

Abbreviations:

HuAb: human antibody

scFv: single-chain variable fragment

IMAC: Immobilized Metal Affinity Chromatography

ELISA: Enzyme-Linked Immunosorbent Assay

OD: Optical Density

IHC: Immunohistochemistry

VH: Heavy Chain

VL: Light Chain

SPR: Surface Plasmon Resonance

PRP: Platelet Rich Plasma

NA-PL: Non Activated Platelets

A-PL: Activated Platelets

BLI: Bio-Layer Interferometry

RU: Relative Units

Introduction

Atherosclerosis is an inflammatory disease associated with the formation of unstable thrombosis-prone atheroma plaques made of large lipid cores, thin fibrous cap and inflammatory cell infiltrates within the walls of arteries.[1] Atherosclerotic plaque rupture is the mechanistic cause of about 75 % of all sudden and often fatal heart attacks.[2] As the risk of plaque rupture is more related to the plaque contents than to the plaque size, molecular imaging modalities have risen as a new imperative. Current studies tend towards the development of non-invasive targeted methods to assess the cellular components that underlie the risk of rupture.[3,4] Molecular imaging requires highly sensitive and specific probes made of a signal detection compound and an affinity ligand for targeting. The affinity ligand should be able to recognize molecules and cells over-expressed during the course of atherogenesis. Inflammation is a well-recognized pathophysiological process involving both innate and adaptive immune cells.[5] Recruitment of monocytes in the vascular wall and macrophage differentiation and proliferation represent a hallmark in the pathology of atherosclerotic lesions.[6] They contribute to the processes that underlie atherogenesis such as lipid accumulation, secretion of pro-inflammatory cytokines, extracellular matrix remodelling. Moreover, the observation of activation and oligoclonal expansion of T cells has suggested the presence of inciting antigens (Ags) that sustain T cell recruitment within coronary lesions.[7] B cells also play a pro or anti-atherogenic role depending on the subtypes (B1(a) or B2), and in atherosclerosis they accumulate both in the atherosclerotic intima and associated adventitia.[8-10] More recently, platelets have come to the forefront as partners of macrophages, T cells and B cells in inflammation and immune responses. They are now recognized as key players in innate and adaptive immune responses [11,12] and notably shown to modulate the T-effector/T-regulator balance via the CD40 ligand.[13,14] Platelet-derived CD40 ligand has also been reported to support B-cell differentiation and

immunoglobulin class switching in mice.[15] Several cytokines released by activated platelets have been demonstrated to modulate monocyte and macrophage function.[16] Moreover platelet–leukocyte interactions largely contribute to OxLDL uptake and foam cell formation.[17] A recent study has underlined the presence of platelets not only in thrombi and intraplaque hemorrhage but also in atheroma burden, around necrotic areas and neovessels, shedding light on the rationale for targeting platelets within atherosclerotic lesions.[18]

Today, antibodies are used for several applications in research, diagnostics, and therapy.[19] Technology improvements are focused on several approaches to manufacturing recombinant human antibodies.[20] Moreover, *in vitro* selection technologies such as antibody phage display or ribosomal display have accelerated the generation of these recombinant human antibodies.[21-23]

To develop a novel non-invasive targeting approach for atheroma, our team previously selected, using *in vitro* phage display biotechnology on activated platelets, a phage-scFv fully human antibody (HuAb) specific to the αIIbβ3 integrin, which is an integrin only expressed on platelets and not on other immune cells.[24] This human antibody was further processed as a whole human IgG_4 molecule in baculovirus system.[18] We proved the maintenance of the bioactivity after grafting onto superparamagnetic nanoparticles dedicated to MRI imaging. However, the chemical functionalization was hard to proceed, time-consuming and we did not succeed in grafting more than one HuAb onto each nanoparticle [18]. To overcome these drawbacks and obtain a better conjugation ratio, another type of protein engineering has been applied to reduce the probe size. A scFv protein composed of the heavy (VH) and light (VL) chains of an antibody linked with a flexible peptide, has been constructed by recombinant DNA technology. The diameter of scFv fragments (5 nm), one-fifth the size of whole IgG, is more suitable for functionalizing relatively small nanoparticles. Compared to much larger forms of antibodies such as Fab, Fab'2 and IgG, scFv have lower retention times in non-target

tissues and exhibit more rapid blood clearance and better penetration into targeted lesions.[25] Moreover, this recombinant form can be generated with tags for purification and site-specific attachment via engineered thiols to avoid loss of bioactivity. There are a variety of recombinant production systems for the generation of scFvs ranging from bacteria, filamentous fungi, insect cell lines to transgenic plants.[20,26] More specifically, studies reported the production of an anti-platelets scFv antibody in transient mammalian cells system (e.g, freestyle HEK 293F cells).[26] However, transient antibody production appears more suitable for small-scale production in antibody screening. Here, TEG4 HuAb needs to be stably expressed as scFv fragments in a quantity so that purification, characterization and further grafting of isolated recombinant fragments could be readily accomplished. Hence, TEG4 HuAb was processed in *Pichia pastoris*. The choice of production in yeast cells was guided by previous experiments where biological activity could only be recovered in the cytoplasm of cells when using *E. coli* as a host expression system. Indeed, despite improvements in fedbatch fermentation production, a proportion of inactive scFv remained in the total purified population.[27] From this point of view, the *Pichia pastoris* expression system is an attractive way due to its ability to secrete a large amount of recombinant protein in the supernatant, thereby facilitating the purification steps.

The aim of the study was thus to produce highly purified and biologically active scFv fragments in a suitable yeast cell expression modality. The biochemical characteristics of the anti-αIIbβ3 scFv were evaluated by ELISA, affinity binding analyses, flow cytometry against platelets and immunohistochemistry (IHC) on atheroma plaques from animal models and human coronary sections. These scFv fragments are ready to be grafted in a site-directed way to nanoparticles for the imaging of atherosclerotic plaques where inflammatory and immune processes increase the risk of instability.

Materials and Methods

Materials

Large-scale expression of TEG4-2c scFv in *Pichia pastoris* was carried out in BIOSTAT® Bplus laboratory fermentor 5L (Sartorius-Stedim Biotech, Germany). Data and set points were monitored with MFCS-Win. Growth media were purchased from Becton Dickinson (Le Pont de Claix, France).

Immobilized Metal Affinity Chromatography (IMAC) was carried out on HisTrap™ excel column (id 5 mL, GE Healthcare, Sweden) containing resin charged with nickel ions. Buffers for chromatographic runs, and reagents were prepared using chemicals of analytical grade from Sigma-Aldrich (Saint Quentin Fallavier, France).

Chromatographic experiments were performed using ÄKTA pilot workstation (GE Healthcare) and were monitored with Unicorn 5.1 software. Protein detection was monitored at 215 and 280 nm.

Spectrophotometric measurements of samples drawn from the fermentor and BCA protein assay measurements were carried out using SAFAS UVmc2 double-beam UV-visible spectrophotometer (Société Anonyme de Fabrication d'Appareillages Scientifiques, Monaco).

Flow cytometry experiments were performed on a FACS Canto I cytometer from BD Biosciences (Le Pont de Claix, France) and monitored using DIVA software.

The absorbance of ELISA assays was read at 405 nm using a CHAMELEON microplate reader from ScienceTec (Les Ulis, France).

Surface Plasmon Resonance (SPR) experiments on purified αIIbβ3 integrin (Kordia Life Sciences, Leiden, The Netherlands) were carried out using the BIAcoreTM 3000 (GE Healthcare Europe GmbH, Velizy-Villacoublay, France) equipped with research-grade CM5 sensor chips. Bio-Layer Interferometry (BLI) experiments on lyophilized platelets (Helena

Biosciences Europe, Queensway S, UK) were performed using an Octet instrument (Octet Red96 Pall Life Sciences, Saint-Germain-en-Laye, France) and HIS2 (anti-penta Histidine Ab) sensors.

Methods

1-Vectors and Strains

The pHOG21 vector, kindly provided by M. Little (Affimed Therapeutics, Lademburg, Germany), pCR4-TOPO and pPICZαA (Invitrogen, Carlsbad, USA) plasmids were used for preparation of DNA constructs. Synthetic oligonucleotides were purchased at Eurogentec (Liege, Belgium). Cloning step was carried out with *Escherichia coli* strain JM109 (NewEnglands Biolabs, Ipswich, MA USA). *Pichia pastoris* strain X33 used for production of recombinant TEG4-2c scFv was obtained from Invitrogen (Carlsbad, CA, USA).

2-Construction of an expression vector for TEG4-2c scFv

The TEG4 scFv DNA fragment provided in the pHOG21 vector previously used for the TEG4 scFv expression in XL1-Blue *E. coli* [16] was used as template to generate a new scFv format containing 2 cysteines into the C-terminal end. The coding sequence was PCR-amplified with *Pfu* Turbo polymerase (Stratagene). The primers (PICTE: 5'-TATCACGTGGCAGGTGCAGCTGGTGG-3' and PIC2C: 5'-TCTAGATTAGCAGCACCCGTGATGGTGATGGTG-3') were used to introduce the 6HisTag-Gly-Cyc-Cys-Stop amino acid sequence. Thirty amplification cycles were performed (30s at 95°C, 45s at 48°C and 1min at 72°C) followed by a final extension of 10 min at 72°C. The PCR product was purified, ligated into pCR4-TOPO plasmid and verified by DNA sequencing (Millegen Technology – France). The resultant plasmid was digested by *Pml*I and

*Xba*I to excise TEG4-6His-Gly-Cys-Cys DNA fragment and ligated into the expression vector pPICZαA (Invitrogen, Carlsbad, USA) containing the Zeocin resistance gene for selection and the AOX1 promoter. The new construction of TEG4-2c scFv is shown in **Fig.1**.

Fig.1: pPICZ*α*A expression vector according to the EasySelect *Pichia* Expression Kit Manual (Invitrogen) and a schematic representation of TEG4-2c scFv with the protein sequence. **(A):** All the featured restriction sites are unique. 5´ AOX1: promoter region of AOX1; TT AOX1: transcription termination of AOX1; PTEF1: promoter of TEF1; PEM7: promoter of EM7; Zeocin resistance: Sh ble ORF; CYC1 TT: transcription termination of CYC1. **(B):** The TEG4-2c scFv coding sequence was cloned between *Pml*I and *Xba*I sites and the protein sequence of recombinant tag-scFv including the 6His-tag and the 2 cysteine are highlighted in green. The α-factor signal sequence is represented in blue and the C-myc tag is highlighted in yellow.

The resultant plasmid was linearized by *Pme*I and transformed into competent *P. pastoris* X-33 cells by electroporation using Gene Pulser II (Bio-Rad, Hercules, CA, USA). Transformant cells were grown on YPDS-Zeocin 150 µg/mL-agar plates and screened again later for their ability to grow on Zeocin™ (Invitrogen, Carlsbad, USA) up to concentrations of 2 mg/ml. Selected clones were tested for the presence of TEG4-2c scFv coding sequence in their genome by colony PCR analysis using the PICTE and PIC2C primers, amplification cycles were preceded by a heating step 3 min at 95°C.

3-Expression and purification of TEG4-2c scFv

Transformed *P. pastoris* cells that exhibited high resistance to Zeocin (up to 2 mg/mL plates) were grown in shake flasks containing 100 ml of buffered glycerol complex medium (BMGY, 1% yeast extract, 2% peptone, 100 mM potassium phosphate buffer at pH 6.0, 13.4g/L YNB, $4x10^{-4}$ g/L biotin, 10 g/L glycerol and 150 µg/mL Zeocin®) until an optical density of 20 was

reached. The culture was inoculated in a 5L bioreactor at 0.2 OD units. The bioreactor conditions were optimized by modification of Narasimhan, J *et al.*[28] The temperature and pH were maintained at 30°C and 6 respectively, and dissolved oxygen levels were maintained at 20% saturation by regulating aeration and agitation in a cascading system. After complete consumption of glycerol in the medium (20 to 24 hours), a methanol fed-batch phase was initiated by adding methanol every 12 h to a final concentration of 0.6%; this phase promotes the induction of scFv production and secretion in the medium. The methanol feed frequency was modified to every 6 h during the 4 latest days of production. Samples were drawn every 24 h to determine the yeast growth profile and scFv production. After 120 h of induction, the culture was harvested and the supernatant frozen at -80°C pending purification steps. Prior to purification, the pH of the broth was adjusted to 7.4 and filtered through a 0.45 µm cellulose acetate membrane.

The expressed recombinant TEG4-2c scFv was purified using IMAC. The HisTrap Excel resin was equilibrated with 50 mM Tris-HCl pH 7.5, 500 mM NaCl (buffer A at a flow rate of 3 mL/min). Typically, 450 to 800 mL *P. pastoris* expression broth supernatant containing the scFv was directly injected into the column. The column was then washed with buffer A until absorbance at 280nm reached the baseline. The elution was carried out into two steps using 5% and 30% buffer B (50 mM Tris-HCl pH 7.5, 500 mM NaCl, 500 mM imidazole) corresponding respectively to 25 mM and 150 mM imidazole. The elution fraction was dialyzed against PBS (NaCl 135 mM, KCl 2.5 mM, Na_2HPO_4 10 mM, KH_2PO_4 1.5 mM pH 7.4) buffer.

4-Protein assay, SDS-PAGE and Dot-blot analysis

Protein quantification of the chromatographic fractions was performed using bicinchoninic acid protein micro-assay (BCA kit, Sigma). Twenty-five microliters samples were incubated

with 200 µL of BCA working reagent and plate was incubated at 37°C for 30 min. The absorbance was measured at 562 nm.

Fractions obtained from chromatographic experiments were analyzed by SDS-PAGE under reducing conditions over 12% polyacrylamide gels. Supernatant and flow through fractions were 5x concentrated by TCA precipitation. Precision plus protein prestained standards (BIO-RAD) were used as molecular weight ladder.

To analyse the efficiency of the yeast cells *P. pastoris* to produce the scFv fragments into the broth medium, 50 µL samples from day 1 to day 5 were blotted on a nitrocellulose membrane using Bio-Dot® Microfiltration Instrument (BIO-RAD). The membrane was blocked with a blocking buffer (TBS Tween with 3% milk powder) for 2 hours. The membrane was again washed twice with TBS-tween, and then incubated with primary antibody (Anti 6His, SIGMA) at 1:1500 dilution overnight at 4°C. Membranes were then washed and probed with a secondary antibody (anti-mouse IgG-HRP Cell Signaling Technology) at 1:5000 dilution.

Colorimetric analysis was performed using Opti4CN (BIO-RAD) kit by gently shaking until color develops.

5-Preparation of Platelet-Rich-Plasma (PRP) and washed platelets

Platelet-rich plasma (PRP) and washed platelets were prepared from the blood of voluntary healthy donors.

PRP was obtained from venous blood anticoagulated with sodium citrate (0.38%, w/v) after centrifugation at 120 *g* for 10 min at room temperature.[29]

For the preparation of washed platelets, venous blood was anticoagulated with citric acid-citrate-dextrose NIH formula A (ACD-A) (1 vol of anticoagulant: 6 vol of blood). After centrifugation at 120 *g* for 10 min, the PRP was collected and mixed with ACD-A (1 vol : 9 vol, PRP) plus 100 nM prostaglandin E_1 and 0.05 U/mL Apyrase [Grade7],[30] Platelets were

sedimented by centrifugation at 1100 *g* for 15 min, washed and adjusted at 10^8/mL in a modified Tyrode's buffer (137 mM NaCl, 2.7 mM KCl, 12 mM $NaHCO_3$, 0.3 mM NaH_2PO_4, 1 mM $MgCl_2$, 5.5 mM glucose, 5 mM HEPES, 0.1% (wt/vol) bovine serum albumin (BSA), pH 7.4.

6-Analysis of TEG4-2c scFv reactivity by Flow cytometry

Analysis on washed platelets

For the analysis of TEG4-2c scFv reactivity on platelets, **w**ashed platelets were activated with 0.5 U/ml human α-thrombin (Fibrindex, Ortho-Diagnostics, Raritan, NJ). Samples of both activated and non-activated platelets were fixed for 30 min with an equal volume of paraformaldehyde (PFA) 2% and then incubated with diluted TEG4-2c scFv.

Aliquots of 10^8 PFA-fixed-washed-platelets/mL (10 µL) [27] non-activated (NA-PL) or activated with thrombin (A-PL) were incubated with 25 µg/mL of TEG4-2c scFv human antibody or PAC-1 commercial IgM antibody (BD Biosciences) [31] targeting the activated αIIbβ3 integrin overnight at 4 °C. After two washes in PBS, a 30 min incubation with secondary Alexa Fluor 488 anti-6His or goat anti-mouse IgM antibodies (1:20) was performed for detection of respectively, the TEG4-2c scFv and the murine PAC-1 antibody. Reactions in the absence of antibodies were used as negative controls.

Analysis on PRP samples

Aliquots of 4 µL of PRP are used in each experiment. Some aliquots are activated with 50 µM thrombin receptor activating peptide (TRAP6; Sigma Aldrich, Saint-Quentin-Fallavier, France). Activated (+TRAP) and non-activated PRP aliquots (-TRAP) were then incubated with diluted TEG4-2c scFv (25 ug/ml) 15 min before adding secondary Alexa Fluor 488 anti-

6His (both 1:20) antibody for another 15 min incubation. Reactions in the absence of antibodies were used as negative controls.

Cells were then resuspended in PBS before analysis on the BD Canto1 cytometer. The forward and wide-angle light scattering and fluorescence intensity from 10,000 platelets were collected using a logarithmic gain.

7-Analysis of TEG4-2c scFv reactivity by ELISA

A 96-well flat-bottom polystyrene microtiter plate (Costar, Corning, NY) was coated with washed thrombin-activated (A-PL) or non-activated platelets (NA-PL) at 10^7 platelets/well or BSA protein 20 µg/mL (Sigma-Aldrich) in 50 mM carbonate-bicarbonate buffer (pH 9.6) overnight at 4°C. The plate was washed three times with PBS (pH 7.4) containing 0.05% Tween 20 (200 µL/well) and blocked with 5% skimmed milk in PBS for 2 h at 37°C. TEG4-2c scFv fragments purified by IMAC or full-length mouse IgG antibody (AP2 antibody targeting αIIbβ3 integrin) [32] were tested on A-PL and NA-PL. After incubation for 2 h at 20°C, the plate was washed and incubated with an anti-6His IgG antibody (GE Healthcare) for 1 h at 37°C to detect scFv fragments or with PBS for full-length mouse antibodies. After washings, 100 µL of a 1:1000 dilution of horseradish peroxidase (HRP)-conjugated anti-mouse IgG (Immunotech, Marseille, France) was added and incubated for 90 min at room temperature. Color was developed with 100 µL of 2;2'-Azino-bis(3-ethylbenzothiazoline-6-sulfonic acid) (ABTS) (Sigma-Aldrich, Saint-Quentin, Fallavier, France) and the absorbance was read at 405 nm using a CHAMELEON microplate reader.

8-Preparation of atheromatous and healthy aorta proteins

All animal experiments were performed in conformity with the Guide for the Care and Use of Laboratory Animals (NIH Publication No. 85–23, revised 1996) and were accredited by the local ethical committee.

Adult male New Zealand rabbits (NZW), weighting from 2.5 kg to 3.0 kg, were obtained from Charles Rivers Laboratories (St Germain sur l'Arbresle, France).

In order to mimic atherosclerosis that develop in humans, rabbits were fed a fat atherogenic diet including 0.3% cholesterol for 8 months and were subjected to surgeries to allow the formation of complex plaques with intramural thrombi. A first surgery was performed to remove endothelial cells from the thoracic until the abdominal aorta using a Fogarty catheter (Fogarty 4F; Edwards Lifesciences). The second surgery consists in an angioplasty using an expandable latex balloon (Maxxum®, Boston Scientific; 20 mm long, diameter of 4.5 mm) under radioscopic guidance from the region of renal arteries to iliac bifurcation. Surgeries were performed under anesthesia by intramuscular administration of 20 mg/kg ketamine and 2 mg/kg xylazin. Anaesthesia was maintained with isoflurane gas (0.25% to 0.35%). As a preventive anti-thrombotic treatment, 1000 µI of heparine (Héparine Choay®, Sanofi Synthélabo) was infused. After surgery 100 mg aspirine (Aspégic® injectable, Sanofi Synthélabo) was administered as analgesia. Aortas from untreated rabbits and balloon-injured aortas from hypercholesterolemic rabbits were extracted from the aortic arch to the iliac bifurcation, washed and fractioned in order to solubilize tissue proteins in T-PER (Thermo Fisher Scientific) or HSB (50 mM HEPES, pH 7.4; 137 mM NaCl; 1% NP-40 (v/v); 2 mM EDTA; 1 mM PMSF; protease inhibitors cocktail (Roche Diagnostics, Meylan, France) lysis buffer. Homogenization was performed using first a Polytron TP-20 Homogenizer (Kinematica, Lucerne, Switzerland) and then a sonicator (3 x 10-seconds pulses at 80% magnitude). After two centrifugations at 13000 g for 45 min at 4°C to remove insoluble material from the supernatant, the protein concentration of every soluble extract was

determined using the Bradford assay kit according to the manufacturer's instructions (Thermo Fisher Scientific).

9-Affinity determination evaluated by SPR

The interactions between the anti-αIIbβ3 TEG4-2c scFv and the integrin αIIbβ3 were analyzed by SPR sensing using BiacoreTM 3000 (GE Healthcare), according to the manufacturer's instructions. HBS-EP buffer (0.01 M HEPES pH 7.4, 0.15 M NaCl, 3 mM EDTA, 0.005% v/v Surfactant P20) (GE healthcare life sciences, France) with 2 mM Ca^{2+} was used as a running buffer. The purified αIIbβ3 was first dialysed in the running buffer, diluted in 10 mM Na-Acetate, pH 5.5, then immobilized onto the sensor surface of a Biacore sensor chip CM5 to an immobilized ligand density (RU) of about 8000, using an amine coupling kit. Then, anti-αIIbβ3 TEG4-2c scFv diluted into the running buffer at concentrations ranging from 90 to 400 nM was allowed to flow through the sensor chip for 5 min at a flow rate of 20 µL/min and dissociation of bound analyte was allowed to proceed for 15 min before chip regeneration with NaOH 20mM.

10-Affinity determination evaluated by BLI: Octet Red96

Octet instrument is a label-free detection system that exploits optical principle to read bimolecular interactions, the bio-layer interferometry (BLI). The interactions between the anti-αIIbβ3 TEG4-2c scFv and blood platelets were analyzed using Octet (Red96) in platelet buffer (NaCl 137 mM, KCl 2 mM, NaH2PO4 0.3 mM, MgCl2 1 mM, Glucose 5.5 mM, Hepes 5 mM, Bicarbonate-Na 12 mM pH6). The purified TEG4-2c scFv was loaded on a HIS2 biosensor (anti-penta Histidine Ab optical fiber based sensor) at 21 µg/mL. Platelets were diluted in PBS, coated into 96 well plate and analyzed at different concentrations: $5x10^5$ to $5x10^8$/mL, corresponding to integrin αIIbβ3 molarities from 42 pM to 42 nM. The plate is

shaken during reading to create an "orbital flow". Controls with no scFv and no platelets were performed to check for nonspecific binding and signal drift, respectively.

11-Immunohistochemistry Analysis on Murine and Human Atherosclerotic Sections

All animal studies were approved under the N° 50120192-A by the Animal Care and Use Committee of Bordeaux, France. All work with tissues from human subjects had been approved by the CPP committee (Comité de Protection des Personnes Sud-Ouest et Outre Mer) of Bordeaux and from the Research Ministry in France (Authorization number DC - 2016- 2724). $ApoE^{-/-}$ mice were fed a high-cholesterol diet for 21 weeks. New Zealand white rabbits were prepared as described in paragraph 8. Human coronary arteries were harvested from patients with end-stage heart failure having undergone heart transplantation. All of the clinical interventions took place at Haut-Lévèque Hospital (Pessac, France). Human tissue specimens were collected after informed consent to use surgical waste for investigational purposes. They were immediately processed and embedded in paraffin.

Paraffin-embedded sections of arterial tissue from mouse, rabbit or human were used in IHC experiments with TEG4-2c scFv (tested between 20 and 40 µg/ml), anti-CD41 (anti-αIIb, working dilution 1:200, Abcam, France), AP2 (anti-αIIbβ3 antibody, 10 µg/mL), RAM11 (working dilution 1:50) and PGM1 (working dilution 10ug/ml) anti-CD68 antibodies targeting rabbit and human macrophages respectively (Dako, Les Ulis, France).

Paraffin-embedded sections were deparaffinised, rehydrated, and heat mediated antigen retrieval was performed with Tris-EDTA pH 9 buffer following the specifications of Abcam, Paris, France (*www.**abcam**.com/ps/pdf/protocols/ihc_p.pdf*). Endogenous peroxidase was then blocked with 3 % H_2O_2 in water, for 15 min. After washing in PBS 1X + 0.025 % Triton

(PBST), nonspecific binding was blocked with PBS 1X + 0.2 % Triton + 2 % bovine serum albumin (BSA) for 1 h at room temperature.

Afterwards, antibodies were applied overnight at 4 °C, diluted at 20 µg/mL in PBS 1X + 1 % BSA. The following day, three washes with PBST were performed. To detect TEG4-2c scFv fragments, an HRP-conjugated antibody specific to 6His (working dilutions 1:250) was applied to the sections for 1 h at room temperature. HRP-conjugated secondary antibodies specific to (1) rabbit IgG H+L (Beckman Coulter), (2) mouse IgG H+L (Beckman Coulter) were respectively applied for commercial primary anti-CD41, RAM-11, PGM1 and AP2 antibodies.

After a further three washes with PBST, staining was performed by adding the peroxidase substrate diaminobenzidine (DAB substrate kit, Eurobio/ABCys, Les Ulis, France) with H_2O_2. It yielded a yellow brown deposit within 10 min at room temperature. After a wash in dH_2O to stop the enzymatic reaction, slides were counterstained in hematoxylin, dehydrated and mounted.

Results

1-Monitoring TEG4-2c scFv large scale production in *Pichia pastoris*

After the transformation of *P. pastoris* with linear pPICZαA-TEG4-2c plasmid, up to 60 clones were selected on 2 mg/mL Zeocin agar plates. The colony PCR analysis confirmed the presence of TEG4-2c scFv gene in 16 tested clones. Six clones were evaluated for their capacity to produce and secrete TEG4-2c scFv in a shake flask. Finally, the clone TEG4-2c A2 was selected for further analysis and the production scaled up in a 5 L benchtop bioreactor.

Five culture batches were carried out on a 5 L benchtop bioreactor and exhibited a similar growth profile (data not shown). The culture conditions were maintained as described in the experimental section. The dissolved oxygen level was maintained throughout the production batch at 20% by a combination of agitation and aeration systems, in a cascading manner to improve the oxygen supply during the growth of cells (**fig.2A**). The yeast growth was exponential during the batch culture with glycerol as the substrate; the glycerol was exhausted after 20 to 24 h culture and the cell density reached 28 OD units corresponding to 8.1 g/L (dry weight).

Fig.2: TEG4-2c scFv production process. A: Fed batch fermentation history plot. Stirring, pO_2 and OD_{600} values are plotted versus time during the cultivation of *P. pastoris* in BMGY medium. Cultures were induced with methanol at t=0 (24 h after starting the batch phase) during the fed batch phase the methanol was added every 12 h or 6h (black arrows) to a final concentration of 0.6%. The average values are shown with error bars representing the standard deviation (n=5). 1 OD_{600} unit was equivalent to 0.29 mg/mL dry weight. **B: Dot-blot analysis of supernatants from recombinant *P. pastoris* culture.** Fifty microliters samples from non-induced culture (NI) and from day 1 to day 5 induced cultures (I1d to I5d) were undiluted (a) or diluted (b=1:10; c=1:50) and blotted on a nitrocellulose membrane. The recombinant TEG4-2c scFv were detected with the Anti-6His antibody and revealed by colorimetric analysis.

A fed-batch phase was initiated by adding methanol every 12 h to induce the scFv production. To optimize the efficiency of scFv production during the 4 last days, the methanol feed frequency was every 6 h. Following each substrate addition event, there was a sharp increase in agitation indicating the active consumption of substrate and sustainable growth of cells. Stirring, which again diminished upon substrate consumption, was raised following the

consecutive methanol injection. During the fed-batch phase, a linear increase in yeast biomass was observed 24 h after induction. A growth rate of 0.23 g $L^{-1}h^{-1}$ was maintained during 5 days; the cell density was also increased by a 4.3 fold and reached 35 g/L (dry weight).

Dot-blot analysis was performed to evaluate the TEG4-2c scFv expression each day after induction in the culture broth. Recombinant TEG4-2c was only produced upon induction of transformed X-33 cells with methanol. This was clearly confirmed by the absence of signal into the samples before methanol feeding and into the samples from X33 *Pichia* cells transfected with the empty pPICZαA plasmid. The anti-αIIbβ3 TEG4-2c scFv was expressed from the first day in a soluble form into the cells culture medium (**Fig. 2B**).

2-Purification of TEG4-2c scFv by IMAC

For the purification of recombinant TEG4-2c scFv, optimal performance was obtained when an intermediate washing step with 25 mM imidazole was used to remove the contaminating proteins weakly bound to the column, after which recombinant TEG4-2c scFv was eluted using 150 mM imidazole (**Fig.3A**).

Fig.3: Purification of recombinant TEG4-2c scFv A: IMAC chromatogram. The HisTrap Excel resin (5 mL) was equilibrated with 50 mM Tris-HCl pH 7.5, 500 mM NaCl (buffer A at a flow rate of 3 mL/min). *Pichia pastoris* expression broth supernatant containing the TEG4-2c scFv was injected into the column. The column was then washed with buffer A until absorbance at 280nm reached the baseline. (Dot Line): The elution was carried out in two steps using 5% and 30% buffer B (50 mM Tris-HCl pH 7.5, 500 mM NaCl, 500 mM imidazole) corresponding respectively to 25 mM and 150 mM imidazole. **B: Electrophoretic analysis of one step IMAC purification of recombinant TEG4-2c scFv.** 12% SDS-PAGE stained with colloidal blue, MW: molecular weight ladder (KDa). [S]: 5x concentrated culture

supernatant. [TF]: 5x concentrated flow-through. W: 25 mM imidazole washing fraction. E: 150 mM elution fraction. E_{PBS}: Elution fraction dialyzed against PBS.

Typically, 30 mg of TEG4-2c scFv were produced and secreted by *P. pastoris* into 1L broth medium after 5 days of growth. The scFv content into this supernatant was estimated to 1.4% of the total proteins. After the IMAC purification, the yield was around 22 mg TEG4-2c scFv from 1L culture medium. This represents a recovery of 70% of produced scFv with a high purity (> to 80%). This one step chromatography led to a 57 fold purer product with highly concentrated solution of TEG4-2c scFv (Table).

Table: IMAC Purification of scFv TEG4-2c produced and secreted by *P. pastoris*. Data are standardized for 1 L culture media; the values are the mean of 7 independent experiments ± SD values.

	Protein[a] (mg/mL)	scFv[b] (µg/mL)	Volume (mL)	Total protein[a] (mg)	Total scFv[ab] (mg)	Step recovery (%)	Step purification (fold)
Supernatant	2.190 ± 0.367	30.7 ± 4.3	1000	2190 ± 367	30.7 ± 4.3	100	0
Flow through	1.983 ± 0.377	ND	1000	1983 ± 377	ND	ND	ND
Wash step	0.167 ± 0.036	16.7 ± 3.3	75 ± 5	12.53 ± 1.64	1.253 ± 0.25	ND	ND
Elution step	0.866 ± 0.136	695 ± 35	31 ± 2	26.85 ± 1.52	21.56 ± 3.01	70.3 ± 0.6	57.35

[a] Protein concentration was determined by BCA protein assay, using bovine serum albumin as standard.
[b,c]TEG4-2c scFv into the supernatant and the purity was estimated by densitometric quantification of corresponding lane of SDS-PAGE 12% acrylamide gel stained by colloidal blue, thanks to Bio-Rad Image Lab™.
ND: not determined.

The eluted fractions were analyzed by SDS-PAGE (**Fig.3B**), which revealed a major band of 35 kDa from the elution step fractions, corresponding to the expected molecular mass of recombinant TEG4-2c scFv. A weaker band of 75 kDa was also present in this lane, but the

mass spectroscopy analysis revealed that TEG4-2c scFv was the major protein present in this fraction (data not shown). This data strongly suggests that the higher molecular weight protein was indeed TEG4-2c scFv dimer.

The elution fraction was dialyzed against PBS buffer. The SDS-PAGE (**Fig.3B-E$_{PBS}$)** shows the purified TEG4-2c scFv as a single thick band with an estimated purity higher than 80%. The profile of TEG4-2c scFv into PBS buffer (used for ELISA and affinity measurement) is similar to the elution fraction (E) obtained at the end of IMAC. The final overall yield of TEG4-2c was 0.7 mg/mL; it represents 70% of initial product. However, upon SDS-PAGE analysis, it was observed that some amount of our protein of interest was also lost in the flowthrough and washing steps.

3-Analysis of TEG4-2c scFv binding to platelets by flow cytometry and ELISA tests

3.1-Flow cytometry analysis using TEG4-2c scFv

Flow cytometry analysis showed a better recognition of washed activated platelets versus non-activated ones (**Fig.4A**). PAC-1, an IgM murine antibody specific to the activated conformation of αIIbβ3 was included as a positive control of the experiment. The slight recognition of resting platelets might be due to their activation during the purification process. Activation of platelets is a problem classically encountered during their handling and processing. To minimize manipulation steps, the binding specificity of TEG4-2c scFv was checked on platelets within plasma (analysis on PRP). The results (**Fig.4B**) highlighted a binding specificity for platelets activated in PRP with TRAP peptide whereas resting platelets were not recognized.

Fig.4: **Binding assessment of TEG4-2c scFv to human platelets by flow cytometry and ELISA tests**. **A**: Binding of TEG4-2c scFv on thrombin-activated human (A-PL) or non-activated–platelets (NA-PL) analysed by flow cytometry. PAC-1 IgM murine antibody serves

as a positive control. Binding of antibody to the platelets was further detected by incubation with Alexa Fluor 488 anti-6His or anti-mouse IgM antibodies. Negative controls were secondary antibody only. Histograms depict representative data ± SD of three independent experiments. Quantitative fluorescence intensities (in Geo mean) are stated under each respective histogram. **B:** Binding of TEG4-2c scFv on TRAP-activated-human (+ TRAP) or non-activated platelets (-TRAP) analysed by flow cytometry. Quantitative fluorescence intensities (in Geo mean) are stated under each respective histogram. **C:** Representative whole cell (A-PL, NA-PL) and purified proteins (αIIbβ3, BSA) ELISA with TEG4-2c scFv. A murine anti-αIIbβ3 antibody AP2 was used as positive control. Negative controls were secondary antibody only. Binding of antibodies was visualized via HRP-6His or HRP-anti-mouse IgG. OD value represents absorbance at 450 nm. Plots represent the mean values ± SD (n=3)

3.2-ELISA tests

The reactivity of TEG4-2c scFv produced in *Pichia pastoris* was then measured on human thrombin-activated and non-activated platelets and on purified αIIbβ3 by ELISA (**Fig.4C**). We have to underline that, here again, the coating of platelets on ELISA wells may itself induce their activation. However, a better recognition of activated platelets is reported with TEG4-2c scFv, especially when using lower concentrations. AP2, a murine antibody directed against αIIbβ3 was included as a positive control of the experiment.

4-Binding of scFv TEG4-2c to αIIbβ3 investigated by SPR and BLI

Affinity of TEG4-2c scFv was determined either by surface plasmon resonance (SPR) with a BIACORE device on purified αIIbβ3 or using the Bio-Layer Interferometry (BLI) technology with an OCTET instrument on lyophilized platelets resuspended from a freeze-dried solution.

4.1-BIACORE analysis

In this first experimental session using SPR technology, TEG4-2c scFv was injected at 3, 6 and 12,5 µg/ml on immobilized αIIbβ3, corresponding respectively to 94, 188 and 390 nM. The binding was concentration-dependent (**Fig.5A**) but the three sensorgrams could not be fitted using the simple Langmuir model, likely because of the presence of a more complex interaction, implying monomers and dimers in the purified fractions.

Fig.5: Binding of scFv TEG4-2c to αIIbβ3 by SPR and to whole platelets by BLI. A: SPR sensorgrams. The ligand αIIbβ3 was immobilized on CM5 chip by amine coupling with a density of 8000 RU. Serial dilutions of TEG4-2c in HBS-EP running buffer were injected over the ligand corresponding to 94, 188 and 390 nM. Sensorgrams show a binding concentration-dependent of TEG4-2c scFv. **B: BLI analysis.** TEG4-2c scFv (ligand) was loaded on HIS2 biosensor (anti-penta Histidine Ab) at 21 µg/mL. Whole platelets (analyte) concentrations converted into αIIbβ3 molarities were: 41.5, 8.3, 4.15, 0.83, 0.415, 0.083 and 0.0415 nM. Additionally one sensor pair was used to record the buffer reference signals. TEG4-2c scFv reacts with αIIbβ3 in its natural conformation in a concentration dependent manner.

4.2-Binding by BLI

This second set of experiments performed using the Octet instrument aimed at determining the interactions between TEG4-2c scFv and blood platelets (**Fig.5B**). This is more informative because this strategy allows evaluating the binding on αIIbβ3 in its natural conformation. TEG4-2c scFv immobilized through an anti-6His coating on an optical fiber based sensor was immersed in a solution of platelets (seven different concentrations were used) contained in the well of a 96- well plate. The plate is shaken during reading to create an "orbital flow". The different platelet concentrations, from $5x10^5$ to $5x10^8$/ml, were converted into integrin αIIbβ3

molarities by taking into account the number of αIIbβ3 per platelet (50 000). Controls with no scFv allowed checking for non-specific binding of the platelets on the sensors. These controls were subtracted from the curves obtained with TEG4-2c scFv. Other controls were also performed with no platelets (only buffer), assessing the signal drift due to the potential release of scFv from sensors.

Octet experiments showed good interactions between TEG4-2c scFv and platelets at nanomolar concentrations superior to 0.4 nM. No Kd could be calculated because no dissociation was observed. However, considering the binding at 0.8 and 4 nM, the affinity should be in the nanomolar range.

5-Evaluation of atheroma burden recognition by IHC and ELISA tests

As the final aim of the project is to target platelets colonizing the plaque, we evaluated the ability of TEG4-2c scFv to recognize platelets within aorta lesional sections of animal models of atherosclerosis as well as aorta sections recovered from human coronary specimens (**Fig.6 A)**. The reactivity was also tested on proteins isolated from the extracted aorta from atheromatous and healthy rabbits by ELISA (**Fig.6 B**).

Fig.6: Comparison of the immunoreactivity of TEG4-2c scFv to atherosclerotic tissues of different species by IHC analysis and ELISA assays. A (**a-r)**: IHC assays on atherosclerotic tissues: similarly to positive controls e.g; anti-CD41 (anti-αIIb) (e), RAM11 and PGM1 (anti-CD68 antibodies targeting rabbit and human macrophages respectively) (k, q) and AP2 (anti-αIIbβ3 antibody) (a; g; m), TEG4-2c scFv specifically recognizes the injured areas of the aorta sections from different species (c; i; o). Binding of antibodies was visualized via HRP-anti-6His (scFv); HRP anti-rabbit IgG (CD41) and HRP anti-mouse IgG (RAM11, AP2). Negative controls were secondary antibody only (b; d; f; h; j; l; n; p; r). Nuclei were counterstained with hematoxylin **B**: ELISA tests on atheromatous and healthy

aorta proteins: TEG4-2c shows a better recognition of atheromatous proteins. RAM11 and AP2 were used as positive controls. Negative controls were secondary antibody only. Binding of antibodies was visualized via HRP-6His or HRP-anti-mouse IgG. OD value represents absorbance at 450 nm. Values represent mean (n=3) ± SD (error bars materialized the SD)

5.1-IHC

The immunohistochemistry data were in accordance with ELISA with a huge recognition of platelets in all analyzed sections (**Fig.6A**). An antibody directed against murine αIIb (anti-CD41) and antibodies directed against rabbit and human macrophages (anti-CD68) over-expressed in the atheroma burden were included as positive controls. We also compared the targeting of TEG4-2c scFv with that of AP2, an antibody we have already demonstrated able to label mouse, rabbit and human platelets.

5.2-ELISA tests

ELISA assay clearly showed a better recognition of atheromatous proteins with TEG4-2c scFv and AP2 antibodies (**Fig.6B**). An anti-CD68 macrophage rabbit antibody was included as positive control. We confirmed by mass spectroscopy analysis (data not shown) that the αIIbβ3 integrin is also present in healthy aorta but to a lesser extent.

Discussion & Conclusion

In the present study, TEG4-2c scFv was expressed at high-level in *Pichia pastoris* using a fed-batch fermentation system monitored by pO_2 level. We produced the TEG4 scFv with cysteine tags at the end of the C-terminal sequence for site-specific conjugation to contrast agents, precluding the loss of reactivity potentially occurring when the grafting process affects antigen-recognition sites. TEG4 scFv had been previously expressed in *E coli*.[27]

Unfortunately, despite optimization tests leading to high yields of cytoplasmic production, proteins also frequently accumulated into inclusion bodies (data not shown). In bacterial systems, many scFv can be produced into the periplasmic space but they are obtained with a very low yield. Higher levels of production can be achieved in inclusion bodies, with the limitation of the presence of insoluble scFv aggregates and the need for subsequent *in vitro* folding that make the use of this bacterial system not attractive for the large scale production of scFv. In addition, many authors have described that the final yield of scFv was only a small percentage of produced proteins with a low specificity for targets.[33,34]

So we chose to use the *Pichia* yeast as an alternative expression system. Indeed, *Pichia pastoris* is an attractive system for low cost-effective large-scale production of heterologous proteins. This type of production, characterized by the secretion of the protein of interest into the culture medium, can be easily scaled up and reach a GRAS (Generally Recognized As Safe) status. The concentration of highly pure TEG4-2c scFv obtained after one chromatography step (IMAC) was up to 600 µg/mL. A production of 30 mg scFv per liter of culture was achieved. This value was lower than that obtained for an scFv anti-carcinoembryonic antigen,[33] but in accordance with the yields obtained for the majority of Fab and antibody fragments expressed in *P. pastoris* [35-37] and sufficient for grafting purposes.

This new scFv format with cysteines included for grafting purposes was tested by ELISA, cytometry and IHC and all the experiments concurred to a specific recognition of platelets, from human or animal model origin and of atheroma issuing from coronary biopsies or animal lesional tissues. Bio-layer interferometry was used for evaluating the affinity of TEG4-2c scFv against platelets because this approach is more relevant than SPR analysis on purified antigen to mimic the *in vivo* behavior. No real Kd value could be extracted from the curves because of an absence of dissociation. This could be explained by the rebinding of the same

platelet on the immobilized ligand because of the presence of 50 000 αIIbβ3 per platelet. Indeed, when the platelet is captured on the surface, one αIIbβ3 can dissociate while another re-binds on the scFv. As a consequence the off-rate is slower than it would be by using isolated αIIbβ3. Nevertheless, the bio-layer interferometry underlines a good affinity of TEG4-2c scFv for platelets with recognition in the nanomolar range. Moreover, the flow cytometry results with PRP are in favor of a preferential recognition of activated platelets. This approach, compared to ELISA assays or cytometry performed on washed platelets is the only one that allows recognition in physiological conditions.

The rationale for targeting activated platelets is that they are highly trapped within atherosclerotic lesions not only in thrombi and intraplaque hemorrhage but also in the atheroma burden, around necrotic areas and neovessels, mainly because of the presence of leaky vessels, blood extravasation and haemorrhage.[18] Preferential recognition of activated platelets is to be considered to avoid *in vivo* elimination of the probe by circulating resting platelets.

An important point to be underlined is that scFv TEG4-2c recognizes human platelets as well as murine or rabbit platelets. The use of a human antibody able to target epitopes on the integrin shared by animal models and humans is of particular interest for pre-clinical studies in animal models of the disease and for direct transfer into the clinic. The use of an antibody of human origin is appealing, considering the need for repeated injections in humans to follow the progression of the pathology. Indeed, the human scFv should limit the induction of anti-antibodies in patients as compared with murine origin; it also avoids any additional humanization step that could impair the reactivity. This antibody equipped with cysteine tags is now ready to be used to functionalize contrast agents for MRI to serve as imaging agents for atherosclerosis.

In conclusion, even if the production of antibody fragments by *P. pastoris* is not always a success story,[38] our findings demonstrated that *P. pastoris* provided TEG4-2c scFv at a high concentration without aggregates and claiming a good purity. Its functionality against activated platelets and atheroma tissues was proven, paving the way for the success of grafting tests. Our results definitely point out the *P. pastoris* expression system as an adapted tool to produce scFv for use in diagnostic or therapeutic applications as well.

Acknowledgments:

Research support: This study was funded by (1) the French National Research Agency Program ANR-07-PCVI-0023 IMATHABIO and ANR-13-BSV5-0018 SVSE5 program named ATHERANOS, (2) the SFR TecSan (Technology for Health) of University of Bordeaux and (3) a public grant from the French National Research Agency within the context of the Investments for the Future Program, referenced ANR-10-LABX-0057 and named TRAIL. We would like to thank Arnaud Vonarburg (from Pall Life Sciences) for support on the Octet Red experiments

References:

1. Libby P, Ridker PM, Hansson GK (2011) Progress and challenges in translating the biology of atherosclerosis. Nature 473: 317-325.
2. Falk E (2006) Pathogenesis of atherosclerosis. J Am Coll Cardiol 47: C7-12.
3. Joshi FR, Lindsay AC, Obaid DR, Falk E, Rudd JH (2012) Non-invasive imaging of atherosclerosis. Eur Heart J Cardiovasc Imaging 13: 205-218.
4. Wildgruber M, Swirski FK, Zernecke A (2013) Molecular imaging of inflammation in atherosclerosis. Theranostics 3: 865-884.
5. Weber C, Zernecke A, Libby P (2008) The multifaceted contributions of leukocyte subsets to atherosclerosis: lessons from mouse models. Nat Rev Immunol 8: 802-815.
6. Fenyo IM, Gafencu AV (2013) The involvement of the monocytes/macrophages in chronic inflammation associated with atherosclerosis. Immunobiology 218: 1376-1384.
7. Burioni R, Canducci F, Saita D, Perotti M, Mancini N, et al. (2009) Antigen-driven evolution of B lymphocytes in coronary atherosclerotic plaques. J Immunol 183: 2537-2544.
8. Kyaw T, Cui P, Tay C, Kanellakis P, Hosseini H, et al. (2013) BAFF receptor mAb treatment ameliorates development and progression of atherosclerosis in hyperlipidemic ApoE(-/-) mice. PLoS One 8: e60430.
9. Kyaw T, Tay C, Hosseini H, Kanellakis P, Gadowski T, et al. (2012) Depletion of B2 but not B1a B cells in BAFF receptor-deficient ApoE mice attenuates atherosclerosis by potently ameliorating arterial inflammation. PLoS One 7: e29371.
10. Kyaw T, Tay C, Khan A, Dumouchel V, Cao A, et al. (2010) Conventional B2 B cell depletion ameliorates whereas its adoptive transfer aggravates atherosclerosis. J Immunol 185: 4410-4419.
11. Herter JM, Rossaint J, Zarbock A (2014) Platelets in inflammation and immunity. J Thromb Haemost 12: 1764-1775.

687 12. Morrell CN, Aggrey AA, Chapman LM, Modjeski KL (2014) Emerging roles for
688 platelets as immune and inflammatory cells. Blood 123: 2759-2767.
689 13. Lievens D, Zernecke A, Seijkens T, Soehnlein O, Beckers L, et al. (2010) Platelet
690 CD40L mediates thrombotic and inflammatory processes in atherosclerosis.
691 Blood 116: 4317-4327.
692 14. Ferdous F, Scott TR (2015) A comparative examination of thrombocyte/platelet
693 immunity. Immunol Lett 163: 32-39.
694 15. Aloui C, Prigent A, Sut C, Tariket S, Hamzeh-Cognasse H, et al. (2014) The signaling
695 role of CD40 ligand in platelet biology and in platelet component transfusion. Int J
696 Mol Sci 15: 22342-22364.
697 16. Daub K, Seizer P, Stellos K, Kramer BF, Bigalke B, et al. (2010) Oxidized LDL-
698 activated platelets induce vascular inflammation. Semin Thromb Hemost 36: 146-
699 156.
700 17. Badrnya S, Schrottmaier WC, Kral JB, Yaiw KC, Volf I, et al. (2014) Platelets mediate
701 oxidized low-density lipoprotein-induced monocyte extravasation and foam cell
702 formation. Arterioscler Thromb Vasc Biol 34: 571-580.
703 18. Jacobin-Valat MJ, Laroche-Traineau J, Lariviere M, Mornet S, Sanchez S, et al. (2015)
704 Nanoparticles functionalised with an anti-platelet human antibody for in vivo
705 detection of atherosclerotic plaque by magnetic resonance imaging.
706 Nanomedicine 11: 927-937.
707 19. Reichert JM (2016) Antibodies to watch in 2016. MAbs 8: 197-204.
708 20. Frenzel A, Hust M, Schirrmann T (2013) Expression of recombinant antibodies. Front
709 Immunol 4: 217.
710 21. Frenzel A, Schirrmann T, Hust M (2016) Phage display-derived human antibodies in
711 clinical development and therapy. MAbs 8: 1177-1194.
712 22. Groves MA, Amanuel L, Campbell JI, Rees DG, Sridharan S, et al. (2014) Antibody VH
713 and VL recombination using phage and ribosome display technologies reveals
714 distinct structural routes to affinity improvements with VH-VL interface residues
715 providing important structural diversity. MAbs 6: 236-245.
716 23. Ahmad ZA, Yeap SK, Ali AM, Ho WY, Alitheen NB, et al. (2012) scFv antibody:
717 principles and clinical application. Clin Dev Immunol 2012: 980250.
718 24. Jacobin MJ, Laroche-Traineau J, Little M, Keller A, Peter K, et al. (2002) Human IgG
719 monoclonal anti-alpha(IIb)beta(3)-binding fragments derived from immunized
720 donors using phage display. J Immunol 168: 2035-2045.
721 25. Hagemeyer CE, von Zur Muhlen C, von Elverfeldt D, Peter K (2009) Single-chain
722 antibodies as diagnostic tools and therapeutic agents. Thromb Haemost 101:
723 1012-1019.
724 26. Hohmann JD, Wang X, Krajewski S, Selan C, Haller CA, et al. (2013) Delayed targeting
725 of CD39 to activated platelet GPIIb/IIIa via a single-chain antibody: breaking the
726 link between antithrombotic potency and bleeding? Blood 121: 3067-3075.
727 27. Robert R, Noubhani AM, Jacobin MJ, Santarelli X, Clofent-Sanchez G (2005)
728 Improvement in production and purification bioprocesses of bacterially
729 expressed anti-alphaIIbbeta3 human single-chain FV antibodies. J Chromatogr B
730 Analyt Technol Biomed Life Sci 818: 43-51.
731 28. Narasimhan Janakiraman V, Noubhani A, Venkataraman K, Vijayalakshmi M,
732 Santarelli X (2016) High yield of recombinant human Apolipoprotein A-I
733 expressed in Pichia pastoris by using mixed-mode chromatography. Biotechnol J
734 11: 117-126.

29. Robert R, Clofent-Sanchez G, Hocquellet A, Jacobin-Valat MJ, Daret D, et al. (2006) Large-scale production, bacterial localization assessment and immobilized metal affinity chromatography purification of a human single-chain Fv antibody against alphaIIb-beta3 integrin. Int J Biol Macromol 39: 51-59.
30. Dabadie M, Valli N, Jacobin MJ, Laroche-Traineau J, Barat JL, et al. (2001) Characterisation, cloning and sequencing of a conformation-dependent monoclonal antibody to the alphaIIbbeta3 integrin: interest for use in thrombus detection. Platelets 12: 395-405.
31. Shattil SJ, Hoxie JA, Cunningham M, Brass LF (1985) Changes in the platelet membrane glycoprotein IIb.IIIa complex during platelet activation. J Biol Chem 260: 11107-11114.
32. Pidard D, Montgomery RR, Bennett JS, Kunicki TJ (1983) Interaction of AP-2, a monoclonal antibody specific for the human platelet glycoprotein IIb-IIIa complex, with intact platelets. J Biol Chem 258: 12582-12586.
33. Freyre FM, Vazquez JE, Ayala M, Canaan-Haden L, Bell H, et al. (2000) Very high expression of an anti-carcinoembryonic antigen single chain Fv antibody fragment in the yeast Pichia pastoris. J Biotechnol 76: 157-163.
34. Joosten V, Lokman C, Van Den Hondel CA, Punt PJ (2003) The production of antibody fragments and antibody fusion proteins by yeasts and filamentous fungi. Microb Cell Fact 2: 1.
35. Eldin P, Pauza ME, Hieda Y, Lin G, Murtaugh MP, et al. (1997) High-level secretion of two antibody single chain Fv fragments by Pichia pastoris. J Immunol Methods 201: 67-75.
36. Takahashi K, Yuuki T, Takai T, Ra C, Okumura K, et al. (2000) Production of humanized Fab fragment against human high affinity IgE receptor in Pichia pastoris. Biosci Biotechnol Biochem 64: 2138-2144.
37. Lange S, Schmitt J, Schmid RD (2001) High-yield expression of the recombinant, atrazine-specific Fab fragment K411B by the methylotrophic yeast Pichia pastoris. J Immunol Methods 255: 103-114.
38. Cupit PM, Whyte JA, Porter AJ, Browne MJ, Holmes SD, et al. (1999) Cloning and expression of single chain antibody fragments in Escherichia coli and Pichia pastoris. Lett Appl Microbiol 29: 273-277.

Figure

Click here to download Figure Fig1.tif

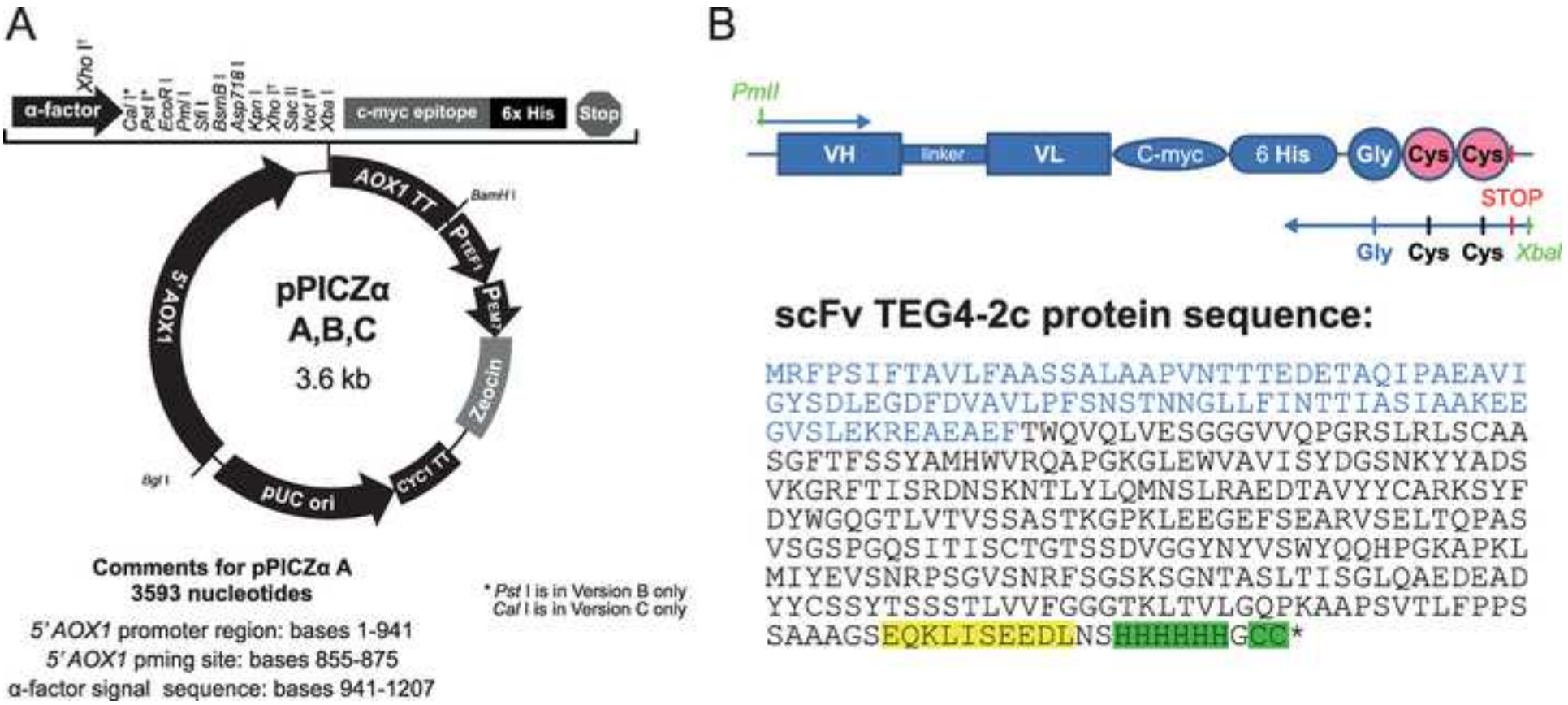

Comments for pPICZα A
3593 nucleotides

5'AOX1 promoter region: bases 1-941
5'AOX1 pming site: bases 855-875
α-factor signal sequence: bases 941-1207

* *Pst* I is in Version B only
Cal I is in Version C only

Figure

Click here to download Figure Fig2.tif

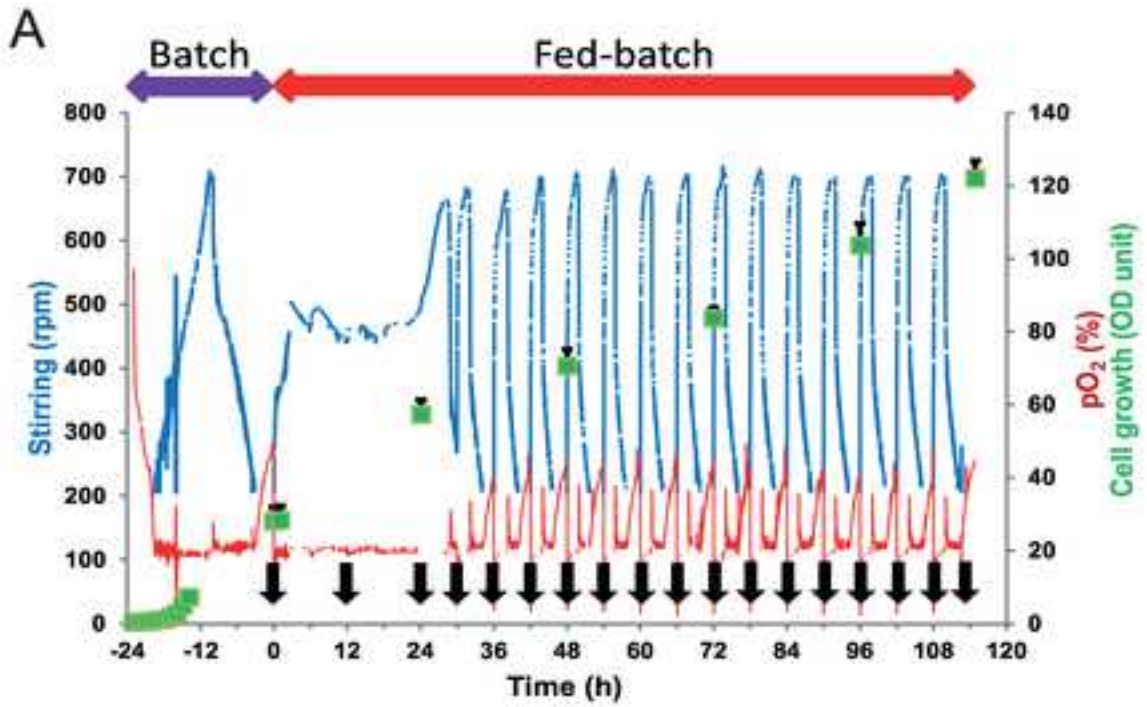

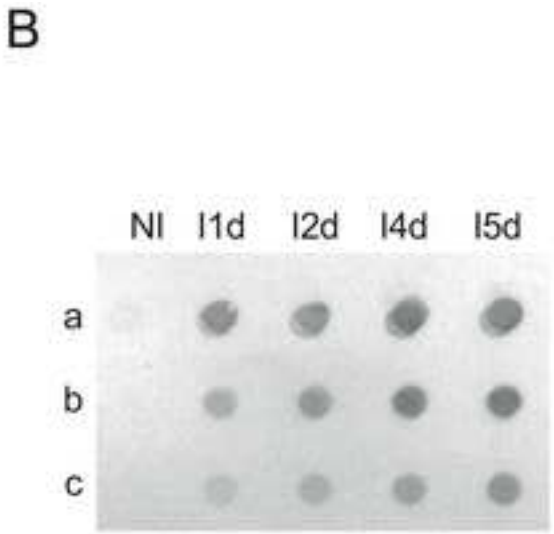

Figure

Click here to download Figure Fig3.tif

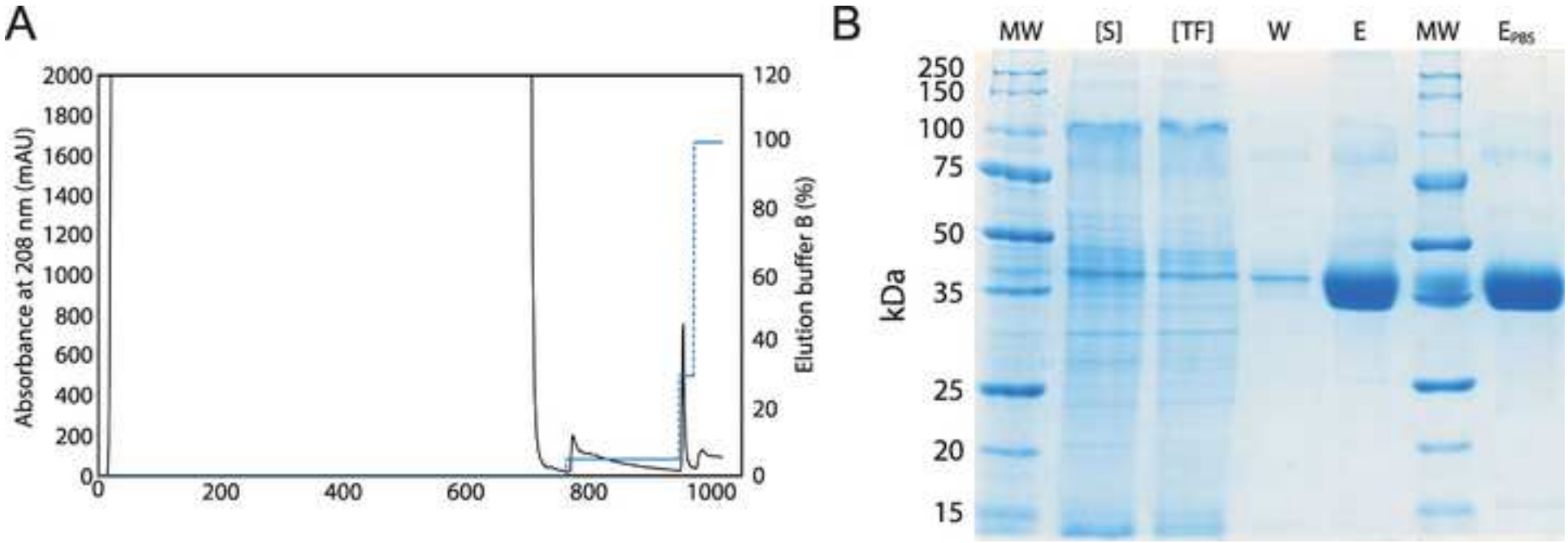

Figure

Click here to download Figure Fig4.tif

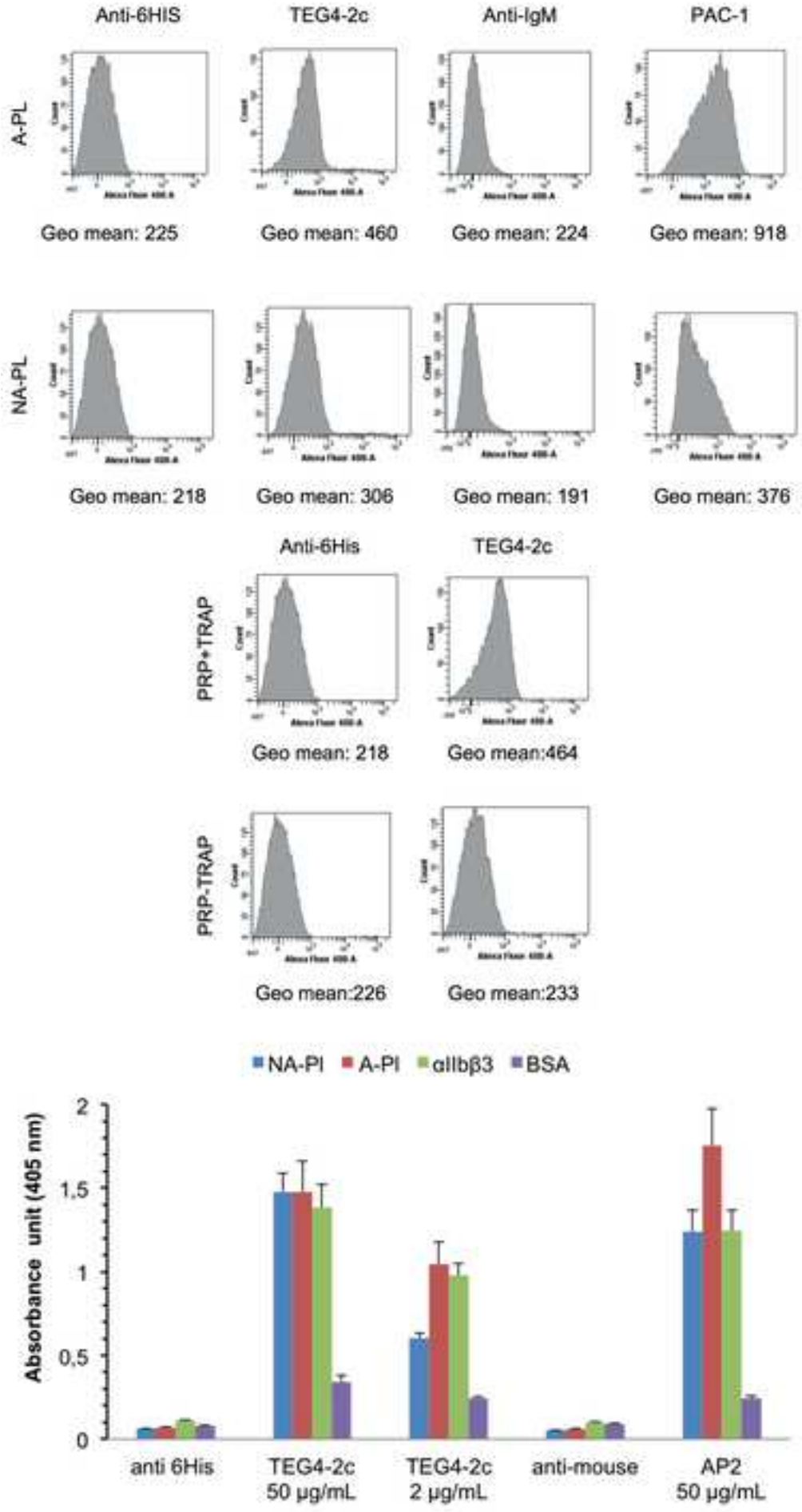

Figure

Click here to download Figure Fig5.tif

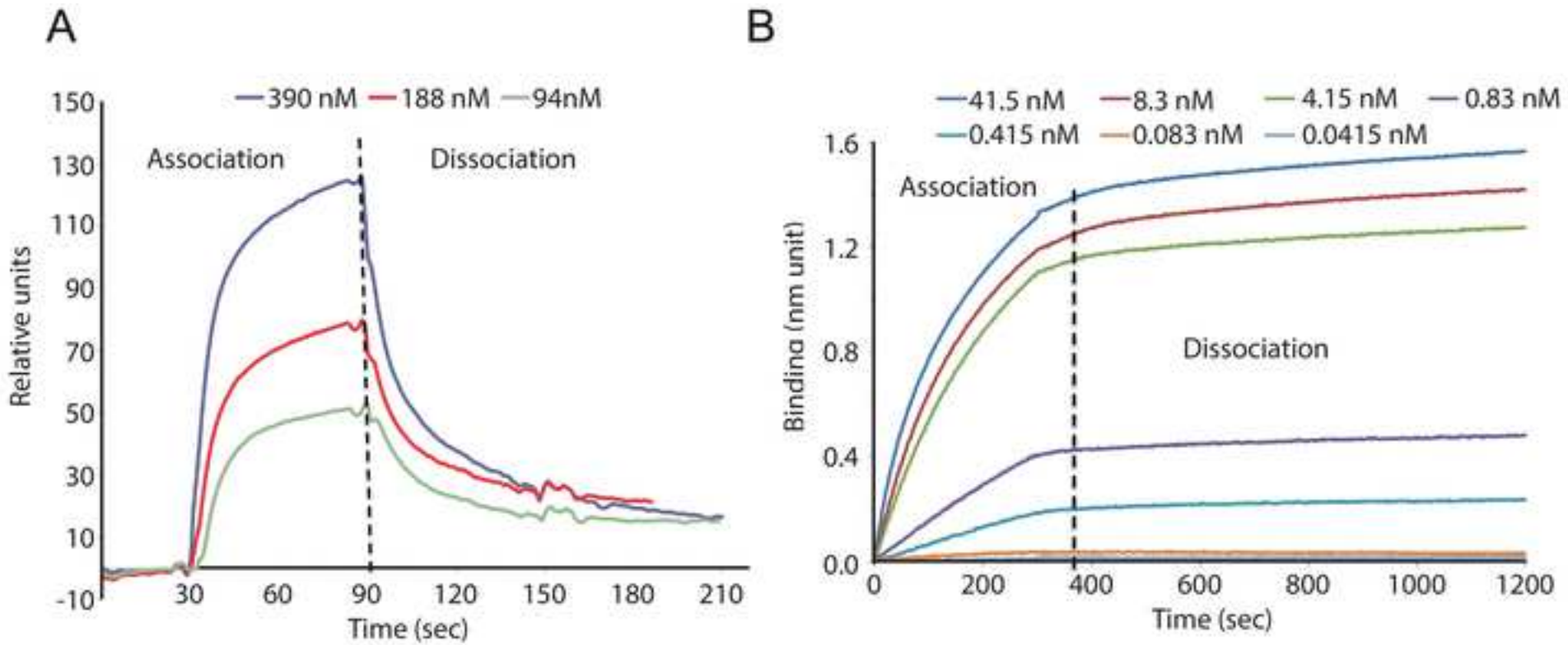

Figure

Click here to download Figure Fig6.tif

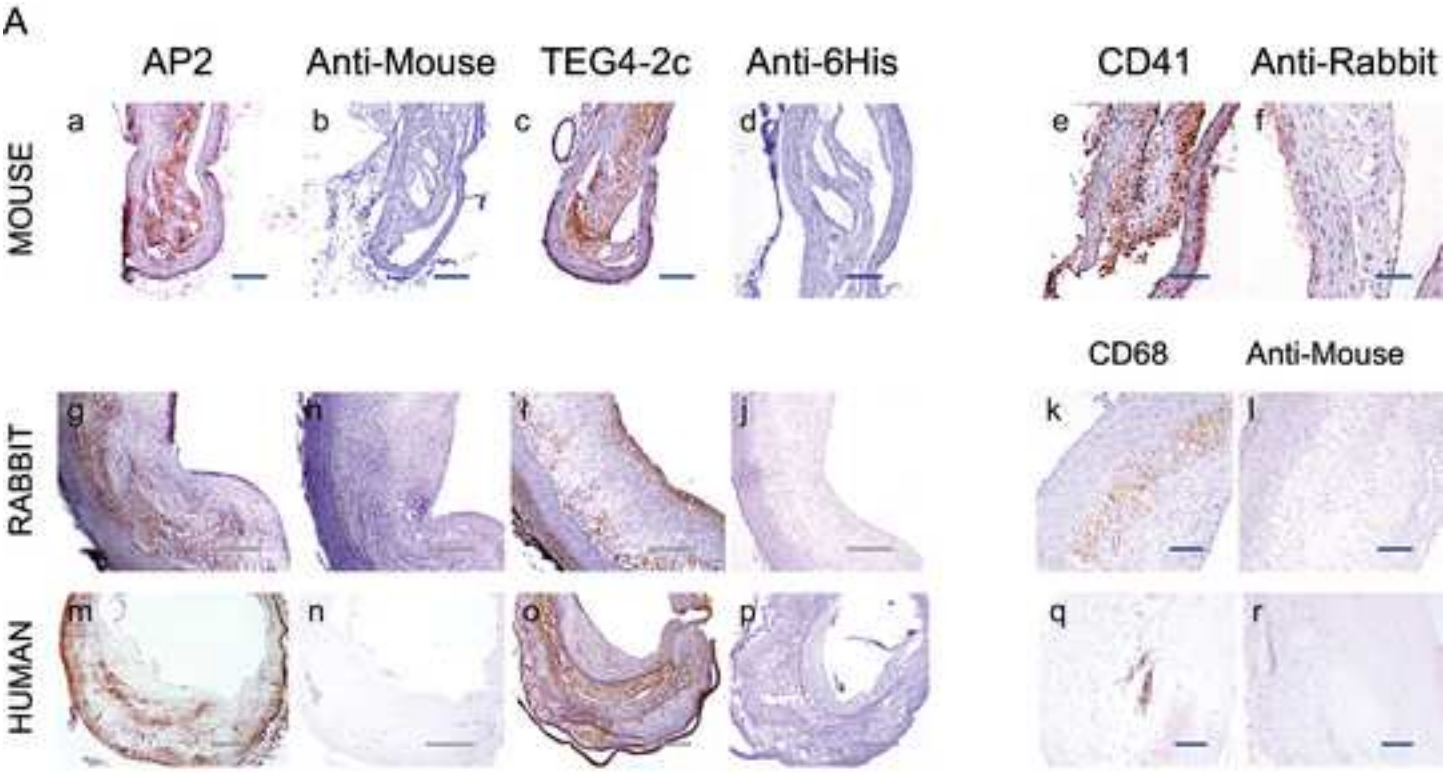

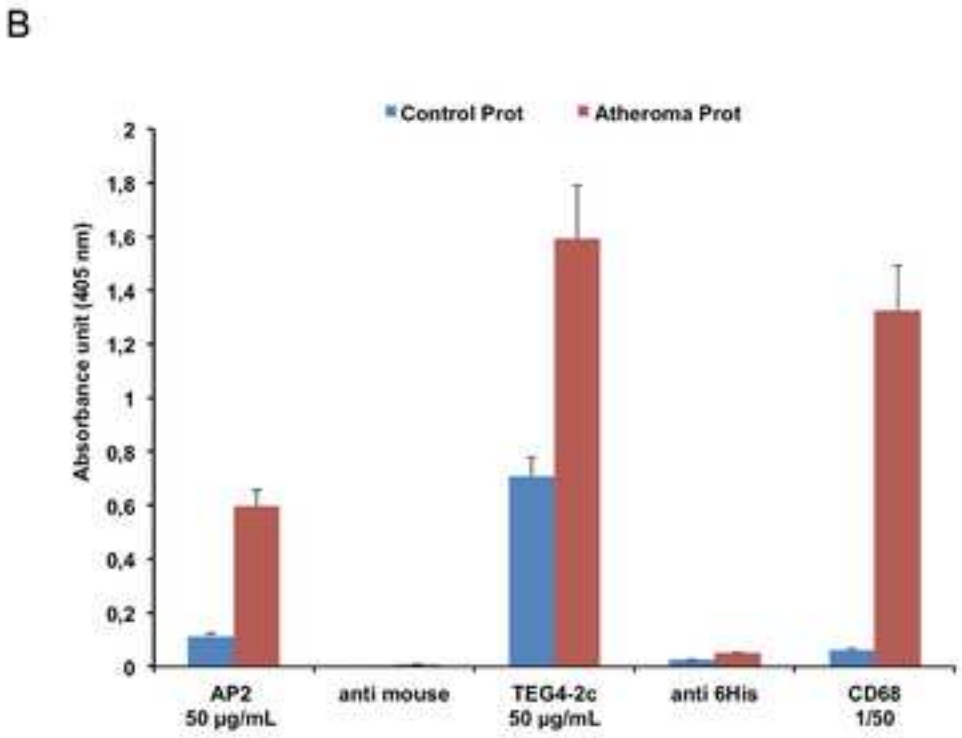

Targeted nanoparticles for multimodal molecular imaging in a mouse model of atherosclerosis

M. Larivière*, C. Lorenzato*, L. Adumeau, A. Hémadou, M-J. Jacobin-Valat, A. Noubhani, X. Santarelli, S. Mornet, J. Laroche-Traineau*, G. Clofent-Sanchez* (* equivalent positions of authors)

Abstract

Cardiovascular diseases are the first cause of sudden deaths worldwide. The majority of them are due to a condition called atherosclerosis, an inflammatory disease of large and medium arteries, resulting in the buildup of atheroma plaques from circulating cholesterol. These plaques evolve under the combined influence of soluble (cytokines) and cellular (macrophages, platelets, etc.) factors. It is their rupture into the blood flow that causes the potentially lethal ischemic accidents. The diagnosis of rupture-prone atheroma requires highly specific molecular markers. Human antibodies (HuAbs) specific for the atheroma lesions have previously been selected by phage display biotechnology. TEG4 HuAb is a promising candidate due to its targeting of activated platelets (integrin αIIbβ3), highly represented within the plaque. Single chain Fragment variable (scFv) fragments were processed from the selected phage-HuAbs and produced in *Pichia pastoris*. They were then used to functionalize original nanoparticles (NP), designed for multimodal imaging, in a regio-selective way to preserve their activity. This was proven by immunohistochemistry (IHC) studies on murine, rabbit and human lesional tissue rich in platelets. Moreover, when multiple copies of scFv fragments were grafted to NPs, kinetics of binding as assessed by Surface Plasmon Resonance (SPR) analyses on integrin αIIbβ3, showed a gradual increase in avidity. Encouragingly, the multi-targeted objects bound to the lesions in *ex vivo* studies, allowing for near infra-red fluorescence (NIRF) and magnetic resonance imaging (MRI) of the atheroma plaque. When injected *in vivo* into animal models of the pathology (ApoE-/- mice), high resolution molecular MRI yielded interesting results.

Introduction

Atherosclerosis is one of the most important health condition worldwide, from which originate most acute cardio-vascular events. Official statistics state that 17.5 million people die each year from cardio-vascular diseases (CVD), 80% of all CVD deaths being due to heart attacks and strokes(1).

Atherosclerosis gradually develops for fifty or more years throughout the life of an individual under the influence of multiple lifestyle, environmental, and genetic factors. It leads to chronic ischemic

complications or acute lethal events like myocardial infarction or stroke. The pathogenesis of atherosclerosis depends on 1/ an increased level of circulating atherogenic lipoproteins, and 2/ local immuno-inflammatory factors.

Primary intimal lesions develop under the influence of local hemodynamic stress, usually at the branching points of major arteries. There, low-density lipoproteins (LDL) accumulate on the endothelial surface, forming structures called fatty streaks, which in turn trigger the recruitment, activation, and differentiation of monocytes into macrophages. Reactive oxygen species (ROS) resulting from the inflammatory environment react with the LDL to form oxidized LDL (oxLDL): when ApoB is oxidized it binds the scavenger receptor of macrophages, thus leading to the formation of LDL-laden macrophages called foam cells(2). Activated endothelial cells (EC) and platelets express adhesion molecules such as P-selectin, intracellular adhesion molecule 1 (ICAM1), or glycoproteins Ibα and αIIbβ3 (GPIbα, GPαIIbβ3), which bind oxLDL and leukocytes (3,4), and provokes the subendothelial accumulation of foam cells, contributing to the development of the plaque(5). In a recent study, we underlined the presence of platelets not only in thrombi and intraplaque hemorrhage (IPH) but also in atheroma burden, around necrotic areas and neovessels, shedding light on the rationale for targeting platelets within atherosclerotic lesions(6).

TEG4, a monoclonal human antibody (HuAb) targeting integrin αIIbβ3 and selected by phage display technology has previously been described(7), and used as a targeting agent for molecular imaging. Indeed, we previously demonstrated that TEG4 can target platelets in atheroma lesions both *in vitro* and *ex vivo.* We also showed that iron nanoparticles (VUSPIO) functionalized with TEG4 were still able to bind platelets both *in vitro* and *ex vivo*, and could be detected by TEM and MRI(6).

In this study, we investigated the effect of multivalent, site-specific grafting of antibody fragments on the reactivity of VUSPIO nanoparticles. In addition, fluorochromes were attached to the surface of the VUSPIO to allow for a multimodal NIRF – MRI detection.

The same activated platelet – reactive TEG4 antibody was produced as a scFv fragment in the yeast *Pichia pastoris*. Compared to full IgGs (150 kDa), scFv fragments (30 kDa), present a reduced size which makes them more suitable for functionalizing relatively small nanoparticles (90 nm).

Furthermore, to better control the Ab to probe conjugation ratio, and increase the particle valence, this Ab was further engineered to possess 2 terminal cysteines that allowed for site directed grafting on the surface of the nanoparticle. Indeed, usual conjugation strategies involve the reaction of amine side chains of the antibodies (Ab), which may be a good strategy for full IgG but presents the risk to degrade the binding sites of smaller Ab fragments and impede their reactivity.

A scFv protein composed of the variable heavy (VH) and light (VL) chains of an antibody linked with a flexible peptide has been constructed by recombinant DNA technology. Two cysteines (amino acids containing thiol functions) were added in the sequence to allow for site-specific conjugation to a maleimide residue. TEG4 HuAb was here processed as scFv fragments in the yeast *Pichia pastoris*.

Avidity and reactivity were assessed as previously described (0) and atheroma imaging was performed in the mouse model ApoE-/-.

Ex vivo binding was first studied via NIRF measurements and MRI, then the functionalized carrier was injected to evaluate its reactivity *in vivo* and its usefulness as an atheroma-specific diagnosis agent.

with the aim to propose a safe, non-invasive diagnosis method

Method

TEG4-2C scFv production (8)

Briefly, the TEG4 scFv DNA fragment was used as a template to generate a new scFv format containing 2 cysteines into the C-terminal end. The coding sequence was PCR-amplified: the primers were used to introduce the 6 HisTag – Gly – Cyc – Cys – Stop amino acid sequence. After control by sequencing, the TEG4 – 6His – Gly – Cys – Cys DNA fragment was introduced into the expression vector pPICZαA containing a Zeocin resistance cassette and transformed in bacteria for amplification. After extraction the plasmid was linearized and transformed into competent *P. pastoris* X-33 cells by electroporation. Transformed yeasts that exhibited high resistance to Zeocin were primarily grown in shake flasks before inoculation in a 5L bioreactor. After 120 h (5 days) of induction, the supernatant was harvested and the expressed recombinant TEG4-2C scFv purified using IMAC. The elution fraction was dialyzed against PBS.

Site specific multivalent grafting onto VUSPIO

VUSPIO nanoparticles synthesis was performed as described by Mornet et al.(6,9). After surface functionalization with heterobifunctional poly(ethylene oxide) chains, derivatization with a near-infrared-emitting dye was carried out in the same team. The remaining primary amine terminal groups were then converted into maleimide functions to allow Ab grafting.

Figure 1 provides an overview of the workflow for this conjugation. An excess of the VUSPIO stock solution is diluted in 1/10 of HEPES buffer 200 mM, pH 7.8, so as to obtain a solution of desired iron concentration in HEPES 20 mM final. Then a heterobifunctional NHS – PEG – maleimide spacer arm is grafted on the surface amines of the VUSPIO nanoparticle. The quantity of NHS ester – PEG3400 – maleimide (MW = 3400 $g.mol^{-1}$, Laysan Bio, Arab, USA) used is 10 times superior to the number of

amine functions on the surface of the VUSPIO, which was around 400 NH2 / VUSPIO for the batch we used. The corresponding PEG quantity is directly solubilized in the VUSPIO suspension, in HEPES buffer 20 mM pH 7.8, and left to react for 2 h at room temperature. At the end of the reaction time, the suspension is washed on a magnetic column (MACS, Miltenyi Biotec, Paris) with a large volume of HEPES buffer 10 mM, pH 7.2 to remove the excess PEG and stop the reaction. The reaction of thiols with maleimides being both oxidation and pH sensitive, a 10 mM pH 7.2 HEPES buffer is vacuum degassed beforehand for at least one hour and saturated with argon gas for this step. In the meantime, the scFv is "activated" by reduction of the N terminal cysteines to make the thiols reactive. A solution of TCEP 10 mM is made fresh and added to the scFv so as to obtain a ratio n(TCEP) / n(scFv) = 20. The reduction is carried out for 30 min at 4°C. TCEP is preferred to other reducing agents because it is known to reduce only the outermost disulfide bonds and has low reactivity (contrary to β-mercaptoethanol for example) for the maleimide present in the next step (10).

Figure 1: Schematic workflow for the conjugation process. 1: an excess NHS – PEG – mal is reacted onto the surface amines of the particle, 2: the VUSPIOs are washed on a magnetic column to remove the unreacted PEG and stop the reaction, 3: scFvs are activated by reduction with TCEP, 4: activated scFv react with the surface maleimide of the VUSPIO for 12 h, 5: the grafting yield is determined via a gel analysis while the excess scFv are cleaned by dialysis.

Following the reaction of the surface amines of the VUSPIO with the NHS ester end of a heterobifunctional NHS – PEG – maleimide molecule, the maleimide function is displayed on the surface of the NP. After washing, the VUSPIO concentration is assessed by spectrophotometry at 480 nm and mixed with scFv in respective quantities calculated to obtain different Ab to particle ratios: R3, R6 and R14. The grafting reaction processes 12 h at 4°C. The conjugated-NP are finally dialyzed (cut-off 100 kDa, Spectra-Por Float-A-Lyzer G2, 1 mL, MWCO 100 kDa, Sigma Aldrich, St Quentin Fallavier, France) against PBS to remove excess scFv. Before this last step a small sample of the reaction medium is analyzed by SDS-PAGE to evaluate the conjugation yield: while the unconjugated scFv is able to migrate freely through the gel, the VUSPIO are retained on top of it by their important size. Each ratio of scFv/VUSPIO is loaded in a way that the initial scFv quantity is equivalent; after migration, the unconjugated scFv quantity is assessed by comparison to an equal amount of free scFv loaded on the same gel. The quantification is performed by image analysis as described in the next paragraph.

Conjugation yield calculation

The conjugation yield was calculated from the gels using the open source image processing program *ImageJ* (https://imagej.nih.gov/ij/ or http://imagej.net).

The Coomassie blue – stained gels were scanned at high resolution (600 dpi). The consecutive bands of interest were selected and plotted to convert their intensity into a measurable area.

> Analyze > Gels > Select First Lane [then] > Plot Lanes ; > Wand (tracing) tool

Several ROI (region of interest) were defined, corresponding to reference scFv lanes and to each conjugation ratio tested. The mean intensity of each lane was measured and normalized with regards to the concentration of the scFv alone.

A lane of known scFv concentration was used as a reference, negative quantification. Quantity of unbound scFv, ratio / reference. Semi-quantitative: comparison.

Noteworthy, whenever it was possible, two lanes of the gel were loaded with the unreacted scFv to serve as a reference for quantification.

Avidity measurement

The avidity of the TEG4-2C scFv before and after grafting to the VUSPIO was assessed by surface plasmon resonance (SPR) sensing on purified αIIbβ3 integrin (Enzyme Research Laboratories, Swansea, UK). The experiments were carried out according to the manufacturer's instructions by Laëtitia Minder and Carmelo Di Primo, at the European Chemistry and Biology Institute (IECB, Pessac, France) using the BIAcoreTM 3000 (GE Healthcare Europe GmbH, Velizy-Villacoublay, France) equipped with research-grade CM5 sensor chips. HBS-P buffer (0.01 M HEPES, pH 7.4, 0.15 M NaCl, 0.005% v/v Surfactant P20) (GE Healthcare, Aulnais-/s-bois, France) with 2 mM Ca2+ was used as a running buffer. Calcium ions were added to allow the good folding of the αIIbβ3 integrin complex.

First the surface of the sensor chip was activated using the Biacore amine coupling kit (GE Healthcare, Aulnais-/s-bois, France), following the manufacturer's instructions.

Afterwards, the purified αIIbβ3 was first dialysed in running buffer, then diluted in acetate buffer 10 mM, pH 4.5 (GE Healthcare, Aulnais-/s-bois, France) to a 30 µg/mL concentration, and finally attached on the surface of the chip following this reaction. The EDC/NHS reaction was stopped using ethanolamine hydrochloride 1 M, pH 8.5. The chip was finally washed using Glycine buffer pH 2.5, followed by NaOH then HBS-Ca running buffer. The common unit for SPR is the resonance unit (RU), which represents 1 pg protein per mm^2.

The scFv and VUSPIO-scFv samples were dialyzed in running buffer, which also served to record the baseline. The chip was regenerated between each sample with NaOH followed by HBS-P Ca.

The scFv alone was flown on the chip at 33, 100, and 300 µg/mL as a control for its affinity to αIIbβ3. The following dilutions of VUSPIO R3, R6, and R14 were assessed: 1/54 for R6 and R14; 1/18, 1/6, ½ for R3, R6, and R14.

Reactivity assessment

The reactivity of TEG4-2C scFv alone, and after grafting to the VUSPIO was confirmed by IHC on paraffin-embedded sections of arterial tissue from mouse, rabbit or human.

All animal studies were approved under the N° 50120192-A by the Animal Care and Use Committee of Bordeaux, France. All work with tissues from human subjects had been approved by the CPP committee (Comité de Protection des Personnes Sud-Ouest et Outre Mer) of Bordeaux and from the Research Ministry in France (Authorization number DC -2016- 2724).

ApoE-/- mice were obtained from Charles River Laboratories and fed a high-cholesterol diet (0.15% cholesterol, Avogadro Western diet, Safe, Augy, France) for 21 weeks to allow for the development of atherosclerotic lesions. Wild-type control C57BL6 mice were used as a negative control (Charles River Laboratories, St Germain sur l'Arbresle, France).

Adult male New Zealand rabbits (NZW) were obtained from Charles Rivers Laboratories, fed a fat atherogenic diet including 0.3% cholesterol for 8 months and subjected to surgeries to trigger the formation of complex plaques with intramural thrombi. Aortas from control untreated rabbits and balloon-injured aortas from hypercholesterolemic rabbits were extracted from the aortic arch to the iliac bifurcation.

Human coronary arteries were harvested from patients with end-stage heart failure having undergone heart transplantation at Haut-Lévèque Hospital (Pessac, France). Human carotid tissue was obtained from patients with life-threatening carotid stenosis receiving endarterectomy surgery at Pellegrin Hospital (Bordeaux, France). Human tissue specimens were collected after informed consent to use surgical waste for investigational purposes.

All tissues were immediately fixed in paraformaldehyde (PFA) 4% (Eurobio, Les Ulis, France) and embedded in paraffin.

To perform immunohistochemistry, the paraffin blocks were thinly sliced (7 µm) and adhered on glass slides. The sections were deparaffinized, rehydrated, and heat mediated antigen retrieval was performed with Tris-EDTA pH 9 buffer following the specifications of Abcam, Paris, France (www.abcam.com/ps/pdf/protocols/ihc_p.pdf). Endogenous peroxidase was then blocked with 3 % H_2O_2 in water, for 15 min. After washing in PBS 1X + 0.025 % Triton (PBST), nonspecific binding was blocked with PBS 1X + 0.2 % Triton + 2 % bovine serum albumin (BSA) for 1 h at room temperature.

Afterwards, VUSPIO alone or antibody-conjugated VUSPIO corresponding to R3, R6 and R14 ratios were applied to the slides, diluted to the same iron concentration so as to compare the avidity of the VUSPIO in each batch. TEG4 Ab alone was applied to the slides in concentrations matching the theoretical Ab content in each VUSPIO dilution to compare their reactivity.

The incubation was carried out overnight at 4 °C, diluted in PBS 1X + 1 % BSA. The following day, three washes with PBST were performed. To detect TEG4-2c scFv fragments, a HRP-conjugated antibody specific to 6His (working dilutions 1:250) was applied to the sections for 1 h at room temperature.

After a further three washes with PBST, staining was performed by adding the peroxidase substrate diaminobenzidine (DAB substrate kit, Eurobio/ABCys, Les Ulis, France) with H_2O_2. It yielded a yellow brown deposit within 10 min at room temperature. After a wash in dH_2O to stop the enzymatic reaction, slides were counterstained in hematoxylin, dehydrated and mounted.

Imaging

All animal studies were approved under the N° 50120192-A by the Animal Care and Use Committee of Bordeaux, France. ApoE-/- mice were obtained from Charles River Laboratories and fed a high-cholesterol diet (0.15% cholesterol, Avogadro Western diet, Safe, Augy, France) for 21 weeks. Wild-type control C57BL6 mice were used as a negative control (Charles River Laboratories, St Germain sur l'Arbresle, France).

Ex vivo

ApoE−/− mice fed a high fat diet or control C57BL/6 wild-type mice were terminally anaesthetized by inhalation of isoflurane. The aorta was exposed and washed by intra-cardiac injection of PBS heparin, then PBS alone. Then a solution of either multivalent TEG4-VUSPIO, IgG cont-VUSPIO or PBS was incubated for 20 min before rinsing and fixing in paraformaldehyde (PFA). The heart and aorta were then removed and embedded in agarose in a glass tube. *Ex vivo* high resolution MR imaging was performed on a horizontal 7 T Biospec system (Bruker, Ettlingen, Germany). T2* maps were calculated from a RF-spoiled multi gradient echo (MGE) images (repetition time TR = 1000 ms, first echo time TE = 3.2 ms, $\Delta TE = 3.6$ ms, number of echoes = 8, $\alpha = 30°$, FOV = 32 x 12 mm², NEx = 32), using the Paravision software (Bruker). Fluorescent images were then acquired on the aforementioned imaging device Fluobeam.

In vivo

Animals were anaesthetized with 2% isoflurane (Belamont, Nicholas Piramal Limited, London, UK) in air for all imaging procedures.

Multivalent TEG4-VUSPIO-Dylight800 particles were injected to ApoE-/- mice, in a quantity corresponding to 4 mg Fe /kg and imaged by MRI and fluorescence imaging. Basal images before injection were acquired for each *in vivo* technique. Non-injected and irrelevant-Ab injected mice served as controls.

MRI was carried out on a horizontal 4.7 T Biospec system (Bruker, Ettlingen, Germany), equipped with a 12 cm gradient insert capable of 200 mT/m maximum strength. T2* weighted multi gradient echo

(MGE) MR sequence were acquired (repetition time TR = 1000 ms, first echo time TE = 3.5 ms, ΔTE = 4.5 ms, α = 60°, NEx = 3). The images were acquired before, immediately after injection and 24 h later.

A section corresponding to the abdominal aorta was imaged using T2star (T2*) map MGE sequences. Before and after injection, Black blood procedure was used to delineate the luminal border of the atheroma plaque, and Bright blood procedure to optimize the MR contrast between blood and iron oxide-labelled plaque. Comparison of MR signal before and after injection was helped by the calculation of a R2* map (=1/T2*) for each voxel, which was done as described previously using the Paravision software.

After the last image was acquired, the animals were humanely killed and dissected, while fluorescence imaging was performed at the Vivoptic facility in Bordeaux, using the Fluobeam imager. A blood sample was immediately retrieved from the cava vein and all remaining blood washed from the circulatory system and organs with a 3 mL PBS heparin (50 U/mL), followed by a 10 mL PBS intracardiac perfusion.

The aorta was removed and embedded in a glass MR tube containing 0.8 % m/v high-grade, low melting-point agarose. MR imaging was performed using a 7 Tesla MRI system as described above.

Results

TEG4-2C scFv production

An average of 30 mg of TEG4-2C scFv were produced and secreted by *P. pastoris* into 1L broth medium after 5 days of growth. After IMAC purification, the yield was around 22 mg TEG4-2C scFv per liter of culture, with a purity superior to 80%. The SDS-PAGE analysis showed the purified TEG4-2C scFv as a single thick band (data not shown) with an estimated purity higher than 80%.

Site specific multivalent grafting

TEG4-2C scFv dialyzed in PBS or MES buffer (**Erreur ! Source du renvoi introuvable.**) were reacted with the VUSPIO in different ratios (from 4 to 32 scFv fragments per VUSPIO, as shown on the graph, **Erreur ! Source du renvoi introuvable.**), and the end product loaded on a gel before dialysis. The unconjugated scFv could then be stained, visualized and quantified by comparison with the scFv alone, loaded in the same amount as theoretically available in the reaction mix. Hence, the VUSPIO-conjugated scFv would be retained at the top of the gel by the massive size of the NPs, while the free TEG4 could migrate freely. **Erreur ! Source du renvoi introuvable.** shows a typical Coomassie-stained SDS-PAGE analysis after the conjugation reaction (left panel). Two scFv/VUSPIO ratios (16 and 32) and two different buffers (MES and PBS) were used in that case. MES buffer disrupts the Ab migration in SDS, showing a spread, blurry band. Right panel curves compares the calculated and theoretical grafting ratios for each buffer. The profiles are similar, roughly linear with a bend from 15 fragments per particle.

Avidity measurements and reactivity validation

The final immobilized αIIbβ3 density on the surface of the SPR chip was 2200 RU.

SPR analysis of the scFv alone and grafted to the VUSPIO nanoparticles showed indeed that TEG4-2C scFv retained its binding capacity to the integrin αIIbβ3 in both settings.

Table 1: TEG4-conjugated VUSPIO data. Iron concentration, VUSPIO equivalent, and scFv concentrations are given for each ratio. VUSPIO molarity is calculated using the formula in ***Erreur ! Source du renvoi introuvable.****.*

scFv/VUSPIO	**R3**	**R6**	**R14**
Fe3+ (M)	0.04	0.04	0.03
VUSPIO (M)	2.72E-7	2.47E-7	1.68E-7
scFv (g/L)	0.0241	0.0469	0.0768
scFv (M)	7.52E-7	1.47E-6	2.40E-6

ScFv alone being monovalent, they are known to have a lower affinity compared to their full IgG counterpart. Because of this, increasing the valence by grafting several fragments should benefit to the avidity of the nanoparticle. To confirm this, each scFv/VUSPIO sample was diluted according to its iron content, in order to assess the avidity of each ratio. Dilutions 1/18, 1/6, and ½ yielded similar results. The representative curves obtained for the 1/6 dilution are shown by **Erreur ! Source du renvoi introuvable.**: SPR sensing confirmed that the VUSPIO binding avidity increases with the number of grafted scFv. The association/dissociation curves represent a quicker association and higher maximum bound analyte for the R14 compared to the R6, itself superior to the R3. However, a Kd couldn't be calculated from these experiments because no sufficient dissociation was measured.

In parallel, immunohistochemistry on rabbit aorta slices showed a specific staining of the areas of platelets accumulation in the atheroma plaque, similar between the scFv fragment alone and its VUSPIO-grafted counterpart as shown by right panel. Interestingly, while the quantity of VUSPIO incubated on the slices was constant, the staining intensity increased with the valence of the particles: A: R3; B: R6, C: R14, consistent with the increased avidity measured by SPR.

Ex vivo imaging

Taking advantage of the bimodal imaging agents injected, both fluorescent and MR images of the aortas were acquired and compared. Fluorescent images were standardized for their respective background using ImageJ software. Successive echo images were used to establish a T2* map of the signal. While the presence of fluorescent particles in the aortic wall is noted by an increased pixel value (color-coded from black to white); the presence of VUSPIO is noted by a decrease in the T2* values (color-coded from cyan to purple). **Erreur ! Source du renvoi introuvable.** shows ApoE-/- mice aortas either uninjected (**Erreur ! Source du renvoi introuvable.**, a, b) or multivalent TEG4-VUSPIO-injected

(**Erreur ! Source du renvoi introuvable.**, c, d, e). The intimal thickening (white arrows) characteristic of atherosclerotic plaque is present in both mice, although it doesn't yield a fluorescent signal, it provokes a decrease of the T2* values (T2* = 11.2 ± 0.7 ms). In the multivalent TEG4-VUSPIO injected mouse, a strong T2* shortening (T2* = 7.0 ± 0.9 ms; **Erreur ! Source du renvoi introuvable.**, e, dashed arrows) also corresponds to an increase in fluorescence (**Erreur ! Source du renvoi introuvable.**, d, dashed arrows), characteristic of plaque labelling.

In vivo imaging

Given the satisfying results obtained *ex vivo*, we decided to inject the nanoparticles to ApoE-/- mice to perform *in vivo* imaging. Immediately after multivalent TEG4-VUSPIO injection, Bright blood images showed a negative contrast in the vessel wall of the atherosclerotic mice which was not observed before injection (**Erreur ! Source du renvoi introuvable.**, b and a, respectively), confirmed by an increase on the R2* map (**Erreur ! Source du renvoi introuvable.**, c and d). Unfortunately, the MR images acquired after 24 h didn't show such a strong negative contrast, and R2* maps were inconclusive (Figure 50, e and f).

Fluorescent biodistribution images didn't show a clear advantage in the take up of multivalent targeted VUSPIO versus untargeted ones. **Erreur ! Source du renvoi introuvable.** represents a typical fluorescence distribution after 24 h in a multivalent TEG4-VUSPIO-injected ApoE-/- mice. *In vivo* (**Erreur ! Source du renvoi introuvable.**, A), the visualization of the aorta is rendered impossible by the tremendous signal displayed by the liver. The kidneys are the only other organs that can be lightly distinguished. *Ex vivo* (**Erreur ! Source du renvoi introuvable.**, B), the most important signal is displayed by the liver, kidneys, and urine, which is relevant with elimination pathways. All particles have been cleared from the blood and didn't distribute into lungs or muscles. Interestingly, the extremely strong signal in the liver creates a halo that impedes correct signal detection from the other organs, so the biodistribution image was acquired again without the liver sample and showed similar results (data not shown).

Discussion

In the previous chapter, we were able to demonstrate the influence of multifunctionalization on the contrast agent avidity and atheroma plaque recognition *in vitro*. To further assess these objects, on top of the iron oxide cores detectable by MR imaging, NIR fluorochromes were added to the VUSPIO platform to allow for fluorescence imaging as a confirmation method. Additionally, Cyril Lorenzato, who recently joined our team as a post-doc, established a MRI protocol using multi-gradient echo sequence parameters to permit the quantification (T2* map) of signal modulation by the VUSPIO nanoparticles.

Using these sequence parameters, combined with NIRF imaging, *ex vivo* reactivity was evaluated in the ApoE-/- mouse model. A specific contrast agent-driven enhancement of the atheroma plaques was detected by MRI at 7 T. Furthermore, NIRF imaging revealed a matching lesion distribution and specific enhancement.

Subsequently, *in vivo* targeting was assessed. NIRF imaging revealed unable to discriminate between the strong unspecific signal due to the accumulation of nanoparticles in the liver, and the signal from the aorta. Biodistribution studies performed on these *in vivo*-injected animals failed to prove a real benefit from VUSPIO multivalent functionalization on plaque recognition. Furthermore, MR imaging yielded mitigate results, as a local negative contrast could be observed in the plaque immediately after injection which wasn't confirmed after 24 h.

Noteworthy, comparison with the previously obtained images(6) was not possible because of the different sequence parameters used. It also seemed that nanoparticles elimination by liver take up was quicker than previously observed.

Interest of multivalence

While we were able to demonstrate the benefit of multivalent grafting *in vitro*, a systematic study of different grafting ratios would allow for evaluating the actual impact of *ex vivo* homing to atherosclerotic lesions.

In vivo experiments with the TEG4-VUSPIO nanoparticles yielded mitigate results, depending on the TEG4 IgG4-VUSPIO or multivalent TEG4 scFv-VUSPIO targeting agent used, or on the conjugated-nanoparticle batch, also depending on acquisition times, immediately after injection or 24 h after. But various reasons could impair *in vivo* the efficient targeting observed *in vitro*.

In vivo targeting

First, the size of our particles should be taken into account. Indeed, in 2008, a study by Briley-Saebo et al.(11) hypothesized that, in order to enter the plaque, rigid objects like USPIO (ultrasmall paramagnetic iron oxide nanoparticles) had to be small enough to fit through the vascular fenestrae of the impaired endothelium. The estimated maximum size was reported to be this of native lipoproteins, up to 25 nm. Of course this could vary from one specie to another, and it is not clear whether 25 nm is a suitable size for mice studies.

This first study took advantage of the passive accumulation in macrophages of dextran-coated nanoparticles. In 2011, lipid-coated USPIO (LUSPIO), inferior to 20 nm in size, and functionalized with antibodies targeting oxidation specific epitopes, showed a superior accumulation in plaque

macrophages than their non-targeted counterpart. They also showed a superior MR signal attenuation than either targeted or untargeted LSPIO, theoretically more potent but displaying a size between 35 and 40 nm which was hypothesized to impair their accumulation in the plaque. Accordingly, the VUSPIO having a size of approximately 90 nm before functionalization, they may not be able to enter through the vascular fenestrae. Yet, in the case of our studies with TEG4 targeting activated platelets, the particle, if not internalized, could bind to the arterial wall of atheroma lesions. However, it is likely that the stringency of arterial blood flow disturbs the particles binding. To overcome these issues, improvements should work at 1/ further increasing the affinity and avidity, 2/ exhibit longer circulation times, and 3/ be able to enter and be retained within the plaque.

This third option has been explored thanks to Gd-loaded micelles. Although superior to 100 nm in size, they were able to squeeze through 25 nm diameter pores and be taken up by macrophages(12,13). Additionally, the formulation of such lipid-based particles may be a key in achieving long circulation times.

References

1. WHO | Cardiovascular diseases (CVDs) [Internet]. WHO. [cited 2016 Aug 22]. Available from: http://www.who.int/entity/cardiovascular_diseases/en/index.html

2. Virmani R, Kolodgie FD, Burke AP, Farb A, Schwartz SM. Lessons From Sudden Coronary Death A Comprehensive Morphological Classification Scheme for Atherosclerotic Lesions. Arterioscler Thromb Vasc Biol [Internet]. 2000 May 1 [cited 2016 Feb 10];20(5):1262–75. Available from: http://atvb.ahajournals.org/content/20/5/1262

3. Insull Jr. W. The Pathology of Atherosclerosis: Plaque Development and Plaque Responses to Medical Treatment. Am J Med [Internet]. 2009 Jan [cited 2016 Feb 10];122(1, Supplement):S3–14. Available from: http://www.sciencedirect.com/science/article/pii/S0002934308010176

4. Nording HM, Seizer P, Langer HF. Platelets in Inflammation and Atherogenesis. Front Immunol [Internet]. 2015 Mar 6 [cited 2016 Nov 1];6. Available from: http://www.ncbi.nlm.nih.gov/pmc/articles/PMC4351644/

5. Badrnya S, Schrottmaier WC, Kral JB, Yaiw K-C, Volf I, Schabbauer G, et al. Platelets mediate oxidized low-density lipoprotein-induced monocyte extravasation and foam cell formation. Arterioscler Thromb Vasc Biol. 2014 Mar;34(3):571–80.

6. Jacobin-Valat M-J, Laroche-Traineau J, Larivière M, Mornet S, Sanchez S, Biran M, et al. Nanoparticles functionalised with an anti-platelet human antibody for in vivo detection of atherosclerotic plaque by magnetic resonance imaging. Nanomedicine Nanotechnol Biol Med [Internet]. 2015 mai [cited 2016 Feb 10];11(4):927–37. Available from: http://www.sciencedirect.com/science/article/pii/S154996341500012X

7. Jacobin M-J, Laroche-Traineau J, Little M, Keller A, Peter K, Welschof M, et al. Human IgG monoclonal anti-alpha(IIb)beta(3)-binding fragments derived from immunized donors using phage display. J Immunol Baltim Md 1950. 2002 Feb 15;168(4):2035–45.

8. Vallet-Courbin A, Larivière M, Hocquellet A, Hémadou A, Sarjapura-Nagaraja P, Laroche-Traineau J, et al. A Recombinant Human Anti-platelet scFv Antibody Produced in Pichia Pastoris for Atheroma Targeting. submitted.

9. Mornet S, Portier J, Duguet E. A method for synthesis and functionalization of ultrasmall superparamagnetic covalent carriers based on maghemite and dextran. J Magn Magn Mater [Internet]. 2005 May [cited 2016 Oct 31];293(1):127–34. Available from: http://www.sciencedirect.com/science/article/pii/S030488530500140X

10. Adumeau L. Développement de stratégies de biofonctionnalisation de surface de nano-objets pour des applications biologiques [Internet]. Bordeaux; 2015 [cited 2016 Sep 8]. Available from: http://www.theses.fr/2015BORD0425

11. Briley-Saebo KC, Mani V, Hyafil F, Cornily J-C, Fayad ZA. Fractionated feridex and positive contrast: In vivo MR imaging of atherosclerosis. Magn Reson Med [Internet]. 2008 Apr 1 [cited 2016 Sep 11];59(4):721–30. Available from: http://onlinelibrary.wiley.com.gate1.inist.fr/doi/10.1002/mrm.21541/abstract

12. Briley-Saebo KC, Amirbekian V, Mani V, Aguinaldo JGS, Vucic E, Carpenter D, et al. Gadolinium mixed-micelles: Effect of the amphiphile on in vitro and in vivo efficacy in apolipoprotein E knockout mouse models of atherosclerosis. Magn Reson Med [Internet]. 2006 Dec 1 [cited 2016 Nov 3];56(6):1336–46. Available from: http://onlinelibrary.wiley.com/doi/10.1002/mrm.21094/abstract

13. Maiseyeu A, Mihai G, Kampfrath T, Simonetti OP, Sen CK, Roy S, et al. Gadolinium-containing phosphatidylserine liposomes for molecular imaging of atherosclerosis. J Lipid Res. 2009 Nov;50(11):2157–63.

Résumé

Le projet de recherche présenté dans ce document a été effectué à l'Université de Bordeaux, au sein de l'UMR CNRS 5536, dans l'équipe « Ciblage de l'athérome » dirigée par le Dr Gisèle Clofent-Sanchez qui a encadré cette thèse. Ce travail vise à proposer une méthode de diagnostic pour une pathologie appelée athérosclérose. En effet, celle-ci est une des maladies cardio-vasculaires qui sont la première cause de décès dans le monde.

L'athérosclérose est une pathologie qui se développe tout au long de la vie, sous l'influence d'une multiplicité de facteurs liés au mode de vie, à l'environnement et à la génétique, et qui peut aboutir aux accidents cardio-vasculaires, notamment infarctus du myocarde ou accidents vasculaires cérébraux. Parmi les facteurs impliqués dans la pathogénèse de l'athérosclérose, certains sont solubles, comme les cytokines pro- ou anti-inflammatoires, les lipoprotéines de faible densité (low density lipoproteins ou LDL) circulant en excès et qui s'accumulent dans la paroi vasculaire, les espèces réactives de l'oxygène impliquées dans l'oxydation de ces LDL ; d'autres sont cellulaires comme les monocytes et macrophages dont la migration et la rétention sous les cellules endothéliales sont à l'origine de la formation de la plaque, les cellules endothéliales qui participent à ce recrutement ; enfin les plaquettes, bien que n'étant pas des cellules, ont un rôle indiscutable dans cette pathogénèse, notamment en aidant le captage des LDL par la paroi vasculaire, en participant au recrutement des monocytes, puis à un stade plus tardif en participant aux thrombi intraplaque ou intraluminal.

L'athérosclérose est une pathologie qui évolue à bas bruit pendant de nombreuses années et n'est pas détectée avant la survenue de signes avant-coureurs ou d'accidents ischémiques souvent mortels. En effet, les méthodes de diagnostic disponibles reposent avant tout sur l'établissement de scores regroupant des critères cliniques (âge, sexe, hypercholestérolémie, hypertension…) et des facteurs de risques associés au mode de vie (tabagisme, sédentarité…). Lorsque le score le justifie, ou en présence de signes cliniques aigus, l'imagerie permet de confirmer la présence des plaques. Cependant, les méthodes traditionnellement utilisées en clinique ne renseignent que sur l'importance du rétrécissement dû à la plaque. Or il est bien connu qu'indépendamment de l'ischémie provoquée par ce rétrécissement, la principale dangerosité des lésions athéromateuses réside dans leur risque de rupture brutale. D'autres modalités cliniques, bien que plus informatives, nécessitent l'introduction d'un cathéter dans les vaisseaux à imager et sont donc hautement invasives : elles présentent plus de risques et une prise en charge plus lourde. Afin de pouvoir proposer une méthode de diagnostic sûre et rapide à une population plus importante de patients à risque, les efforts de recherche se concentrent actuellement sur la mise au point d'agents de contraste pour l'imagerie non invasive, principalement l'imagerie nucléaire ou l'imagerie de résonance magnétique. En effet, ces méthodes sont très utilisées en clinique et les appareils sont donc disponibles. Le défi à relever

réside dans la mise au point d'une méthode permettant de cibler spécifiquement les lésions vasculaires en évitant la génération de bruit de fond.

Dans cette optique, l'imagerie moléculaire permet de s'adresser spécifiquement à l'un -ou plusieurs- des nombreux acteurs impliqués dans la déstabilisation des plaques d'athérome : le candidat idéal représente un bon compromis entre spécificité de la cible et sa forte représentation dans la zone d'intérêt. L'agent de contraste proposé dans ce projet est composé d'une plateforme VUSPIO (Versatile UltraSmall Particle of Iron Oxide) et d'un fragment d'anticorps humain, couplés de manière contrôlée par une méthode régio-sélective.

L'équipe « ciblage de l'athérome » possède une expertise particulière dans la technologie de phage display à partir de banques d'anticorps humains. Grâce à cette méthode, des anticorps spécifiques de l'athérosclérose ont été sélectionnés par deux méthodes. Une première méthode *in vitro* sur plaquettes a permis d'identifier des anticorps reconnaissant l'intégrine αIIbβ3, spécifique des plaquettes activées (1). Parmi les anticorps issus de cette sélection, le TEG4 a été bien décrit pour sa capacité à reconnaître les lésions athéromateuses (2) et représente l'anticorps modèle pour cette étude. Des sélections ultérieures, opérées *in vivo* chez des animaux modèles, ont permis d'isoler des anticorps reconnaissant spécifiquement la plaque d'athérome(3), mais dont la cible moléculaire n'est pas connue. Ces anticorps ont été étudiés pour leur capacité de fixation *in vivo*, et d'autre part des tests protéomiques ont été entrepris afin d'identifier leurs cibles (thèse d'Audrey Hémadou).

Ces différents anticorps ont été produits et testés sous plusieurs formats (anticorps entiers ou fragments) afin d'étudier leur intérêt pour l'imagerie multimodale de l'athérosclérose chez la souris modèle ApoE -/-.

Une première étude, en cours lors de mon arrivée dans l'équipe et à laquelle j'ai collaboré, a eu pour objet de démontrer la faisabilité du ciblage de la particule VUSPIO par l'anticorps anti-intégrine αIIbβ3 TEG4. L'anticorps entier était greffé à la surface des nanoparticules par une conjugaison thiol – maléimide, l'introduction de groupement thiols se faisant de manière aléatoire sur les amines libres de la structure via le réactif de Traut. Les VUSPIO ainsi ciblées étaient capables de se fixer aux lésions athéromateuses *in vitro* sur coupes de tissu fixés, mais également *ex vivo* dans des aortes de souris ApoE-/-, permettant leur détection en IRM haute résolution. Ces résultats ont été publiés dans la revue *Nanomedicine: Nanotechnology, Biology and Medicine* (2).

Une première partie de mon projet a permis (i) de comparer plusieurs anticorps pour leurs capacités de reconnaissance de la plaque d'athérome *in vivo* ; (ii) de mettre au point la méthode d'imagerie de fluorescence chez la souris. Pour cette étude, un kit commercial a été utilisé, les candidats anticorps (IgG ou scFv-Fc) ont été marqués par un fluorophore émettant dans le proche infrarouge afin de permettre l'imagerie des tissus profonds. Malgré cette précaution il

s'est rapidement avéré qu'imager l'aorte *in vivo* n'était pas possible par cette méthode, notamment en raison de l'accumulation hépatique très importante de l'anticorps marqué. Les animaux ont donc dû être sacrifiés et la méthode d'imagerie adaptée pour permettre de comparer les données obtenues de manière semi-quantitative.

Une seconde partie de cette thèse a eu lieu en Australie, dans le laboratoire du Dr Christoph Hagemeyer, ACBD, Monash University, Melbourne. Le Dr Hagemeyer et son équipe sont spécialisés dans la production d'anticorps sous format de scFv comportant une séquence de reconnaissance pour l'enzyme bactérienne sortase. Ceci permet une conjugaison site-spécifique a une grande variété de substrats nucléophiles, notamment des fluorochromes, de la biotine ou une cage de chélate pour capturer des radioéléments (Cu64 par exemple). Cette méthode a été mise en œuvre avec succès pour 2 des anticorps issus de la sélection *in vivo* : C3.3 et H2.1 ; elle a permis de prouver le maintien de leur réactivité envers la plaque d'athérome après conjugaison. En revanche, les premiers tests engagés pour l'imagerie PET – CT chez la souris ApoE-/- n'ont pas été concluants, et la méthode devra être adaptée. Cette étude a été reprise par Samuel Bonnet qui a commencé en 2016 une thèse dans l'équipe de Gisèle Clofent-Sanchez à Bordeaux ; il aura à cœur de pérenniser le partenariat avec l'équipe australienne et de mener à bien l'imagerie nucléaire de l'athérosclérose, il est prévu qu'il se rende sur place. Ces travaux feront donc certainement l'objet d'une publication ultérieure.

Enfin, sur la base des travaux antérieurs de l'équipe, j'ai travaillé à l'amélioration de l'agent de contraste VUSPIO-TEG4 en réalisant un objet multifonctionnel et multimodal : un fluorochrome émettant dans le proche infrarouge a été ajouté aux nanoparticules d'oxyde de fer pour valider la méthode en s'affranchissant des principales faiblesses de l'IRM (faible sensibilité) et de l'imagerie de fluorescence (faible résolution). En partenariat avec le Dr Abdelmajid Noubhani à l'IPB, des fragments d'anticorps de type scFv, comportant une cystéine terminale ont été produits dans *Pichia pastoris* (4). Ce TEG4 scFv 2C a pu être couplé de manière site-spécifique sur les VUSPIO grâce aux bras espaceurs portant une fonction maléimide (thèse de Laurent Adumeau, sous la direction du Dr Stéphane Mornet). La diminution de taille de l'anticorps (30 kDa au lieu de 150) a permis d'augmenter les ratios de conjugaison et d'obtenir des particules d'avidité supérieure, ce qui a été démontré par SPR (Biacore). Les tests *in vitro* sur coupe de tissu athéromateux montrent également une reconnaissance des lésions qui augmente avec la valence des particules. L'injection *ex vivo* dans des aortes de souris a montré une rétention préférentielle des objets ciblés sur les sites lésés. En revanche, il semblerait que l'injection *in vivo* ne permette pas l'accrochage des nanoparticules à la plaque dans le flux sanguin. Ces travaux ont été soumis à la revue PlosOne.

1. Jacobin M-J, Laroche-Traineau J, Little M, Keller A, Peter K, Welschof M, et al. Human IgG monoclonal anti-alpha(IIb)beta(3)-binding fragments derived from immunized donors using phage display. J Immunol Baltim Md 1950. 2002 Feb 15;168(4):2035–45.

2. Jacobin-Valat M-J, Laroche-Traineau J, Larivière M, Mornet S, Sanchez S, Biran M, et al. Nanoparticles functionalised with an anti-platelet human antibody for in vivo detection of atherosclerotic plaque by magnetic resonance imaging. Nanomedicine Nanotechnol Biol Med [Internet]. 2015 mai [cited 2016 Feb 10];11(4):927–37. Available from: http://www.sciencedirect.com/science/article/pii/S154996341500012X

3. Deramchia K, Jacobin-Valat M-J, Vallet A, Bazin H, Santarelli X, Sanchez S, et al. In Vivo Phage Display to Identify New Human Antibody Fragments Homing to Atherosclerotic Endothelial and Subendothelial Tissues. Am J Pathol [Internet]. 2012 Jun [cited 2016 Aug 1];180(6):2576–89. Available from: http://www.sciencedirect.com/science/article/pii/S0002944012002337

4. Vallet-Courbin A, Larivière M, Hocquellet A, Hemadou A, Parimala S-N, Laroche-Traineau J, et al. A Recombinant Human Anti-Platelet scFv Antibody Produced in Pichia pastoris for Atheroma Targeting. PloS One [Internet]. 2017 [cited 2017 Feb 8];12(1):e0170305. Available from: http://journals.plos.org/plosone/article?id=10.1371/journal.pone.0170305

Nanoparticles functionalized with human antibodies for multimodal molecular imaging of atherosclerosis

Because cardiovascular diseases are the leading cause of death in the world, providing clinicians with reliable and straightforward imaging techniques to identify "vulnerable" patients from the general population appears like the Holy Grail of the cardiovascular field. Atherosclerosis, identified as the underlying condition for most acute cardiovascular events, is characterized by the constitution of a lipid-rich atheroma plaque, driven both by excess cholesterol and inflammation, which eventual rupture triggers clotting into the blood flow. It involves a wealth of cellular and molecular actors, which are so many potential markers for molecular imaging, aiming at deciphering how to warn clinicians about the possible occurrence of myocardial infarction or stroke. Here, human antibodies (HuAbs) selected by phage-display for their recognition of over-expressed biomarkers of the pathology are proposed as targeting ligands. They were further engineered for site-specific grafting, either by introducing Cysteine or Sortase recognition tags, and used to target contrast agents for MRI, fluorescence, or PET imaging. In vitro and ex vivo validation studies were carried out on atheroma sections of animal models. In vivo studies in the ApoE-/- mouse model were realized with the anti-platelet TEG4 HuAb using MRI, which provided insights on the biological relevance and feasibility to detect platelets-rich, high-risk atheroma plaques. The development of contrast agents useful in multi-modality imaging, and multi-functionalized with HuAbs is underway. It should serve as an accurate molecular imaging method for atherosclerosis, furthermore easily translated into the clinical arena.

Keywords: atherosclerosis, human antibodies, antibodies engineering, targeted contrast agents, site-specific functionalization, magnetic resonance imaging, near-infrared fluorescence.

Nanoparticules fonctionnalisées avec des anticorps humains pour l’imagerie moléculaire multimodale de l’athérosclérose

L'athérosclérose, à l’origine de la plupart des maladies cardiovasculaires telles que l'infarctus du myocarde ou l'AVC, est la principale cause de décès dans le monde. Les cliniciens ont donc besoin de techniques d'imagerie fiables pour identifier les patients «vulnérables» porteur d’athérome à haut risque d'occlusion thrombotique. Cette pathologie est une maladie inflammatoire qui implique beaucoup d'acteurs cellulaires et moléculaires, parmi lesquels les cellules endothéliales et immunitaires, les lipoprotéines, les cellules apoptotiques et les plaquettes. L'imagerie moléculaire visant à détecter ces acteurs avant la survenue d'événements cardiovasculaires dramatiques est en plein essor.Des anticorps humains (HuAbs) sélectionnés par phage-display pour reconnaître des biomarqueurs de la pathologie sont ici proposés comme ligands servant à fonctionnaliser des vecteurs pour l'imagerie IRM, de fluorescence ou TEP. Les HuAbs ont été modifiés, en introduisant soit des Cystéines soit un site de reconnaissance pour la Sortase, afin de développer un greffage site-spécifique. Les agents ciblant ont été validés in vitro et ex vivo sur des coupes d'athérome de modèles animaux. Des résultats prometteurs ont été obtenus en injectant dans des souris ApoE-/- l’anticorps antiplaquettaire TEG4, apportant ainsi de nouvelles connaissances sur la biologie de l'athérome et la preuve de concept d'une possible détection des plaques à haut risque riches en plaquettes. Des améliorations sont en cours pour développer des agents de contraste multi-fonctionnalisés avec des HuAbs et permettant de réaliser une imagerie moléculaire multimodale de l'athérosclérose facilement transposable en clinique.

Mots clés : athérosclérose, anticorps humains, ingénierie d’anticorps, agents de contraste ciblés, fonctionnalisation site-spécifique, imagerie de résonance magnétique, fluorescence proche-infrarouge

---

CNRS UMR5536 - Équipe Ciblage de l’athérome

146, rue Léo Saignat 33076 Bordeaux Cedex